

Molecular dynamics in non-polymeric
binary glass formers studied
with ^{31}P - and ^2H -NMR

eingereicht an der Bayreuther Graduiertenschule für Mathematik und
Naturwissenschaften zur Erlangung des Doktors der
Naturwissenschaften (Dr. rer. nat.)

vorgelegt von
Björn Pötzschner
geboren am 21. September 1986 in Hof

Die vorliegende Arbeit wurde in der Zeit von März 2011 bis August 2017 in Bayreuth am Lehrstuhl Experimentalphysik II unter Betreuung von Herrn Professor Dr. Ernst Rössler angefertigt.

Vollständiger Abdruck der von der Bayreuther Graduiertenschule für Mathematik und Naturwissenschaften (BayNAT) der Universität Bayreuth genehmigten Dissertation zur Erlangung des akademischen Grades eines Doktors der Naturwissenschaften (Dr. rer. nat.).

Dissertation eingereicht am: 17.08.2017

Zulassung durch das Leitungsgremium: 28.09.2017

Wissenschaftliches Kolloquium: 18.07.2018

Amtierender Direktor: Prof. Dr. Dirk Schüler

Prüfungsausschuss:

Prof. Dr. Ernst Rössler (Gutachter)

Prof. Dr. Michael Vogel (Gutachter)

Prof. Dr. Werner Köhler (Vorsitzender)

Prof. Dr. Hans-Werner Schmidt

Content

I. Abstract.....	6
II. Kurzdarstellung	8
III. Extended Abstract	11
1. Introduction.....	11
2. The glass transition in neat systems.....	12
2.1 Main relaxation in neat systems	12
2.2 Secondary relaxation in neat systems.....	17
3. Binary glass formers	22
3.1 Main relaxation in binary mixtures– state of the art	22
3.2 Experimental results: α -process	28
3.3 Secondary relaxations in binary mixtures – state of the art	43
3.4 Experimental results: β -process	46
4. Dendrimers	54
4.1 State of the art	54
4.2 Experimental results.....	55
5. NMR Spectroscopy.....	62
5.1 Experimental and theoretical basics	62
5.1.1 The spin and its interactions.....	62
5.1.2 NMR Spectra.....	64
5.1.3 Relaxation phenomena	66
5.1.4 Correlation function	67
5.1.5 2D NMR spectra.....	68
5.2 Simulations.....	70
5.2.1 Random walk simulations	70
5.2.2 Graphical user interface and examples.....	73
IV. Publications	77
1. List of Publications	77
2. Individual contribution to the publications	78
3. Further publications	80
4. Publication I.....	81

5. Publication II.....	91
6. Publication III	107
7. Publication IV	121
References	132
List of figures and permissions for reuse	152
Acknowledgements	157
Eidesstattliche Versicherung	159

I. Abstract

Polymer-plasticizer systems show a decoupling of the dynamics of both components and the existence of large dynamic heterogeneities especially for the low- T_g (plasticizer) component. The question arises, whether these effects depend on the polymer character or whether they are intrinsic to binary systems, including non-polymeric systems. Therefore, we studied the low- T_g component tricresyl phosphate (TCP, $T_g = 206$ K) mixed with a specially synthesized high- T_g spirobichroman derivative (DH 379, $T_g = 382$ K) and a second mixture consisting of tripropyl phosphate (TPP, $T_g = 134$ K) and another spirobichroman derivative (SBC, $T_g = 356$ K). The dynamics of TCP and TPP were probed by ^{31}P NMR in the whole concentration range, while the SBC component was deuterated and thus was selectively investigated by ^2H NMR. Different NMR methods (Echo spectra, two-dimensional NMR spectra, stimulated echo measurements, analysis of the spin-lattice and spin-spin relaxation times) reveal the reorientational dynamics of the main and secondary relaxation.

For all concentrations, two main relaxation processes with two distinct T_g are identified by dielectric spectroscopy (DS), T_{g1} and T_{g2} . The faster one (α_2 -process) is attributed to the dynamics of the low- T_g component. It shows increasing dynamic heterogeneities of the reorientational dynamics, described by a broad distribution of $G(\ln\tau_{\alpha_2})$, with decreasing concentration of the low- T_g component, as demonstrated by all NMR observables. This is reflected by an increasing stretching of the stimulated echo correlation function, from a more or less exponential decay at high concentrations to a quasi-logarithmic decay at low concentrations. 2D NMR spectroscopy reveals, that the dynamic heterogeneities are of transient nature, i.e. a dynamical exchange between fast and slow moving molecules within the broad $G(\ln\tau_{\alpha_2})$ occurs. The slower process (α_1 -process) is associated with the dynamics of the high- T_g component. However, there are indications that a fraction of the low- T_g component also takes part in the slow α_1 -process. In contrast to the α_2 -process, the α_1 -process broadens only weakly when adding the low- T_g component and is comparable to the main relaxation in a neat glass former. Furthermore, the plasticizer effect (α_1) and the anti-plasticizer effect (α_2), respectively, are observed. In the range $T_{g2} < T < T_{g1}$, i.e. in the arrested high- T_g matrix (α_1 -process), the molecules of the low- T_g component involved in the α_2 -process still show an isotropic liquid-like motion as proven with 1D and 2D NMR spectra. Further, a crossover of the temperature dependence of $\tau_{\alpha_2}(T)$ from a non-Arrhenius to an Arrhenius-like behavior, at low concentrations of the low- T_g component, is observed below T_{g1} . This change in the temperature dependence also leads to a decrease of T_{g2} at low concentrations and thus leads to

a maximum in T_{g2} (c_{low-Tg}). The dynamical behavior of the α_2 -process is attributed to intrinsic confinement effects.

Exploiting the sensitivity of ^2H and ^{31}P NMR echo experiments, the secondary process (β) was studied in the system TPP/SBC in the entire concentration range. The β -process of neat TPP is rediscovered in the mixture with unchanged time constants. The NMR spectra (for short interpulse delays) in the slow and fast exchange limit are very similar with only slightly changed spectral widths (ca. 1%). Thus, a spatially highly restricted motion with angular displacements below $\pm 10^\circ$ is performed. Yet, increasing the interpulse delay, TPP shows echo spectra typical of a small angle motion with decreasing intensity in the center of the spectra. At the same temperatures, very similar line shape effects are recognized in the ^2H NMR spectra of the SBC component in the mixture, not observed in neat SBC. It appears that the TPP molecules enslave the SBC molecules to perform a similar hindered reorientation with the same time constant as TPP. In addition, the temperature dependence of the spin-lattice relaxation becomes the same for both components at low temperature. Taking into account the different coupling constants, the amplitude of the β -relaxation is estimated to be smaller in the high- T_g component. At lowest weight concentrations ($c_{TPP} \leq 20\%$) one finds indications that the β -process starts to disintegrate, i.e. not all molecules take part in the β -relaxation any longer, as expected for $c_{TPP} \rightarrow 0$. Altogether, we conclude that the β -process is a cooperative process. Summarizing, all dynamical features reported in polymer additive systems or polymer blends are also observed in the non-polymeric systems.

Furthermore, the dynamics of bulk polypropylene imine (PPI) dendrimers of generation 2-5 were investigated. A secondary process, traces of which are observed in the ^2H NMR spin-lattice relaxation time and in the ^2H NMR spectra, exhibits features characteristic of a typical β -process. Moreover, ^2H NMR identifies amino end group jumps with a broad distribution of correlation times $G(\ln\tau)$. The characteristics of the main relaxation are essentially independent of generation and the dendrimers exhibit a glass point T_g of about 200 K.

II. Kurzdarstellung

Polymer-Weichmacher Systeme zeigen eine Entkopplung der Dynamik beider Komponenten und große dynamische Heterogenitäten, insbesondere in der nieder- T_g (Weichmacher) Komponente. Es stellt sich die Frage ob diese Effekte nur vom Polymercharakter der Komponenten abhängen oder ob sie intrinsisch für binäre Systeme, insbesondere auch für niedermolekulare Systeme sind. Deshalb untersuchten wir die nieder- T_g Komponente Trikreslyphosphat (TCP, $T_g = 206$ K) in einer Mischung mit einer speziell synthetisierten spirobichromanen hoch- T_g Komponente (DH 397, $T_g = 382$ K) und eine zweite Mischung aus Tripropylphosphat (TPP, $T_g = 134$ K) und einer weiteren spirobichromanen Komponente (SBC, $T_g = 356$ K). Die Dynamik von TCP und TPP wurde mit Hilfe von ^{31}P NMR im gesamten Konzentrationsbereich untersucht, während die deuterierte SBC Komponente selektiv mit Hilfe von ^2H NMR gemessen wurde. Verschiedene NMR Methoden (Echospektren, zweidimensionale NMR Spektren, Messungen des stimulierten Echos, der Spin-Gitter und Spin-Spin Relaxationszeiten) offenbarten die Reorientierungsdynamik der Haupt- und Sekundärrelaxation.

Im gesamten Konzentrationsbereich wurden zwei Hauptrelaxationen mit zwei verschiedenen T_g 's, T_{g1} und T_{g2} , mit Hilfe von dielektrischer Spektroskopie (DS) gefunden. Der schnellere Prozess (α_2 -Prozess) wird der Dynamik der nieder- T_g Komponente zugeordnet. Alle NMR Observablen zeigen eine Zunahme der dynamischen Heterogenitäten der Reorientierungsdynamik der nieder- T_g Komponente mit sinkender Konzentration der nieder- T_g Komponente, welche durch eine breite Verteilung $G(\ln\tau_{\alpha_2})$ beschrieben werden. Dies spiegelt sich in der zunehmenden Streckung der mit der Stimulierten-Echo-Methode gemessenen Korrelationsfunktionen wider, von einem mehr oder weniger exponentiellen bei hohen Konzentrationen bis hin zu einem quasi-logarithmischen Zerfall bei niedrigen Konzentrationen der nieder- T_g Komponente. 2D NMR Spektroskopie zeigt, dass die dynamischen Heterogenitäten transienter Natur sind, d.h. es findet ein dynamischer Austausch innerhalb von $G(\ln\tau_{\alpha_2})$ zwischen sich schnell und langsam bewegenden Molekülen statt. Der langsame Prozess (α_1 -Prozess) wird der Dynamik der hoch- T_g Komponente zugeschrieben. Allerdings gibt es Hinweise darauf, dass ein Teil der nieder- T_g Komponente auch am langsamen α_1 -Prozess teilnimmt. Beim Hinzufügen der nieder- T_g Komponente verbreitert sich der α_1 -Prozess nur leicht und ist vergleichbar mit der Hauptrelaxation in reinen Glasbildnern, im Gegensatz zum α_2 -Prozess. Weiterhin wird der Weichmacher (α_1) beziehungsweise der Anti-Weichmacher (α_2) Effekt beobachtet. Innerhalb der arretierten hoch- T_g Matrix (α_1 -

Prozess), vollführen die Moleküle der nieder- T_g Komponente, welche am α_2 -Prozess teilnehmen, immer noch eine isotrope flüssigkeitsähnliche Bewegung im Temperaturbereich $T_{g2} < T < T_{g1}$, wie mit Hilfe von 1D und 2D NMR Spektren gezeigt wird. Bei niedrigen Konzentrationen der nieder- T_g Komponente wird unterhalb von T_{g1} eine Veränderung in der Temperaturabhängigkeit von $\tau_{\alpha_2}(T)$ von einem nicht-Arrhenius zu einem Arrhenius Verhalten beobachtet. Diese Veränderung in der Temperaturabhängigkeit führt außerdem zu einer Wiederabnahme von T_{g2} bei niedrigen Konzentrationen und führt auf diese Weise zu einem Maximum in T_{g2} ($c_{\text{nieder-}T_g}$). Das dynamische Verhalten des α_2 -Prozesses wird auf intrinsische „confinement“ Effekte zurückgeführt.

Der Sekundärprozess (β) wurde im System TPP/SBC im gesamten Konzentrationsbereich unter Ausnutzung der Empfindlichkeit der ^2H and ^{31}P NMR Echo-Experimente studiert. Der β -Prozess von reinem TPP wird in der Mischung mit unveränderten Zeitkonstanten wiederentdeckt. Die NMR Spektren (für kurze Zwischenpulsabstände) im schnellen und langsamen Grenzfall ähneln sich stark mit nur leicht veränderten spektralen Breiten (ca. 1%). Daraus wird geschlossen, dass eine räumlich eingeschränkte Bewegung mit Winkelveränderungen der molekularen Achse von weniger als 10% durchgeführt wird. Wenn allerdings der Zwischenpulsabstand erhöht wird, zeigt TPP Echo-Spektren mit abnehmender Intensität in der Mitte der Spektren, welche typisch für einen Kleinwinkelprozess sind. Im selben Temperaturbereich werden sehr ähnliche Linienformeffekte in den ^2H NMR Spektren der SBC Komponente in der Mischung beobachtet, welche im Reinsystem nicht beobachtbar sind. Es scheint als versklaven die TPP Moleküle die SBC Moleküle dahingehend, dass sie eine ähnliche räumlich eingeschränkte Bewegung mit der gleichen Zeitkonstante wie TPP, durchführen. Weiterhin wird bei niedrigen Temperaturen die Temperaturabhängigkeit der Spin-Gitter Relaxation für beide Komponenten gleich. Wenn die verschiedenen Kopplungskonstanten der Komponenten berücksichtigt werden, lässt sich abschätzen, dass die Amplitude der β -Relaxation in der hoch- T_g Komponente kleiner als in der nieder- T_g Komponente ist. Bei niedrigen Gewichtskonzentrationen ($c_{\text{TPP}} \leq 20\%$) finden sich Hinweise, dass der β -Prozess anfängt zu zerfallen. Es nehmen nicht mehr alle Moleküle am β -Prozess teil, was für $c_{\text{TPP}} \rightarrow 0$ erwartet wird. Insgesamt schließen wir, dass der β -Prozess ein kooperativer Prozess ist. Zusammenfassend ist zu sagen, dass die dynamischen Eigenschaften von Polymer-Additiv Systemen oder Polymermischungen auch in nicht-polymeren Systemen gefunden werden.

Weiterhin wurde die Dynamik von Polypropylenimin (PPI) Dendrimeren der Generation 2-5 im Reinsystem untersucht. Ein Sekundärprozess, dessen Spuren in der ^2H NMR Spin-Gitter Relaxationszeit und in den ^2H NMR Spektren beobachtet wurden, zeigt Eigenschaften, welche

charakteristisch für einen typischen β -Prozess sind. Zusätzlich identifiziert ^2H NMR die Amino-Endgruppen Sprünge, welche eine breite Verteilung von Korrelationszeiten $G(\ln\tau)$ zeigen. Die Eigenschaften der Hauptrelaxation, welche ein T_g von ungefähr 200 K aufweist, sind im Wesentlichen unabhängig von der Generation.

III. Extended Abstract

1. Introduction

While the crystal phase is the thermodynamically stable phase below the melting point T_m , almost every molecular liquid or polymer can be supercooled below T_m given a sufficiently high cooling rate. For temperatures below T_m one speaks of a supercooled liquid, provided that no crystallization occurs. For even lower temperatures below the glass transition temperature T_g , it is called a glass. The transport coefficients continuously change while supercooling the liquid, e.g. the viscosity increases over many orders of magnitude within a small temperature range below T_m . Likewise, the structural relaxation becomes very slow and thus the metastable liquid is still stable on a macroscopic timescale. Below T_g , the structural relaxation does not take place on the experimental timescale anymore, an “isostructural” state, the glass, is formed.

In contrast to the crystal phase with its translational symmetry, in the glass state there is no long ranged order, but a disordered structure similar to that of the liquid phase. The glass transition, being defined as the strong increase of the transport coefficients below T_m , is phenomenologically understood today, especially the evolution of the main (structural) and secondary relaxation. However, there is still no satisfying theoretical model to describe the crossover from a liquid to the glass state.

Binary glasses, i.e. glasses consisting of two components, have a wide field of application, especially in the chemical and plastics industry. While binary systems consisting of components with similar T_g form homogeneous mixtures, systems with a dynamical asymmetry, i.e. systems consisting of two components with strongly different T_g , display relaxation behavior that is not fully understood. In particular, the components are dynamically decoupled and thus show two distinct T_g . Mainly polymer blends and polymer plasticizer systems, i.e. mixtures consisting of a polymer and a low molecular component, are the content of recent research. Systems consisting of two low molecular components are less studied, especially systems with a large T_g contrast, i.e. a large difference between the T_g of the components.

In this work, component selective ^2H and ^{31}P NMR are applied to unravel the dynamics of these mixtures regarding their main and secondary relaxation. The main questions are, whether the dynamical behavior observed in polymer plasticizer systems is similar in mixtures of low molecular components and whether mainly the T_g contrast determines the dynamic of these

systems. Further, the dynamics of PPI dendrimers (repetitively branched molecules), are investigated with the aid of dielectric spectroscopy, field cycling NMR and solid-state NMR. The thesis is organized as follows. In chapter 2.1, the glass transition in neat systems is described. Further, secondary relaxations, especially the Johari-Goldstein secondary relaxation, are characterized in chapter 2.2. In chapter 3, two state of the art chapters provide an overview of the research done on the main (chapter 3.1) and secondary (chapter 3.3) process in binary systems, followed by the experimental results (chapter 3.2 and 3.4) obtained in the framework of this thesis (Publications II-IV). In chapter 4, the dynamics of PPI dendrimers are examined (Publication I). Chapter 5.1 provides information on the theoretical and experimental basics needed to understand this work. Finally, in chapter 5.2 a self-written graphical user interphase program to obtain NMR observables from random walk simulations is presented.

2. The glass transition in neat systems

2.1 Main relaxation in neat systems

When supercooling a liquid below its melting temperature T_m and avoiding crystallization, its viscosity η continuously increases until it reaches values typical of a solid ($\eta \geq 10^{12}$ Pa*s) near its glass transition temperature T_g . This increase of viscosity is associated with an enormous slowdown of the structural relaxation (α -relaxation) time τ_α , reaching values on the timescale of seconds. Associated with the structural relaxation is the reorientational relaxation due to the coupling of translational and rotational motion typically observed in supercooled liquids. The temperature dependence of the reorientational relaxation time and the viscosity is very similar as shown in figure 2.1.

When cooling down to low temperatures, where the structural relaxation becomes very slow, the entropy $S(T)$ and the volume $V(T)$ show a change in their temperature dependence. Correspondingly, a step in their first derivatives is observable. Since relaxation is not possible on the experimental timescale anymore, these quantities depend on the cooling rate. The glass transition temperature T_g is conventionally defined as the temperature when the structural relaxation time τ_α reaches 100 s. This corresponds to the temperature where the heat capacity shows a step in calorimetric measurements when applying a cooling rate of $R = 10$ K/min. The glass state below T_g can be described as an arrested isostructural state.

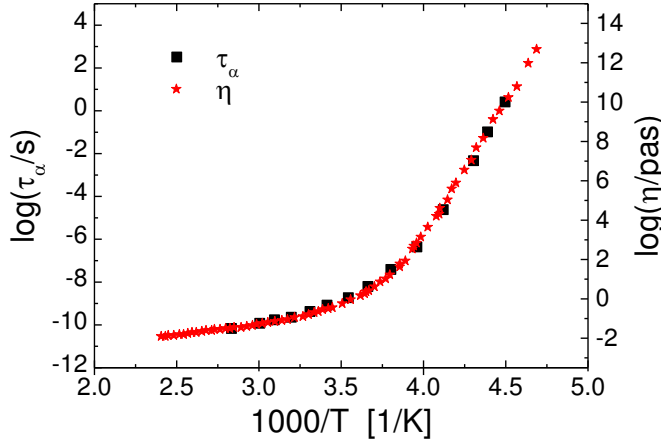


Figure 2.1: Reorientational correlation times τ_α (left y-axis) of salol (phenyl salicylate) as a function of the inverse temperature as obtained by dielectric spectroscopy [1]. Further, viscosity data is shown (right y-axis) [2].

The α -relaxation time $\tau_\alpha(T)$ shows a non-Arrhenius temperature dependence often interpolated by the phenomenological Vogel-Fulcher-Tammann (VFT) equation [3]

$$\tau_\alpha = \tau_0 \exp\left(\frac{D}{T-T_\infty}\right) \quad (2.1)$$

whereby D , τ_0 and T_∞ are empirical parameters. The VFT equation interpolates the time constants well at low temperatures close to T_g but fails for molecular liquids at high temperatures ($T > T_m$). Thus, other interpolations, e.g. considering a temperature dependent activation energy, are suggested [4-6].

While in simple liquids well above T_m a Debye relaxation in the frequency domain is observed, which corresponds to an exponential correlation function of the main relaxation in the time domain, the correlation function of the structural (α -) relaxation at temperatures near T_m and in the supercooled state follows a non-exponential decay. Figure 2.2 displays the time dependence of the reorientational correlation function of the second Legendre polynomial (due to the particular NMR interaction, see chapter 5.1) $C_2(t)$ as obtained by solid-state NMR in the glass former tricresyl phosphate (TCP).

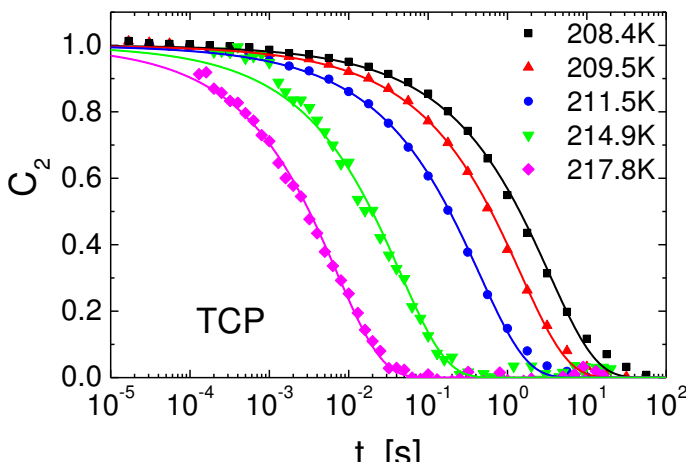


Figure 2.2: Reorientational correlation function $C_2(t)$ of TCP at different temperatures as obtained by ^{31}P NMR stimulated echo measurements. Interpolations (solid lines) by a stretched exponential (Kohlrausch) function with $\beta_K \approx 0.6$ (see eq. 3.2). Data from [7].

The non-exponential long-time decay can be described with a stretched exponential (Kohlrausch) function [8,9]

$$C = A \cdot \exp\left(-\left(\frac{t}{\tau_K}\right)^{\beta_K}\right) \quad (2.2)$$

The stretching parameter is typically around $\beta_K = 0.4 - 0.85$ for neat glass formers [10]. In neat glass formers time-temperature superposition (TTS) [11] or frequency-temperature superposition (FTS), respectively, is fulfilled in a large temperature range, i.e. the shape of the long-time decay of the correlation function does not change with temperature, and master curves $C(t) = \hat{C}(t/\tau_\alpha)$ can be obtained by shifting the data on the logarithmic timescale.

One reason causing the stretching of the correlation function is the occurrence of dynamic heterogeneities, i.e. a distribution of correlation times $G(\ln\tau_\alpha)$ determines the correlation function $C(t)$ [12]. The idea is, that each subensemble has an essentially exponential correlation decay but the subensembles in distinct environments show different mobility, and thus different correlation times. This leads to a non-exponential overall correlation function. The presence of these dynamic heterogeneities was shown through various experiments like 4D-NMR experiments [13,14], non-resonant dielectric spectral hole burning [15,16], and photo bleaching experiments [17]. Furthermore, 2D and 3D simulations as well as theoretical work was put into effect to characterize these dynamical heterogeneities [18-21]. The lifetime of these dynamical heterogeneities was detected to be on the timescale of the structural relaxation [22], while a temperature dependent characteristic length scale was found to be on the order of some nanometers [12,14,23,24]. As example, figure 2.3 shows the single-particle displacements of a simulation of a binary Lennard-Jones mixture in two dimensions [20]. The length of the arrows corresponds to the velocity of the particles. Clearly dynamic heterogeneities in the form of spatially divided regions of fast and slow moving molecules are recognizable.

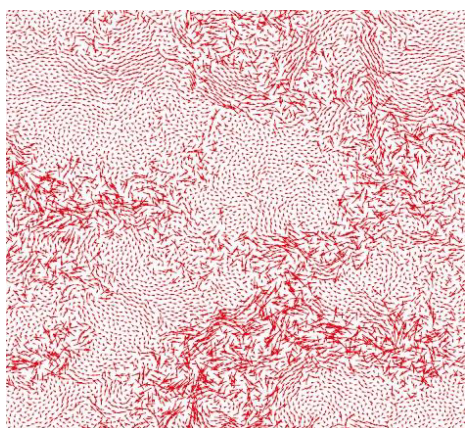


Figure 2.3: Single-particle displacements recorded during the simulation of a binary Lennard-Jones mixture in two dimensions on a timescale comparable to the structural relaxation. Reprinted from [20].

Instead of measuring the correlation function $C(t)$ in the time domain, one can measure in the frequency domain via linear response experiments like dielectric spectroscopy (DS) or depolarized light scattering (DLS) which yields the susceptibility χ . The dissipative part χ'' of the susceptibility is shown in figure 2.4 as obtained by DLS measurements on propylene carbonate. The peak at low frequencies corresponds to the main relaxation while the intensity at higher frequencies originates from secondary processes (see next chapter). The χ'' itself is connected to the spectral density $J(\omega)$ via the fluctuation dissipation theorem $\chi'' \sim \omega J(\omega)$, while the spectral density is given as the Fourier transform of the correlation function (see eq. 5.16).

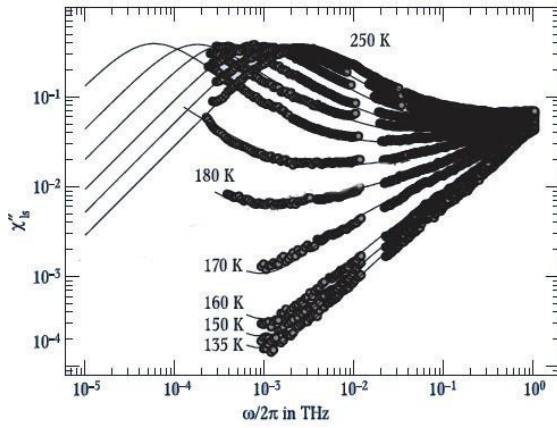


Figure 2.4: Depolarized light scattering spectra $\chi''(\omega)$ for propylene carbonate (black dots, from ref. [25]). The solid lines are solutions of MCT describing the fast dynamics and the α -relaxation. Figure adapted from [26].

A promising theoretical concept to describe the glass transition and yielding detailed predictions for the shape of the susceptibilities is the mode coupling theory (MCT). The MCT characterizes the glass transition through a set of non-linear differential equations for the density fluctuations [27-31]. Their time dependent density correlation function $\phi(t)$ is described by a set of generalized harmonic oscillator differential equations containing a retardation term, which correlates the density correlation $\phi(t)$ at the time t to all $\phi(t')$ for times $t' < t$. In its simplest form, it holds [29]:

$$\ddot{\phi}(t) + \Omega^2 \phi(t) + \Omega^2 \int_0^t m(t-t') \dot{\phi}(t') dt' = 0 \quad (2.3)$$

The retardation term (the term containing $m(t-t')$) is the key of MCT and reproduces the so-called “cage effect”, that means the caging of a particle through its neighboring particles for short times. The MCT predicts a critical temperature T_c , where a dynamic phase transition occurs, i.e. with cooling below T_c the system shows a crossover from a liquid to a glass. It turns out that traces of the transition at T_c are experimentally found well above T_g . However,

no divergence of η is observed at T_c as predicted by the MCT. Thus, an extension of the theory is necessary to describe the actual situation [32]. Experimental results [26] (see figure 2.4) and molecular dynamics simulations of rigid diatomic molecules [33-35] give a good validation of the MCT regarding the evolution of $\chi''(\omega, T)$ during the transition from a simple liquid to a moderate viscous liquid.

Other theoretical models are based on the growing length scale of the cooperative behavior of the main relaxation with decreasing temperature like the random first order transition theory (RFOT) [36-38], the dynamic facilitation concept [38] or the frustration-limited domain approach [4]. Furthermore, elastic models are proposed like the elastically cooperative activated barrier hopping theory [6,39].

2D NMR experiments (see chapter 5.1) propose a motional model for the reorientation of the molecules due to the main relaxation in supercooled liquids. The molecular reorientation mainly consists of small angle jumps similar to the Brownian diffusion observed at high temperatures and a small fraction of large angle jumps [40] as illustrated in figure 2.5, where a typical spatial trace of a molecular axis is displayed.

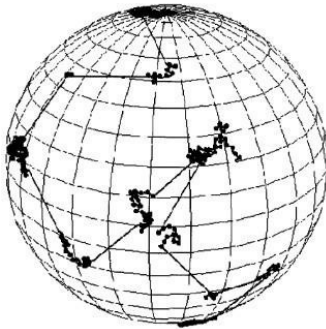


Figure 2.5: Motional model for the molecular reorientation of the α -process. The trace on the sphere surface resembles the orientation trajectory of a molecular axis. Reprinted from [41].

The huge timescale of τ_α from picoseconds ($T \gg T_m$) to seconds ($T \ll T_m$) must be covered by different measurement methods. Therefore, neutron scattering (NS, 10^{-12} s to 10^{-8} s), depolarized light scattering (DLS) with a double monochromator (DM, 10^{-12} s to 10^{-8} s) and a Tandem-Fabry-Perot-interferometer (TFPI, 10^{-12} s to 10^{-8} s), or with photon-correlation spectroscopy (PCS, 10^{-8} s to 10^2 s) as well as dielectric spectroscopy (DS, 10^{-12} s to 10^{-2} s), field cycling nuclear magnetic resonance (FC NMR, 10^{-9} s to 10^{-5} s), and solid-state NMR (10^{-5} s to 10^2 s) is typically applied [42].

2.2 Secondary relaxations in neat systems

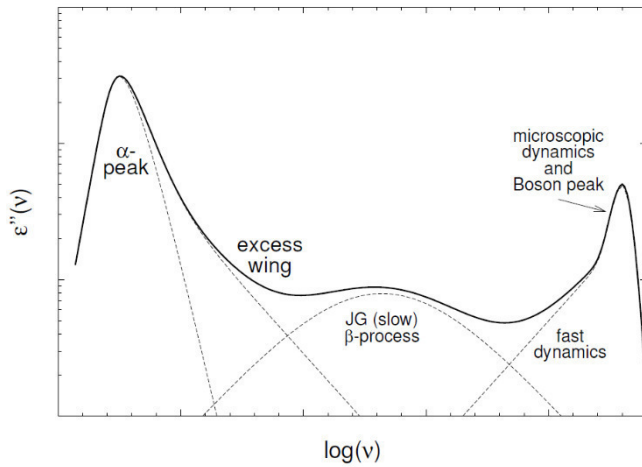


Figure 2.6: A sketch of the dielectric loss spectrum for glass forming systems with the main relaxation and all secondary processes. Reprinted from [43].

Until now, mainly the α -process was described, i.e. the long-time or low-frequency behavior of the dynamics. Now we focus on secondary relaxations. Figure 2.6. shows an overview of possible secondary processes which can occur between the α -process and the microscopic dynamics (the high frequency end of the intermolecular dynamics; also seen in figure 2.4 at high frequencies): The fast secondary relaxation predicted first by MCT, the slow β -process or Johari-Goldstein (JG) process and the excess wing.

The excess wing may be regarded as some kind of hidden secondary relaxation which may separate from the α -process under pressure or aging [44,45] or as an intrinsic feature of the α -relaxation [46,47]. The β -process was first proposed to be of intramolecular origin. It was argued that the movement of side-groups in polymers or in molecules with internal degrees of freedom causes the β -relaxation [48]. In 1970 Johari and Goldstein showed that also systems consisting of small rigid molecules show a secondary relaxation and that the β -process must be of intermolecular origin and be an intrinsic feature of the glass state [49-51]. This so-called Johari-Goldstein (JG) β -process is also discovered in ionic glasses [52]. An excess wing was also observed in metallic glass formers [53]. Mainly, the β -process is probed by dielectric spectroscopy, but also neutron scattering [54,55] and mechanical relaxation [48,56] can be applied, while in light scattering (LS) measurements no secondary relaxation can be observed so far. Yet, the excess wing is found in LS [46].

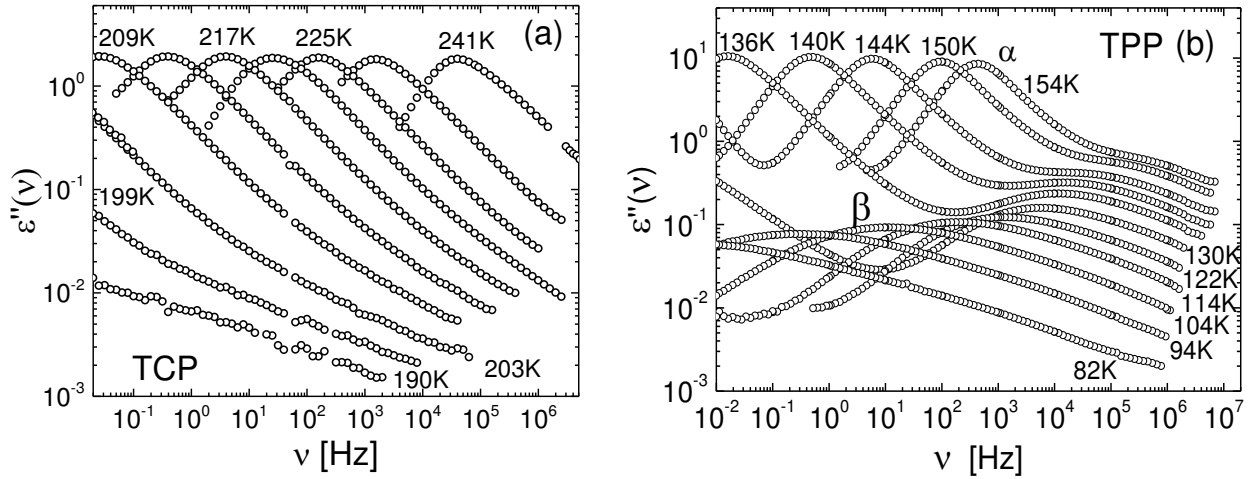


Figure 2.7: (a) Dielectric spectra of the type A glass former tricresyl phosphate (TCP) (reprinted from Publication II). (b) DS spectra of the type B glass former tripropyl phosphate (TPP) (adapted from Publication III).

Regarding the manifestation of the secondary relaxations, one may distinguish between so-called type A and type B glass formers [57]. The former shows no JG secondary relaxation but rather an excess wing, as shown in figure 2.7 (a). On the other hand, type B glass formers show a separated β -relaxation as seen in figure 2.7 (b). Here, a second peak at low temperatures is seen in the frequency window, while the main relaxation is already “arrested” on macroscopic timescales at these temperatures [57]. In some cases, a β -process as well as an excess wing are found [47,57,58].

According to Ngai et al. [58-60] one may distinguish between “generic” secondary relaxations and those processes reflecting structural particularities of the glass forming molecules. The pressure dependence of the secondary relaxation may be an important classification criterion [58-60]. It is shown, that for generic β -processes both relaxations (α and β) have the same T - p dependence, i.e. τ_α and τ_β shift in the same way when changing the temperature T and the pressure p . Thus, a strong connection between the JG- β - and α -process was suggested, i.e. it is a precursor for the main relaxation. Other secondary relaxations may originate from the intrinsic movement of molecular parts and show a different pressure and temperature dependence.

Below T_g , the β -process is seen as a broad, usually symmetric peak in the DS spectra (see figure 2.7 (b)) which is often described by a log-Gaussian distribution of the correlation times [61]. The spectra broaden with decreasing temperature, and can be described by a temperature independent activation energy distribution $g(E)$ [62,63]. The mean time constant $\langle\tau_\beta\rangle$ of the secondary process follows an Arrhenius temperature dependence typically of a thermally activated process with activation energies in the range of $E/k_b = 11 - 26 T_g$ [64,65]. While

below T_g , the relaxation strength of the β -process is almost temperature independent, it strongly increases with raising the temperature above T_g [63,66,67]. This may be attributed to the softening of the glass which leads to a lower extend of spatial hindrance as suggested by NMR experiments, (see below, figure 2.8 and 2.9) [68]. At even higher temperatures both processes, α and β , often merge [69].

The origin of the JG β -process is not completely understood yet. Johari and Goldstein proposed so-called “islands of mobility”, where groups of molecules retain a higher mobility compared to their surrounding in the glass [49,51,70]. However, NMR experiments [71,72] as well as solvation studies [73] proved that all molecules take part in the relaxation process, at least in neat simple glass formers.

The underlying molecular mechanism of the secondary relaxation was investigated by ^2H NMR techniques in structural glasses [71,74,75] as well as in plastic crystals [76,77]. For example, the lineshape of the NMR solid-echo spectra (see chapter 5.1) is sensitive to small angle reorientations, especially the intensity in middle of the spectra at $\omega = 0$ decreases, when increasing the solid-echo interpulse delay. Figure 2.8 displays such interpulse dependent spectra for the deuterated type A glass former glycerol- d_5 (a) and for the deuterated type B glass former toluene- d_5 (b). Line shape changes are only observed in toluene: for long interpulse delays the intensity in the middle of spectra decays to zero; a clear sign that all molecules participate in the relaxation process. According to these NMR experiments, the β -process yields a small correlation loss at short times for all sub-ensembles of molecules until the main relaxation leads to a complete loss of the correlation at longer times, as proposed before by Williams and Watts [78]. It was shown that a spatially restricted multi-step reorientation is the underlying mechanism for the β -process. A so-called wobbling “within-a-cone” or “on-a-cone” (cf. figure 2.8 (d)) model was proposed [72,77,79-81]. Here the molecular axis reorients within or on the circumference of a cone with half opening angle χ . These models reproduce the measured interpulse dependent spectra (cf. figure 2.8 (c), and figure 5.6)

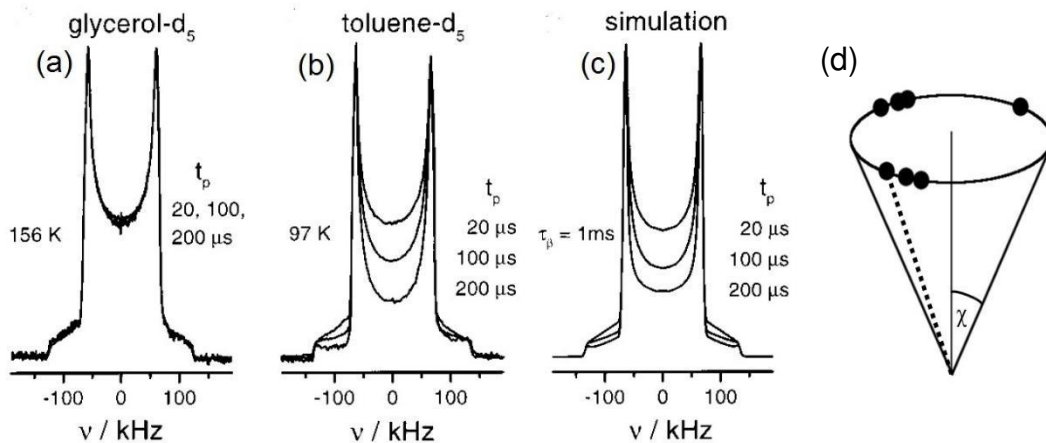


Figure 2.8: Interpulse t_p dependent ^2H NMR solid-echo spectra of glycerol-d₅ (a) and toluene-d₅ (b). (c) Simulated spectra, assuming a motion on the circumference of a cone with half opening angle $\chi = 6^\circ$. Figures adapted from [74]. (d) “Motion-on-a-cone”-model. The molecular axis (dashed line) reorients on the circumference of a cone with opening angle χ .

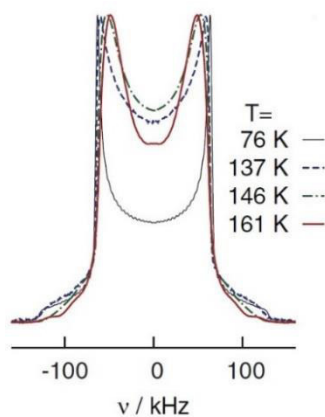


Figure 2.9: Temperature dependent ^2H NMR spectra of the plastically crystalline phase of cyano cyclohexane for a short interpulse delay $t_p = 20 \mu\text{s}$, demonstrating the effect of the β -process at $T > T_g$. Figure reprinted from [76].

While χ is typically smaller than 10° below T_g , the opening angle increases above T_g , which can explain the increase of the DS relaxation strength at temperatures higher than T_g [76,77,79,82]. In the plastically crystalline phase of cyano cyclohexane, no merging of the β -process with the α -process is observable, so the secondary relaxation can be observed even at temperatures higher than T_g . The increase of χ is reflected in the ^2H spectra in the fast motion limit (even for short t_p), i.e. at temperatures where the β -process is fast compared to the experimental NMR timescale, as illustrated in figure 2.9. For temperatures below T_g , no influence of the β -process is seen at a short interpulse delay of $t_p = 20 \mu\text{s}$ due to the small reorientational angle (black spectrum). Above T_g , a motionally averaged spectrum (red spectrum) with a smaller coupling constant $\overline{\delta_Q}$ (compared to δ_Q at low temperatures) in the fast motion limit of the β -process is observed due to the increased spatial exploration of the molecular axis (compare chapter 5.2.2; figure 5.5).

Recently, indications were found that the β -process may exhibit some kind of anisotropy which reflects the particular molecular structure [83]. For example, experiments in toluene-d₃ suggest that the β -process only involves fluctuations around its pseudo C₂-axis since no significant interpulse dependent line shape changes in the spectra occur [83]. This is also indicated by measurements of the ²H spin-lattice relaxation time [84]. In contrast, as discussed above, measurements on toluene-d₅ show interpulse dependent spectra whose intensity in the middle of the spectra decays to zero implying that all deuterons take part in the secondary relaxation. This implies that also the C-D bond parallel to the C₂-axis must take part in the reorientation and thus indicates a reorientation of the C₂-axis [72]. These inconsistent results are not understood yet. An anisotropic motion of toluene solely around the C₂-axis does not explain the dielectric activity of the β -process which is observed, since such kind of motion would not change the dipole moment.

In simulations of Lennard-Jones binary mixtures of rigid asymmetric, dumbbell-shaped molecules, many experimentally observed features of the JG- β -process could be reproduced like the two step correlation function [78], the strong increase of the relaxation strength of the β -process above T_g , and the merging of the α - and the β -relaxation at higher temperatures [85,86]. However, the large angle jumps of the molecules found even in the glass state are at variance with experimental results (see above).

3. Binary glass formers

3.1 Main relaxation in binary mixtures— state of the art

The dynamics of so-called asymmetric binary mixtures consisting of two glass formers with significantly different T_g of their components are more complex than in neat systems. A single step in DSC measurements was observed in early works [87], which has been regarded as a necessity for miscibility [88]. Meanwhile, a dynamic decoupling with two distinct T_g is reported for binary mixtures consisting of miscible polymer blends [89-92], for polymer plasticizer systems [93-98], and for mixtures consisting of two low molecular components with a large T_g contrast [99]. Besides DSC, other methods like dielectric spectroscopy, NMR spectroscopy and neutron scattering were carried out to investigate polymer blends [100], the technologically relevant polymer additive (a low molecular low- T_g component) systems [47,99,101-107], and non-polymeric mixtures [108-112].

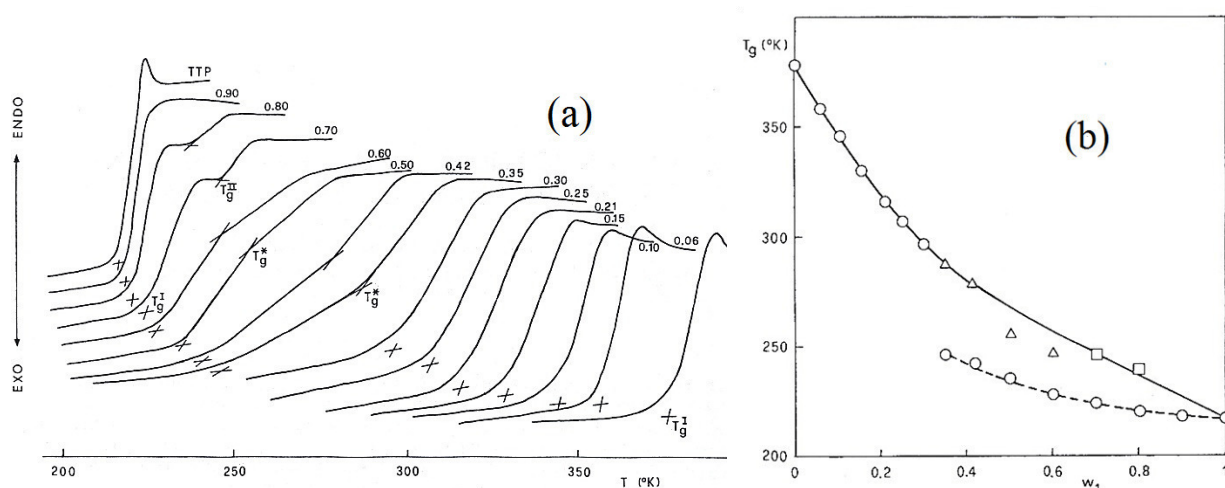


Figure 3.1: (a) DSC measurements of the system tritolyl phosphate (TTP) in polystyrene (PS). At high TTP concentrations two separated steps are seen (left), while at low concentration only a single step is observed (right). (b) $T_g(C_{TTP})$ curve as obtained from the DSC measurements. The lines are a guide for the eye. The lower curve displays the T_g of the TTP, the upper curve the T_g of PS. Figures reprinted from [94].

The dynamic decoupling is clearly seen with the help of DSC measurements in the system tritolyl phosphate (TTP) in polystyrene (PS), for example, which has a T_g contrast of around 150 K [94]. Figure 3.1 shows measurements in the whole concentration range. At high PS concentrations only one step is seen. With increasing additive concentration first two different slopes in the DSC curve and then two resolved steps are observable, clearly identifying two

glass transitions temperatures T_{g1} , associated with the PS component, and T_{g2} , associated with the TPP component. The corresponding $T_g(c_{TPP})$ values are shown in figure 3.1 (b). It seems that the dynamic decoupling takes place in the whole concentration range, although T_{g2} values at lowest concentrations are missing. Further, one of the main features of asymmetric binary glass forming mixtures, namely the plasticizer effect is seen for the high- T_g component, i.e. the acceleration of the dynamics in the mixture reflected by the decreasing $T_{g1}(c_{TPP})$ with increasing additive concentration. Also the anti-plasticizer effect reflected by the increasing $T_{g2}(c_{TPP})$ in the mixture, i.e. the slowing down of the dynamics in the mixture for the low- T_g component, is observed. The plasticizer effect is more pronounced, the higher the T_g contrast, i.e. the higher the difference of the T_g of the components, is [113,114].

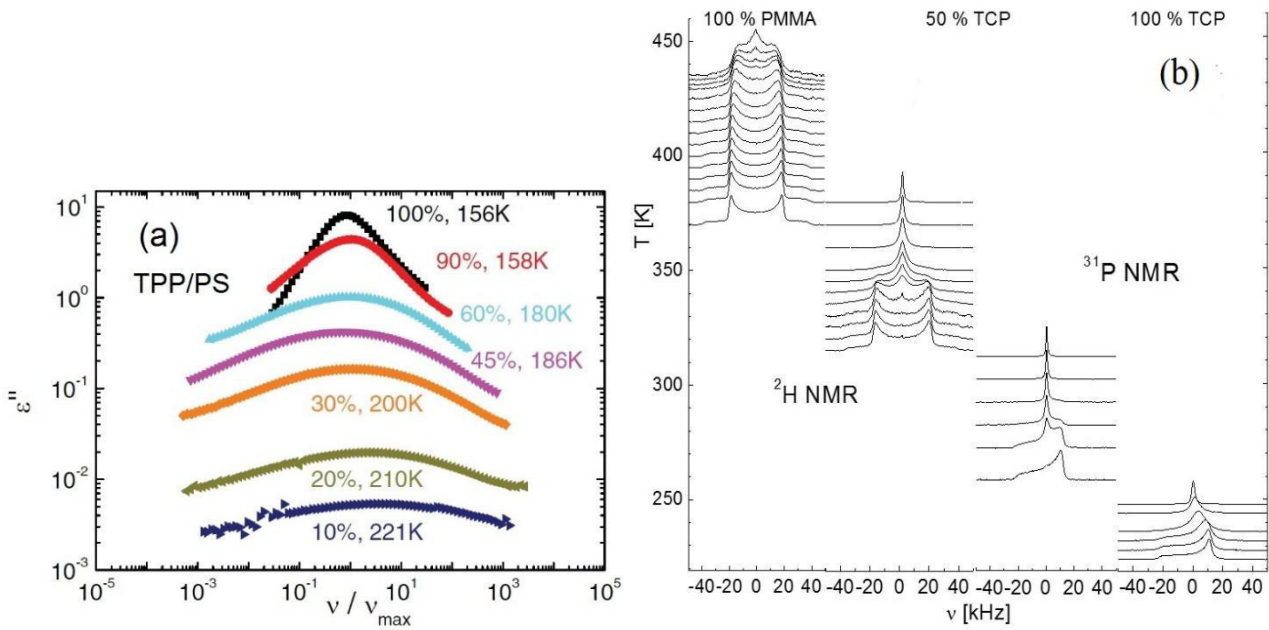


Figure 3.2: (a) DS spectra of TPP in the mixture TPP/PS for the concentrations $c_{TPP} = 100\%$ down to $c_{TPP} = 10\%$. Adapted from [106]. The frequency axis for each spectrum is shifted with respect to the frequency of the maximum of the spectrum. (b) ^2H and ^3P NMR spectra of the system TCP/PMMA for neat PMMA (left row), neat TCP (right row) and in the $c_{TCP} = 50\%$ (mass concentration) mixture (middle rows). Figure adapted from [104]. The baseline of the spectra corresponds to the temperature at which they were measured.

Figure 3.2 (a) illustrates another prominent feature of asymmetric binary glass forming mixtures. Here, DS spectra of the additive component tripropyl phosphate (TPP) in the system TPP/polystyrene (PS) are shown in the whole concentration range from neat TPP down to the mass concentration $c_{TPP} = 10\%$ [106]. With decreasing concentration, the DS spectra strongly

broaden, first mainly on the low frequency flank, then also on the high frequency side, reflecting strong dynamic heterogeneities for the low- T_g component in the mixture as revealed by NMR (cf. below). These heterogeneities increase with decreasing concentration of the low- T_g component. In contrast, the high- T_g component shows only slightly broadened dielectric spectra. Further, the broadening of the spectra of the low- T_g component is temperature dependent. Thus, FTS does not hold any longer [114].

Binary systems were also investigated by NMR allowing to probe both components selectively. This is shown in figure 3.2 (b) for the system tricresyl phosphate (TCP) in polymethyl-methacrylate (PMMA) [104]. The deuteration of PMMA enables to measure both components selectively with ^2H and ^{31}P NMR. Also here, the plasticizer and anti-plasticizer effect are well observable in the NMR spectra. The line collaps from the powder spectrum to a liquid line, which occurs around the temperature at which the condition $\tau_\alpha \approx 10^{-6}$ s holds, is shifted to lower temperatures for PMMA and to higher temperatures for TPP in the mixture. Further, the decoupling of the dynamics of the two components is recognized: The phosphorus component shows a Lorentzian line, reflecting isotropically liquid-like reorientation at temperatures around 300 K, while the PMMA component is still arrested on the NMR timescale as seen by the rigid solid-state spectrum.

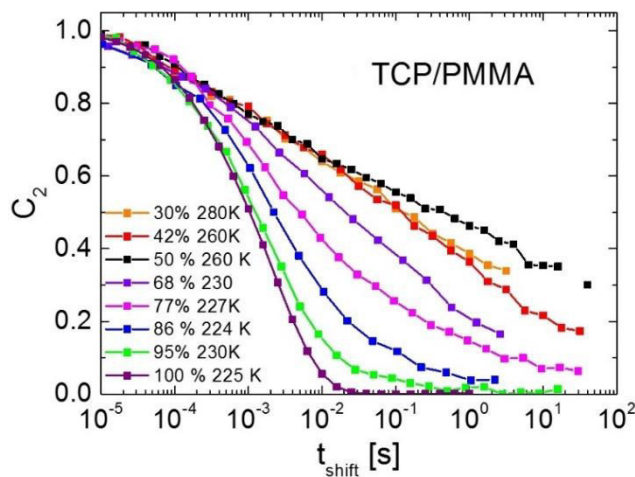


Figure 3.3: Reorientational correlation functions $C_2(t)$ of the system TCP/PMMA for TCP concentrations as indicated. Figure reprinted from [115].

While at low temperatures typical solid-state powder spectra and at high temperatures liquid-like Lorentzian lines are measured, at intermediate temperatures so-called “two-phase“ spectra are observable (cf. figure 3.2 (b) middle right row). They were interpreted that way, that at the same temperature “fast” and “slow” (on the NMR timescale) subensembles of TCP molecules are present. Thus, the appearance of such “two-phase” spectra is a direct sign for pronounced dynamic heterogeneities, i.e. a broad distribution of correlation times $G(\ln\tau_\alpha)$ [41] usually not

observed in neat systems. Those heterogeneities are also reflected in the reorientational correlation functions accessible by the NMR stimulated echo technique as figure 3.3 shows. Here, the correlation decay of TCP in the system TCP/PMMA gets more and more stretched with decreasing additive concentration until the correlation function decays quasi-logarithmically. This behavior is in accordance with the strong broadening in the DS spectra shown in figure 3.2 (a).

The strong dynamical heterogeneities in mixtures are often explained due to local concentration fluctuations which cause a distribution of correlation times. The concentration variations are typically attributed to thermally driven concentration fluctuations [116-118], or so-called self-concentration effects [119,120] or even a combination of both [121,122]. The transient nature of the dynamic heterogeneities was confirmed by 2D NMR exchange spectra, even below T_{gl} [106,123,124]. There, a dynamic exchange of “slow” and “fast” molecules on a timescale comparable to the mean structural relaxation time of the low- T_g component, occurs.

A logarithmic decay of the correlation function was reported in Monte Carlo simulations of mixtures consisting of soft sphere particles with different size [125,126] for the component of high mobility, while the correlation function of the large particles is only slightly broadened. The dynamical decoupling is also seen in similar simulations [127]. Here the large particles exhibit a standard glass transition, controlled by the cage effect, while the small particles remain mobile within the more or less arrested matrix of the large particles. With increasing particle density, the small particles first show a sub-diffusive behavior until they perform a localization transition in the confinement of the arrested matrix of the large particles. Sub-diffusive behavior and a localization transition were also found in simulations for a Lorentz gas [128] and MCT works on mixtures with large and small particles [129]. Correspondingly, MCT in so-called quenched-annealed systems (systems, in which the small molecules reorientate in a matrix of “arrested” large particles, which are “in a disordered configuration sampled from a given probability distribution” [130]) predicts higher order singularities. Near these singularities, logarithmic correlation decays and a sub-diffusive behavior is observable [130].

In a set of recent publications in 2011 and 2012 Blochowicz and coworkers investigated the systems methylenetetrahydrofolate (MTHF) in PS of different molecular weights [107] and MTHF in tristyrene [112] by means of DSC, DS, NS, dynamic light scattering (DLS) and NMR. As these publications inspired the present work, they will be discussed here in detail. The authors were able to observe two different T_g in DSC measurements for low MTHF concentrations. The two T_g are assigned to the main relaxations of both components. DS measurements, mainly probing the MTHF component due to its large dipole moment, discovered three processes (cf. figure 3.4), called α_1 , α_2 and β . The α_1 -process was assigned to the main relaxation of the PS component and the α_2 -process to that of the MTHF component.

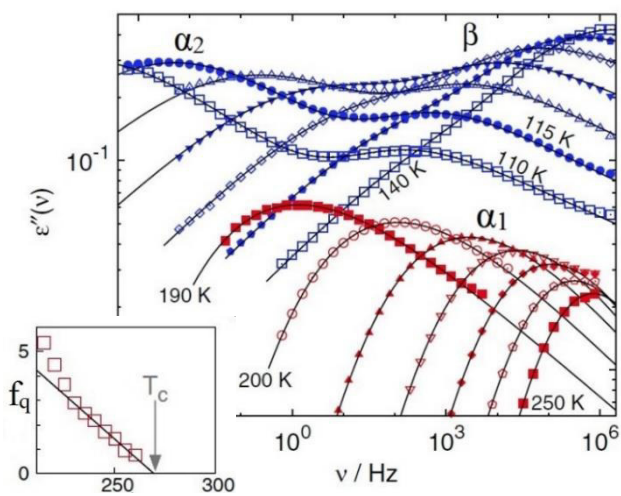


Figure 3.4: DS measurements of the system MTHF in PS60k for the $c_{MTHF} = 50\%$ (mass concentration) mixture. The α_1 -process (PS) (red points), the α_2 -process (MTHF) and the β -process (blue points) are observable. The inset shows $f_q(T) = (\Delta\epsilon_{\alpha 1} - \Delta\epsilon_{PS})/\Delta\epsilon_{total}$, (with $\Delta\epsilon_i$ being the relaxation strengths), i.e. the fraction of MTHF molecules participating on the α_1 -process. Figures adapted from [107].

For temperatures below a critical temperature T_c the relaxation strength of the α_1 -process ($\Delta\epsilon_{\alpha 1}$) increases and is higher than the relaxation strength expected from the contribution of the PS component ($\Delta\epsilon_{PS}$). The following scenario was proposed: Two dynamically different MTHF fractions exist, a comparably fast one (α_2) reorienting in the “arrested” matrix of the high- T_g component below the upper T_g and a slow one (α_1) participating in the reorientation of the “slow” PS component. Above a critical temperature T_c the contribution of the MTHF on the α_1 -process vanishes, while with decreasing temperature more and more MTHF molecules take part in the slow reorientation of PS (see inset figure 3.4). Blochowicz and coworkers proposed a type A scenario for the glass transition of the low- T_g component as predicted by MCT [130-132] and identified in simulations [133]. The non-ergodicity parameter f (here the fraction of “arrested” MTHF molecules) continuously increases from zero to a non-zero value below T_c , in contrast to the glass transition of the high- T_g component or in neat systems, where the long time limit of the correlation function jumps from zero to a finite value at the critical temperature T_c (type B glass transition).

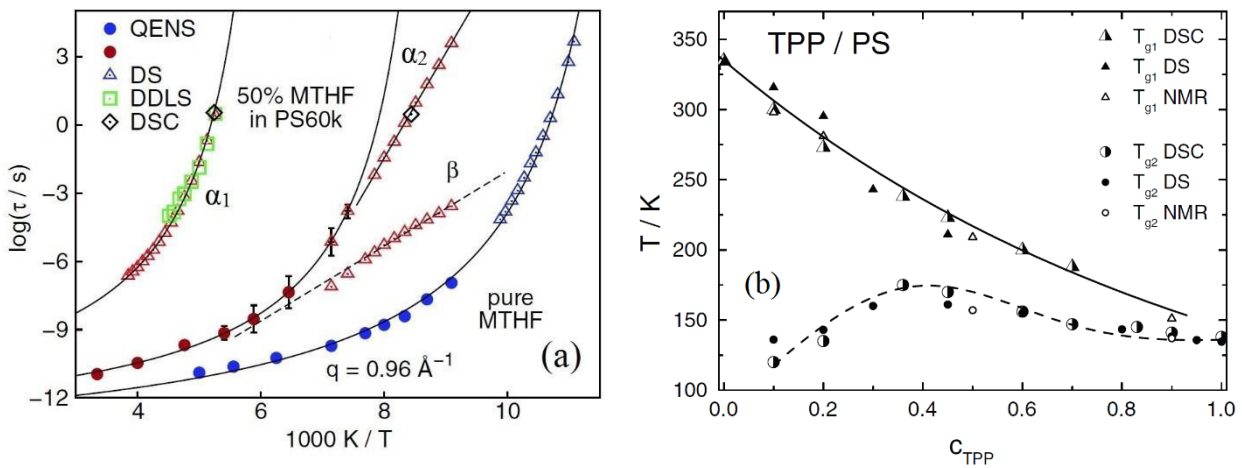


Figure 3.5: (a) Relaxation times of the system MTHF/PS60k for the α_1 -, α_2 - and β -process obtained by quasi-elastic neutron scattering (QENS) (circle), DS (triangle), depolarized dynamic light scattering (DDLS) (square), and DSC (diamond) measurements. Pure MTHF and the mixture with $c_{MTHF} = 50\%$ in PS are shown. Adapted from [107]. (b) Concentration dependent T_{g1} and T_{g2} for both main relaxations α_1 and α_2 in the system TPP/PS. Reprinted from [106].

In addition, a crossover of the temperature dependence of $\tau_{\alpha_2}(T)$ from a VFT to an Arrhenius behavior below the upper T_{g1} (α_1 -process), when the matrix (τ_{α_1}) is arrested, was found by Blochowicz and coworkers (cf. figure 3.5 (a)). This “fragile-to-strong” transition is also observed in the system TPP/PS [106]. The temperature dependence of $\tau_{\alpha_2}(T)$ of the low- T_g component is similar to supercooled liquids inside nanometer pores (confinement) [115,134-139].

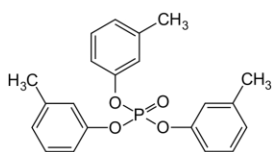
In another study, the glass transition temperatures T_{g1} and T_{g2} for both processes are obtained in the whole concentration range as shown in figure 3.5 (b) [106]. The T_{g1} decreases monotonously from the glass transition temperature of the neat high- T_g component to values similar to the T_g of the neat low- T_g component reflecting the “plasticizer effect”. The T_{g2} of the additive first increases with decreasing additive concentration, shows a maximum and decreases again for low concentration, which was not observed so far.

3.2 Experimental results: α -process

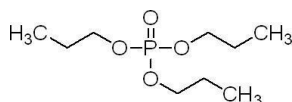
While polymer mixtures and polymer additive systems were extensively investigated in the last decades, binary mixtures consisting of two low molecular components were only rarely measured due to the fact that only a small T_g contrast (e.g. $\Delta T_g = 109$ K for the system MTHF/TCP [115]) could be reached in these systems. Therefore, in the present work (Publications II,III and IV), binary systems consisting of TCP and TPP as low- T_g components and especially synthesized spirobichroman high- T_g derivatives called DH 379 and SBC (see figure 3.6) were mixed to obtain large T_g contrasts of up to 220 K. The DS measurements were carried out by F. Mohamed as a part of her PhD thesis. All NMR results were collected within the framework of this dissertation.

The objective of this work is to compare the dynamics of these non-polymeric, dynamically asymmetric mixtures to that of the well known polymer plasticizer system. Questions like the following arise: Do the systems show a similar behavior like in polymer additive systems, i.e. is only the T_g contrast the important factor determining the dynamic behavior of the mixtures? Which kind of glass transition (type A or B) does the low- T_g component perform within the matrix of the high- T_g component? Does the low- T_g component also participate in the main relaxation of the high- T_g component, as found for polymer additive systems? As for $c_{low-T_g} > 0$ two main relaxations are observed, the question arises what happens for $c_{low-T_g} \rightarrow 0$. Can the low- T_g component in this case be used as a probe for the dynamics of the high- T_g component and vice versa for $c_{low-T_g} \rightarrow 1$? Furthermore, the TPP component as well as DH 379 and SBC show a β -process in the neat systems, and therefore the behavior of the secondary relaxations in the mixtures is also of substantial interest (see chapter 3.4), especially if all molecules of both components participate in the secondary relaxation as indicated in first experiments [68]. The chemical structures of the used components are shown in figure 3.6.

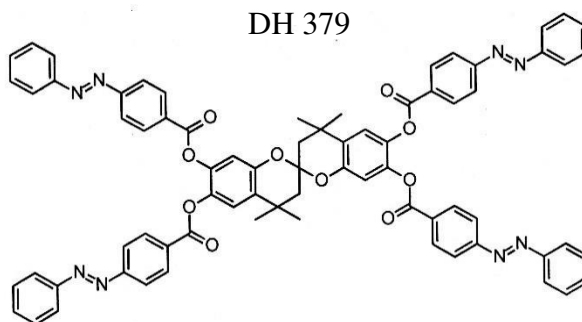
Tricresyl phosphate (TCP)



Tripropyl phosphate (TPP)



DH 379



SBC

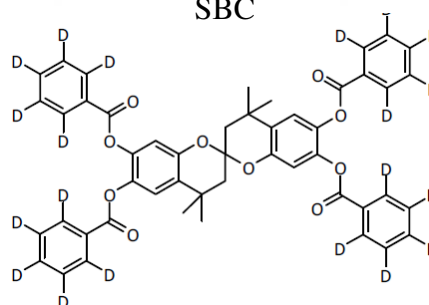


Figure 3.6: TCP (up left, $T_g = 206$ K, $M_{mol} = 368.4$ g/mol), DH 379 (up right, $T_g = 382$ K, $M_{mol} = 1205.3$ g/mol), TPP (bottom left, $T_g = 134$ K, $M_{mol} = 224.23$ g/mol) and SBC (bottom right, $T_g = 356$ K, $M_{mol} = 809.0$ g/mol).

The components TCP and DH 379 (Publication II) with a T_g contrast of $\Delta T_g = 176$ K and TPP and SBC ($\Delta T_g = 222$ K, Publication III, IV) were mixed and investigated. In both systems the low- T_g component contains phosphorus and thus can be selectively investigated by ^{31}P NMR. Further, the SBC was deuterated for ^2H NMR measurements, while the DH 379 was studied by the unselective ^1H NMR. DS measurements in the two mixtures mainly probe the low- T_g components due to their larger relaxation strengths compared to that of the high- T_g components. Both mixtures show the tendency to demix at high temperatures ($T > 300$ K) followed by a crystallization of the high- T_g component. Thus, measurements above room temperature could not be carried out in the systems. Due to this tendency to crystallize, all measurements, NMR and DS, were performed twice and the samples were regularly optically checked to assure the presence of a homogeneous mixture. While NMR measurements in the whole concentration range were possible for both mixtures, only concentrations down to $c_{TPP} = 61\%$ could be investigated by DS in the system TPP/SBC due to the different sample preparation. The mixture always crystallized at lower concentrations when filled into the DS sample holder, while in the case of NMR the binary system could be prepared at high temperatures and then quenched to low temperatures, where the mixture is stable. In the case of TCP/DH 379 DS could cover the whole concentration range. Further, DSC measurements could not be performed in the mixtures due to this problem. Since both systems TCP/DH 379

and TPP/SBC show a similar dynamical behavior in the mixtures, the main results will be discussed in parallel.

In figure 3.7. (a) dielectric spectra ($c_{TCP} = 34\%$ in the system TCP/DH 379) typical of the mixtures are shown. After subtracting the conductivity contribution (open symbols) two distinct processes are revealed in the DS data at high temperatures. As will be clear when discussing the temperature and concentration dependence of the time constants (see figure 3.8 (a)), the high-frequency process, called α_2 , has to be addressed to the dynamics of the low- T_g component (here TCP), while the low-frequency process, called α_1 , reflects the dynamics of the high- T_g component (here DH 379). Clearly, both processes and therefore the dynamics of the components are decoupled in the mixtures. This decoupling is found in the whole concentration range, even at very high additive concentrations (see figure 3.7 (b)), two distinct processes can be distinguished, although they are very close together and the α_1 -process is only seen as a shoulder in the DS data. This is in contrast to Blochowicz and coworkers [107,112] who proposed a merging of the two processes at high concentrations of the faster component (cf. inset figure 3.9). Furthermore, the α_2 -relaxation peak of the additive (TPP or TCP) gets significantly broader with decreasing additive concentrations, in particular on the low-frequency side, implying growing dynamic heterogeneities in the mixture. It also becomes broader upon cooling, leading to a failure of FTS.

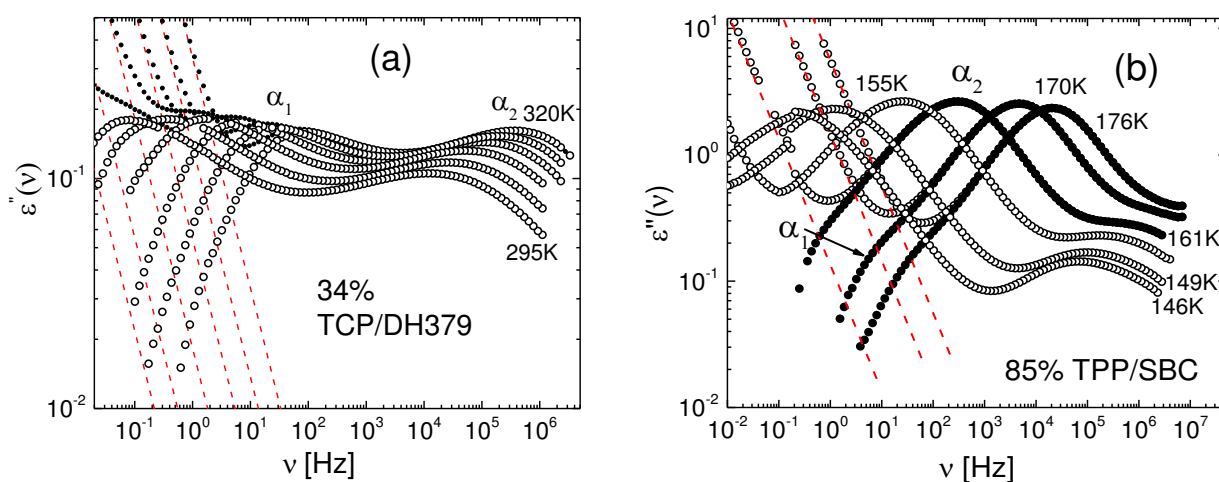


Figure 3.7: (a) DS spectra of the $c_{TCP} = 34\%$ mixture in the system TCP/DH 379 (filled circles). For high temperatures, the conductivity contribution (red dashed lines) is subtracted (open circles). Figure adapted from Pub. II. (b) DS spectra of the $c_{TPP} = 85\%$ mixture of the system TPP/SBC (open circles). Again, the conductivity contribution (red dashed lines) is subtracted (filled circles) for high temperatures. Figure adapted from Pub. III.

Figure 3.8 displays an overview over the temperature dependence of the time constants of both processes in the system TCP/DH 379 obtained by the DS and NMR (see below) measurements. Following the concentration dependence of $\tau_{\alpha 1}$ (filled symbols) and $\tau_{\alpha 2}$ (open circles) it is now clear that the processes have to be addressed to the dynamics of DH 379 and TCP, respectively. The plasticizer and the anti-plasticizer effect are clearly seen for both components. With increasing concentration of the low- T_g component, the dynamics of the high- T_g component accelerates, i.e. $\tau_{\alpha 1}$ decreases while the dynamics of the low- T_g component slows down with increasing concentration of the high- T_g component, i.e. $\tau_{\alpha 2}$ increases. The time constants of the α_2 -process follow a VFT behavior for concentrations higher than $c_{TCP} = 48\%$, while for the α_1 -process too little data points are available to apply a VFT fit.

For lower concentrations, deviations from the VFT behavior in the low- T_g component are observable (see figure 3.8 (b)). For the $c_{TCP} = 34\%$ mixture a crossover from a VFT behavior at high temperatures to an Arrhenius behavior at low temperatures is found. This crossover takes place at temperatures around the T_g of the high- T_g component (T_{gI}). With the arresting of the slow component, a so-called “fragile-to-strong” [140] transition appears to occur. In contrast, in the $c_{TCP} = 20\%$ mixture the low- T_g component seems to show an Arrhenius behavior at all temperatures. However, too few data points above T_{gI} exist to make a clear statement on the type of temperature dependence at high temperatures. The low- T_g component appears to experience intrinsic confinement effects below the upper glass transition temperature, quite analogue to the behavior of supercooled liquids in nanopores [135,138]. A similar crossover was observed in the polymer plasticizer system TPP/PS [106]. As will be demonstrated by NMR experiments below, the α_2 -process at low concentrations does not reflect a secondary relaxation despite the Arrhenius temperature dependence of $\tau_{\alpha 2}$ typically observed for a β -process.

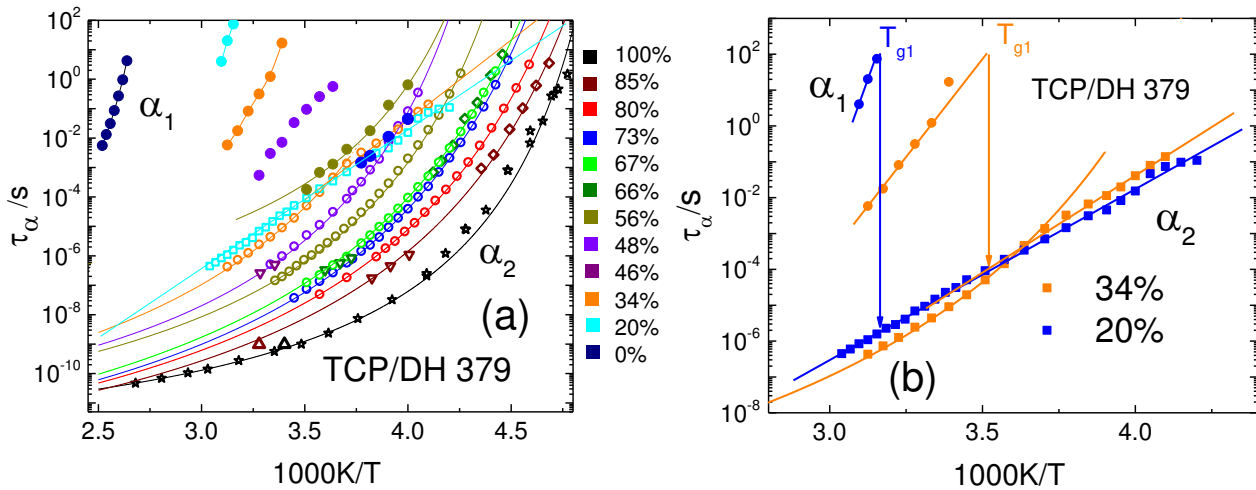


Figure 3.8: (a) Time constants $\tau_\alpha(T)$ for the mixture TCP/DH 379 for concentrations as indicated (see color code); α_2 -process as obtained from dielectric spectroscopy (open circles), NMR stimulated echo (open diamonds), T_1 minimum (open up triangle), T_2 data (open down triangle), neat TCP from ref. 141 (open stars) and α_1 -process from dielectric spectroscopy (filled circles). Lines are fits with a VFT or Arrhenius function. (b) Reorientational time constants in the mixture TCP/ DH 379 for $c_{TCP} = 20\%$ and for $c_{TCP} = 34\%$. The arrows indicate the estimated T_{g1} . A crossover from non-Arrhenius to Arrhenius behavior is observed close to T_{g1} . Figures reprinted from Pub. II.

The $T_g \equiv T(\tau_\alpha = 100 \text{ s})$ in dependence of the TCP concentration obtained from the time constants in figure 3.8 (a) by extrapolating the time constants to $\tau_\alpha = 100 \text{ s}$ are shown in figure 3.9. As mentioned above, no merging of both processes even at high TCP concentrations occurs. Furthermore, while T_{g1} monotonously decreases with increasing c_{TCP} , the T_g of the low- T_g component exhibits a maximum. So far, this is only observed by recent similar experiments in TPP/PS (cf. figure 3.5 (b)) [106]. However, in the previous works from Blochowicz and coworkers [107,112] (see inset figure 3.9 for the system MTHF/tristyrene) no maximum at low temperatures was observed, as well as a merging of both processes was proposed at high concentrations of the low- T_g component.

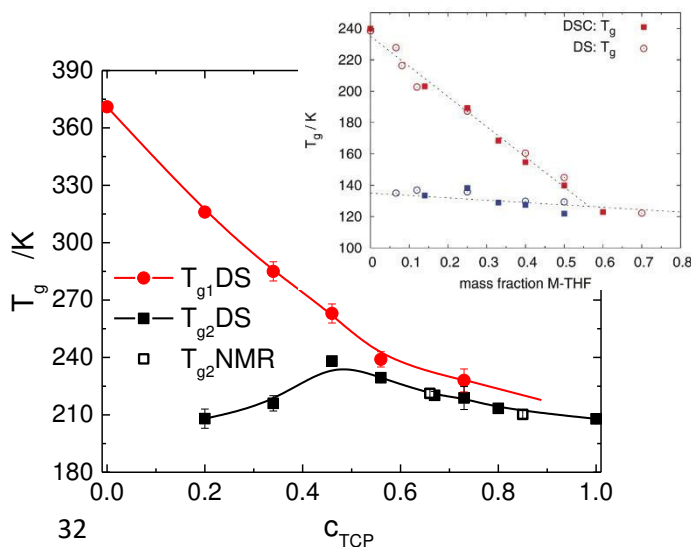


Figure 3.9: Concentration dependence of the glass transition temperatures for both processes, α_1 (red circles) and α_2 (black squares) in the mixture TCP/DH 379 with guides for the eye (solid lines) and error bars. Figure adapted from Pub. II. Inset: Both T_g in the system MTHF/tristyrene. Reprinted from [112].

In the following, the NMR results achieved within this thesis, regarding the α_1 - and the α_2 -process, will be presented. Component selective NMR measurements in the system TPP/SBC reveal the dynamics of both components. The TPP component is investigated by ^{31}P NMR, while the deuterated SBC is probed by ^2H NMR. This is shown in figure 3.10 for ^{31}P NMR Hahn-echo and in figure 3.11 for ^2H NMR solid-echo spectra (see chapter 5.1 for further details). At low temperatures the limit of rigid molecules is reached for both components, i.e. typical powder spectra controlled by the chemical shift anisotropy (CSA) or quadrupolar interaction, respectively, are recognized. With increasing temperatures a transition to a liquid-like Lorentzian line is observable for TPP and for SBC. For high SBC concentrations the line collapse takes place above the accessible temperature window. Furthermore, for highest temperatures and low concentrations $c_{\text{TPP}} \leq 39\%$ spectral changes (two additional peaks in the middle of the spectra appear) due to the phenyl group jumps of the deuterated SBC component are recognizable in the ^2H NMR spectra. The most prominent feature of polymer plasticizer systems is rediscovered in the NMR spectra in this non-polymeric system, namely the “plasticizer” and the “anti-plasticizer” effect. The spectral transition, taking place when the reorientational correlation time τ_α is on the timescale of the NMR echo measurements $1/\delta$, shifts to lower temperatures for the high- T_g component with increasing concentration of the small component and to higher temperatures for the low- T_g component, with increasing concentration of the high- T_g component. That means, the dynamics of the slow component accelerate while the dynamics of the fast component slows down in the mixture. This is seen in both systems and is also observed in the DS spectra, as mentioned above.

Dynamic heterogeneities of the low- T_g ingredients, typical of polymer additive systems can also be seen in the mixtures investigated. Taking a closer look at the spectral transition of TPP in figure 3.10, it is obvious that the crossover from the powder spectra to the Lorentzian lines in the mixture is not a direct collapse any longer as in the neat system, but shows a temperature region in which “two-phase” spectra (a superposition of a Lorentzian line and a rigid powder spectrum, see. chapter 5.1.) are present. These spectra reflect the existence of slow ($\tau_{\alpha 2} \ll 1/\delta_{\text{CSA}}$) and fast ($\tau_{\alpha 2} \gg 1/\delta_{\text{CSA}}$) subensembles at the same temperature and can be analyzed in terms of the weighting factor $W(T)$ (see chapter 5.1, eq. 5.10). It is the fraction of molecules performing a liquid-like motion leading to a Lorentzian line and is shown in the inset of figure 3.10 for the system TPP/SBC. The temperature range in which two-phase spectra occur increases with decreasing TPP concentration up to almost 100 K at low concentrations and is the NMR fingerprint of a broad distribution of correlation times $G(\ln\tau_{\alpha 2})$ in agreement with DS. The strong broadening of $G(\ln\tau)$ is only observed for the α_2 -process. The α_1 -process is only weakly broadened, but enough to also observe two-phase spectra,

although in a very small temperature window (e.g. 220 K until 240 K for $c_{TPP} = 59\%$ in the system TPP/SBC, see figure 3.11).

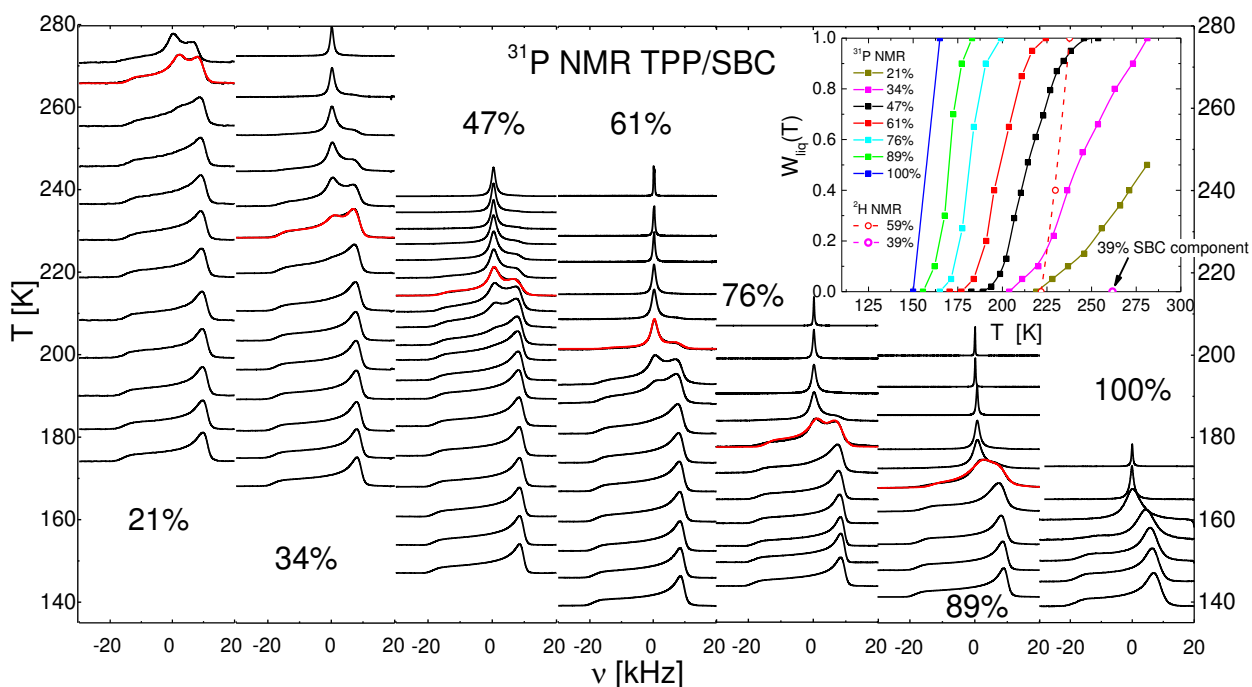


Figure 3.10: ^{31}P NMR spectra of TPP in the mixture TPP/SBC for the concentrations as indicated. The red lines are two-phase fits. The baseline corresponds to the temperature at which the spectra were measured. Inset: Weighting factor $W(T)$ from the ^{31}P NMR spectra (TPP) and the ^2H NMR spectra (SBC) for concentrations c_{TPP} as indicated. For neat TPP the two points at $W_{liq} = 0$ and $W_{liq} = 1$ indicate the temperature at which the spectral collapse starts and ends, respectively. For $c_{TPP} = 39\%$ the highest temperature at which a ^2H solid-state spectrum is measured is indicated. Figures reprinted from Pub. III.

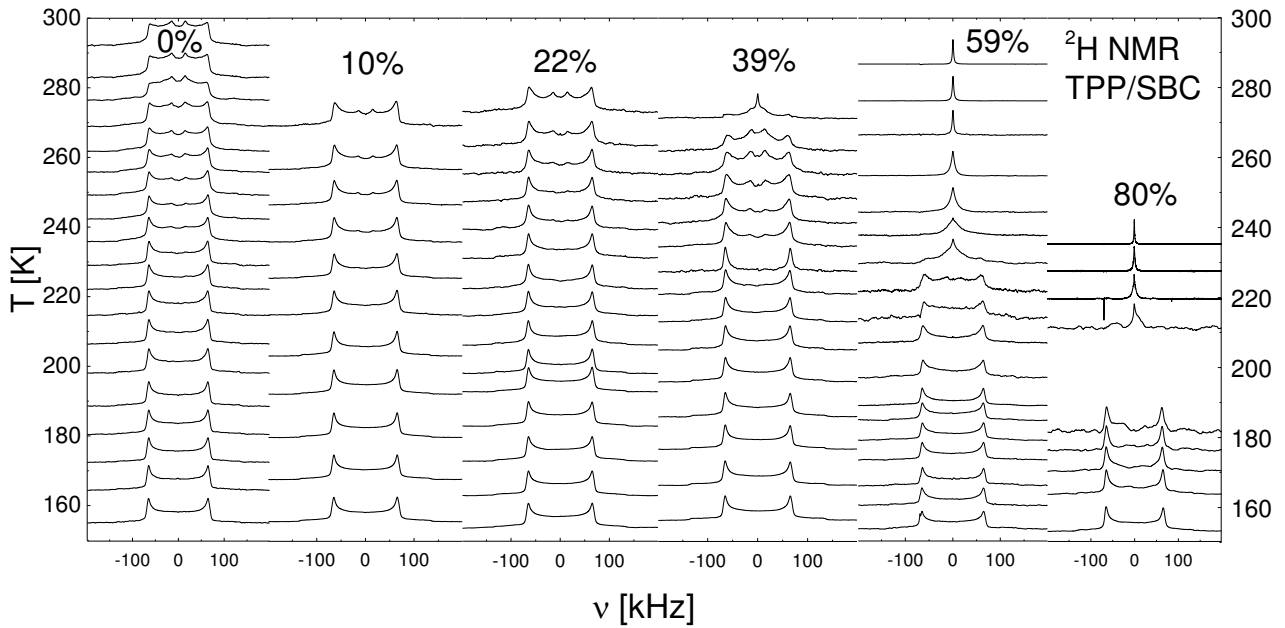


Figure 3.11: ^2H NMR spectra of SBC in the mixture TPP/SBC for concentrations as indicated. The baseline of the spectra corresponds to the temperature at which they were measured. Figure adapted from Pub. III.

The fact that the weighting factor $W(T)$ of TPP, indicating the fraction of liquid-like moving molecules, is larger than zero at temperatures where $W(T)$ of the SBC component is still zero, indicates that a fraction of the TPP molecules performs an isotropic liquid-like motion within the essentially arrested SBC matrix. For example, for $c_{\text{TPP}} = 61\%$ $W(T)$ is almost 1 for TPP while it is still 0 for SBC ($c_{\text{TPP}} = 59\%$) at $T \approx 225$ K, so all TPP molecules perform an isotropic reorientation while the SBC component is completely arrested on the NMR timescale. Due to the isotropic motion, it can be ruled out that the α_2 -process reflects a secondary relaxation, even for the low concentration samples, where an Arrhenius temperatures dependence of $\tau_{\alpha_2}(T)$ is found. Also there, a central Lorentzian line is found in the two-phase spectra reflecting isotropic dynamics.

Now the question arises if the dynamical heterogeneities of the low- T_g component are only a result of the extreme broadening of the α_2 -relaxation, or if a fraction of molecules of the low- T_g component also takes part in the relaxation of the high- T_g component as stated by Blochowicz et. al. [107,112] and also recognized by Bock et. al. [105,106] for polymer additive systems. Both groups analyzed the DS relaxation strength of the α_1 -relaxation and found more intensity than expected solely from the high- T_g component. They addressed the additional intensity to a fraction of the low- T_g component participating in the α_1 -relaxation.

To test this for our systems, the DS measurements were reevaluated (s. figure 3.7 (a), (b)). We calculated the expected quotient of the dielectric relaxation strengths $(\Delta\varepsilon_1/\Delta\varepsilon_2)_{\text{calc}} = \frac{(1-c_{\text{TPP}/\text{TCP}})\Delta\varepsilon_{1n}T_1}{c_{\text{TPP}/\text{TCP}}\Delta\varepsilon_{2n}T_2}$ with $\Delta\varepsilon_{1n}$ being the measured relaxation strength of the neat systems and assuming a Curie law and ideal mixing and compared it to the measured quotient $(\Delta\varepsilon_1/\Delta\varepsilon_2)_m$ for all concentrations accessible in both systems. In the formula above, the mass concentration can be used instead of the molar concentration due to the comparable density of all components. A participation of the low- T_g component in the slow α_1 -process would lead to a significant increase of the α_1 -relaxation strength in the mixture since the relaxation strength of the neat low- T_g components is much higher than the relaxation strength of the neat high- T_g component (by a factor of 11 for TPP/SBC and a factor of 5 for TCP/DH 379). The results are shown in table 1. Since little fluctuations of the ratio of relaxation strengths with temperature are present, average values are taken.

System	70%	85%	20%	34%	46%	56%	67%	73%	80%
	TPP/SBC	TPP/SBC	TCP/DH						
			379	379	379	379	379	379	379
$(\Delta\varepsilon_1/\Delta\varepsilon_2)_m$	0.12	0.035	1.85	0.8	0.55	0.25	0.24	0.18	0.1
$(\Delta\varepsilon_1/\Delta\varepsilon_2)_{\text{calc}}$	0.04	0.016	0.85	0.42	0.25	0.17	0.11	0.08	0.05

Table 1: Calculated and measured quotient of relaxation strengths of the α_1 - and α_2 -process for $c_{\text{TPP}} = 70\%$, and 85% in the system TPP/SBC, and for all concentrations measured in the system TCP/DH 379.

The measured signal intensity is by a factor of 2 to 3 too high for all concentrations in both systems. Although ideal mixing may not apply, the measured ratios are significantly higher than the calculated and almost independent of the concentration. Thus, we conclude that a pronounced fraction of TPP/TCP molecules participates in the slow relaxation process of the SBC/DH 379 molecules.

In contrast to the results of Blochowicz et al., that with decreasing temperature more and more additive molecules take part in the relaxation of the high- T_g component, no definite temperature dependence of the relaxation strength $\Delta\varepsilon_1$, and therefore of the fraction of molecules participating on the slow process, was found.

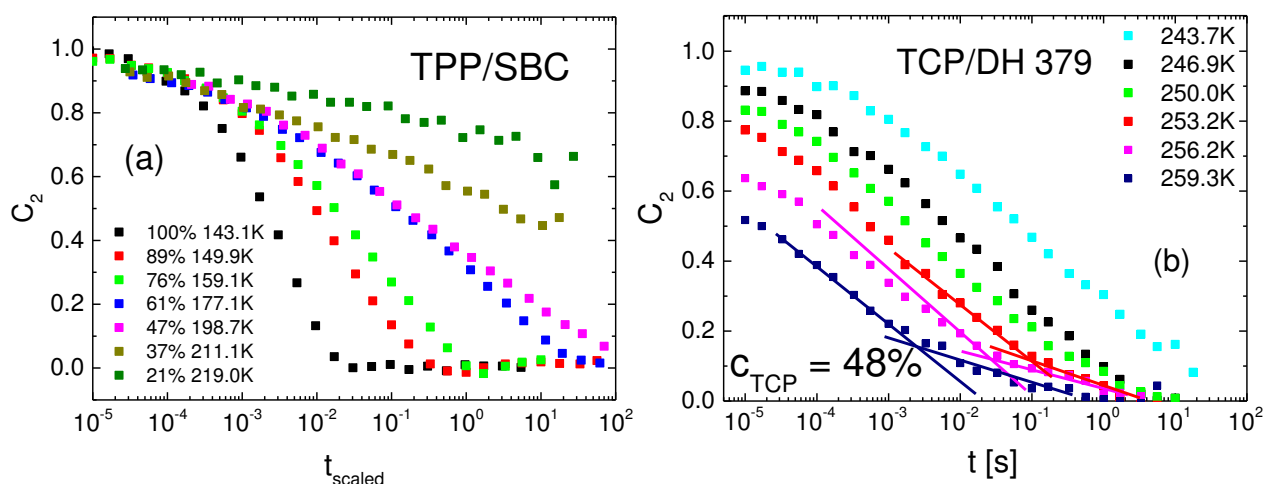


Figure 3.12: (a) ^{31}P NMR reorientational correlation functions $C_2(t)$ in the system TPP/SBC for concentrations indicated with a scaled time axis for a better comparability of the different concentrations. Figure reprinted from Pub. III. (b) Correlation functions $C_2(t)$ in the system TCP/DH 379 for the concentration $c_{TCP} = 48\%$. Figure adapted from Pub. II.

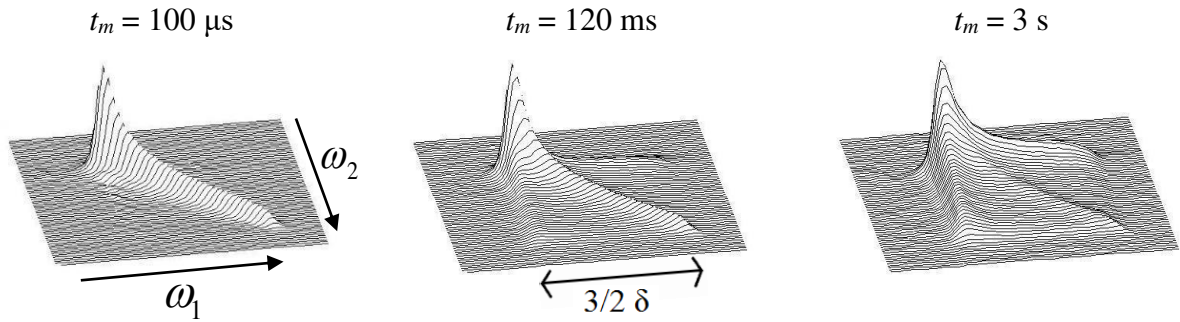
The reorientational correlation function $C_2(t)$ was measured for different concentrations with the stimulated echo technique (see eq. 5.17-5.20, chapter 5.1) to further investigate the dynamics. They are shown in figure 3.12. A progressive stretching of the correlation functions with decreasing concentrations of the low- T_g component is observed. For lowest concentrations, the correlation function decays quasi-logarithmic over more than 7 decades in time (compare figure 3.12. (a)). In contrast, as mentioned above, the α_1 -process is only slightly stretched compared to the stretching of the neat high- T_g component (see Publication III). From the correlation decays at higher concentrations and from the relaxation data (T_1 , T_2 , see figure 3.22, chapter 3.4) time constants were obtained and added to figure 3.8 (a). NMR and DS results fit well together.

Since the low- T_g component takes part in both processes α_1 and α_2 clearly distinguishable in the DS measurements, a bimodal behavior in the ^{31}P NMR observables might be expected as well. This is not seen yet. Neither the weighting factor $W(T)$, nor the correlation function $C_2(t)$ nor the spin-lattice relaxation functions show some clear bimodal behavior. Only for $c_{TCP} = 48\%$ in the system TCP/DH 379 the correlation functions shown in figure 3.12 (b) may give some hint for the appearance of a fast and a slow process (two different slopes in the correlation functions can be identified, see solid lines).

It was shown that the TCP and TPP molecules in an asymmetric binary mixture show a very broad distribution of correlation times $G(\ln\tau_{\alpha 2})$ and reorient isotropically within the arrested matrix of the high- T_g components. Furthermore, there are indications that also some low- T_g molecules take part in the reorientation of the high- T_g component. To gain further insight on the nature of these dynamic heterogeneities, 2D NMR spectra were measured, as shown in figure 3.13 and 3.14 for the system TCP/DH 379. A 2D spectrum measures the probability that a molecule has the NMR frequency ω_1 before a certain mixing time and ω_2 after the mixing time. Thus, the reorientational behavior of the molecules is directly accessible (see chapter 5.1 for further details).

Figure 3.13 top row shows the 2D ^{31}P NMR spectra in the $c_{TCP} = 66\%$ mixture in the system TCP/DH 379 for a temperature ($T = 231.8$ K) for which no 1D “two-phase” spectrum but a solid-state powder spectrum is observed. For short mixing times t_m (left) only a powder spectrum along the diagonal ($\omega_1 = \omega_2$) similar to the 1D spectrum is observable, reflecting no reorientation on the timescale of the mixing time. With increasing mixing times (middle) intensity in the whole (ω_1, ω_2) -plane is found, indicating that reorientation occurs. For long mixing times almost all the intensity is distributed among the (ω_1, ω_2) -plane, showing that almost all molecules reorient isotropically. Little diagonal intensity remains even for $t_m = 3$ s indicating that some molecules are still rigid on this timescale due to the very broad correlation time distribution $G(\ln\tau_{\alpha 2})$. The spectra were simulated with the random walk method and a random jump model (see chapter 5.2). Therefore, a Kohlrausch function with $\beta_K = 0.35$ (as obtained from the stimulated echo measurement at this temperature) and $\tau_\alpha = 0.5$ s is assumed as the distribution from which the waiting time t_w is drawn. The simulated spectra are shown in figure 13 bottom row. The experimental spectra are reproduced very well for the same mixing times as used in the experiment. Since the spectra are reproduced by a unimodal $G(\ln\tau_{\alpha 2})$, we assume that the diagonal intensity disappears for slightly longer times (which are outside the accessible experimental window) and complete reorientational spectra (see eq. 5.21) are expected.

$T = 231.8 \text{ K}, c_{TCP} = 66\%$



Simulations (RJ), $\tau_\alpha = 0.5 \text{ s}, \beta_K = 0.35$

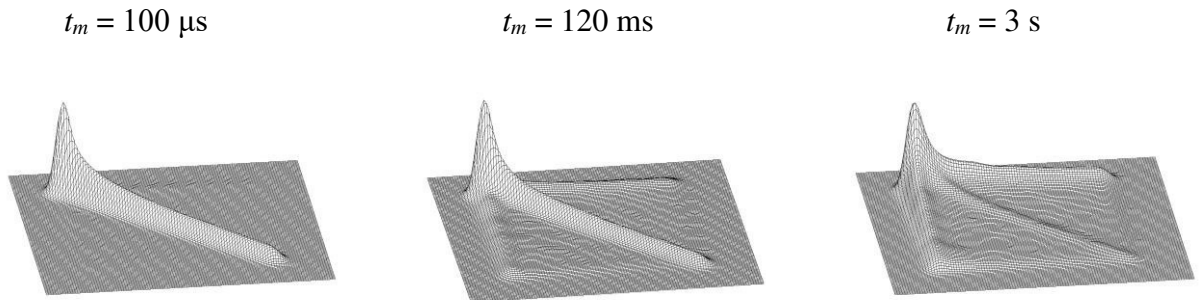


Figure 3.13: Top row: ^{31}P 2D NMR spectra for $c_{TCP} = 66\%$ in the system TCP/DH 379 at the temperature $T = 231.8 \text{ K}$ are shown in a stack plot representation for mixing times of $t_m = 100 \mu\text{s}$ (left), $t_m = 120 \text{ ms}$ (middle) and $t_m = 3 \text{ s}$ (right).

Bottom row: Simulated 2D spectra with the random walk method and a random jump (RJ) model (see chapter 5.2) for the same mixing times as used in the measured spectra. A Kohlrausch function with $\beta_K = 0.35$ and $\tau_\alpha = 0.5 \text{ s}$ is assumed as the distribution from which the waiting times t_w are drawn.

$T = 267.7 \text{ K}, c_{TCP} = 48\%$

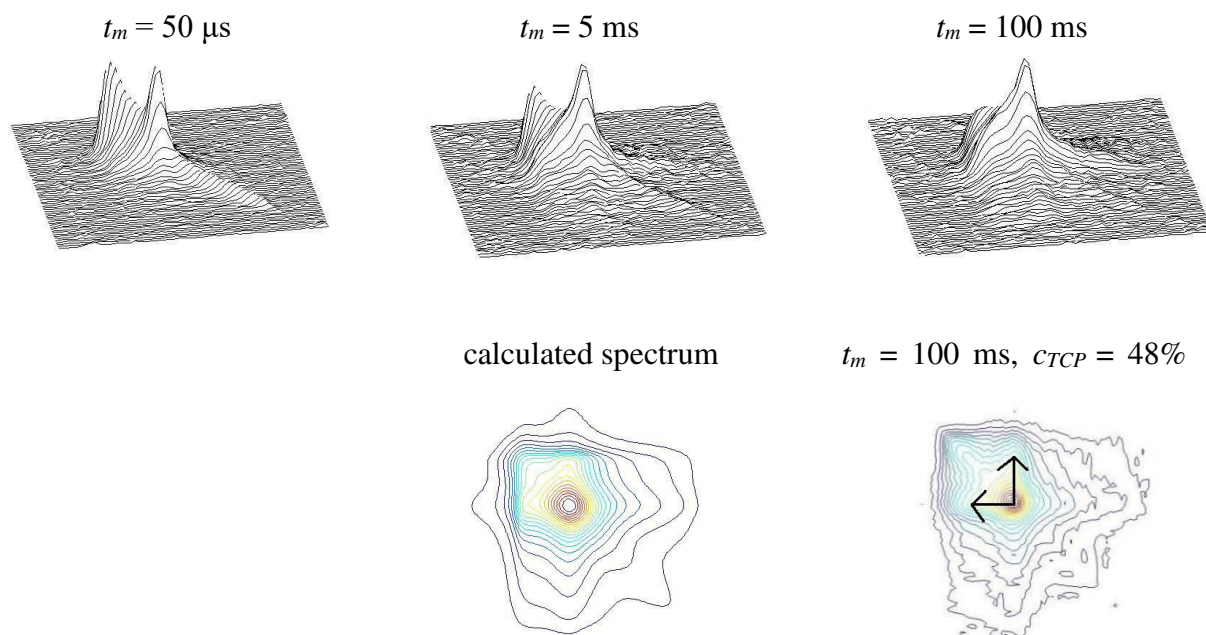


Figure 3.14: Top row: ^{31}P 2D NMR spectra for $c_{TCP} = 48\%$ in the system TCP/DH 379 for mixing times of $t_m = 50 \mu\text{s}$ (left), $t_m = 5 \text{ ms}$ (middle) and $t_m = 100 \text{ ms}$ (right) in a stack plot representation at $T = 267.7 \text{ K}$ are displayed.

Bottom row: The $t_m = 100 \text{ ms}$ spectrum of $c_{TCP} = 48\%$ shown in the contour plot representation (right) compared to a calculated spectrum (left).

Figure 3.14 top row shows 2D exchange spectra for increasing mixing times in the $c_{TCP} = 48\%$ TCP/DH 379 sample for a temperature at which a 1D two-phase spectrum was measured. For short mixing times only signal along the diagonal is detected with a similar spectral pattern as the 1D spectrum at this temperature. This implies that there are molecules which perform no reorientation during the mixing time ($\omega_1 = \omega_2$) and molecules which perform a fast isotropic reorientation ($\langle \omega_{1,2} \rangle = 0$). For longer mixing times more complex spectra occur. The intensity is spread over the whole (ω_1, ω_2) -plane in a particular pattern. The spectra consist of 4 sub spectra, a diagonal spectrum, a reorientational spectrum a 2D Lorentzian line in the middle and an exchange spectrum (see chapter 5.1, eq. 5.21 to 5.24). The features are better seen in the bottom line of figure 3.14 where the spectrum in contour plot representation for longest mixing time is compared to a calculated spectrum (see chapter 5.1). Apparently, there is signal intensity on the $(\omega_1 = 0, \omega_2)$ and $(\omega_1, \omega_2 = 0)$ (indicated with arrows in figure 3.14 bottom

right) lanes. This cross like pattern can only be reproduced if one assumes a fraction of molecules that perform a fast liquid-like reorientation before the mixing time and is arrested after the mixing time and vice versa. Similar spectra were found for all concentrations in both mixtures and in many binary mixtures [106,124]. This clearly demonstrates that the dynamical heterogeneities of the α_2 -process are of transient nature, which means molecules in the fast/slow motion limit exchange with molecules in the slow/fast motion limit on a timescale comparable to the relaxation time τ_α .

The exchange in the $c_{TCP} = 48\%$ sample is expected to take place within the dynamic heterogeneities due to the α_2 -process, since the measurements are done at temperatures around T_{g1} , where the α_1 -process (possibly including additive molecules at this temperature) is much too slow compared to the mixing time. This is not any longer the case at high concentrations since both T_g are very close. The measurements (e.g. for $c_{TCP} = 85\%$) took place slightly above both T_g , and a separation of both processes in the 2D spectra is not possible. Bock et al. [106] stated, that in the system TPP/PS the TPP molecules involved in the α_1 -process do not participate in the exchange, due to the fact that some intensity on the diagonal remains also for long mixing times. This cannot be asserted for this system, since only little diagonal intensity remains for longer mixing times (see figure 3.14 top row right)) and it is not clear if it disappears for even longer mixing times (which are outside the NMR time window).

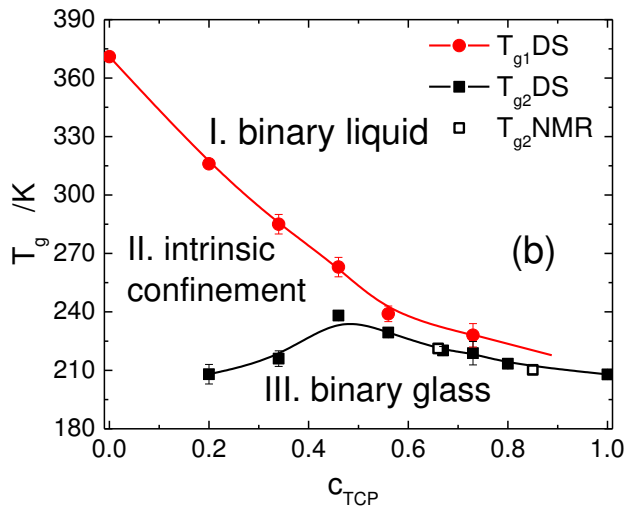


Figure 3.15: Mass concentration dependence of the glass transition temperatures T_g for both processes, α_1 (red circles) and α_2 (black squares) in the mixture TCP/DH 379 with guides for the eye (solid lines). Three “phases” can be distinguished. Figure reprinted from Pub. II.

Finally, by combining all results, some kind of “phase diagram” of the binary mixture TCP/DH 379 can be drawn (see figure 3.15). When plotting $T_{g1}(c_{TCP})$ and $T_{g2}(c_{TCP})$ three dynamical regimes can be distinguished. At high temperatures the mixture behaves like a binary super cooled liquid (I.), both components reorient isotropically and are dynamically decoupled. When cooling below T_{g1} , the low- T_g component still performs an isotropic liquid-

like reorientation in the arrested matrix consisting of the high- T_g component and a fraction of molecules of the low- T_g component (II.). Finally, below the glass transition temperature of the low- T_g component, both components are arrested and form a binary glass (III.). The maximum is a result of the change to the Arrhenius temperature dependence of the relaxation times at lower concentrations due to the “fragile-to-strong” transition [106]. The activation energies of the α_2 -process decrease with lower additive concentrations and thus also the slopes of $\tau_{\alpha_2}(T)$ decrease, which leads to a reduced T_{g2} at low concentrations. In the system TPP/SBC the whole “phase diagram” could not be obtained due to the limited DS data but a similar behavior as in TCP/DH 379 is implied.

Altogether, it is to state that most features discovered in polymer additive systems or polymer blends are also rediscovered in systems consisting of two low molecular components. Two separated main relaxation processes were identified, the faster associated with the low- T_g component, the slower related to the high- T_g component. They show the plasticizer and anti-plasticizer effect, respectively. NMR measurements imply that the low- T_g molecules reorient isotropically (α_2) even at temperatures where a rigid matrix (α_1), consisting of the high- T_g component and a fraction of the low- T_g components molecules, is present. So, the α_2 -process can not reflect a secondary process, although below T_{g1} it shows a similar behavior as a JG secondary relaxation, especially the Arrhenius temperature dependence. The dynamics of the low- T_g component is governed by a very broad distribution $G(\ln\tau_2)$ of correlation times resulting in quasi logarithmic correlation functions at low additive concentrations. Similar features as found for supercooled binary liquids are observed in the confinement of nanometer-sized pores, like the broad $G(\ln\tau_2)$ or the “fragile-to-strong” transition of the temperature dependence of the time constants. We suggest that the high- T_g component in the asymmetric mixtures provides an intrinsic confinement for the low- T_g component and that mainly the T_g contrast of the neat systems and not the specific molecular structure of the components governs the dynamical behavior in binary mixtures as indicated also by simulations [125-128] and MCT [129,130] works. Surprisingly, no temperature dependence of the fraction of low- T_g molecules participating in the reorientation of the high- T_g component is found as stated by Blochowicz and coworkers [107]. Thus, we cannot make a statement on the kind of glass transition the low- T_g component in the matrix of the high- T_g component performs.

Finally the questions arises what happens in the concentration limits $c_{low-T_g} \rightarrow 0$ or 1. For $c_{low-T_g} \rightarrow 1$ figure 3.15 suggests very similar dynamics of both processes. The plasticizer effect becomes so strong, that both T_g become almost the same. This is even better indicated in the dielectric spectra of TPP/SBC (figure 3.7 (b)). The α_2 maximum for $c_{TPP} = 85\%$ almost “absorbs” the α_1 maximum. Both are only separated by 2.5 decades in time compared to a

separation of 4 decades in time for $c_{TCP} = 70\%$ (see Publication III). Extrapolating to $c_{TCP} \rightarrow 100\%$, both relaxation times should become almost indistinguishable. For $c_{low-T_g} \rightarrow 0$ two species of the low- T_g molecules have to be distinguished, the ones performing the α_2 - and those performing the α_1 -process. Both processes are well separated at low c_{low-T_g} . For $c_{TCP} = 20\%$ over six decades in time separate both processes, while the separation increases with decreasing TCP concentration, strongly indicating that no merging of both processes occurs at low concentrations. For $c_{low-T_g} \rightarrow 0$ the α_2 -process, of course, has to disappear, because only few low- T_g molecules are in the probe and therefore no cooperative process of the low- T_g molecules can be present anymore. The low- T_g molecules are completely surrounded by the high- T_g molecules. Supposedly, the low- T_g molecules take only part in the α_2 -process for lowest c_{low-T_g} and consequently probe the dynamics of the high- T_g component.

3.3 Secondary relaxation in binary mixtures – state of the art

While the secondary relaxation in neat systems is described in chapter 3.1, we now extend the discussion to binary systems. The investigation of the secondary process in mixtures provides further insight into the nature of this process. Many experiments in binary mixtures were already carried out [68,82,108,110,112,142 -148] and the phenomenology of the β -process turns out to be even more puzzling than in neat systems.

First of all, the relaxation times τ_β of the β -process as well as their distribution $G(\ln\tau_\beta)$ as a function of the concentration do not change significantly in many mixtures as shown for TPP/PS [142], MTHF/tristyrene [112] and many more [82,110,144]. This is demonstrated in figure 3.16 for the system toluene/PCB54 [110]. In the whole concentrations range the relaxation times are almost identical and similar to those of neat toluene. However, the time constants of the β -process decrease in mixtures consisting of water and propylene glycol [147].

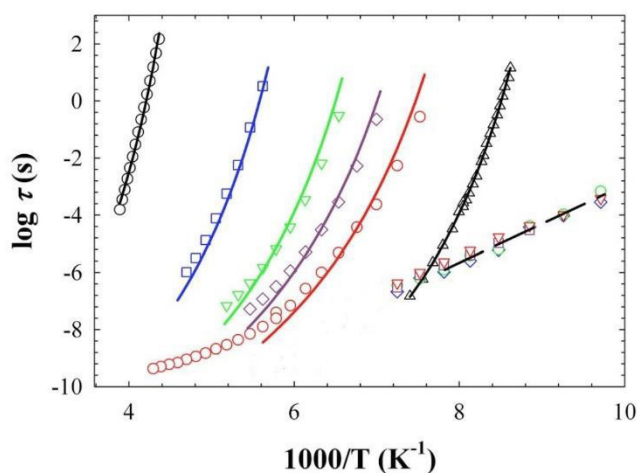


Figure 3.16: Time constants of main and secondary relaxation of the system toluene/PCB54 for mass concentrations $c_{PCB54} = 70\%$ (blue), 50% (green), 35% (dark pink) and 20% (red). The τ_β of neat toluene is indicated as a dashed line. Further, the τ_α of neat PCB54 (black circles) and neat toluene (black up triangles) are shown. Figure adapted from [110].

Besides DS measurements also NMR spectra were measured, especially with the echo method (see. chapter 2.2 and 5.1) analogue to measurements in neat systems. Similar line shape effects were found [68,82,142]. To quantize these line shape effects due to the secondary relaxation, the NMR line shape parameter R was introduced [71], being defined as the intensity in the middle of a spectrum ($\omega = 0$) normalized to the intensity at the singularities ($\omega = \pm\delta/2$) (see chapter 5.1, eq. 5.11). As shown in chapter 2.2. the intensity in the middle and thus the $R(t_p)$ values of the spectra decay for longer interpulse delays t_p when a small-angle reorientation is within the experimental NMR time window ($\tau_\beta \approx 10^{-6}$ s). In most neat systems $R(t_p)$ decays to zero for large t_p indicating that all molecules take part in the secondary relaxation. Deviations from this behavior were found in binary mixtures.

For the systems toluene- $d_{3/5}$ /PCB54 and toluene- d_5 /picoline the $R(t_p)$ does not decay to zero anymore for low toluene concentration as demonstrated in figure 3.17 (a), (b) for toluene/PCB54 [82]. The $R(t_p)$ value at a temperature, where the sensitivity of the line shape to the secondary relaxation is maximal, is shown. For molar concentrations lower than $c_{add} < 0.59$ a concentration dependent fraction $(1-\zeta)$ of molecules does not take part in the secondary relaxation. So-called “islands of rigidity” were postulated, referring to the “islands of mobility” first proposed by Johari and Goldstein [50].

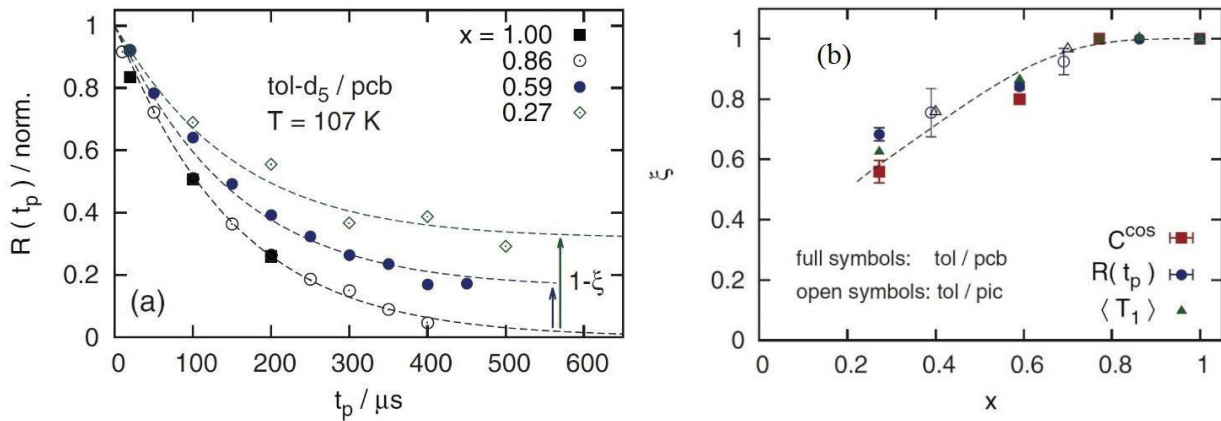


Figure 3.17: (a) Normalized ^2H NMR line shape parameter $R(t_p)$ for the system toluene-d₅/PCB54 for different molar concentrations and varying interpulse delays. (b) Molar concentration dependent fraction ζ of toluene molecules (obtained by different NMR measurement techniques) which take part in the secondary relaxation for the systems toluene/PCB54 and toluene/picoline. Figures reprinted from [82].

Another system investigated is the mixture TPP/PS [142]. The type A glass former PS does not show a secondary relaxation in the bulk, while TPP does. Component selective ^{31}P and ^2H NMR on TPP and on deuterated PS, respectively, revealed that both components in the mixture participate in the secondary relaxation introduced by TPP. The ^2H NMR spectra of PS show the typical line shape effects of a restricted small angle motion at the same temperature as TPP measured by ^{31}P NMR in the mixture (cf. figure 3.18.) and in the neat system [142]. The TPP molecules seem to “enslave” the PS molecules to perform a similar small angle motion as the TPP component, a result also observed before in the system toluene/2-picoline [68]. Furthermore, there are indications that “islands of rigidity”, i.e. fractions of immobile molecules, occur also in this system for both components for lower concentrations (c_{TPP} (mass concentration) $< 50\%$), which indicates the disintegration of the secondary relaxation for $c_{\text{TPP}} \rightarrow 0$. Additionally, in the mixture both components show the same temperature dependence of the relaxation time T_1 at low temperatures, while in the neat components the T -dependence is different. This is a strong hint that both component have a very similar activation energy distributions $g(E)$. However, it is still not sure whether the spatial extent of the secondary relaxation of both components is alike. The enslavement of the polymer molecules was interpreted as a sign for the cooperativity of the secondary relaxation.

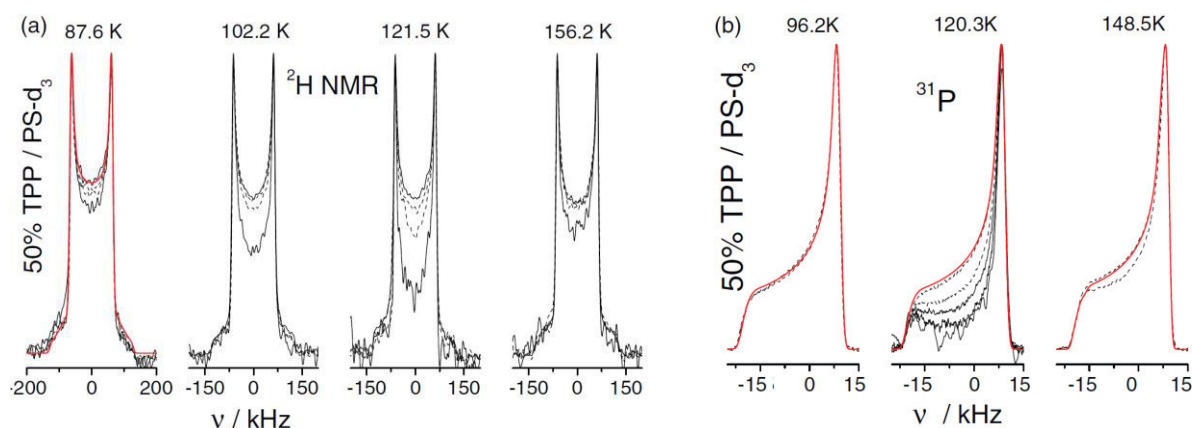


Figure 3.18: (a) Interpulse delay dependent ($t_p = 20 \mu\text{s}$, $40 \mu\text{s}$, and $80 \mu\text{s}$) ^2H NMR spectra of PS in the mixture $c_{\text{TPP}} = 50\%$ (mass concentration) TPP/PS- d_3 for different temperatures. (b) Interpulse delay dependent ($t_p = 20 \mu\text{s}$, $200 \mu\text{s}$, $400 \mu\text{s}$, $800 \mu\text{s}$ and $1600 \mu\text{s}$ for $T = 120.3 \text{ K}$, else only the spectra for $t_p = 20 \mu\text{s}$ and $200 \mu\text{s}$ are shown) ^{31}P NMR spectra of TPP in the mixture $c_{\text{TPP}} = 50\%$ TPP/PS- d_3 . Figures reprinted from [142].

3.4 Experimental results: β -process

The secondary relaxation in non-polymeric binary mixtures was investigated based on the system TPP/SBC. This mixture is well-suited for this task since both components are type-B glass formers and therefore exhibit a β -process (compare figure 2.7 (b) for DS measurements of TPP). Again, the DS results were collected by Fathia Mohamed as a part of her PhD thesis. All NMR result are obtained in the context of the present dissertation. They are found in Publication IV.

The time constants τ_β of the secondary relaxations in the neat systems and in the mixtures obtained by DS and NMR echo experiments are shown in figure 3.19 together with the relaxation times τ_α of the main relaxation in the neat components. The β -process of TPP (β_2) was experimentally accessible in the whole concentration range, while the secondary relaxation of SBC (β_1) was only observable in the neat system, due to the fact that in the mixtures the main relaxations α_1 and α_2 featuring the plasticizer and anti-plasticizer effect, respectively, occur on similar timescales as the β_1 -process.

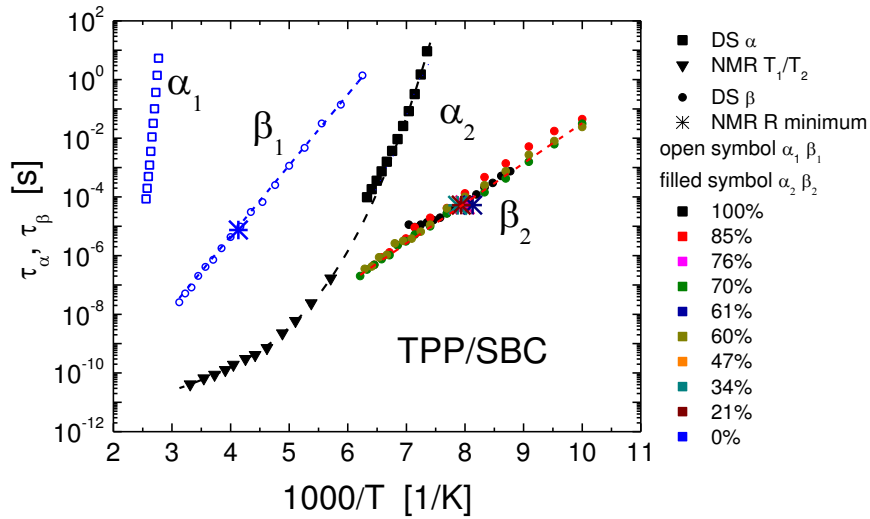


Figure. 3.19: Time constants of the main and secondary relaxations α_1 , α_2 , β_1 and β_2 , respectively, in the neat components SBC (index 1) and TPP (index 2) and for the β_2 -process in the mixture TPP/SBC for concentrations as indicated. Every symbol is coded by relaxation process, measurement method and concentration. The lines are guides for the eye. Figure reprinted from Publication IV.

Both β -processes show an Arrhenius temperature dependence typical of a secondary relaxation with activation energies of $E_{\beta_1} \approx 15.6 RT_g$ and $E_{\beta_2} \approx 23.5 RT_g$. The time constants of the β_2 -process do not change with concentration even down to $c_{TPP} = 21\%$, a result found for many binary glass forming systems (compare chapter 3.3. and figure 3.16) [82,110,112,142,144].

In order to gain further insight into the nature of the secondary relaxation in the mixture, component selective NMR echo measurements were carried out. As discussed in chapter 2.2 and 3.3 NMR Hahn- (^{31}P) and solid- (2H) echo spectra are very sensitive on small angle reorientations when the interpulse delay t_p is systematically increased. Therefore interpulse dependent spectra were measured in the whole concentration range and are exemplarily shown for the $c_{TPP} = 34\%$ (^{31}P NMR) and the 39% (2H NMR) mixture in figure 3.20 (middle rows) together with the spectra for the neat systems (left and right row).

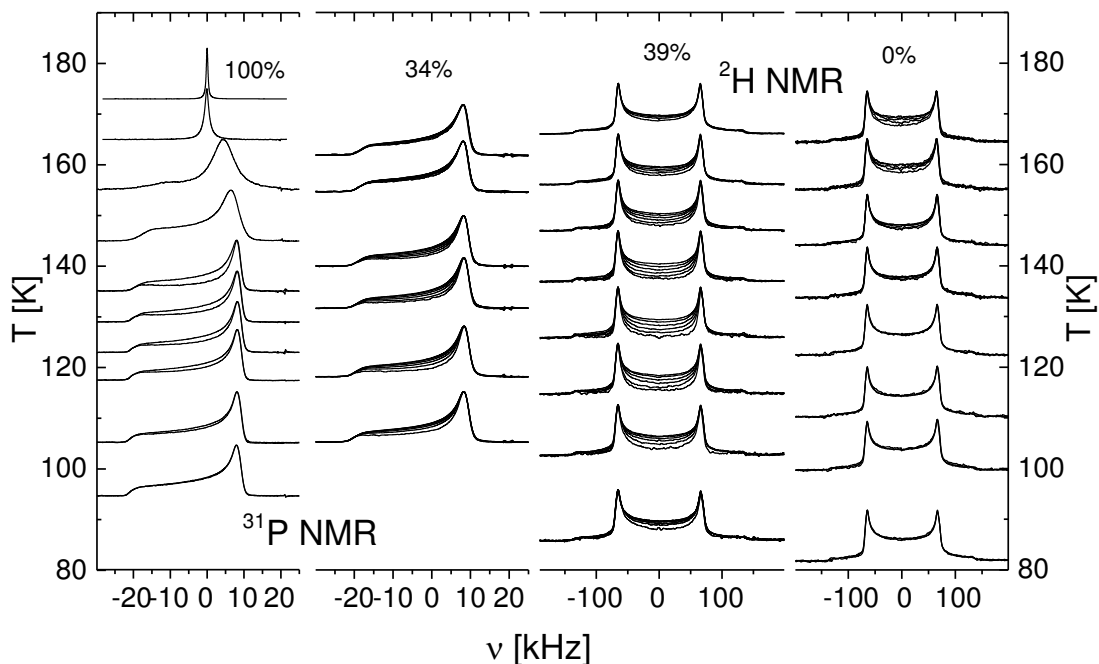


Figure 3.20: Temperature and inter-pulse dependent ^{31}P and ^2H NMR echo spectra of the neat systems TPP (100%) (left) [149] and SBC (0%) (right), as well as in the mixtures with $c_{\text{TPP}} = 34\%$ (middle left) and with $c_{\text{TPP}} = 39\%$ (middle right). The baseline of the spectra corresponds to the measurement temperature. At each temperature, spectra with different inter-pulse delays are shown: $t_p = 25 \mu\text{s} - 280 \mu\text{s}$ for ^2H NMR, $t_p = 20 \mu\text{s} - 920 \mu\text{s}$ for $c_{\text{TPP}} = 34\%$ and $t_p = 20 \mu\text{s}$, and $200 \mu\text{s}$ for neat TPP; at high temperatures for neat TPP only spectra with $t_p = 20 \mu\text{s}$ are shown. Figure reprinted from Publication IV.

For neat TPP as well as for TPP in the $c_{\text{TPP}} = 34\%$ mixture line shape effects associated with the β_2 -process are clearly recognized in the ^{31}P Hahn-echo spectra. In particular, one observes that the spectral changes are weak at high as well as at low temperatures, but strong at intermediate temperatures. This is typical of a relaxation process passing through the NMR time window. For neat SBC no signature of a secondary process is seen by ^2H NMR at lower temperatures, while at higher temperatures ($T > 150 \text{ K}$) spectral changes due to the β_1 -process are observable. In the mixture, line shape changes typical of small angle reorientations are well recognizable also for SBC at the same temperatures, where the β_2 -process of TPP causes the line shape changes in the ^{31}P spectra. It appears, that the TPP component enslaves the SBC component to perform a similar small-angle movement as the TPP molecules do. The neglectable change of the spectral width (ca. 1%) between spectra in the slow motion (low temperatures) and fast motion (high temperatures) limit of the secondary process indicates angular displacements lower than $\pm 10^\circ$ degrees (compare chapter 5.2, figure 5.5.) involved in the β_2 -process for both components.

To quantify the spectral changes caused by the β_2 -process, the $R(t_p)$ values of both components and all concentrations are compared in figure 3.21 in a temperature region where the line shape effects are most pronounced ($\tau_\beta \approx 1/\delta$). As described (see chapter 3.3. and 5.1), this quantity turned out to be a reliable measure of the subtle spectral changes caused by the β -process [142]. In the case of SBC (^2H NMR), the $R(t_p)$ decay is about a factor of 6 faster than for TPP (^{31}P NMR). When assuming comparable amplitudes of the β -process in both components, this is expected due to the larger coupling constant in the case of ^2H NMR ($\delta_Q \approx 6 \delta_{\text{CSA}}$). But for each component the decay of $R(t_p)$ occurs on the same timescale and reaches zero for long times for $c_{\text{TPP}} > 21\%$. In accordance with Vogel et. al. [74] we conclude that all molecules take part in the small angle process as it is observed for neat systems. The spectra of subensembles of molecules not taking part in the process would not be affected by the spectral changes due to long interpulse delays. A residual value R_∞ for long times would occur.

For low concentrations the situation changes. For the TPP component a $R(t_p) > 0$ for long times remains ($R_\infty \approx 50\%$ for the $c_{\text{TPP}} = 21\%$ mixture and $R_\infty \approx 80\%$ for the $c_{\text{TPP}} = 10\%$ mixture), showing that a large fraction of TPP molecules is now arrested and does not take part in the β_2 -process any longer. For the SBC component a similar change is observed, however only for the lowest concentration of $c_{\text{TPP}} = 10\%$. But it cannot be decided whether a residual intensity remains (a corresponding fit yields $R_\infty \approx 20\%$) or whether the $R(t_p)$ decays slower, indicating a lower extend of angular displacement, since the time constant of the $R(t_p)$ decay also depends on it. In any case, this disintegration of the β_2 -process is expectable, since for $c_{\text{TPP}} \rightarrow 0\%$ the secondary relaxation must completely disappear.

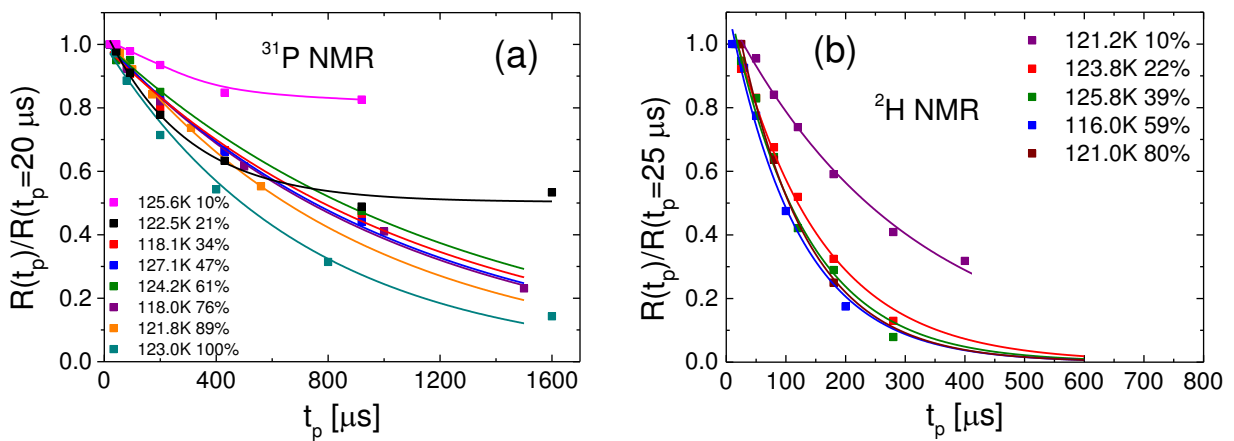


Figure 3.21: Normalized ($R(t_p = t_{p,\text{minimal}}) = 1$) spectral shape parameter $R(t_p)$ at temperatures where the influence of the secondary relaxation on the line shape is maximal for all concentrations measured by ^{31}P NMR for TPP (a) and measured by ^2H NMR for SBC (b). Solid lines are fits by exponential functions, except for $c_{\text{TPP}} = 10\%$ and 21% in (a); here only guides for the eye are shown. Figures reprinted from Publication IV.

In addition, the spin-lattice relaxation time T_1 for both components was studied over the entire concentration range (see figure 3.22). At high temperatures the ^{31}P NMR relaxation minimum due to the α_2 -process is observed in the case of TPP (figure 3.22 (a)). With decreasing concentration the minimum shifts to higher temperatures and to higher relaxation times due to the anti-plasticizer effect and the increasing dynamic heterogeneities of the α_2 -process, i.e. due to the distribution $G(\ln\tau_\alpha)$ becoming broader. At low temperatures, the relaxation is caused by the β_2 -process. There, the relaxation times for all concentrations coincide, which is a hint that amplitude and time constants of the β_2 -process do not essentially change in the mixtures. Although not all TPP molecules, according to the analysis of the echo spectra, take part in the β_2 -process any longer for low concentrations, the mobile fraction appears to control the T_1 relaxation time due to spin diffusion.

For the SBC component, the temperature dependence of the spin-lattice relaxation time is shown in figure 3.22 (b). At high temperatures, a broad minimum is seen caused by the effect of both the α_1 -process and the additional fast phenyl group jumps. The latter were identified in the solid-echo spectra (cf. figure 3.11). At low temperatures, the relaxation due to the β_2 -process is essentially the same for $c_{\text{TPP}} \geq 22\%$. But for $c_{\text{TPP}} = 10\%$ higher relaxation times were obtained, which is interpreted as a sign for the disintegration of the secondary relaxation. This effect is seen in the ^2H NMR spin-lattice relaxation time due to the less efficient spin diffusion in deuteron relaxation. Furthermore, it is remarkable that for both components the same temperature dependence of the spin-lattice relaxation time at low temperatures is observable, a result also found in the system TPP/PS [142], which is a sign for a similar correlation time distribution $G(\ln\tau_\beta)$.

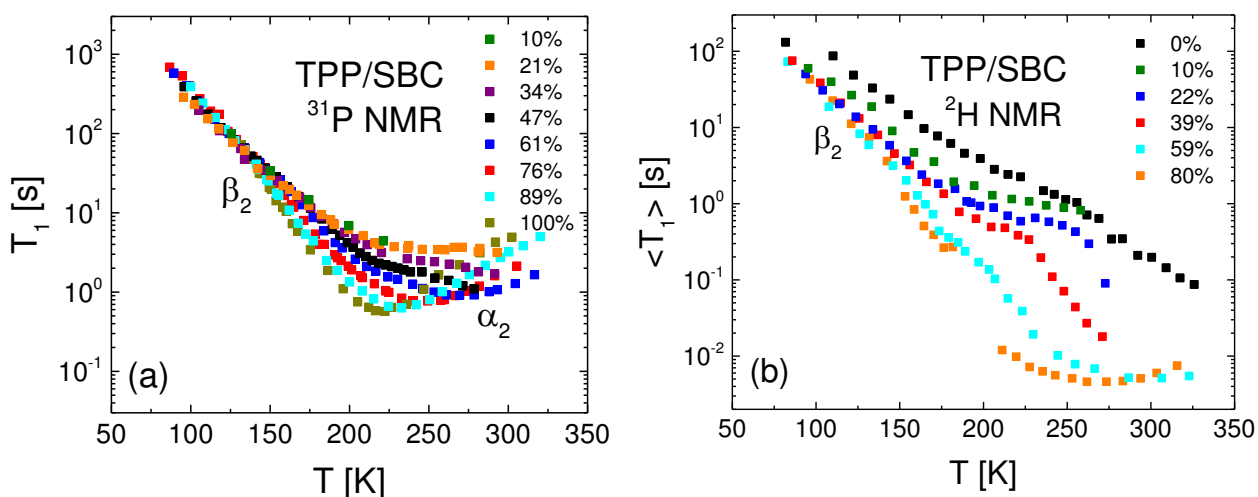


Figure. 3.22: (a) Spin-lattice relaxation time of TPP in the neat system and in the mixtures for concentrations indicated. (b) $\langle T_1 \rangle$ relaxation data of SBC in the neat system and in the mixtures for concentrations indicated. Figures reprinted from Publication IV.

Given that the ^{31}P and ^2H NMR spin-lattice relaxation times show the same temperature dependence, yet $T_1(^{31}\text{P}) > T_1(^2\text{H})$, one may ask the question whether the difference in the absolute values of the relaxation rate R_1 is solely caused by the different coupling constants or whether the amplitude of the spectral density is different for SBC and TPP in the mixture. Thus, the susceptibility $\chi''(T) = \omega_L J(T, \omega_L) = \omega_L / (K_i * T_1)$ is calculated at low temperatures where the β_2 -process determines the relaxation assuming that $J(\omega_L) \approx J(2\omega_L)$ (^2H NMR) (see chapter 5.1, eq. 5.12 and 5.14: for the corresponding coupling constant K_i it holds $K_{CSA} = \frac{2}{15} \left(\frac{3}{2} \delta_{CSA} \right)^2$ and $K_Q = \frac{2}{15} \delta_Q^2$, respectively). The susceptibility is shown in figure 3.23. It is to mention that the relaxation rate $R_1 = 1/T_1$ has to be used in the above equation to calculate $\chi''(T)$ which is not equal to $1/\langle T_1 \rangle$ for a stretched relaxation function as it is the case for the ^2H NMR measurements. However, the difference is small since the stretching is not very large, so we refrained from determining the relaxation rates and used the $1/\langle T_1 \rangle$ data. The normalized susceptibility $\chi''(T)$ can be split into two fractions, one describing the relaxation of the α -process (f) and one describing the spatial restricted β -process ($1-f$) [150]. In the glass ($T < T_{g2}$), the contribution of the α -process can be ignored and one gets $\chi''(T) = (1 - f) \chi''_{\beta}(T)$. The quantity $(1 - f)$ reflects the relaxation strength of the β -process and is linked to the extent of angular displacement of the molecules.

Figure 3.23 shows that both components have the same T -dependence of $\chi''(T)$, as expected from the T_1 measurements. One recognizes that $\chi''(T)$ of SBC is about a factor of seven lower than that for TPP. Since $\chi''(T)$ for both components shows the same temperature dependence the difference in the susceptibility must be assigned to a lower relaxation strength, which is a measure of the “spatial exploration” of the molecular axis, indicating smaller angular displacements of the SBC molecules compared to those of the TPP molecules. This is a reasonable result considering the larger size of the SBC molecules. Further, we compared the susceptibility of TPP in the system TPP/PS [106] to this mixture (open triangles in figure 3.23). Surprisingly, the $\chi''(T)$ values are the same for TPP in TPP/PS; it seems that the characteristics of the secondary relaxation in TPP are completely independent of the second component in the mixture.

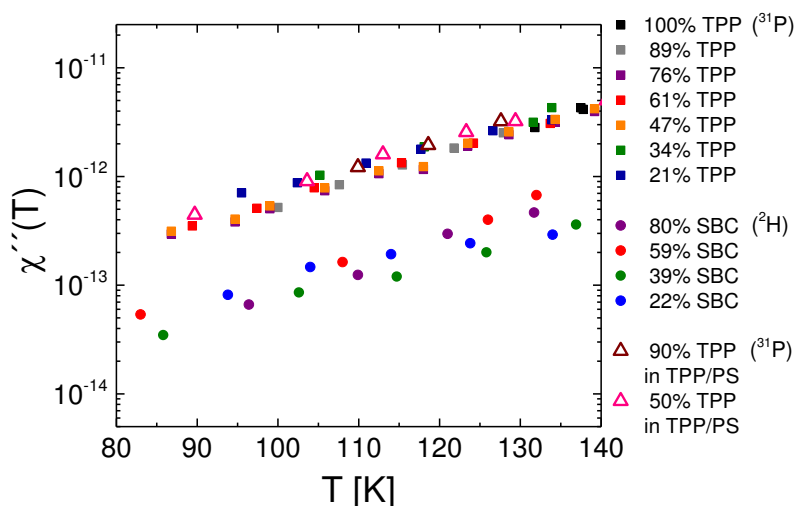


Figure 3.23: Normalized susceptibility $\chi''(T) = \omega_L J(T, \omega_L)$ of neat TPP and TPP in the mixture and of the SBC component in the mixture for concentrations as indicated. For comparison, $\chi''(T)$ data from the system TPP/PS is added [149] showing the same behavior as in the TPP/SBC mixture. Figure reprinted from Publication IV.

Finally, the question regarding the extent of cooperativity of the β -process in the mixture arises. In the first place, the similar time constants of neat TPP and in the mixture (cf. figure 3.19) as well as the independence of the characteristics of the β_2 -process on the second component (see figure 3.23) might indicate a local process independent of the spatial environment of the TPP molecules. However, the TPP component seems to enslave the SBC molecules to perform a small angle reorientation on a similar time scale (see figure 3.20) and with the same temperature dependence (figure 3.23), which is a clear sign of cooperativity. One may argue that the intermolecular dipole-dipole interaction between the protons of TPP and the deuterons of SBC is the cause of the line shape changes. However, the significant decrease of the ^2H NMR relaxation times in the mixtures compared to the neat system at higher TPP concentrations is a strong hint that the SBC component indeed performs a small angle reorientation. One can rule out that the dipole-dipole interaction causes the lower T_1 because the influence due to dipole-dipole coupling can be neglected, since for the ratio of the relaxation rates of the dipolar (DD) over the quadrupolar (Q) interaction holds $R_1^{DD}/R_1^Q = (\delta_{DD}/\delta_Q)^2 \approx (5/100)^2$ [151]. An even larger influence of the induced secondary relaxation on the relaxation time was found in the system TPP/PS [142].

The high activation energy of the β -process ($E_{\beta 2} \approx 23.5 RT_g$) is a clue for cooperativity [152,153]. Additionally, the disintegration of the β_2 -process at low TPP concentrations (see figure 3.21) is a further strong argument for the cooperativeness of the process in the mixture. The concept of “islands of mobility” of Johari and Goldstein [49,51,70] might be reintroduced at low additive concentrations. The fraction of arrested molecules may form some kind of “islands of rigidity”, a phenomenon also discovered in the system toluene/picoline, toluene/PCB54 (see figure 3.17) and TPP/PS [142]. There, the occurrence of “islands of rigidity” sets in at the molar concentrations $c_n = 40\%$ and $c_n = 60\%$, respectively [82]. This is

similar to the system TPP/SBC, where “island of rigidity” occur for molar concentrations $c_n \leq 48\%$.

Most features described here are also found in polymer plasticizer systems (see chapter 3.3). Therefore, similar to the behavior of the main relaxation in binary mixtures, also the features of the β -relaxations seem to be independent from the kind of the binary systems and from the particular molecular structure of the components involved in the mixture.

Furthermore, it is to mention that in the case of SCB only the side groups may possibly reorient due to the induced β -process, since the motion of the core is not probed in the ^2H NMR experiments. To continue the investigation of the β -process, especially regarding the involvement of the type A (no β -process in the neat system) component, one may carry out DS experiments, with a type A component which governs the DS signal, to possibly observe the increasing of the relaxation strength of the β -process in the mixtures when the type A molecules also takes part in this process. Also, further NMR experiments may shed light on the behavior of the type A component. One might consider mixtures with a fully deuterated type B low- T_g component and measure the spectra of the type A high- T_g component with ^{31}P or ^{13}C NMR to completely rule out any influence of the intermolecular dipole-dipole (proton-deuteron) interaction on the line shape of the type A component.

4. Dendrimers

4.1 State of the art

Dendrimers, first synthesized almost 40 years ago in 1978 [154] are repetitively branched molecules. In the center of the dendrimer is a functional core, then segments with uniform length and functionality f (number of new branches per generation +1) are added with each generation, starting with $G = 0$ for the center. Since the mass ($\sim (f-1)^G$) grows faster than the volume ($\sim G^3$) of the dendrimers the number of generations is limited. The application field of dendrimers is very broad, reaching from the use as MRI contrast agents [155], as drug or gene deliverers [156-158] or as drugs themselves [157] to the use as catalysts [159]. Regarding the structure and the dynamics of dendrimers, many experimental investigations, including NMR relaxation measurements on dendrimers in solution [160-163], simulations, and theoretical work [164-172] were carried out. Dendrimers in bulk are only rarely investigated, in contrast to dendrimers in solution. Further, some rheology [173,174,175] and dielectric measurements [176] were carried out.

Concerning the bulk dynamics, the Poly(propylene imine) (PPI) dendrimers investigated here are viscous liquids at room temperature. The dynamics of dendrimers are similar to polymers below their entanglement mass M_e (cf. tube reptation model [177]), as no entanglement effects are observed in rheological measurements on polyamidoamine (PAMAN) [173] and PPI dendrimers [174], but a partial interpenetration [178] was suggested. This leads to a much lower viscosity as in entangled polymers. With increasing generation the outer branches of the dendrimer turn inwards as MD simulations show [178,179]. The gyration radius of the dendrimers is reported to scale with the number of monomers N between $R_g \sim N^{1/3}$ [180] and $R_g \sim N^{0.24}$ [179]; the latter is approached for a high number of generations.

Molecular dynamics (MD) [166] and Brownian simulations together with theoretical calculations of a viscoelastic model of dendrimers [168] showed that additionally to the α -process further slower modes appear. Three relaxation processes can be distinguished: the reorientation of the dendrimer as a whole, the reorientation of the branches of the dendrimer, the so-called breathing modes, and the local reorientation of a segment (α -process). Experimentally, a secondary relaxation, as typically seen in molecular glass formers, is observed in carbosilane dendrimers [181], while in PAMAN dendrimers even three fast processes were detected, successively addressed to the “local fluctuations of branch ends”, the “interplay between molecular architecture and hydrogen bonding to the neighboring chains” and “the motion of amide groups on the surface of the dendrimers” [176].

4.2 Experimental results

The results described in this chapter were the outcome of a project distributed among our work group. The dielectric measurements were carried out by F. Mohamed and the field cycling (FC) results were obtained by M. Hofmann, both as a part of their PhD thesis. The NMR results were obtained in the context of this work. They were reported in Publication I.

PPI dendrimers were studied in the bulk. The generations 2, 3, 4, and 5 were examined with the help of dielectric spectroscopy, ^2H solid-state NMR and field cycling (FC) NMR. Field cycling NMR [42,182-185] is able to reveal the local as well as the slower collective polymer dynamics [186,187]. The PPI dendrimer of the generation 2 ($\text{C}_{40}\text{N}_{14}\text{H}_{96}$) is shown in figure 4.1. A di-aminobutane core builds the center. For higher generations two further branches (functionality $f=3$) replace the hydrogen atoms at each amino end group's nitrogen. An almost generation independent T_g of around 200 K is revealed by DSC measurements. The dendrimers were obtained from SyMO-chem BV. The different generations have the following molecular masses: G2: 773.3 g/mol; G3: 1686.8 g/mol; G4: 3513.9 g/mol; G5: 7198.1 g/mol.

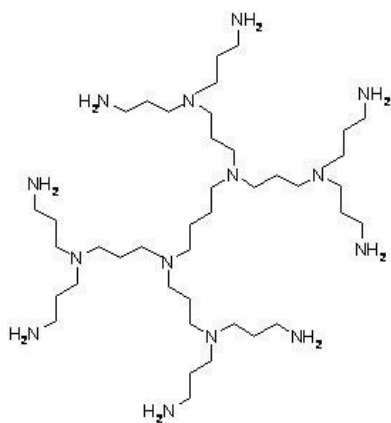


Figure 4.1: Structure of the PPI dendrimer of generation $G = 2$ with molar mass $M = 773.3$ g/mol. The center is given by a diaminobutane core. For each generation two further $\text{CH}_2\text{-CH}_2\text{-CH}_2\text{-NH}_2$ branches are attached at the amino end group nitrogen atoms.

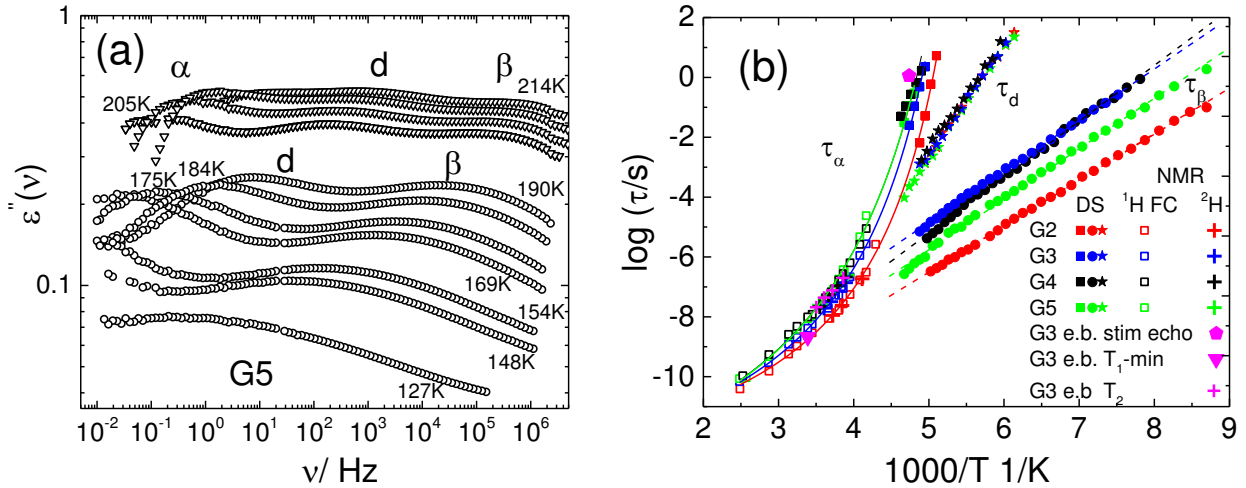


Figure 4.2: (a) Dielectric spectra, after the subtraction of the conductivity contribution, of the PPI dendrimer ($G = 5$) for temperatures as indicated. The main relaxation (α) and two secondary (d, β) processes are distinguishable. Figure adapted from Publication I. (b) Time constants of the PPI dendrimers for all generations as obtained from DS, FC NMR and ^2H solid-state NMR. For the end branch deuterated dendrimer (G3 e.b., see below) time constants from the stimulated echo measurements (pink pentagon), the T_1 minimum (pink down triangle), and the T_2 relaxation times (pink cross) were obtained. Figure adapted from Publication I.

Three rather broad relaxation processes were observed in the DS spectra at high temperatures (see figure 4.2 (a)) for all generations. The slowest is addressed to the segmental relaxation (α -process). The two other processes (named β - and d -process) behave like secondary relaxations as will be clear below. At low temperatures ($T < T_g$) these two processes are clearly distinguishable. The amplitude of both processes decreases below T_g . While the relaxation attributed to the β -process broadens with decreasing temperature, typical for a secondary relaxation, the width of the d -relaxation is temperature independent. Thus, FTS applies for the latter process, which is usually not observed for secondary relaxations.

The time constants for the main relaxation obtained from the different measurement methods, including NMR (see below), are shown in figure 4.2 (b). They only weakly change with generation. The relaxation time exhibits a typical VFT behavior yielding to a T_g close to the T_g obtained from the DSC measurements. The time constants of the d - and β -process show an Arrhenius temperature dependence typical of secondary relaxations. The dynamic of the d -process is independent of the generation while the time constants of the β -process vary somewhat with generation, but no trend is recognizable. A very high activation energy of $E_a = 42 RT_g$ is found for the d -process, while for the β -relaxation an E_a of 18 – 21

RT_g is obtained, which is typical for a JG secondary relaxation [65]. Two secondary relaxations are also found in hyperbranched polymers [188-190] and assigned to the reorientation of certain molecular groups, e.g. like methoxy (end-) groups. However, the reorientation of the amino end groups can be excluded as a source for the d-process, as the dipole moment does not change by 180° jumps, and therefore this movement is not seen in DS measurements.

Of further interest are the slow (slower than the main relaxation) dynamics of the dendrimers. As field cycling NMR is an excellent method to investigate polymer dynamics, FC NMR measurements were also carried out on the dendrimer samples of all generations available. From the relaxation measurements, susceptibility master curves $\chi''(\omega*\tau_\alpha)$ were constructed assuming FTS (see [185] for further details). The normalized susceptibilities are shown in figure 4.3.

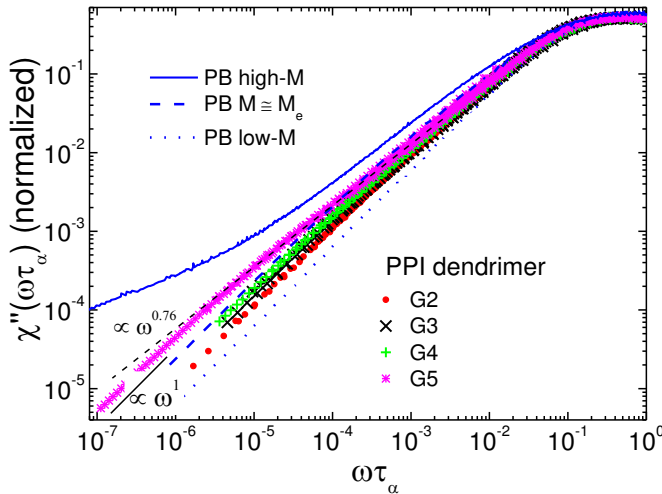


Figure 4.3: Normalized susceptibility $\chi''(\omega\tau_\alpha)$ master curves as obtained by FC NMR for the PPI dendrimers of all generations G2 to G5. Data for the polymer polybutadiene (PB) with low molecular weight M (blue dotted line), an M on the order of the entanglement mass M_e (blue dashed line), and with high M (blue solid line) are shown. Figure adapted from Publication I.

Three different relaxation regimes can be distinguished in figure 4.3. The main relaxation at $\omega\tau_\alpha \approx 1$ (from the necessary frequency shifts of the FC NMR susceptibilities, to create the master curve with the α -peak at $\omega\tau_\alpha \approx 1$, further time constants τ_α are obtained and added in figure 4.2 (b)); an additional relaxation intensity at $\omega\tau \ll 1$ when compared to $\chi''(\omega\tau_\alpha)$ of the low- M PB (dotted line, PB low- M), which gets increasingly pronounced with growing dendrimer generation; and the terminal relaxation at low frequencies with an exponent close to one. The behavior of the dendrimers is similar to that of unentangled polymers (compare $\chi''(\omega\tau_\alpha)$ of PB for a molar mass M on the order of the entanglement mass (blue dashed line)). In comparison with entangled PB (high- M PB, blue solid line in figure 4.3), no entanglement is seen, as also observed in rheological measurements [173,174,191].

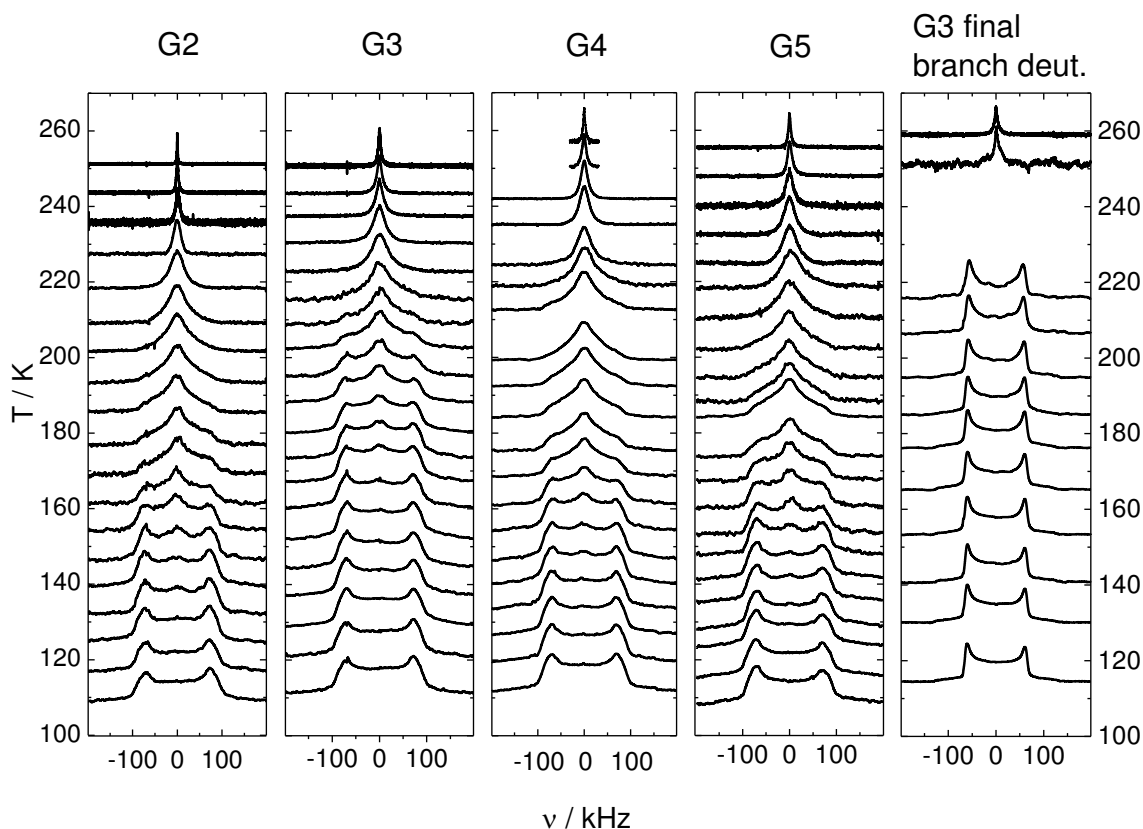


Figure 4.4: ^2H NMR Spectra for generation G2 to G5 of the amino group deuterated dendrimer and for the end branch deuterated dendrimer of Generation 3 (from left to right). The baseline of each spectrum indicates the measurement temperature. Figure adapted from Pub. I.

As part of the present work, solid-state ^2H NMR spectra were measured. For the ^2H measurements the dendrimers were deuterated (by stirring the dendrimers in deuterated water for two days at 45°C) at the amino end groups (which will be called amino group deuterated dendrimer) for all generations. For $G = 3$ also a sample with deuteration in the end branches ($\text{CD}_2\text{-CHD-CH}_2\text{-NH}_2$) (which will be called end branch deuterated dendrimer) but not including the NH_2 group was especially synthesized to avoid the measurement of the amino group jump in the NMR experiments. The ^2H NMR spectra are shown in figure 4.4 for all generations of the amino group deuterated dendrimer and the end branch deuterated dendrimer of generation 3. At low temperatures solid-state spectra with an asymmetry parameter of $\eta = 0.15$ are observable for the amino group deuterated dendrimers, while the asymmetry vanishes ($\eta = 0$) for the end branch deuterated dendrimer. With increasing temperature there is no direct line collapse from solid-state to liquid spectra in the case of the amino group deuterated dendrimers, but two-phase spectra consisting of a weighted sum of the rigid solid-state spectrum and a motionally averaged spectrum due to the fast amino group two-site jumps are found. An example of such a two-phase spectrum is shown in figure 4.5 (a). It can be described as a superposition of the rigid solid-state and the motionally averaged spectrum with

a weighting factor of $W = 0.5$. Further, an angle of 104° between the ND_2 bond directions has to be assumed to fit the motionally averaged sub spectrum well. When increasing the temperature even further, the rigid solid-state spectral part in the two-phase spectra disappears, and the spectra can now be described as a superposition of the fast exchange spectrum of the two-site amino jumps and a Lorentzian line reflecting a liquid on the NMR timescale. At highest temperatures only a Lorentzian line is seen. The collapse of the solid-state spectrum to the Lorentzian line takes place at similar temperatures for all generations in agreement with the almost identical T_g values found by DS and DSC. In the case of the end branch deuterated dendrimer the spectrum directly collapses from a solid-state spectrum to a Lorentzian line at slightly higher temperatures (220 K - 250 K) than for the amino group deuterated dendrimer of the same generation (G3) (200 K - 240 K). A possible cause for this may be the slightly different coupling constant, asymmetry parameter, and molecular weight between the end branch deuterated generation 3 dendrimer and the amino group deuterated dendrimer.

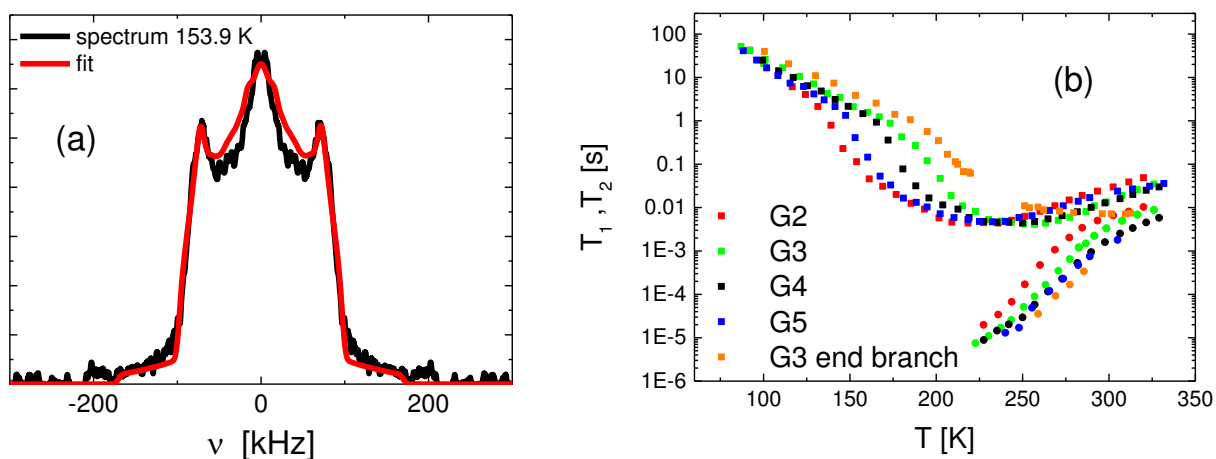


Figure 4.5: (a) Spectrum (symmetrized, black line) of the amino group deuterated $G = 3$ PPI dendrimer at $T = 153.9$ K. The fit (red line) is a superposition of a solid-state and a motionally averaged spectrum due to fast NH_2 jumps (see text) with a weighting factor of $W = 0.5$. Figure reprinted from Pub. I. (b) ^2H NMR T_1 and T_2 relaxation times of all generations of the amino group deuterated dendrimers and of the end branch deuterated dendrimer of generation $G = 3$ (G3 end branch).

In figure 4.5 (b) relaxation times of all generations of the amino group deuterated and of generation 3 of the end branch deuterated dendrimers are shown. At low temperatures similar spin-lattice relaxation times are found for all generations, which must be addressed to the relaxation due to the β -process, which appears at similar temperatures and timescales in all generations (compare figure 4.2 (b)). At higher temperatures a broad minimum is observed for

the amino group deuterated dendrimers. If one compares the time constants of the α -process (see figure 4.2 (b)) with the time constant obtained from this minimum it becomes clear that it cannot be caused by the main relaxation, but is the result of the fast 2-site amino group jumps. The expected minimum due to the main relaxation at higher temperatures is covered by the minimum due to the amino group jumps. In the case of the end branch deuterated dendrimer the T_1 minimum appears at higher temperatures (ca. 300 K), which is caused by the α -process. This is confirmed when comparing the time constant obtained from this minimum (pink down triangle in figure 4.2 (b)) to the time constants of the main relaxation. Furthermore, from the spin-spin relaxation data in the fast motion limit ($\tau_\alpha \ll 1/\delta_Q$) time constants were calculated along eq. 5.15 (cf. pink crosses figure 4.2 (b)). They also agree with the FC NMR and DS time constants.

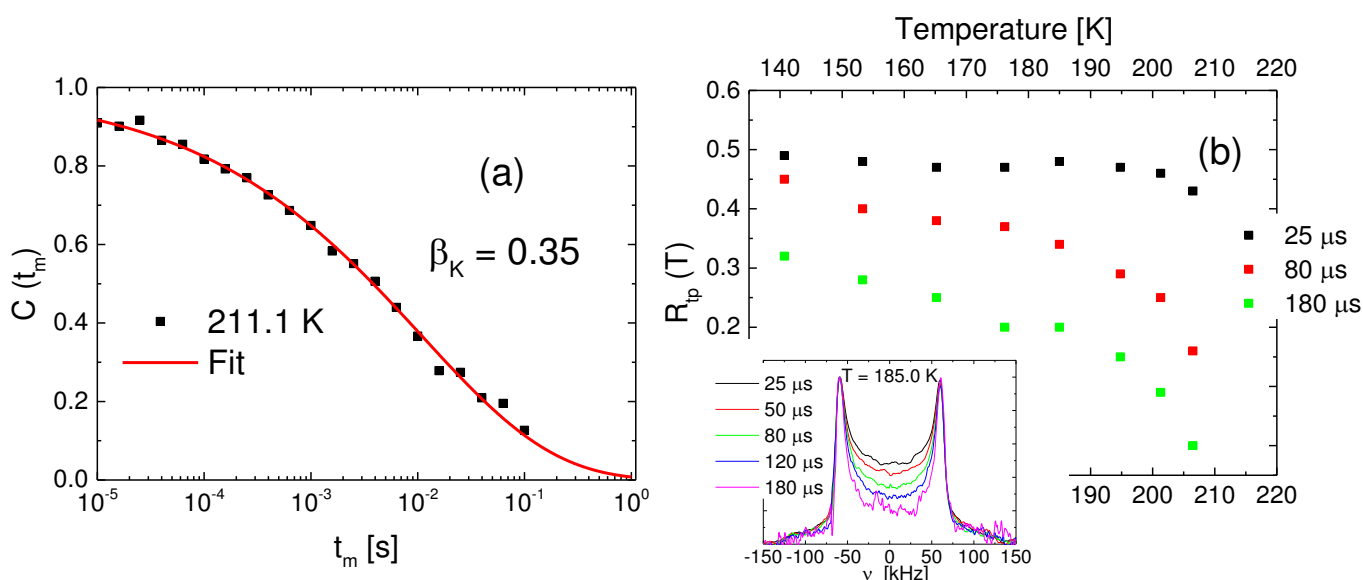


Figure 4.6: (a) Correlation function of the end branch deuterated G3 dendrimer at $T = 211.1$ K. (b) The line shape parameter $R_p(T)$ for the G3 end branch deuterated dendrimer. Inset: Interpulse dependent ^2H NMR spectra at $T = 185.0$ K.

Beyond that, applying the stimulated echo technique (see chapter 5.1), a correlation function of the end branch deuterated dendrimer was obtained (see figure 4.6 (a)). The respective time constant, given by a Kohlrausch fit, is added in figure 4.2 (b) (pink pentagon). It fits well to the time constants obtained by DS. The stretching parameter of $\beta_K = 0.35$ found in the ^2H NMR correlation function when applying a Kohlrausch fit [8,9] is comparable to the stretching parameter of $\beta_{CD} = 0.3$ obtained by a Cole Davidson [192-194] fit (it theoretically holds

$\beta_K \approx \beta_{CD} + 0.1$ for $0.2 < \beta_{CD} < 0.8$) of the dielectric data (see figure 4.2 (a)) and coincides with the stretching typically found in polymers [195].

Finally, to investigate the secondary relaxation with NMR, interpulse dependent spectra were recorded (compare chapter 3.4 and 5.1, eq. 5.11) for the G3 end branch deuterated dendrimer. The line shape parameter $R_{lp}(T)$, used to characterize the subtle changes of the solid-echo spectra, is shown in figure 4.6 (b). It decreases from low to high temperatures. A significant line shape effect due to a small angle reorientation is observable at temperatures below T_g (compare inset figure 4.6 (b)). Comparing the probed timescale ($1/\delta_Q$) with the time constants in figure 4.2 (b) it is clear that the decrease of $R_{lp}(T)$ for longer interpulse delays must be addressed to the β -process. However, no minimum in $R_{lp}(T)$, as observed in the binary mixtures in chapter 3.4, is observable, since the timescales of the β -process and the main relaxation are too close together and the influence of the main relaxation (strong decrease of $R_{lp}(T)$ for $T \geq 200$ K) on $R_{lp}(T)$ is observable before the β -process causes the minimum.

Altogether, we see different types of dynamics on quite different time scales in PPI dendrimers. Local fast dynamics, attributed to a JG β -relaxation and another dendrimer specific relaxation process, called d-process, whose origin is still unknown, but may be of cooperative nature, as the high activation energy is a typical sign for it [152,153], are observed in DS measurements. The main relaxation is detected with all three measurement methods with agreeing time constants between FC NMR, DS and solid-state NMR. Further, ^2H NMR observes the amino end group jump in the amino group deuterated dendrimers. Traces of a small angle process, which is associated with the β -process found in DS, are observed in the ^2H NMR spin-lattice relaxation times and in the ^2H NMR spectral line shapes. The d-process is probably not observable with ^2H NMR spectroscopy since the timescale of this process is too slow to influence the NMR observables like spectra or relaxation times. At low frequencies, FC NMR observes further relaxation intensity, similar to the breathing modes found in computer simulations and in calculation of a viscoelastic model of the dendrimer [168]. Thus, the spectral intensity found in the FC NMR susceptibility can be identified with the reorientation of whole branches of the dendrimer.

5. NMR Spectroscopy

5.1 Experimental and theoretical basics

5.1.1 The spin and its interactions

The nuclear spin \hat{I} as a quantum mechanical property of the nucleus represents its total angular momentum. It results from the coupling of the spins and the orbital angular momentums of the neutrons and protons. Since a pair of protons or neutrons always couple to a total spin of zero in their ground state, only nuclei with an uneven proton and/or neutron number possess a nuclear spin. This leads to a total spin of $I = 1/2$ for ^{31}P with an uneven number of neutrons and $I = 1$ for ^2H with one proton and one neutron.

The nuclear spin is coupled to the magnetic moment of the nucleus, as

$$\vec{\mu} = \gamma \vec{I} \quad (5.1)$$

holds, with γ being the gyromagnetic ratio of the nucleus. In an external magnetic field $\vec{B}_0 = B_0 \vec{e}_z$ the energy of the moment $\vec{\mu}$ and thus the spin is described by the Zeeman interaction analogue to the classical energy of a magnetic moment in a magnetic field:

$$\hat{H}_Z = -\vec{\mu} \cdot \vec{B} = -\gamma \vec{I} \cdot \vec{B} = -\gamma B_0 \hat{I}_Z \quad (5.2)$$

If a radio frequency (RF) signal with the Larmor frequency $\omega_L = \gamma B_0$ is applied to the system, transitions between the different spin states can occur and a NMR signal can be detected, provided that a population difference (which is given by the Boltzmann distribution if the system is in thermal equilibrium) between the different states is present.

The Zeeman interaction caused by the external field is not the only interaction influencing the total spin energy of the system. The “local field” provides an additional contribution to the total energy. Therefore, for instance, the quadrupolar interaction for $I \geq 1$ nuclei (for ^2H) and the chemical shift anisotropy (CSA) dominating for $I = 1/2$ nuclei (for ^{31}P) has to be taken into account. The dipole-dipole (DD) coupling between nuclei of the same kind (homonuclear DD coupling) or between nuclei of a different kind (heteronuclear DD coupling) has to be further considered.

The quadrupolar interaction results from the interplay of the non-symmetric charge distribution of the nucleus with the electric field gradient (resulting from the surrounding chemical bonds) at the site of the nucleus and is the dominating interaction for nuclei with spin $I \geq 1$. The electric dipole moment of the nucleus vanishes since the wave function of the

nucleus has a defined parity $|\Psi(r)|^2 = |\Psi(-r)|^2$. Thus, in first approximation, the quadrupole moment Q of the nucleus determines the interaction energy. The respective Hamiltonian reads [196]:

$$\hat{H}_Q = \frac{eQ}{2I(2I-1)\hbar} \hat{V} \hat{I} \quad (5.3)$$

Whereby $V_{i,j} = \frac{\partial^2 \Phi}{\partial r_i \partial r_j}$ with $i,j = [x,y,z]$ is the electric field gradient tensor, e the elemental charge and Φ the electric potential.

When applying first order perturbation theory one gets

$$\hat{H}_Q = \frac{eQ}{2I(2I-1)\hbar} V_{ZZ}^{LF} \frac{1}{2} (3\hat{I}_Z \hat{I}_Z - \hat{I} \hat{I}). \quad (5.4)$$

After expression of V_{ZZ}^{LF} in the PAS system of the molecule, the transition frequency correction with respect to the Zeeman interaction reads

$$\Delta\omega_Q = \frac{E_Q}{\hbar} = \pm \frac{\delta_Q}{2} (3\cos^2\theta - 1 - \eta \sin^2\theta \cos(2\varphi)) \quad (5.5)$$

with the coupling constant $\delta_Q = \frac{3}{4} \frac{eQ}{\hbar} V_{ZZ}^{PAS}$, the anisotropy parameter $\eta = \frac{V_{yy} - V_{xx}}{V_{zz}}$ and (θ, φ) being the spherical angles between the PAS system and the external magnetic field. The plus and minus sign result from the two possible transitions of the $I = 1$ spin (between $m_I = 1$ and $m_I = 0$ and between $m_I = -1$ and $m_I = 0$). The quadrupolar interaction is independent of the strength of the external field.

For $I = 1/2$ nuclei, the quadrupole moment of the nucleus vanishes and the CSA interaction dominates if the DD interaction is neglectable. In this case, the energetic shift results from the diamagnetic shielding of the external field due to the electrons surrounding the nuclei. The field at the site of the nucleus is thus not the external field \vec{B}_0 but a local field given by

$$\vec{B}_{local} = \vec{B}_0 + \vec{B}_{shield} = \vec{B}_0 - \tilde{\sigma}_L \vec{B}_0 = (1 - \tilde{\sigma}_L) \vec{B}_0 \quad (5.6)$$

with the chemical shielding tensor $\tilde{\sigma}^{PAS}$, with $\sigma_{ij}^{PAS} = 0$ for $i \neq j$, being diagonal in its principal axis system but not necessarily in the laboratory frame ($\tilde{\sigma}_L$). Thus, the Hamiltonian for the CSA interaction can be written as

$$\hat{H}_{CSA} = -\gamma \vec{I} \tilde{\sigma}_L \vec{B}_0 \quad (5.7)$$

As \vec{B}_0 is given in the laboratory frame, the CSA tensor $\tilde{\sigma}^{PAS}$ has to be transformed into the laboratory system. Further, the secular approximation is applied, i.e. contributions to \hat{H}_{CSA} resulting from the local contribution to the B -field ($\tilde{\sigma}_L \vec{B}_0$) perpendicular to the external field are neglected due to the presence of the strong magnetic field in z -direction. This leads to a NMR frequency shift of $\Delta\omega = \Delta\omega_{iso} + \Delta\omega_{CSA}(\theta, \varphi)$ with the isotropic chemical shift $\Delta\omega_{iso}$, which is independent of the molecular orientation and the chemical shift anisotropy (CSA) $\Delta\omega_{CSA}$ which depends on the angles (θ, φ) between the PAS system of the molecule and \vec{B}_0 , as it is the case for the quadrupolar interaction. The frequency shift due to the CSA is then given by

$$\Delta\omega_{CSA} = \frac{\delta_{CSA}}{2} (3\cos^2\theta - 1 - \eta\sin^2\theta \cos(2\varphi)) \quad (5.8)$$

with the CSA parameter $\delta_{CSA} = \omega_L \sigma_z$ and the asymmetry parameter $\eta = \frac{\sigma_y - \sigma_z}{\sigma_z}$, whereby $\sigma_i = \sigma_{ii} - \sigma_{iso}$ with $i = [x, y, z]$ and $\sigma_{iso} = \frac{1}{3}(\sigma_{xx} + \sigma_{yy} + \sigma_{zz})$ holds [123]. The frequency shift is now dependent on the external field, since $\delta_{CSA} = \omega_L \sigma_z = \gamma B_0 \sigma_z$.

5.1.2 NMR Spectra

To measure the NMR spectra one applies a radio frequency (RF) pulse with the intensity $B_I(t) = B_I \cos(\omega_{RF} t)$ and $\omega_{RF} \approx \omega_L$ in x or y direction

$$\hat{H}_{RF} = \gamma B_1(t) \vec{I}_{x,y} \quad (5.9)$$

Since the motional equation for the density matrix $\hat{\rho}(t)$ of the spin system (von Neumann equation) for the total Hamiltonian $\hat{H}_Z + \hat{H}_{RF}$ is hard to solve, one transforms the system into the so-called rotating frame, i.e. a coordinate system that rotates around the z -axis with the Larmor frequency ω_L [197]. In this system, the contribution of the Zeeman interaction vanishes and the RF-pulse becomes static in first approximation. Thus, the von Neumann equation can be easily solved. In a semi classical picture, the remaining Hamiltonian only turns the magnetization $\vec{M} = \sum_i^N \vec{\mu}_i$ (with number of spins N) around the x/y -axis. In experiments often 90° or 180° pulses are applied, for example for a 90° pulse it holds $\frac{\pi}{2} = \gamma B_1 t_p$, i.e. the pulse length t_p is determined by the B_I field and the nucleus.

After applying a 90° pulse with a coil in the respective direction, the magnetization is turned into the x,y plane and then precesses freely (free induction decay (FID)) around the z-axis. Different subensembles of the sample precess with slightly different $\Delta\omega$ due to the “local field” (see eq. 5.5 and 5.8), resulting from the different orientations (θ, φ) of the subensembles in a powder (i.e. the angles (θ, φ) between the molecular axis and the external field are equally distributed on the sphere surface) sample, for example. The magnetization induces a current in the coil, which can be detected and yields the NMR spectrum of the sample after Fourier transformation of the NMR signal.

Since death time effects after the first pulse prevent an immediate recording of the signal (FID), echo pulse sequences are applied to obtain the broad solid-state NMR spectra. For ^{31}P NMR a Hahn-echo pulse sequence (90° - t_p - 180°) is applied [198]. The second pulse leads to a refocusing of the magnetization of the different subensembles so that at $t = t_p$ after the second pulse an echo signal appears, which is identical to the original FID in the case of rigid molecules. Otherwise, the shape of the echo depends on the interpulse delay t_p . In the case of ^2H NMR a solid-echo is applied (90° - t_p - 90°) [199]. During the ^{31}P NMR experiment ^1H - ^{31}P dipolar decoupling is applied to eliminate the effects of the heteronuclear dipole-dipole interaction between the phosphorus and the hydrogen atoms. The homonuclear DD interaction between the phosphorus nuclei can be neglected in the investigated systems due to the large distance between two atoms.

At low temperatures, when no reorientation of the molecules is present on the experimental timescale, a solid-state spectrum is observed. With increasing temperature the spectrum continuously collapses to a liquid-like Lorentzian line in glass formers. The line collapse typically occurs within a few Kelvin for neat systems. For the glassy mixtures investigated here, instead of a direct collapse, a broad temperature region with so-called two-phase spectra is observable. The two-phase spectra are a weighted superposition of a solid-state $S_{Solid}(\omega)$ and a liquid-like spectrum $S_{Lorentz}(\omega)$ [200]

$$S(\omega; T) = W(T)S_{Lorentz}(\omega) + (1 - W(T))S_{Solid}(\omega) \quad (5.10)$$

with the weighting factor $W(T) = \int_{-\infty}^{\ln\tau_{cut}} G(\ln\tau) d\ln\tau$. The cut-off time τ_{cut} is given by the typical time scale of the experiment $\tau_{cut} \approx 1/\delta$ (see eq. 5.5 and 5.8), and $G(\ln\tau)$ is the corresponding distribution of reorientational correlation times of the molecules.

When prolonging the echo pulse interval t_p from short times (typically 20 μs for a normal solid-state NMR spectrum) to large t_p , (up to over 1 ms, $t_p < T_2$) the spectral shape becomes sensitive to small angle reorientations of the molecules during the experiment [201]. As the

angle dependent frequency shift $\Delta\omega(\theta)$ has its highest slope at $\Delta\omega = \frac{1}{4}\delta$ (see eq. 5.5 and 5.8, and assuming $\eta = 0$, as it is the case for most of our samples), the change of the NMR frequency due to a small angle reorientation during the experiment is maximal in this frequency region. Small reorientations are then recognized at high t_p as a decay of the intensity near the middle of the spectra, because the second pulse will not refocus the subensembles with a significant changed phase due to the reorientation. The line shape parameter $R(t_p)$, being defined as the intensity in the middle of a spectrum ($\omega = 0$) normalized to the intensity at the singularities ($\omega = \delta/2$ for ^{31}P NMR, $\omega = \pm\delta/2$ for ^2H NMR) quantifies the subtle changes of the spectra due to the influence of secondary relaxations [142,197]:

$$R(t_p) = \frac{S(\omega=0;t_p)}{S(\omega=\frac{\delta}{2};t_p)} \quad (5.11)$$

The R value is typically minimal at the temperature where the timescale of the β -relaxation coincides with the time scale of the experiment, therefore the time constant of the β -process can be obtained from the temperature of the R minimum along $\tau_\beta(T_{Rmin}) = 2\pi/\delta$ [197].

5.1.3 Relaxation phenomena

The application of RF pulses destroys the thermal equilibrium of the spin system. The return to the equilibrium state takes place due to two relaxation processes (in the case of $I = \frac{1}{2}$; in the case of $I > \frac{1}{2}$ the situation is more complex, but I refrain from a further discussion as almost always only the relaxation times T_1 and T_2 are important for my measurements). They originate from the coupling of the system to the lattice, called spin-lattice relaxation (T_1), and from the coupling to other spins, called spin-spin relaxation (T_2). Fluctuations in the electromagnetic field caused by molecular motion, which are described by the spectral density $J(\omega)$, enable the spins to perform state transitions between their energy levels. In the case of the spin-lattice relaxation, energy is transferred between the spin system and the lattice, which enables transitions between the different spins states and thus the buildup of the equilibrium magnetization in z-direction. Therefore $J(\omega_L)$ at the transition frequency ω_L may not vanish. The spin-spin relaxation is a purely entropic process; no energy transfer to the lattice is involved, and it leads to a loss of the transversal magnetization. The relations between the relaxation times and the spectral density can be calculated analogue to the BPP equations for the dipole-dipole interaction [202] and one gets in the case of a symmetric interaction tensor ($\eta = 0$) and a fast ($\tau_\alpha \ll 1/\delta$) isotropic motion [196] for ^{31}P NMR ($I = 1/2$)

$$\frac{1}{T_1} = \frac{2}{15} \left(\frac{3}{2} \delta_{CSA} \right)^2 [J(\omega_L)] \quad (5.12)$$

$$\frac{1}{T_2} = \frac{2}{90} \left(\frac{3}{2} \delta_{CSA} \right)^2 [4J(0) + 3J(\omega_L)] \quad (5.13)$$

and for ^2H NMR ($I = 1$)

$$\frac{1}{T_1} = \frac{2}{15} \delta_Q^2 [J(\omega_L) + 4J(2\omega_L)] \quad (5.14)$$

$$\frac{1}{T_2} = \frac{1}{15} \delta_Q^2 [3J(0) + 5J(\omega_L) + 2J(2\omega_L)]. \quad (5.15)$$

The spin-lattice relaxation time was measured with the saturation recovery pulse sequence at low temperatures and with the inversion recovery pulse sequence at high temperatures. The spin-spin relaxation time was obtained with the Carr-Purcell-Meiboom-Gill (CPMG) pulse sequence [203,204] or directly from the line width of the Lorentzian line, at temperatures where inhomogeneous broadening due to the field inhomogeneity can be neglected. It holds $\Delta\omega = 2/T_2$, with $\Delta\omega$ being the full width of the Lorentzian line.

5.1.4 Correlation function

The spectral density $J(\omega)$ mentioned above is connected to the reorientational correlation function of the molecules $C(t)$ via the Fourier transformation:

$$J(\omega) = \frac{1}{2} \int_{-\infty}^{\infty} C(t) e^{-i\omega t} dt \quad (5.16)$$

The reorientational correlation function is directly accessible in NMR with the stimulated echo pulse sequence [123]. In the case of ^{31}P NMR a three pulse sequence (90° - t_{ev} - 90° - t_m - 90°) is applied which is similar to the Hahn-echo sequence but the 180° echo pulse is split into two parts separated by the mixing time t_m . During the mixing time the molecules can reorient, which leads to an intensity loss of the stimulated echo signal. The echo amplitude is measured for different mixing times t_m and constant evolution times t_{ev} . For ^2H NMR an additional echo pulse is added after the third pulse (90° - t_{ev} - 45° - t_m - 45° - t_p - 90°) due to the short evolution times used (ca. 5 μs). When the phase of the second pulse is shifted by 90° with respect to the first

pulse the intensity at the echo maximum $I(t_m; t_{ev})$ reflects the sine-sine correlation damped by the T_1 relaxation (or by the quadrupolar relaxation T_{1Q} in the case of ^2H NMR) [13]:

$$I(t_m; t_{ev}) \propto \langle \sin(\omega(0)t_{ev}) \sin(\omega(t_m)t_{ev}) \rangle \exp\left(-\left(\frac{t_m}{T_{1/1Q}}\right)\right) = F_{t_{ev}}^{sin}(t_m) \exp\left(-\left(\frac{t_m}{T_{1/1Q}}\right)\right) \quad (5.17)$$

The function $F_{t_{ev}}^{sin}(t_m, t_{ev})$ can be separated into a constant residual correlation F_∞ for long times, which is only dependent on the evolution time and the geometry of the underlying motional process, and a mixing time dependent part $F(t_m, t_{ev})$ [205]:

$$F_{t_{ev}}^{sin}(t_m, t_{ev}) = (1 - F_\infty(t_{ev}))F(t_m, t_{ev}) + F_\infty(t_{ev}) \quad (5.18)$$

In the case of small evolution times it holds:

$$\lim_{t_{ev} \rightarrow 0} \langle \sin(\omega(0)t_{ev}) \sin(\omega(t_m)t_{ev}) \rangle = \langle \omega(0)\omega(t_m) \rangle t_{ev}^2 \quad (5.19)$$

Therefore, with eqs. 5.5 and 5.8 it becomes clear that for a vanishing asymmetry parameter $\eta = 0$ the correlation function $C_2(t_m)$ of the second Legendre polynomial of the reorientation $P_2(\theta) = (3\cos^2\theta - 1)$ is probed. Explicitly,

$$C_2(t_m) = \frac{\langle P_2(\theta(0)) P_2(\theta(t_m)) \rangle}{P_2(\theta(0))^2} \quad (5.20)$$

In contrast, via DS the correlation function of the first Legendre polynomial $P_1(\theta) = \cos\theta$ is accessible as the Fourier transformation of the measured susceptibility ε'' divided by the frequency ($\frac{\varepsilon''(\omega)}{\omega} = \frac{\chi''(\omega)}{\omega} = J_1(\omega)$) [66].

5.1.5 2D NMR spectra

With a 2D NMR spectrum $S(\omega_1, \omega_2; t_m)$ one can directly track the reorientation of the molecules, which is linked to the NMR frequency ω , during the mixing time. Therefore, one is able to observe the reorientation at temperatures for which a 1D solid-state powder spectrum is present up to mixing times on the order of the spin-lattice relaxation time T_1 . More specifically, a 2D spectrum measures the joint probability to find molecules with frequency ω_1 before and ω_2 after the mixing time, assuming that no significant reorientation during the evolution time and during the detection of the signal after the mixing time, occurs. It can be expressed as the

product of the a priori probability $P(\omega_1)$ to find a molecule with ω_1 before the mixing time, which is given by the 1D spectrum $S(\omega_1)$, and the conditional probability $P(\omega_2, t = t_m; \omega_1, t = 0)$ that a molecule has a frequency ω_2 after the mixing time if it had ω_1 before the mixing time.

To obtain a 2D NMR spectrum $S(\omega_1, \omega_2; t_m)$ in the case of $I = 1/2$ the TPPI (time proportional phase incrementation) technique is used [123]. Analogue pulse sequences as for the stimulated echo are applied but one measures alternately the cosine ($90^\circ_{x,y}-t_{ev}-90^\circ_{x,y}-t_m-90^\circ-t_p-180^\circ$) and sine part ($90^\circ_{x,y}-t_{ev}-90^\circ_{y,x}-t_m-90^\circ-t_p-180^\circ$) of the spectrum while linearly incrementing the evolution time t_{ev} , starting with $t_{ev} = 0$ (therefore, the fourth echo pulse is added to overcome the dead time). A subsequent 2D Fourier transformation yields the 2D spectrum. Depending on the timescale of the reorientation, different limiting cases can be distinguished. If a 1D solid-state spectrum is present and isotropic reorientation with a complete loss of correlation takes place during the mixing time (i.e. $t_m \gg \tau_a \gg 1/\delta$), ω_1 becomes independent of ω_2 and the spectrum in the case of $I = 1/2$ is given by [124]

$$S_{reo}(\omega_1, \omega_2) = S_{SS}(\omega_1)S_{SS}(\omega_2) \quad (5.21)$$

with the 1D solid-state spectrum $S_{SS}(\omega_1)$.

Similarly, if no reorientation takes place ($\tau_a \gg t_m$), the spectrum is given by

$$S_{dia}(\omega_1, \omega_2) = S_{SS}(\omega_1)\delta(\omega_1 - \omega_2) \quad (5.22)$$

as $P(\omega_2, t = t_m; \omega_1, t = 0) = 0$ for $\omega_1 \neq \omega_2$ and $P(\omega_2, t = t_m; \omega_1, t = 0) = 1$ for $\omega_1 = \omega_2$ holds, i.e. only intensity on the diagonal $\omega_1 = \omega_2$ is expected.

If all molecules are in the fast motion limit ($\tau_a \ll 1/\delta$) the 2D spectrum is given by

$$S_{liq}(\omega_1, \omega_2) = S_L(\omega_1)S_L(\omega_2) \quad (5.23)$$

with the 1D Lorentzian line $S_L(\omega)$.

Finally, if the molecules are in the fast motion limit before the mixing time and in the slow motion limit after the mixing time (e.g. because of a dynamical exchange within a broad $G(\ln\tau_a)$) and vice versa, an exchange spectrum is measured:

$$S_{ex}(\omega_1, \omega_2) = S_{SS}(\omega_1)S_L(\omega_2) + S_L(\omega_1)S_{SS}(\omega_2) \quad (5.24)$$

In binary systems with very broad correlation time distributions, the 2D spectra can often be described as a weighted superposition of all four cases discussed above [104,124].

5.2 Simulations

Another project of the present dissertation was to write a Graphical User Interface (GUI) program to comfortably simulate NMR observables like 1D and 2D spectra or correlation functions while employing random walk simulations of different motional models. With the aid of such a tool, the measured observables can be compared to the simulated observables and conclusions regarding the underlying motional process of the different detectable processes like the α -process, the β -process or discrete jumps of distinct molecular groups can be drawn [40,206]. The GUI development environment of MathlabR2009b was used to create the program. In the following an overview over the random walk simulations, how to obtain the respective NMR observables, and the GUI with some example simulations is given.

5.2.1 Random walk simulations

The basic idea of random walk simulations is to calculate the trajectory $(\theta, \varphi)(t)$ of the molecular axis on the surface of a sphere for a sufficient high number of molecules for a distinct stochastically motional model. Since the NMR frequency ω is only dependent on this molecular orientation, the time dependent $\omega(t)$ is then available for all molecules. From the knowledge of $\omega(t)$ the NMR observables are calculable. The exact procedure will be depicted in the following.

To create a trajectory for one molecular axis, at first a starting orientation (θ_0, φ_0) is randomly drawn out of the set $(\theta_0 \in [0, \pi], \varphi_0 \in [0, 2\pi[)$ with the aid of a random number generator. Not all starting angles (θ_0) are equally probable since the (θ, φ) are isotropically distributed on the sphere surface for a glass or super-cooled liquid and thus a θ_0 near the equator of the sphere is more probable than a θ_0 near the poles. This has to be considered later when the sum over all molecules is calculated. The contributions of the respective trajectories to the whole NMR signal have to be weighted with the $\sin(\theta_0)$ (see below, eq. 5.28 and 5.29).

In the next step the waiting time τ_w until the next jump or reorientation takes place is drawn. A stretched exponential distribution with the stretching parameter β for the waiting times τ_w is applied. Thus, it holds for the waiting time

$$\tau_w = (-\ln r)^{1/\beta} * \tau_{avr} \quad (5.25)$$

whereby $r \in [0,1]$ is an equally distributed random number and τ_{avr} the average waiting time. Now the new orientation of the molecular axis $(\theta_1, \varphi_1)(t_1)$, $t_1 = \tau_w$, has to be calculated. The jump angles $(\theta_{jump}, \varphi_{jump})$ are calculated according to the motional model. For example, for an isotropic random jump model it holds $\varphi_{jump} = 2\pi r$. For the polar angle $\theta_{jump} = \arccos(1-2r)$ must be chosen, since the probability for a distinct θ is $P(\theta) = \sin(\theta)$ (s. above) and θ should be chosen from the set $[0, \pi]$. The new orientation (θ_1, φ_1) can be calculated while applying a coordinate transformation along the negative jumping angles $(-\theta_{jump}, -\varphi_{jump})$. The new orientation $(\theta_1, \varphi_1) = (\theta_0, \varphi_0)'$ is given by the transformed coordinates $(\theta_0, \varphi_0)'$ of the old orientation (θ_0, φ_0) . These steps are repeated until the experimental duration $t_{exp} = \sum_i \tau_{wi}$ is reached. As a result the trajectory $(\theta, \varphi)(t)$ is obtained.

The program varies depending on the simulated pulse sequence and the desired NMR observable. For a 1D NMR spectrum or a stimulated echo simulation the phases $ph(t)$ of the NMR signal of all molecules are needed. The time dependent NMR frequency $\omega(t)$ is easily calculated along eq. 5.5 or 5.8 from the trajectory. The phase is given at any time by $ph(t+dt) = ph(t) + \omega(t)*dt$, therefore it holds

$$ph(t) = \int_{t=0}^t \omega(t') dt' \quad (5.26)$$

This is only valid for an FID without applying any echo pulses, but further pulses can easily be taken into account. One just has to invert the phase at the time t_p when the echo pulse is applied. Thus, the phase after an echo pulse at $t = t_p$ is given by

$$ph(t) = \int_{t=t_p}^t \omega(t') dt' - \int_{t=0}^{t=t_p} \omega(t') dt' \quad (5.27)$$

Thus, the phases are known at distinct time steps according to the drawn waiting times τ_{wi} . To calculate the whole NMR signal of all simulated molecules, the subsignal of each molecule needs to be known at common time steps. Therefore, the phase is calculated at the distinct time steps $t = dw*m$ with $m \in \left[0; \frac{t_{exp}}{dw}\right] \cup m \in \mathbb{N}$ which are multiples of a chosen dwell time dw . Finally, the simulated NMR signal (FID or echo) is given by the weighted sum over all molecules

$$S_{NMR}(t) = \sum_{k=1}^n [e^{-iph_k(t)} * \sin(\theta_{0k})] \quad (5.28)$$

whereby n is the total number of simulated molecules and $ph_k(t)$ and $\sin(\theta_{0k})$ are the phase and weighting of the respective molecule with index k . After a Fourier transformation, starting at the echo maximum in the case of a solid- or Hahn-echo, the NMR spectra are obtained.

For the simulation of a stimulated echo pulse sequence the same procedure as described above is used to calculate the NMR signal before and after the mixing time. During the mixing time only the orientation of the molecules is calculated. The only difference is, that the signal after the mixing time (whereby it holds $ph(t_e+t_m) = 0$) has to be weighted with the sine (for the sine-sine correlation function), or the cosine (for the cosine-cosine correlation function), respectively, of the phase at the end of evolution time $t = t_e$. Thus, it holds for the NMR signal of the sine-sine correlation function after the mixing time:

$$S_{NMR}(t) = \sum_{k=1}^n [e^{-iph_k(t)} * \sin(\theta_{0_k}) * \sin(ph_k(t_e))] \quad (5.29)$$

For the cosine-cosine correlation function the $\sin(ph_k(t_e))$ has to be replaced by the $\cos(ph_k(t_e))$. The correlation is then given by the intensity of the sine or cosine part, respectively, of the signal at the echo maximum normalized to the starting intensity at $t = 0$.

In the case of 2D NMR spectra, the calculation of the spectra is simpler. Assuming that no reorientation on the NMR timescale ($1/\delta$) occurs during the evolution time and during the detection of the signal after the mixing time, only the frequencies and therefore the orientations before and after the mixing time are needed. The initial frequency $\omega_1(\theta_i, \varphi_i)$ is given from the starting orientation (θ_i, φ_i) . Then the jump process according to the underlying motional model is repeated until the simulation time $t = \sum_j \tau_{wj}$ reaches the mixing time t_m . From the final orientation (θ_f, φ_f) the final frequency $\omega_2(\theta_f, \varphi_f)$ is calculated. The 2D spectrum $S(\omega_1, \omega_2)$ is divided into N^2 equal segments $\{[\omega_{1k}, \omega_{1k}+\Delta\omega] [\omega_{2k}, \omega_{2k}+\Delta\omega]\}$, with $\omega_{ik} = [-\omega_r + k * \Delta\omega]$; $i = 1,2$; $k = [0, N-1] \cup k \in \mathbb{N}$; $\Delta\omega = \frac{2\omega_r}{N}$, and $[-\omega_r, \omega_r]$ being the frequency range of the spectrum in each dimension and N the number of segments per dimension. Then the calculated (ω_1, ω_2) are just counted whilst adding the weighting $\sin(\theta_i)$ of the starting angles to a counter for the respective segment the tuple belongs to. For a sufficiently large number ($N \geq 10000$) of (ω_1, ω_2) the 2D spectrum emerges.

5.2.2 Graphical user interface and examples

The graphical user interface (GUI) (see figure 5.1) enables to modify all experimental parameters like the number of spins, the average waiting time before jumps, the interpulse delay of the echo, the coupling constant and a lot more. Further, the motional model can be selected from a number of predefined models like isotropic random jump or the motion on the circumference of a cone with a distinct opening angle, but also a user-defined reorientation angle distribution can be entered. There are different GUI's for the different experiments like 1D or 2D spectra or the simulation of the stimulated echo pulse sequence. The simulation starts by pressing the start button and returns the spectrum or the respective NMR signal and correlation in the case of the stimulated echo sequence.

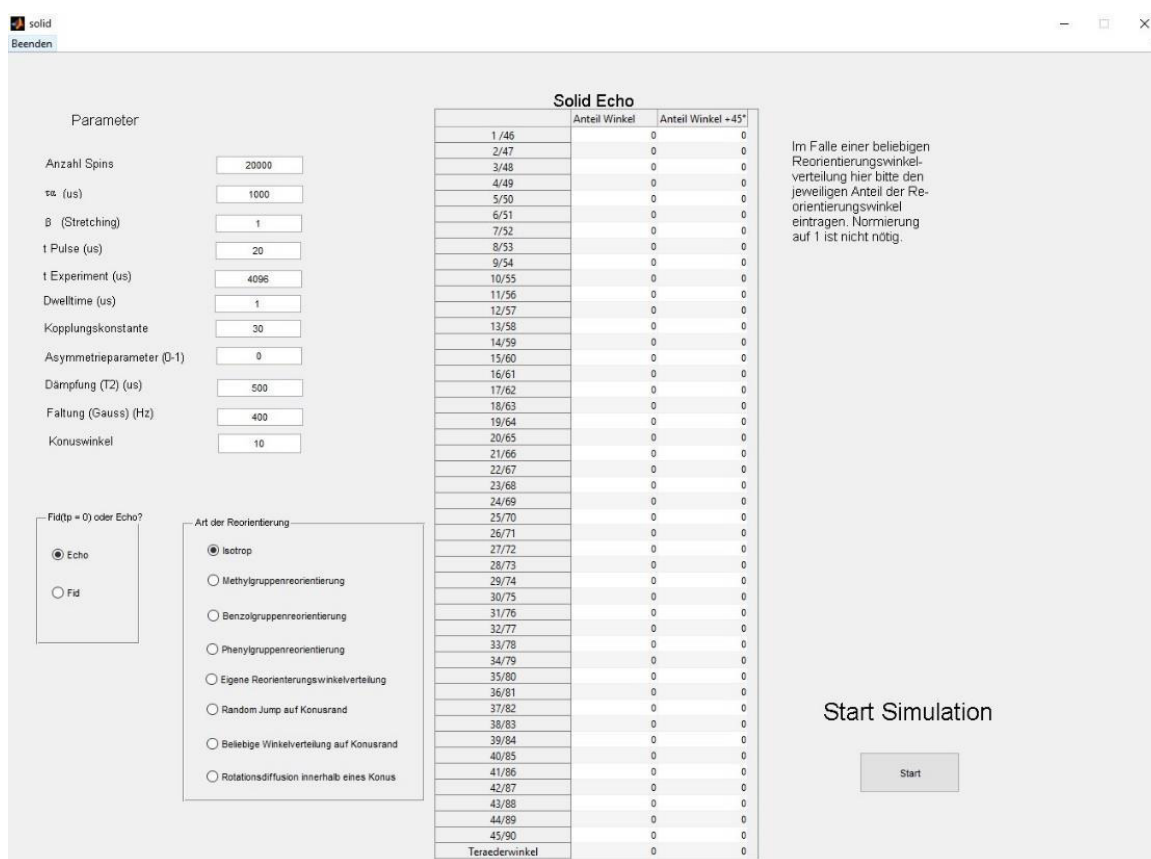


Figure 5.1: GUI of the program for 1D ^2H NMR spectra. On the left side all parameters can be modified and it can be chosen whether an echo should be applied or if only the FID shall be calculated. The motional model is selectable in the lower box. With the table on the right side, a distinct reorientational angle distribution can be defined.

In the following some example spectra and calculations are displayed. Figure 5.2 shows solid-echo spectra ($\eta = 0$) of a methyl group jump for different waiting times. For long waiting times (1000 μs) the spectrum is in the slow motion limit, a typical Pake spectrum with $\delta_Q = 120$ kHz is observed. With decreasing waiting times, the spectral shape starts to change and fulfills a line shape change typical of the tetrahedral jumps of the methyl group. For very short waiting times (0.01 μs) the spectrum reflects the fast motion limit of this threefold jump with an averaged spectral width of $\bar{\delta} = 1/3 \delta_Q$, as expected.

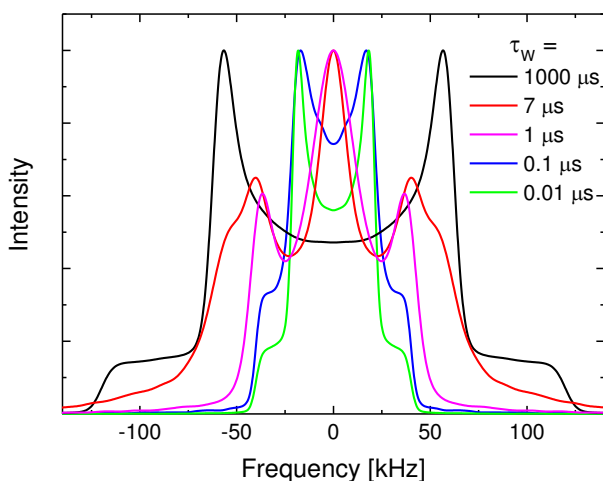


Figure 5.2: Random walk simulation of ^2H solid-echo spectra for a threefold methyl group jump. The spectrum collapses from a broad Pake spectrum for long waiting times to a motional averaged Pake spectrum in the fast motion limit.

For the same motional model the sine-sine and cosine-cosine stimulated echoes were calculated. The residual correlation $F_\infty(t_{ev})$ (see eq. 5.18) of the correlation function depends on the geometry of the underlying motion and the evolution time t_{ev} (see chapter 5.1). So one may compare a measured residual intensity $F_\infty(t_{ev})$ to a calculated one for different motional models and may draw conclusions on the kind of underlying motion. Figure 5.3 shows the $F_\infty(t_{ev})$ for a methyl group jump.

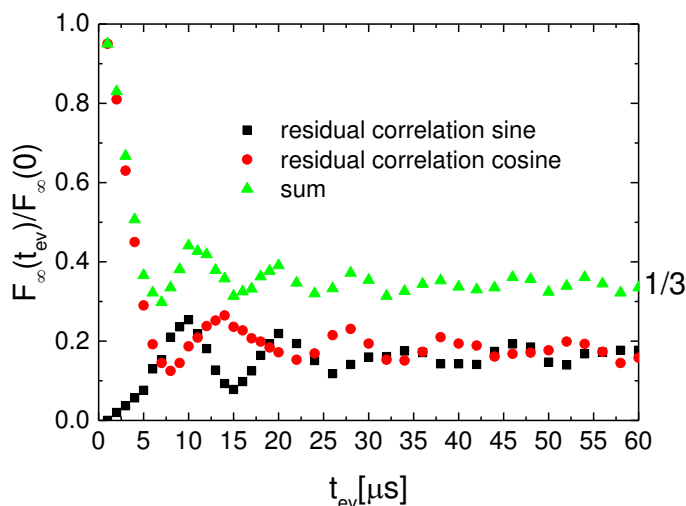


Figure 5.3: Calculated residual correlation $F_\infty(t_{ev})$ normalized to $F_\infty(0)$ for the methyl group jump for the sine-sine and cosine-cosine stimulated echo pulse sequence. The sum of both approaches the value $1/3$.

For short evolution times the cosine-cosine residual correlation starts at one, which is just the intensity of the FID and the sine-sine part starts at zero, then both parts oscillate against each other and approach a residual correlation of 1/6 for long evolution times. The sum of both parts approaches the value 1/3, which is quite reasonable due to the three side jump. The orientation of a molecule before and after the mixing time coincides with a probability of 1/3.

Finally, a 2D spectrum for the methyl group model for long mixing times $t_m \gg \tau_w$, i.e. all molecules reorient, is shown in figure 5.4. The ellipse like structure reflects the 109° tetrahedral angle. Also here, 1/3 of the intensity stays on the diagonal, apparently showing no reorientation, but just reflecting the molecules who have the same orientation before and after the mixing time.

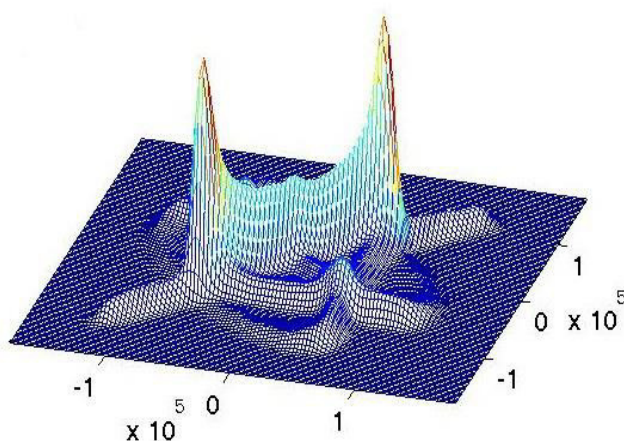


Figure 5.4: Simulated 2D ^2H NMR spectrum with $\delta_Q = 120$ kHz for the threefold methyl group jump ($t_m \gg \tau_w$).

The next example shows the influence of the opening angle in the “motion-on-a-cone” model, which is applied to describe the spectral changes observed in the β -process. In this model, the molecular axis reorients with random jumps on the circumference of a cone with the (half) opening angle χ (see figure 2.8 (d)). Figure 5.5 shows the solid-echo spectra with an interpulse delay of $t_p = 20 \mu\text{s}$ for $\chi = 5^\circ$ (left) and for $\chi = 20^\circ$ (right). The average waiting times between the jumps decreases from 10000 μs (slow motion limit) to 0.02 μs (fast motion limit) from bottom to top. For the small opening angle both spectra in the fast and slow motion limit almost coincide. For waiting times between these extreme cases the spectra only slightly decay in the middle of the spectra. In the case of the large opening angle, the spectral width in the fast motion limit strongly decreases from $\delta = 120$ kHz to ca. $\bar{\delta} = 100$ kHz. For waiting times in between, transition spectra are observed. This shows that the extend of spatial exploration of the molecules involved in the secondary process is observable in the fast motion limit of the NMR spectra and that for small reorientation angles no significant spectral changes for short t_p , as observed in the systems discussed in the present work, occur. However, when

increasing the interpulse delay t_p significantly the intensity in the middle of the spectra also decays for small opening angles (see figure 5.6). With this model, the spectral changes due to the β -process observed in this work can be reproduced.

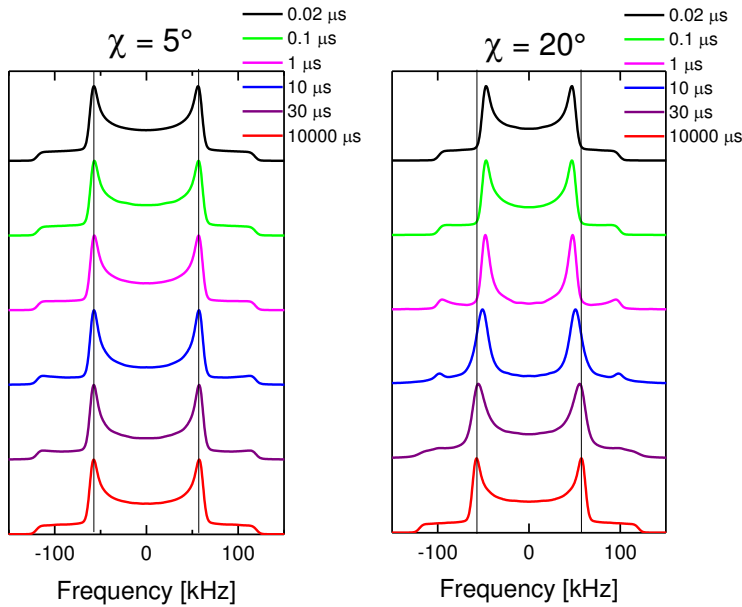


Figure 5.5: Solid-echo Pake spectra ($\delta = 120$ kHz) for a “motion-on-a-cone” model for an (half) opening angle of $\chi = 5^\circ$ (left) and $\chi = 20^\circ$ (right). The average waiting time decreases from bottom to top. The interpulse delay is $20 \mu\text{s}$.

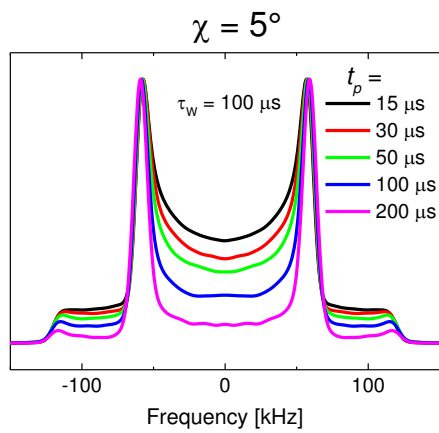


Figure 5.6: Solid-echo Pake spectra ($\delta = 120$ kHz) for a “motion-on-a-cone” model for an (half) opening angle of $\chi = 5^\circ$. The average waiting time is $\tau_w = 100 \mu\text{s}$. The interpulse delay t_p increases from $15 \mu\text{s}$ to $200 \mu\text{s}$.

IV. Publications

1. List of Publications

Publication I: F. Mohamed, M. Hofmann, B. Pötzschner, N. Fatkullin, and E. A. Rössler: *Dynamics of PPI Dendrimers: A Study by Dielectric and ^2H NMR Spectroscopy and by Field-Cycling ^1H NMR Relaxometry*, *Macromolecules* 48, 3294 (2015). <http://dx.doi.org/10.1021/acs.macromol.5b00486>

Publication II: B. Pötzschner, F. Mohamed, A. Lichtinger, D. Bock, and E. A. Rössler: *Dynamics of asymmetric non-polymeric binary glass formers—A nuclear magnetic resonance and dielectric spectroscopy study*, *J. Chem. Phys.* 143, 154506 (2015). <http://dx.doi.org/10.1063/1.4932981>

Publication III: B. Pötzschner, F. Mohamed, C. Bächer, E. Wagner, A. Lichtinger, R. Minikejew, K. Kreger, H.-W. Schmidt, and E. A. Rössler: *Non-polymeric asymmetric binary glass-formers. I. Main relaxations studied by dielectric, ^2H NMR, and ^{31}P NMR spectroscopy*, *J. Chem. Phys.* 146, 164503 (2017). <http://dx.doi.org/10.1063/1.4980084>

Publication IV: B. Pötzschner, F. Mohamed, C. Bächer, E. Wagner, A. Lichtinger, D. Bock, K. Kreger, H.-W. Schmidt, and E. A. Rössler: *Non-polymeric asymmetric binary glass-formers. II. Secondary relaxation studied by dielectric, ^2H NMR, and ^{31}P NMR spectroscopy*, *J. Chem. Phys.* 146, 164504 (2017). <http://dx.doi.org/10.1063/1.4980085>

2. Individual contribution to the publications

Pub. I: I performed and analyzed all NMR measurements on the generation 2 to 5 of the PPI dendrimers. All dielectric measurements and analysis were carried out by F. Mohamed as part of her PhD thesis, while the field cycling data and its analysis was done by M. Hofmann as part of his PhD thesis.

Pub. II: I performed and analyzed all ^1H NMR and ^{31}P NMR measurements of the mixture TCP/DH 397 for all concentrations except for neat TCP. The data of the neat component was obtained by D. Bock. All dielectric measurements and analysis in the mixtures were carried out by F. Mohamed as part of her PhD thesis, while the neat system of DH 379 was measured by A. Lichtinger as part of her bachelor thesis.

Pub. III: I performed and analyzed all ^2H NMR and ^{31}P NMR measurements of the mixture TPP/SBC except the ^{31}P NMR measurements on the $c_{\text{TPP}} = 47\%$ mixture which was measured and analyzed by C. Bächer as part of his bachelor thesis and the ^2H NMR measurements on the $c_{\text{TPP}} = 59\%$ mixture, which was measured and analyzed by E. Wagner as part of his diploma thesis. All dielectric measurements and analysis in the mixtures were carried out by F. Mohamed as part of her PhD thesis, while the neat system of the undeuterated SBC component was measured by A. Lichtinger as part of her bachelor thesis and the neat system of the deuterated SBC component was measured by R. Minikejew. The workgroup of H.-W. Schmidt synthesized and performed DSC measurements on all high- T_g components.

Pub. IV: I performed and analyzed all ^2H NMR and ^{31}P NMR measurements of the mixture TPP/SBC except the ^{31}P NMR measurements on the $c_{\text{TPP}} = 47\%$ mixture which was measured and analyzed by C. Bächer as part of his bachelor thesis and the ^2H NMR measurements on the $c_{\text{TPP}} = 59\%$ mixture, which was measured and analyzed by E. Wagner as part of his diploma thesis. D. Bock contributed the

measurements of the interpulse dependent ^{31}P NMR spectra of neat TPP. All dielectric measurements and analysis in the mixtures were carried out by F. Mohamed as part of her PhD thesis, while the neat system of the undeuterated SBC component was measured by A. Lichtinger as part of her bachelor thesis. The workgroup of H.-W. Schmidt synthesized and performed DSC measurements on all high- T_g components.

3. Further publications

- S. Adishchev, D. Bock, C. Gainaru, R. Kahlau, B. Micko, N. Petzold, B. Pötzschner, and E. A. Rössler: *Reorientational Dynamics of Organophosphate Glass Formers - a Joint Study by ^{31}P NMR, Dielectric Spectroscopy and Light Scattering*, Z. Phys. Chem. 226, 1149 (2012). <http://dx.doi.org/10.1524/zpch.2012.0281>
- D. Bock, R. Kahlau, B. Micko, B. Pötzschner, G. J. Schneider, and E. A. Rössler: *On the cooperative nature of the β -process in neat and binary glasses: A dielectric and nuclear magnetic resonance spectroscopy study*, J. Chem. Phys. 139, 064508 (2013). <http://dx.doi.org/10.1063/1.4816374>
- D. Bock, R. Kahlau, B. Pötzschner, T. Körber, E. Wagner, and E. A. Rössler: *Dynamics of asymmetric binary glass formers. II. Results from nuclear magnetic resonance spectroscopy*, J. Chem. Phys. 140, 094505 (2014). <http://dx.doi.org/10.1063/1.4865945>
- B. Schmidtke, N. Petzold, B. Pötzschner, H. Weingärtner, and E. A. Rössler: *Relaxation Stretching, Fast Dynamics, and Activation Energy: A Comparison of Molecular and Ionic Liquids as Revealed by Depolarized Light Scattering*, J. Phys. Chem. B 118, 7108 (2014). <http://dx.doi.org/10.1021/jp412297u>

4. Publication I

Publication I

Dynamics of PPI Dendrimers: A Study by Dielectric and ^2H NMR Spectroscopy and by Field-Cycling ^1H NMR Relaxometry

F. Mohamed, M. Hofmann, B. Pötzschner, N. Fatkullin, and E. A. Rössler

Macromolecules 48, 3294 (2015)

Doi: 10.1021/acs.macromol.5b00486

© 2015 The American Chemical Society

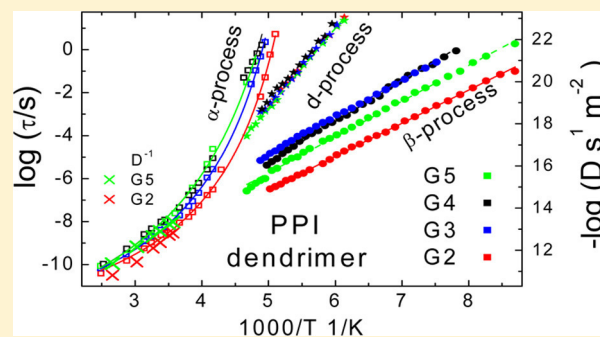
Dynamics of PPI Dendrimers: A Study by Dielectric and ^2H NMR Spectroscopy and by Field-Cycling ^1H NMR Relaxometry

F. Mohamed,[†] M. Hofmann,[†] B. Pötzschner,[†] N. Fatkullin,[‡] and E. A. Rössler^{*,†}

[†]Experimentalphysik II, Universität Bayreuth, 95440 Bayreuth, Germany

[‡]Institute of Physics, Kazan Federal University, Kazan 420008, Tatarstan Russia

ABSTRACT: We investigate bulk poly(propyleneimine) dendrimers of generation (G) 2–5 by dielectric spectroscopy (DS), solid-state ^2H NMR, and field-cycling ^1H NMR relaxometry (FC ^1H NMR) in a large temperature range (120–400 K). Three relaxation processes are identified by DS: a main (α -) relaxation ($T > T_g$) and two secondary processes ($T < T_g$). The α -process exhibits a super-Arrhenius temperature dependence typical of glass-forming liquids and changes only weakly with G , yielding $T_g \sim 200$ K. The temperature dependence of the secondary relaxations is governed by an Arrhenius law. While one secondary process exhibits features characteristic for glasses, the other is atypical. Its time constant is virtually independent of G , and its spectral width does not increase with lowering temperature as is usually observed for sub- T_g relaxations. Regarding FC ^1H NMR probing the dispersion of the spin–lattice rate R_1 in the frequency range 200 Hz–30 MHz, transformation to the susceptibility representation, $\chi''(\omega) \equiv \omega R_1(\omega)$, and applying frequency–temperature superposition, an effective frequency range of 9 decades is covered by a master curve $\chi''(\omega\tau_\alpha)$. In addition to the segmental time $\tau_\alpha(T)$, which complements the results from DS up to high temperatures, a longer terminal relaxation $\tau_t(T)$ is identified. In between, an intermediate power-law regime is observed in $\chi''(\omega\tau_\alpha)$ with an exponent of about 0.8. The broad relaxation spectrum is attributed to local dynamics, breathing modes, and overall tumbling and diffusion of the dendrimer molecule. In the low-frequency limit, $R_1(\omega)$ is determined by intermolecular relaxation from which the molar mass dependence of the translational diffusion coefficient can be estimated. We find $D(M) \propto M^{-1.2 \pm 0.2}$.



1. INTRODUCTION

Dendrimers as a special type of macromolecular architecture offer an interesting field of investigations in physics and chemistry.^{1–5} Starting from a central point with a functionality f , segments of uniform length again with functionality f are attached. Thereby “shells” of segments are created, and each shell defines a generation starting with $G = 0$ for the functional center. Dendrimers are thus perfectly monodisperse, and as mass grows faster than volume, the number of generations G is limited. Yet, the actual maximum depends on the chemistry of the segment. The latter also strongly determines structure and dynamics of the dendrimers.

Here we focus on bulk poly(propyleneimine) (PPI) dendrimers with $f = 3$. Generations 2–5 can be synthesized and purchased commercially. At room temperature they constitute liquids of high viscosity, and cooling below the glass transition temperature T_g (around 200 K) yields transparent glasses. The dendrimer structure is soft enough to allow for partial interpenetration, however, the extent of which decreases with generation.⁶ Entanglement effects, as in the case of long-chain polymers, do not occur.^{7,8} Correspondingly, the viscosity is significantly lower than in entangled linear polymers.⁷ According to MD simulations, the dendrimers become more compact and spherical as the generation number grows, and also dendra turn

inward.^{6,9} Thus, the end amine groups are spread more and more uniformly over the entire dendrimer volume. The overall density profile decreases gradually from the center to the surface of the molecule while the radius of gyration scales approximately with the cubic root of the number of segments. This structural picture sketched by simulation data essentially agrees with experimental studies.^{3,6,9}

While several studies on the solution behavior were published, up to our knowledge not many experiments were done attempting to unravel the dynamics in bulk dendrimers. Values of T_g for neat and end group modified PPI, linear and nonlinear rheological behavior, and the M dependence of the zero-shear viscosity were reported.⁸ Detailed rheological results were also reported for polyamidoamine (PAMAM) dendrimers.⁷ No entanglement (rubber) plateau was observed in the dynamic modulus, indicating, as mentioned, the absence of entanglement effects. Altogether, one finds a relaxation behavior showing some reminiscence of melts of polymer chains below their entanglement molar mass. That is, in addition to segmental dynamics determined by the glass transition phenomenon,⁴ a

Received: March 6, 2015

Revised: April 17, 2015

Published: May 4, 2015

spectrum of slower modes appears. Indeed, the Rouse model¹⁰ was applied to reproduce the rheological behavior, yet deviations were found.⁷ Also, secondary relaxation processes as usually observed in molecular glasses were reported for other dendrimers.^{11,12} A number of MD simulations as well as theoretical approaches deal with the dynamics of particular dendrimer models.^{4–6,9,13–17}

In the present work we investigate the dynamics of PPI dendrimers by dielectric and NMR spectroscopy. A large temperature range is covered (120–400 K) comprising the melt ($T > T_g$) as well as the glassy state ($T < T_g$). In the case of NMR we present results from solid-state ²H NMR and from field-cycling (FC) ¹H NMR relaxometry. The latter technique has gained new momentum with the availability of commercial spectrometers.^{18–22} In contrast to existing NMR studies on dendrimers mostly in solution,^{23–26} which characterize the spin–lattice relaxation time T_1 at a few frequencies (magnetic fields), the FC method probes the frequency dependence of the relaxation rate $1/T_1 = R_1(\omega)$ usually in the frequency ($\omega/2\pi$) range 10 kHz–20 MHz. Taking recourse to a self-built FC relaxometer,²⁸ we were able to reach a low-frequency limit of 200 Hz. Converting the relaxation data to the susceptibility representation $\chi''(\omega) \equiv \omega R_1(\omega)$ and applying frequency–temperature superposition (FTS), an approach well-known from rheological studies,²⁷ a large effective frequency range is covered by a master curve $\chi''(\omega\tau_\alpha)$. It reveals both local and collective segmental dynamics.^{29–33} Here $\tau_\alpha = \tau_\alpha(T)$ denotes the time scale of the local segmental dynamics. The evolution of $\chi''(\omega\tau_\alpha)$ with molar mass M will be compared to that of linear polymers. Moreover, as the low-frequency dispersion is determined by translational dynamics, we are able to extract the diffusion coefficient $D(M)$.

2. EXPERIMENTAL SECTION

2.1. Systems. We investigated the dynamics of PPI dendrimers in bulk, which were purchased from SyMO-Chem BV (University of Eindhoven) and used without further treatment. In the case of FC ¹H NMR the samples were degassed to remove paramagnetic oxygen. The chemical structure of generation 2 is shown in Figure 1. For each further

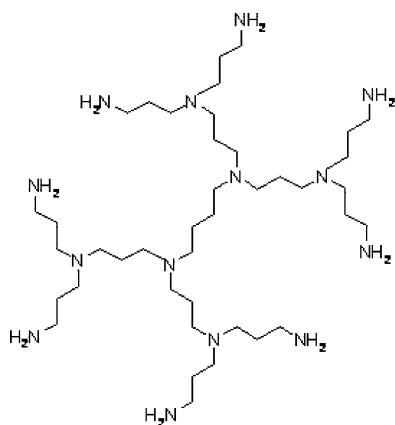


Figure 1. Idealized structure of the PPI dendrimer of generation 2.

generation the number of amine end groups doubles. We investigated dendrimers of generation 2 (G2), 3 (G3), 4 (G4), and 5 (G5); higher generations are not available for this type of dendrimer. For the ²H NMR investigations, the amine end groups were deuterated by dissolving the dendrimers in deuterated water and evaporating the water again. The procedure was repeated twice. The glass transition temperature T_g was determined by DSC experiments (cf. Table 1).

2.2. Dielectric Spectroscopy. Dielectric measurements were carried out with an Alpha-A Analyzer by Novocontrol, which allows for frequency-resolved measurements of the dielectric permittivity in the range 10^{-2} – 10^6 Hz. Temperature stability was ± 0.2 K controlled by a Quatro-H temperature controller (Novocontrol). The absolute accuracy is better than ± 0.5 K. The sample cell is designed as described in ref 34 and guarantees constant plate distance while cooling.

In most of the PPI dendrimer samples a pronounced dc conductivity is observed in the dielectric loss $\epsilon''(\omega)$ ($T > T_g$), which is subtracted by using the expression $\epsilon_{dc}''(\omega) = \sigma_{dc}/(\epsilon_0\omega)$ (cf. Figure 12). All time constants were estimated by “peak picking”; i.e., the condition $\tau_i = 1/(2\pi\nu_{max,i})$ was applied. In the case of the two secondary processes (“d” and “b”) a sum of a distribution of correlation times $G(\ln \tau)$ appropriate for thermally activated relaxation processes³⁵ was chosen for interpolating the dielectric spectra, explicitly

$$\epsilon^*(\omega) = \Delta\epsilon \int_{-\infty}^{\infty} \frac{G(\ln \tau)}{1 + i\omega\tau} d \ln \tau + \epsilon_\infty \quad (1)$$

with

$$G(\ln \tau) = AN_\beta \frac{1}{b_\beta \left(\frac{\tau}{\tau_\beta}\right)^{a_\beta} + \left(\frac{\tau}{\tau_\beta}\right)^{-a_\beta b_\beta}} + (1-A)N_d \frac{1}{b_d \left(\frac{\tau}{\tau_d}\right)^{a_d} + \left(\frac{\tau}{\tau_d}\right)^{-a_d b_d}} \quad (2)$$

and the normalization factors

$$N_{i \in \{d, \beta\}}(a_i, b_i) = \frac{a_i(1+b_i)}{\pi} b_i^{b_i/(1+b_i)} \sin\left(\frac{\pi b_i}{1+b_i}\right) \quad (3)$$

The coefficients A and $(1-A)$ define the relative weight of the individual contributions. The parameter a causes a symmetric broadening of the distribution while the “asymmetry parameter” b only affects its short time flank. After Laplace transformation, the resulting susceptibility peak is symmetrically broadened by a , which is also the exponent of the power-law asymptotically approached by the peak’s low-frequency flank. The exponent of the power-law asymptote of the high-frequency flank is given by the product ab .

2.3. ²H NMR. Solid-state ²H NMR spectra of the end group deuterated dendrimers are dominated by the interaction of the nuclear quadrupolar moment with the electric field gradient (EFG), and the NMR angular frequency depends on the spherical angles (θ, ϕ) between the EFG tensor axis and the magnetic field direction³⁶

$$\omega_Q(\theta, \phi) = \pm \delta_Q/2(3 \cos^2 \theta - 1 - \eta \sin^2 \theta \cos(2\phi)) \quad (4)$$

where $\omega_Q(\theta, \phi)$ is the shift of the resonance frequency with respect to the Larmor frequency ω . The parameter δ_Q is the anisotropy and η the asymmetry parameter of the EFG tensor. In the case of an isotropic distribution of tensor orientations and $\eta = 0$, a so-called Pake spectrum is observed, which is measured with a solid-echo pulse sequence.³⁶ At high temperatures the two-site reorientation of the dendrimer’s amine groups becomes faster than the NMR time scale ($\tau_{\text{jump}} \ll 1/\delta_Q$), which leads to a motion-averaged powder spectrum with $\bar{\eta}$ close to one (cf. below and Figure 6). In the case of an isotropic reorientation occurring at even higher temperatures a Lorentzian line typical for a liquid results. Under the condition $1/\delta_Q \gg \tau_\alpha \gg \omega^{-1}$, for which effects from the crossover to a solid-state spectrum and from field inhomogeneity, respectively, can be ignored, the full half-width $\Delta\nu$ of the line is related to the transversal relaxation time T_2 via $\Delta\nu = 1/\pi T_2$, and one can estimate the reorientational correlation time τ_α from³⁷ $1/T_2 = (1/5)\bar{\delta}_Q^2(1 + \bar{\eta}^2/3)\tau_\alpha$ where $\bar{\delta}_Q = 2\pi \cdot 90$ kHz is the motionally averaged anisotropy parameter and $\bar{\eta} = 0.9$ due to the fast 180° two-site jumps.

The ²H NMR experiments were performed on an upgraded Bruker Avance DSX spectrometer and a 300 MHz Oxford cryomagnet. The ²H Larmor frequency is $\omega = 46.067$ MHz for a magnetic field of 7 T. The pulse length of a $\pi/2$ pulse was 2.8 μ s. The recovery delay after applying a saturation sequence of 5 $\pi/2$ pulses was at least $4T_1$ and 8-fold phase

Table 1. Properties of the Investigated PPI Dendrimers: Molecular Formula, Molar Mass, Number of Amine Groups, Glass Transition Temperature (T_g) from DSC and Dielectric Relaxation (DS), Activation Energy E_A/R , and Attempt Time τ_∞ of the β -Process

generation	molecular formula	molar mass [g/mol]	no. of amine end groups	T_g [K] (DSC)	T_g [K] (DS)	$E_A/R(\beta)$ [K]	$\tau_\infty(\beta)$ [s]
2	$C_{40}N_{14}H_{96}$	773.3	8	195	196	3522	5×10^{-15}
3	$C_{88}N_{30}H_{208}$	1686.8	16	198	200	3914	2×10^{-14}
4	$C_{184}N_{62}H_{432}$	3513.9	32	204	204	4282	5.2×10^{-15}
5	$C_{372}N_{126}H_{880}$	7198.1	64	200	200	3868	5.5×10^{-16}

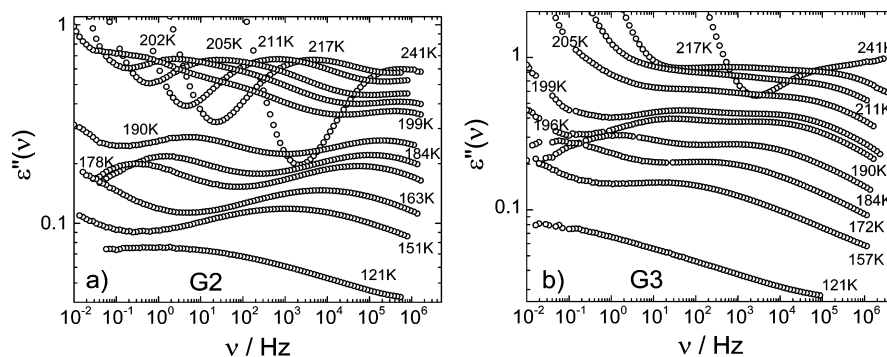


Figure 2. (a) Dielectric spectra of PPI dendrimer G2 as measured for temperatures 121 to 241 K as indicated. (b) Analogous spectra of PPI dendrimer G3 from 121 to 241 K.

cycling was applied for collecting the solid-echo spectra with a pulse delay of 10 μ s. The home-built ^2H NMR probe was cooled by liquid nitrogen with a CryoVac Konti cryostat and an Oxford ITC-503 temperature controller with temperature accuracy better than ± 1 K and temperature stability better than ± 0.2 K.

2.4. Field Cycling ^1H NMR. The spin–lattice relaxation time T_1 describes the recovery of the nuclear magnetization toward its equilibrium value. Its frequency dependence can be studied by applying the FC technique where the external magnetic field is switched between a variable relaxation field B and a constant detection field.¹⁸ The angular frequency is given by the Larmor frequency $\omega = \gamma B$, where γ denotes the gyromagnetic ratio. Usually, T_1 reflects intra- and intermolecular relaxations contributions, and the measured rate $R_1 = 1/T_1$ is given by $R_1(\omega) = R_1^{\text{intra}}(\omega) + R_1^{\text{inter}}(\omega)$.^{18,37} The role of the two relaxation paths was elucidated by not only measuring the fully protonated system but also the dendrimer with the protons at the amine groups exchanged by deuterons used for the ^2H NMR experiments (cf. above).

Rewriting the Bloembergen–Purcell–Pound (BPP) expression in the susceptibility representation yields^{29–33,37}

$$\omega R_1(\omega) = C[\chi''(\omega) + 2\chi''(2\omega)] \equiv 3C\omega J_{\text{NMR}}(\omega) = 3C\chi''_{\text{NMR}}(\omega) \quad (5)$$

where $\chi''(\omega) = \omega J(\omega)$ is the susceptibility with the spectral density $J(\omega)$, and C denotes the coupling constant of the magnetic dipole–dipole interaction. In the case of intramolecular relaxation $J(\omega)$ is given by the Fourier transform of the rank-two reorientational correlation function $C_2(t)$ of a dendrimer segment, more precisely of the internuclear vectors of the proton spin pairs in the segment. Although $\chi''_{\text{NMR}}(\omega)$ and $J_{\text{NMR}}(\omega)$ are actually weighted sums, in the case of a broad distribution of correlation times, both quantities are essentially indistinguishable on logarithmic scales from $\chi''(\omega)$ and $J(\omega)$, respectively, besides the factor of 3.

As said, the actually measured relaxation rate contains both intra- and intermolecular contributions and follows a similar equation like eq 5. Thus, the spectral density splits up into two parts. While the intra part reflects segmental reorientation, the inter part probes translational motion. The correlation functions $C_2(t)$ and $C_{\text{trans}}(t)$ exhibit quite different long-time behavior. While $C_2(t)$ decays stretched exponentially for long times, $C_{\text{trans}}(t)$ follows a power law $t^{-3/2}$ reflecting Fickian diffusion and therefore will always dominate the total correlation function in the limit of long times.^{38–40} Thus, at low frequencies the relaxation dispersion $R_1(\omega)$ follows a square root law, explicitly

$$R_1(\omega) = R_1^{\text{intra}}(\omega) + R_1^{\text{inter}}(\omega) = R_1(0) - \frac{B}{D^{3/2}}\sqrt{\omega} \quad (6)$$

with

$$B = \frac{\pi}{30}(1 + 4\sqrt{2})\left(\frac{\mu_0}{4\pi}\hbar\gamma_{\text{H}}^2\right)^2 n_s$$

and the spin density $n_s = 7.3 \times 10^{28} \text{ m}^{-3}$ in the case of the dendrimers. This relation was recently exploited to determine the diffusion coefficient $D(T)$ in simple liquids⁴⁰ as well as in polymers,⁴¹ and it will be employed here to estimate the $D(T, M)$ of the PPI dendrimers.

As a large temperature range is covered, local segment dynamics as well as dendrimer specific dynamics are probed and one is able to construct master curves $\chi''_{\text{NMR}}(\omega\tau_\alpha)$ extending over many decades in time by assuming frequency–temperature superposition (FTS). Specifically, the individual data sets measured at different temperatures are shifted solely horizontally to obtain best overlap.^{30–33} The master curves $\chi''_{\text{NMR}}(\omega\tau_\alpha)$ thus combine $R_1(\omega)$ results from a broad temperature range and yield “isofrictional” spectra which allow comparing the results for different dendrimer generations. As the high-frequency part reflects the α -dynamics, which is interpolated by a Cole–Davidson function, the construction of the master curves provides the time constants $\tau_\alpha(T)$.^{29–33} For simple liquids, no spectral contribution at $\omega\tau_\alpha < 1$ in excess to the Debye behavior $\chi''(\omega) \propto \omega^{-1}$ is observed except for some weak intermolecular contributions. Any additional low-frequency relaxation thus reflects dendrimer specific dynamics.

The dispersion of the spin–lattice relaxation time T_1 was monitored by a STELAR FFC 2000 relaxometer, which allows measurements in the temperature range 160–420 K and in (Larmor) frequency range 10 kHz $\leq \nu \leq 20$ MHz.^{18,30} The accuracy and stability of the temperature measurements are typically ± 1 K. Concerning G4 and G5 the $T_1(\omega)$ measurements performed in Bayreuth were complemented by two data sets obtained at the Technical University of Darmstadt. There, a home-built relaxometer allows for extremely low frequencies via active field stabilization and stray field compensation.²⁸ The lower limit is 200 Hz being well below the limitations of the STELAR machine and even below the earth’s magnetic field. This gives access to extremely slow dendrimer dynamics.

The magnetization curves for all dendrimers investigated feature a monoexponential decay at $T < 300$ K. With temperature growing the decay curves develop an increasingly stretched form which is well describable by a stretched exponential function $\propto \exp[-(t/T_1^K)^\beta]$. The

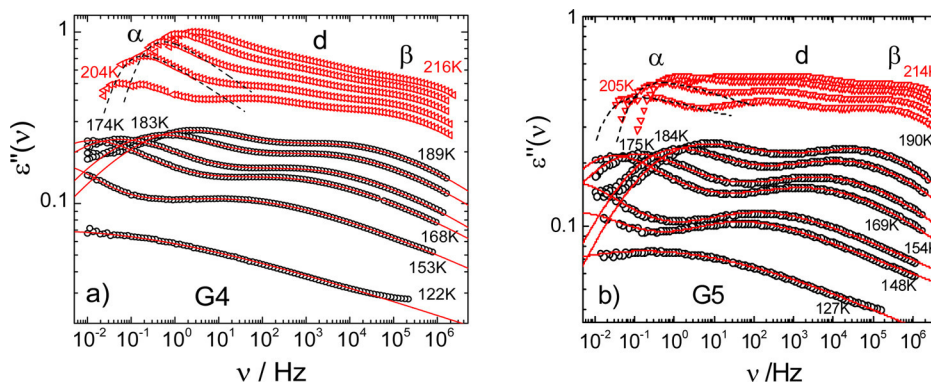


Figure 3. Dielectric loss after subtracting the dc conductivity contribution of PPI dendrimer G4 (a) and G5 (b); red triangles: $T > T_g$ in 3 K steps; black circles: $T < T_g$ (selected data); solid red lines: fits by a sum of two subspectra along eq 2 corresponding to d - and β -processes; dashed black lines: Cole–Davidson fits of the α -relaxation.

(mean) relaxation time follows from $\langle T_1 \rangle = T_1^k \beta^{-1} \Gamma(\beta^{-1})$ which is generally used in this work. The stretching parameter decreases only slightly between $\beta = 1$ at low temperatures and $\beta \approx 0.8$ at $T \approx 400$ K.

3. RESULTS

3.1. Dielectric Spectra. Figure 2 shows dielectric spectra as measured at different temperatures for the generation G2 and G3 of the PPI dendrimer. In Figure 11 we display the corresponding spectra of G4 and G5. Three rather broad and barely separated relaxation processes are recognized at high temperatures. The relaxation peak at lowest frequencies is partly covered by a dc conductivity contribution, most obviously for G3, G4, and G5 (cf. Figures 11 and 12). With decreasing temperature the low-frequency peak leaves the acquisition window and the other two relaxations become better resolved while shifting to lower frequencies. In addition, below T_g their amplitudes appear to decrease and their widths to broaden. This is typical for secondary processes in molecular glasses.⁴² Figure 3 shows the DS spectra of G4 and G5 after subtracting the dc contribution (see Figure 12). Above T_g (data marked in red) the three relaxation processes can be distinguished. Inspecting also the corresponding spectra of G2 (Figure 2) and G3 (Figure 12), one can conclude that relaxation patterns are rather similar for all generations: PPI dendrimers show three relaxation processes which we call, for reasons becoming clear below, α , d (d for dendrimer), and β , according to the order of their appearance in the DS frequency window upon cooling. At lowest temperatures only the β -relaxation can be probed in the given frequency window.

In order to extract time constants for α , d , and β -relaxation, we take the estimate $\tau_i = 1/(2\pi\nu_{\max})$. The results for all generations are shown in Figure 4. Close to T_g (measured by DSC, cf. Table 1) the segmental time constant $\tau_\alpha(T)$ exhibits a strong temperature dependence and reaches values of the order of seconds. This is typical of the structural relaxation (α -process) in supercooled liquids or polymer melts and justifies this assignment. Moreover, the time constants fit well to the high-temperature data compiled by the NMR techniques (cf. below) included in Figure 4. Considering all data the temperature dependence is describable by a Vogel–Fulcher–Tammann (VFT) law. Because of quite similar T_g the different $\tau_\alpha(T)$ almost coincide around 200 K. In Table 1, T_g values obtained via the condition $T_g = T(\tau_\alpha = 100 \text{ s})$ are compared to those from DSC experiments; very good agreement is found. We note that also the dc conductivity $\sigma(T)$ extracted from the original data

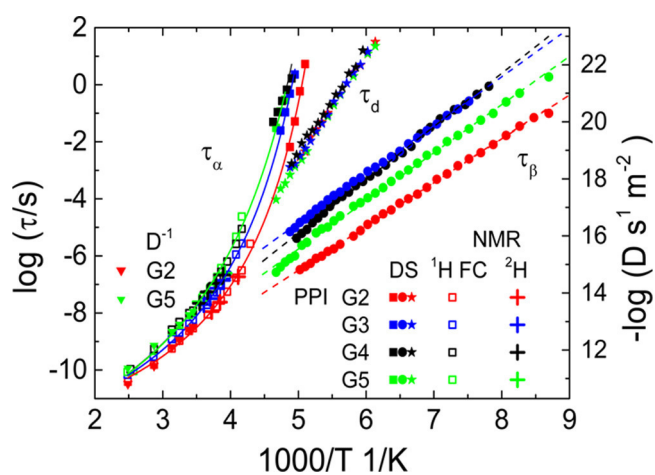


Figure 4. Time constants of the PPI dendrimers for the different relaxations identified by the different techniques. Structural relaxation times τ_α : dielectric spectroscopy (DS, filled squares), FC ^1H NMR (open squares), solid-state ^2H NMR (crosses). Time constants τ_d and τ_β of the d - and the β -process as provided by DS (stars and circles, respectively); the color code for the generations is given in the legend. Solid lines: VFT interpolations for $\tau_\alpha(T)$; dashed lines: Arrhenius fits for d - and β -process. Triangles: diffusion coefficient $D(T)^{-1}$ referred to the right ordinate.

exhibits a temperature dependence similar to that of $\tau_\alpha(T)$. Usually, dc conduction in molecular liquids or polymers originates from diffusion of ionic impurities. Thus, conductivity is coupled to the viscosity of the host. Concerning the stretching parameter of the α -relaxation, we find a value $\beta_{\text{CD}} = 0.3$ when applying a Cole–Davidson function.⁴³

The other two relaxations (d and β) show an Arrhenius temperature dependence of their time constants characteristic for secondary processes in glasses ($T < T_g$) (cf. Figure 4). The d -relaxation displays a time constant which is virtually independent of the number of generations while that of the β -relaxation shows some differences. Yet, no systematic trend can be identified. The Arrhenius law for the d -process yields a rather high activation energy $E_A/R = 8520 \text{ K}$ ($E_A/RT_g \cong 42$) and an attempt time $\tau_\infty = 5.3 \times 10^{-22} \text{ s}$, which is exceptionally low. Regarding the β -process, E_A and τ_∞ are listed in Table 1. Its activation energy is found in the range $18 < E_A/RT_g < 21$. The corresponding τ_∞ values range within $5 \times 10^{-16} - 2 \times 10^{-14} \text{ s}$, which is typical for β -processes in glasses.⁴²

Below T_g a quantitative interpolation of the DS spectra is possible using the distribution $G(\ln \tau)$ defined in eq 2. The asymmetry parameter b was kept constant. The corresponding fits are included in Figure 3 and well reproduce the spectra. As demonstrated in Figure 5, the parameter ab of the β -process

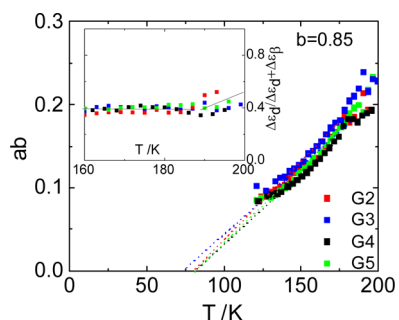


Figure 5. Temperature dependence of the spectral shape parameter ab (cf. eq 2) of the β -process; asymmetry parameter b is kept constant. Inset: temperature dependence of the dielectric strength of the d -process with respect to that of the sum of both β - and d -processes.

decreases essentially linearly upon cooling, which is the typical trend of a β -process in glasses,⁴² while the parameter ab of the d -process is temperature-independent for all generations. Thus, this relaxation is atypical. In order to illustrate directly the spectral changes of the secondary relaxations, we display in Figure 13a rescaled spectra of G2, for which $\epsilon''(\omega)/\epsilon''_{d,\max}$ is plotted versus $\nu/\nu_{d,\max}$ with $\epsilon''_{d,\max}$ and $\nu_{d,\max}$ denoting the height and frequency of the d -relaxation peak, respectively. Figure 13b shows the analogous scaling for the β -process. It is apparent that FTS applies for the d -process while the β -relaxation broadens upon cooling, so FTS does not hold for the latter. Finally, the inset of Figure 5 displays the temperature dependence of the relative dielectric strength of the d -process. The ratio does not change and is temperature independent below T_g while it tends to increase above T_g .

3.2. Solid-State NMR. Figure 6 shows the ^2H NMR spectra for all the generations of PPI dendrimers beginning with G2 in the left column to G5 in the right column in a temperature range from 110 to 240 K. The temperature at which the spectra were

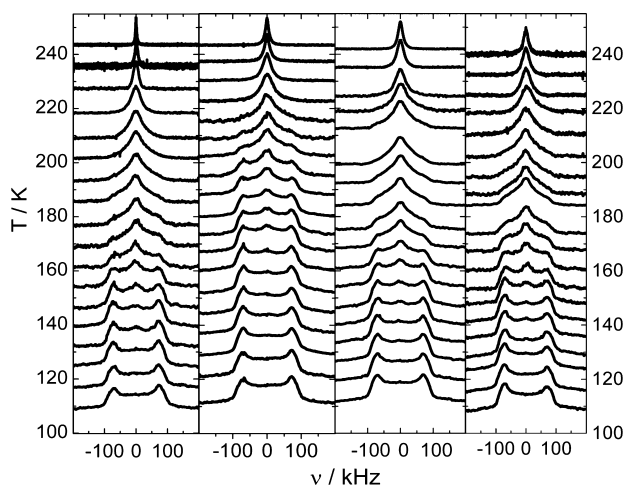


Figure 6. ^2H NMR spectra for generation G2 to G5 (from left to right). The baseline of each spectrum indicates the temperature at which the spectrum was measured.

measured is given by the baseline of the spectra. At lowest temperatures a typical Pake spectrum with a small asymmetry parameter $\eta \approx 0.15$ is observed for all G (cf. Figure 7). At highest temperatures a Lorentzian line shows up characteristic of fast isotropic (liquid-like) reorientation. In between features of spectra with an anisotropy parameter close to one are discovered, indicating fast 180° two-site jumps of the ND_2 groups according to their symmetry. Concerning the transition to the liquid line the spectra of different G essentially agree. Thus, the liquid dynamics do not significantly change, in agreement with very similar T_g values (cf. Table 1). Yet, some differences are observed for the transition from the low-temperature Pake spectrum to the motionally averaged spectrum of the fast amine group jumps.

In order to quantitatively describe the solid-state spectra ($T \leq 180$ K), a weighted superposition of two subspectra, namely a Pake spectrum and a motionally averaged spectrum due to the fast jumps of the amine group, is assumed. Examples of calculated spectra are shown in Figure 7. An angle of 104° between the two ND_2 bond directions has to be assumed to reproduce the experimental subspectrum with the motion-averaged anisotropy parameter $\bar{\eta} \approx 0.92$. The large temperature range 120–180 K (G2, G4, G5) (130–190 K for G3) in which the spectra must be described by a superposition of the two subspectra indicates dynamical heterogeneities regarding the two-site jump of the ND_2 group. In other words, the jump process, actually taking place also below T_g , is determined by a broad distribution of jump times. This behavior is typical of glasses that exhibit static density fluctuations.^{44,45} Figure 7 shows such a “two-phase” spectrum for G2 at 153.9 K and a fit with a superposition of a 50% solid state spectrum and a 50% motionally averaged spectrum due to the ND_2 jumps. At higher temperatures (180–210 K for G2, G4, G5; 190–220 K for G3) the solid-state line collapses to a liquid-like Lorentzian line. The width $\Delta\nu$ of the Lorentzian line at high temperatures is taken to estimate the time constant of the α -process (cf. Experimental Section). The extracted time constants $\tau_\alpha(T)$ fit well to those from FC ^1H NMR as is shown in Figure 4.

3.3. Field-Cycling ^1H NMR. Figure 8a shows typical relaxation rates $R_1(\omega) = 1/T_1(\omega)$ for the PPI dendrimer G5 as a function of frequency $\nu = \omega/2\pi$. For all temperatures one recognizes pronounced dispersion, becoming stronger at low temperatures where the local dynamics determines the relaxation. At $T = 393$ K the measurements for G4 and G5 were extended to lower frequencies by applying a home-built spectrometer which covers significantly lower frequencies (cf. Experimental Section). As described, the relaxation rates are transformed into the susceptibility representation via $\omega/T_1 = \chi''(\omega)$. Then master curves $\chi''_{\text{NMR}}(\omega\tau_\alpha)$ are constructed by applying FTS which collapses different data sets collected at several temperatures in the range 220–400 K.³² The resulting master curves for G2–G5 are shown in Figure 8b and can be characterized by three relaxation regimes. At frequencies around the relaxation maximum ($\omega\tau_\alpha \cong 1$) the glass transition determines the segmental relaxation. Here, by construction, all master curves agree. In the regime $\omega\tau_\alpha \ll 1$ excess relaxation is observed when compared to the susceptibility of a low- M liquid (oligo-butadiene $M = 460$ g/mol,³⁰ cf. Figure 8b) which does not exhibit any polymer dynamics. The excess relaxation becomes more pronounced with growing generation number G . It can be specified by a power law ω^α with an apparent exponent α weakly changing from 0.87 (G2) to 0.76 (G5). At even lower frequencies the curves turn back to a behavior with an exponent very close to one. This is typical for the terminal relaxation. The $\chi''_{\text{NMR}}(\omega\tau_\alpha)$

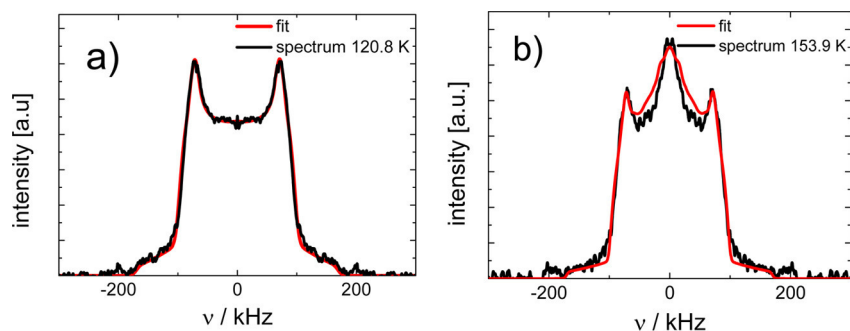


Figure 7. Examples of ^2H NMR spectra (symmetrized) fitted to a “two-phase” model. (a) Spectrum of PPI dendrimer G3 at $T = 120.8$ K (black line) and fit with a solid-state spectrum with $\eta = 0.15$ (red line). (b) Spectrum of G2 at $T = 153.9$ K (black line) and fit (red line) with a superposition of a 50% solid-state and 50% motionally averaged spectrum ($\eta \approx 0.9$).

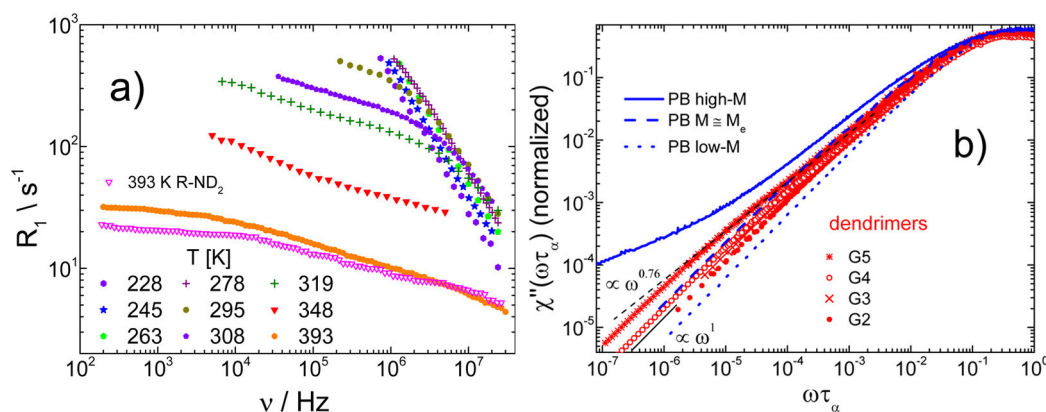


Figure 8. (a) Spin–lattice relaxation rate $R_1(\nu)$ of the fully protonated dendrimer G5 as a function of frequency ν , obtained by FC ^1H NMR; in addition, at $T = 393$ K data for the end group-deuterated dendrimer G5. (b) Normalized (by area) susceptibility master curves of the (fully protonated) PPI dendrimers of different generations; for comparison master curves of polybutadiene for $M = 460$ g/mol (simple liquid, dotted blue line), $M = 2000$ g/mol $\approx M_e$ (unentangled, dashed blue line), and for $M = 87\,000$ g/mol (entangled, blue line) are shown.

curves show some similarity with the FC ^1H NMR results for unentangled (linear) polymers like polybutadiene (PB, $M = 2000$ g/mol,³³ data included in Figure 8b), i.e., PB with M below the entanglement molar mass M_e . However, high- M (entangled) PB³³ displays a quite different behavior (PB, $M = 87$ kg/mol $\gg M_e$, data included in Figure 8b). In the latter case a second power-law regime with an even lower exponent is recognized at lowest frequencies, a finding which is typical for entanglement polymer dynamics.³³ This second power-law is absent for the dendrimers; that is, they do not show entanglement effects, a fact well-known from rheological studies.⁷ Upon constructing the master curves $\chi''_{\text{NMR}}(\omega\tau_\alpha)$ the time constants $\tau_\alpha = \tau_\alpha(T)$ are obtained and included in Figure 4. They well extend the data sets from DS to high temperatures and also agree perfectly with those from solid-state ^2H NMR.

As discussed in the Experimental Section, performing ^1H NMR always raises the question to what extent the spin–lattice relaxation is actually determined by the intramolecular reorientation-mediated relaxation and whether there is some significant contribution from intermolecular relaxation reflecting also translational diffusion. In order to address this question, we compare in Figure 9 the FC ^1H susceptibility master curves for the fully and the partially deuterated dendrimer G5 (original $R_1(\omega)$ data is shown in Figure 8a). Indeed, differences are observed, in particular at low frequencies; the susceptibility of the end group deuterated dendrimer is reduced due to the suppression of some of the intermolecular relaxation contributions. Thus, the relaxation rate of the fully protonated samples

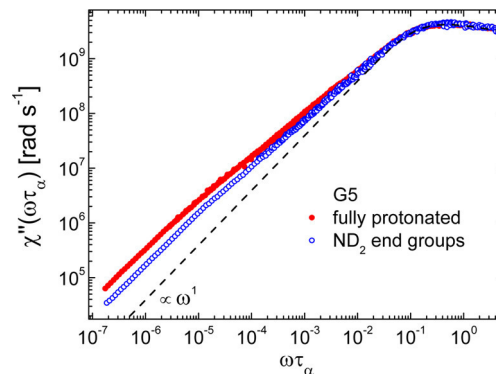


Figure 9. Comparing the FC ^1H NMR susceptibility master curve for fully and end group deuterated dendrimer G5. Dashed line: simple liquid (Debye) limit.

contains a significant intermolecular contribution. This can be exploited to estimate the diffusion coefficient $D(T, M)$ for the different generations along eq 6.

Figure 10 presents the relaxation rates measured at the highest temperature $T = 393$ K as a function of the square root of angular frequency. At the lowest frequencies a linear behavior is observed from which $D(M)$ is extracted when inserting the spin density $n_s = 7.3 \times 10^{28} \text{ m}^{-3}$ in eq 6. The latter is calculated from the molecular structure and mass density $\rho \approx 1 \text{ g cm}^{-3}$ (from the supplier) and only slightly depends on G . The inset of Figure 10 shows the change of D with M . We find $D(M) \propto M^{-1.2 \pm 0.2}$ (cf.

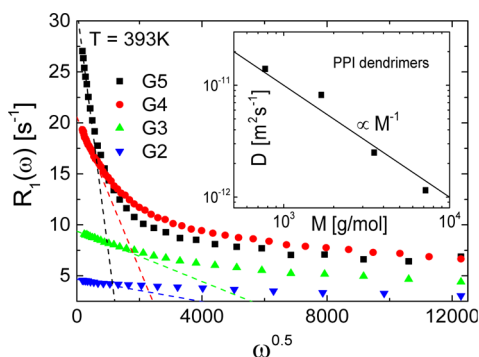


Figure 10. Spin–lattice rate $R_1(\omega)$ at 393 K as a function of the square root of angular frequency. The slope of the linear part at lowest frequencies (dashed line) yields the diffusion coefficient D (cf. eq 6). Inset: D as a function of M with corresponding power-law fit.

inset). This result will be reconsidered in the Discussion. The temperature dependence of D closely follows, as expected, that of the reciprocal segmental time $1/\tau_\alpha(T)$ (see Figure 4).

4. DISCUSSION

The dynamics of PPI dendrimers is investigated by several techniques addressing segmental (“local”) and polymer specific (“collective”) dynamics. Concerning the local dynamics, as revealed by DS and ^2H NMR, the dendrimers show features well-known from amorphous polymers and molecular glass-formers.^{42,46} The main (structural or α -) relaxation only weakly changes with generation and follows a super-Arrhenius temperature dependence. Correspondingly, T_g is virtually independent of G , in agreement with previous studies,⁸ but in contrast to other dendritic macromolecules.⁴⁷ The spectral width of the α -process is broad but similar to polymers.⁴⁸ Yet, some influence of heterogeneous dynamics within the dendrimers reflecting different mobilities in different “shells”, as documented by NMR studies^{23–26} as well as theoretical work,^{5,16,17} may additionally broaden the α -relaxation. This fact may also explain the weak nonexponential relaxation observed in the present study, yet most of the dynamic heterogeneities are averaged out due to spin diffusion in the present case of ^1H NMR. Secondary relaxations occur, which appear to merge with the structural relaxation above T_g . Below T_g their time constants follow an Arrhenius law. One of the secondary relaxations (d -process) displays time constants that virtually do not change with G and its spectral shape does not change with temperature. In addition, the attempt frequency is unphysically high. A temperature-independent spectral shape of the relaxation is usually found

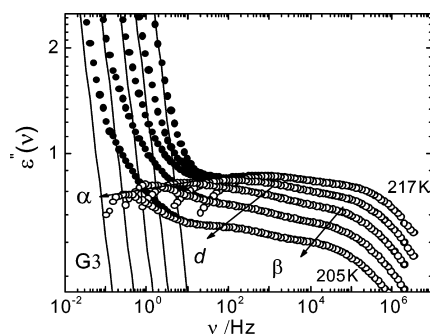


Figure 12. Dielectric spectra of PPI dendrimer G3 (filled symbols) for temperatures $T = 217, 214, 211, 208,$ and 205 K. Lines: dc conductivity contribution. Open symbols: susceptibility after subtracting the conductivity contribution.

for cooperative processes like the α -process.⁴⁶ Thus, we may speculate whether the d -process is of cooperative nature and reflects internal motion of the dendrimers which still can proceed in the structurally frozen state, i.e., below T_g . As proven by ^2H NMR, the amine end groups undergo a two-site jump governed by a broad distribution of jump times reflecting (static) density fluctuations in the glass state.^{44,45} The latter process is not probed by DS as the dipole moment does not change by a 180° jump. We plan to run ^2H NMR experiments on PPI dendrimers deuterated only in the core. Then the amine group reorientation will not obscure the ^2H spectral features characteristic of main and secondary relaxations.

The other secondary process displays features typical of a β -process (also Johari–Goldstein process) in amorphous systems.⁴² Although there are conflicting interpretations of its nature,⁴⁹ according to ^2H NMR investigations in molecular glasses ($T < T_g$) it is attributed to small-angle displacements of the segments, and a wobbling-on-a-cone model reproduces the salient NMR findings.^{50,51} Secondary processes in dendrimers were also reported by other research groups.^{11,12} For example, a quite similar relaxation scenario with an α -process and two secondary relaxations virtually not changing with generation was found in PAMAM dendrimers.¹² Also, hyperbranched polymers show a relaxation time map highly resembling that of the present PPI dendrimers, in particular, also two secondary relaxations are observed.^{52–54}

The collective polymer dynamics, in addition to local dynamics, are revealed by FC ^1H NMR ($T > T_g$). Here we note that the collective dynamics are not probed by dielectric measurements since already the local segmental dynamics (α -process) leads to a complete loss of the correlation as is the case

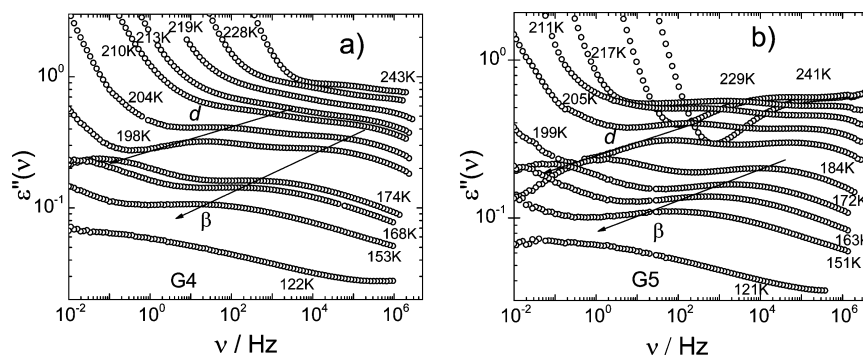


Figure 11. Dielectric spectra of PPI dendrimer G4 (a) and G5 (b) including the dc conductivity masking the structural relaxation (α -process).

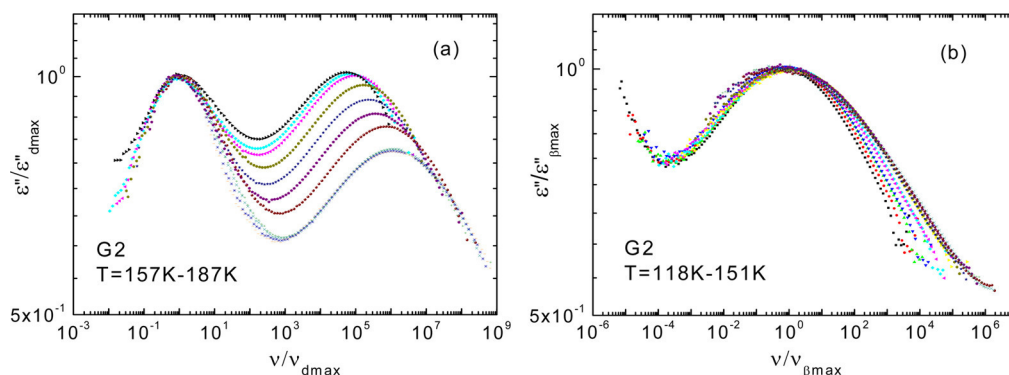


Figure 13. (a) Rescaled dielectric spectra of PPI dendrimer G2; dielectric permittivity ϵ'' is rescaled by maximum height $\epsilon''_{d,\max}$ and frequency ν by $\nu_{d,\max}$ of the d -relaxation peak in a temperature range $T = 157$ – 187 K. (b) Dielectric data are rescaled with respect to the β -relaxation peak in $T = 118$ – 151 K.

of so-called type B polymers (Stockmayer notation⁵⁵). Frequency–temperature superposition works well and susceptibility master curves $\chi''(\omega\tau_\alpha)$ extending over 9 decades in (reduced) frequency are obtained. Clear evidence of additional dynamics much slower than the local dynamics is found. The construction of the master curves provides $\tau_\alpha(T)$ which complements the data from dielectric spectroscopy and ²H NMR; summarized, 12 decades in $\tau_\alpha(T)$ are covered. Between the local dynamics (α -process) and the terminal relaxation time τ_t of the collective dynamics an intermediate relaxation regime can be approximated by a power-law with an exponent around 0.8 depending weakly, yet systematically on G . When compared with results for linear polymers, some resemblance with Rouse dynamics is recognized. Entanglement can be excluded, a fact well-known also from rheological studies.⁷ The FC ¹H NMR susceptibility also shows some features that were recently reported by theory¹⁴ as well as simulations.^{5,13–17} Yet, quantitative comparison is not possible since no fully realistic models were considered. Qualitatively, local dynamics at high, breathing modes at intermediate, and overall tumbling and diffusion of the whole dendrimer molecule at low frequencies can be distinguished in accordance with our experimental findings.

Exploiting the universal low-frequency dispersion law, the diffusion coefficient $D(M)$ is estimated from the low-frequency relaxation rate $R_1(\omega)$, a relation $D(M) \propto M^{-1.2 \pm 0.2}$ is found. Of course, having only four generations at hand the change with M is small, and the extracted exponent should be taken with caution. Nevertheless, to our knowledge this is the first report of $D(M)$ for bulk PPI dendrimers. We note that our approach extracting D from the low-frequency dispersion of T_1 was recently applied for linear polymers⁴¹ as well as simple liquids,⁴⁰ and good agreement with field gradient NMR was found. Again, attempting to understand the M dependence appears somewhat speculative as only five generations of PPI generations can be synthesized. Nevertheless, we want to propose some scaling arguments, the details of which will be discussed in a forthcoming publication. They are meant to provide a semiquantitative understanding. In any case, the rheological behavior of dendrimers certainly depends on details of their structure.

In first approximation, a dendrimer can be considered as a viscoelastic ball with constant density and a radius scaling as $R \propto N^{1/3}$ with N denoting the number of segments. In a coordinate system fixed within the dendrimer any segment has a well-defined average position \vec{r} with respect to which thermal fluctuations lead to a displacement $\vec{u}(\vec{r};t)$. The vector $\vec{u}(\vec{r};t)$ satisfies a diffusion equation with adequate boundary conditions and a diffusion coefficient D_α being on the order of the segmental

diffusion coefficient. The thus derived (longest) relaxation time of such breathing modes scales as $\tau_{\text{breath}} \propto R^2/D_\alpha \propto N^{2/3}$ with $\tau_\alpha \ll \tau_{\text{breath}} \ll \tau_t$. In order to estimate the longest relaxation connected with translational diffusion, the friction coefficient of a (large) dendrimer with its environment is assumed to be proportional to the number f of surface segments for N going to ∞ , i.e., $f \propto R^2 \propto N^{2/3}$. Hence, self-diffusion scales as $D \propto (k_B T/f) \propto D_\alpha N^{-2/3} \propto (b^2/\tau_\alpha) N^{-2/3}$, where b is a characteristic segment length. Hence, the time during which the dendrimer diffuses over a distance of about its linear size will scale as $\tau_{\text{trans}} \propto (R^2/D) \propto \tau_\alpha N^{4/3}$. Regarding rotation the same M scaling is expected within this model. The spin–lattice relaxation at $\omega\tau_\alpha \leq 1$ is determined by these three types of motions. It appears that the breathing time τ_{breath} cannot be resolved from the experimental susceptibility (cf. Figure 9); only an intermediate power-law regime is found. Yet, in any case, the low-frequency part of spin–lattice relaxation is determined by translations and rotations of the entire dendrimer molecule. Given this coarse-grained description for $D(M)$, the actually observed M dependence $D(M) \propto M^{-1.2 \pm 0.2}$ can be explained by finite size effects due to the rather small M range investigated. In addition, for these small molar masses the extent of penetration is large, i.e., comparable with the radius, which will increase the exponent of $D(M)$. Qualitatively, our mathematically simple model may be regarded as continuous limit of the discrete viscoelastic models recently proposed.^{5,13–17} Its advantage is that it takes into account excluded volume interactions between the dendrimer's arms.

5. CONCLUSIONS

We investigated bulk PPI dendrimers of generation (G) 2–5 by dielectric spectroscopy (DS), solid-state ²H NMR, and field-cycling (FC) ¹H NMR relaxometry in a large temperature range of 120–400 K, above and below the glass transition temperature $T_g = 200$ K. Three relaxation processes are identified by DS; a main (α -) relaxation ($T > T_g$) and two secondary processes ($T < T_g$). The α -process exhibits a super-Arrhenius temperature dependence typical of glass-forming liquids. The secondary relaxations are governed by an Arrhenius temperature law. While one secondary process exhibits features characteristic of a β -process in amorphous systems, the other one is atypical and thus possibly specific to dendrimers. Its spectral width does not vary with temperature and exhibits time constants independent of G . Regarding FC ¹H NMR probing the dispersion of the spin–lattice relaxation rate $R_1(\omega)$, applying susceptibility representation, $\chi''(\omega) \equiv \omega R_1(\omega)$, and frequency–temperature superposition a large effective frequency range is covered by the master curve $\chi''(\omega\tau_\alpha)$. Its construction yields $\tau_\alpha(T)$; thereby, together

with results from DS, 12 decades in $\tau_\alpha(T)$ are covered. The obtained master curve $\chi''(\omega\tau_\alpha)$ provides evidence of dynamics much slower than the local dynamics. An intermediate power-law regime is identified which covers the frequency range between the terminal relaxation and local relaxation. In accordance with theoretical models and computer simulations reported in the literature, we identify three processes: local reorientations at high, breathing modes at intermediate, and overall tumbling of the dendrimer at low frequencies. Estimating the diffusion coefficient $D(M)$ from the universal low-frequency dispersion law of $R_1(\omega)$, the $D(M) \propto M^{1.2 \pm 0.2}$ is found. Discussing some scaling arguments, we derive $D(M) \propto M^{-2/3}$. This deviation may be connected to the relatively small range of molar masses that can be investigated in the case of PPI dendrimers.

AUTHOR INFORMATION

Corresponding Author

*E-mail: ernst.roessler@uni-bayreuth.de (E.A.R.).

Notes

The authors declare no competing financial interest.

ACKNOWLEDGMENTS

The authors are indebted to F. Fujara and B. Kresse (Technical University Darmstadt) for giving the opportunity to measure the $R_1(\omega)$ dispersion at extremely low frequencies. We also thank Maxim Dolgushev (University of Freiburg) for providing unpublished results where he shows the relevance of intermolecular relaxation contribution. Financial support by Deutsche Forschungsgemeinschaft (DFG) through grant RO 907/17 is appreciated.

REFERENCES

- (1) Bosman, A. W.; Janssen, H. M.; Meijer, E. W. *Chem. Rev.* **1999**, *99*, 1665.
- (2) Jean, M. J.; Fréchet, D. A. T. *Dendrimers and Other Dendritic Polymers*; John Wiley & Sons, Ltd.: New York, 2002.
- (3) Ballauff, M.; Likos, Ch. N. *Angew. Chem., Int. Ed.* **2004**, *43*, 2998.
- (4) Karatasos, K. *Macromolecules* **2006**, *39*, 4619.
- (5) Markelov, D. A.; Lyulin, S. V.; Gotlib, Y. Y.; Lyulin, A. V.; Matveev, V. V.; Lahderanta, E.; Darinskii, A. A. *J. Chem. Phys.* **2009**, *130*, 044907.
- (6) Zacharopoulos, N.; Economou, L. G. *Macromolecules* **2002**, *35*, 1814.
- (7) Uppuluri, S.; Morrison, F. A.; Dvornic, P. R. *Macromolecules* **2000**, *33*, 2551.
- (8) Tande, B. M.; Wagner, N. J.; Kim, Y. H. *Macromolecules* **2003**, *36*, 4619.
- (9) Götze, I. O.; Likos, C. N. *Macromolecules* **2003**, *36*, 8189.
- (10) Doi, M.; Edwards, S. F. *The Theory of Polymer Dynamics*; Oxford Science Publications: Oxford, 1986.
- (11) Trahasch, B.; Stühn, B.; Frey, H.; Lorenz, K. *Macromolecules* **1999**, *32*, 1962.
- (12) Mijovic, J.; Ristic, S.; Kenny, J. *Macromolecules* **2007**, *40*, 5212.
- (13) Gotlib, Y. Y.; Markelov, D. A. *Polym. Sci., Ser. A* **2007**, *49*, 1137.
- (14) Markelov, D. A.; Lahderanta, E.; Gotlib, Y. Y. *Macromol. Theory Simul.* **2010**, *19*, 158.
- (15) Dolgushev, M.; Berezovska, G.; Blumen, A. *Macromol. Theory Simul.* **2011**, *20*, 621.
- (16) Kumar, A.; Biswas, P. *Phys. Chem. Chem. Phys.* **2013**, *15*, 20294.
- (17) Markelov, D. A.; Dolgushev, M.; Gotlib, Y. Y.; Blumen, A. *J. Chem. Phys.* **2014**, *140*, 244904.
- (18) Kimmich, R.; Anardo, E. *Prog. Nucl. Magn. Reson. Spectrosc.* **2004**, *44*, 257.
- (19) Kruk, D.; Herrmann, A.; Rössler, E. A. *Prog. Nucl. Magn. Reson. Spectrosc.* **2012**, *63*, 33.
- (20) Kimmich, R. *Principles of Soft-Matter Dynamics*; Springer: Berlin, 2012.
- (21) Meier, R.; Kruk, D.; Rössler, E. A. *ChemPhysChem* **2013**, *14*, 3071.
- (22) Fujara, F.; Kruk, D.; Privalov, A. F. *Prog. Nucl. Magn. Reson. Spectrosc.* **2014**, *82*, 39.
- (23) Meltzer, A. D.; Tirrell, D. A.; Jones, A. A.; Inglefield, P. T.; Hedstrand, D. M.; Tomalia, D. A. *Macromolecules* **1992**, *25*, 4541.
- (24) Meltzer, A. D.; Tirrell, D. A.; Jones, A. A.; Inglefield, P. T. *Macromolecules* **1992**, *25*, 4549.
- (25) Malveau, C.; Baille, W. E.; Zhu, X. X.; Ford, W. T. *J. Polym. Sci., Part B: Polym. Phys.* **2003**, *41*, 2969.
- (26) Pinto, L. F.; Correa, J.; Martin-Pastor, M.; Riguera, R.; Fernandez-Megia, E. *J. Am. Chem. Soc.* **2013**, *135*, 1972.
- (27) Rubinstein, M.; Colby, R. H. *Polymer Physics*; Oxford University Press: New York, 2003.
- (28) Kresse, B.; Privalov, A. F.; Herrmann, A.; Hofmann, M.; Rössler, E. A.; Fujara, F. *Solid State Nucl. Magn. Reson.* **2014**, *59*, 45.
- (29) Kariyo, S.; Gainaru, C.; Schick, H.; Brodin, A.; Novikov, V. N.; Rössler, E. A. *Phys. Rev. Lett.* **2006**, *97*, 207803.
- (30) Kariyo, S.; Brodin, A.; Gainaru, C.; Herrmann, A.; Schick, H.; Novikov, V. N.; Rössler, E. A. *Macromolecules* **2008**, *41*, 5313.
- (31) Herrmann, A.; Kariyo, S.; Abou Elfadl, A.; Meier, R.; Gmeiner, J.; Novikov, V. N.; Rössler, E. A. *Macromolecules* **2009**, *42*, 5236.
- (32) Hofmann, M.; Herrmann, A.; Abou Elfadl, A.; Kruk, D.; Wohlfahrt, M.; Rössler, E. A. *Macromolecules* **2012**, *45*, 2390.
- (33) Herrmann, A.; Kresse, B.; Gmeiner, J.; Privalov, A. F.; Kruk, D.; Fujara, F.; Rössler, E. A. *Macromolecules* **2012**, *45*, 1408.
- (34) Wagner, H.; Richert, R. *J. Phys. Chem. B* **1999**, *103*, 4071.
- (35) Blochowicz, T.; Gainaru, C.; Medick, P.; Tschirwitz, C.; Rössler, E. A. *J. Chem. Phys.* **2006**, *124*, 134503.
- (36) Spiess, H. W.; Sillescu, H. *J. Magn. Reson.* **1981**, *42*, 381.
- (37) Abragam, A. *The Principles of Nuclear Magnetism*; Clarendon Press: Oxford, 1961.
- (38) Harmon, J. F.; Muller, B. H. *Phys. Rev.* **1969**, *182*, 400.
- (39) Sholl, C. A. *J. Phys. C: Solid State Phys.* **1981**, *14*, 447.
- (40) Kruk, D.; Meier, R.; Rössler, E. A. *Phys. Rev. E* **2012**, *85*, 020201.
- (41) Meier, R.; Herrmann, A.; Hofmann, M.; Kresse, B.; Privalov, A. F. *Macromolecules* **2013**, *46*, 5538.
- (42) Kudlik, A.; Benkhof, S.; Blochowicz, T.; Tschirwitz, C.; Rössler, E. A. *J. Mol. Struct.* **1999**, *479*, 201.
- (43) Böttcher, C. J. F.; Bordewijk, P. *Theory of Electronic Polarization*; Elsevier Scientific Polarization: Amsterdam, 1978.
- (44) Rössler, E. A.; Taupitz, M.; Börner, K.; Schulz, M.; Vieth, H.-M. *J. Chem. Phys.* **1990**, *92*, 5847.
- (45) Böhmer, R.; Diezemann, G.; Hinze, G.; Rössler, E. A. *Prog. Nucl. Magn. Reson. Spectrosc.* **2001**, *39*, 191.
- (46) Petzold, N.; Schmidtke, B.; Kahlau, R.; Bock, D.; Meier, R.; Micko, B.; Kruk, D.; Rössler, E. A. *J. Chem. Phys.* **2013**, *138*, 12A510.
- (47) Wooley, K. L.; Hawker, C. J.; Pochan, J. M.; Frechet, J. M. J. *Macromolecules* **1993**, *26*, 1514.
- (48) Abou Elfadl, A.; Kahlau, R.; Herrmann, A.; Novikov, V. N.; Rössler, E. A. *Macromolecules* **2010**, *43*, 3340.
- (49) Johari, G. P. *J. Non-Cryst. Solids* **2002**, *307*, 317.
- (50) Vogel, M.; Rössler, E. A. *J. Chem. Phys.* **2001**, *115*, 10883.
- (51) Micko, B.; Tschirwitz, C.; Rössler, E. A. *J. Chem. Phys.* **2013**, *138*, 154501.
- (52) Garcia-Bernabe, A.; Diaz-Calleja, R.; Haag, R. *Macromol. Chem. Phys.* **2006**, *207*, 970.
- (53) Turkey, G.; Sangoro, J. R.; Rehim, M. A.; Kremer, F. *J. Polym. Sci., Part B: Polym. Phys.* **2010**, *48*, 1651.
- (54) Sangoro, J. R.; Turkey, G.; Rehim, M. A.; Jacob, C.; Naumov, S.; Ghoneim, A.; Kaerger, J.; Kremer, F. *Macromolecules* **2009**, *42*, 1648.
- (55) Stockmayer, W. H. *Pure Appl. Chem.* **1967**, *15*, 539.

5. Publication II

Publication II

Dynamics of asymmetric non-polymeric binary glass formers—A nuclear magnetic resonance and dielectric spectroscopy study

B. Pötzschner, F. Mohamed, A. Lichtinger, D. Bock, and E. A. Rössler

J. Chem. Phys. 143, 154506 (2015)

Doi: 10.1063/1.4932981

© 2015 AIP Publishing LLC

Dynamics of asymmetric non-polymeric binary glass formers—A nuclear magnetic resonance and dielectric spectroscopy study

B. Pötzschner, F. Mohamed, A. Lichtinger, D. Bock, and E. A. Rössler^{a)}

Experimentalphysik II, Universität Bayreuth, 95440 Bayreuth, Germany

(Received 22 June 2015; accepted 29 September 2015; published online 21 October 2015)

We study a dynamically asymmetric binary glass former with the low- T_g component m-tri-cresyl phosphate (m-TCP; $T_g = 206$ K) and a spirochroman derivative as a non-polymeric high- T_g component ($T_g = 382$ K) by means of ^1H nuclear magnetic resonance (NMR), ^{31}P NMR, and dielectric spectroscopy which allow component-selectively probing the dynamics. The entire concentration range is covered, and two main relaxation processes with two T_g are identified, T_{g1} and T_{g2} . The slower one is attributed to the high- T_g component (α_1 -process), and the faster one is related to the m-TCP molecules (α_2 -process). Yet, there are indications that a small fraction of m-TCP is associated also with the α_1 -process. While the α_1 -relaxation only weakly broadens upon adding m-TCP, the α_2 -relaxation becomes extremely stretched leading to quasi-logarithmic correlation functions at low m-TCP concentrations—as probed by ^{31}P NMR stimulated echo experiments. Frequency-temperature superposition does not apply for the α_2 -process and it reflects an isotropic, liquid-like motion which is observed even below T_{g1} , i.e., in the matrix of the arrested high- T_g molecules. As proven by 2D ^{31}P NMR, the corresponding dynamic heterogeneities are of transient nature, i.e., exchange occurs within the distribution $G(\ln\tau_{\alpha_2})$. At T_{g1} a crossover is found for the temperature dependence of (mean) $\tau_{\alpha_2}(T)$ from non-Arrhenius above to Arrhenius below T_{g1} which is attributed to intrinsic confinement effects. This “fragile-to-strong” transition also leads to a re-decrease of $T_{g2}(c_{m\text{-TCP}})$ at low concentration $c_{m\text{-TCP}}$, i.e., a maximum is observed in $T_{g2}(c_{m\text{-TCP}})$ while $T_{g1}(c_{m\text{-TCP}})$ displays the well-known plasticizer effect. Although only non-polymeric components are involved, we re-discover essentially all features previously reported for polymer-plasticizer systems. © 2015 AIP Publishing LLC. [<http://dx.doi.org/10.1063/1.4932981>]

I. INTRODUCTION

The dynamical properties of binary glass forming systems, especially of polymer-additive systems, were subject of intensive research during the last decades.^{1–7} Recent studies indicate that the main quantity which appears to determine the dynamics is the “contrast” of the glass transition temperature T_g , i.e., the T_g difference of the neat components.^{8–10} For similar T_g of the components, a binary system forms a dynamically rather homogeneous system. Yet, for such dynamically “asymmetric” mixtures, two T_g are well documented^{3,8–10} and, consequently, pronounced dynamic heterogeneities are expected. Their occurrence is, in particular, well documented by nuclear magnetic resonance (NMR) which allows to selectively probe the dynamics of each component provided that different NMR nuclei, e.g., ^2H and ^{31}P are used.^{7,10–16}

Recently, in the case of dielectric spectroscopy (DS) probing only the low- T_g component in several polymer-plasticizer systems two relaxation processes, namely, α_1 and α_2 were found,^{8–10,16} in addition to a secondary (β) relaxation observed at low temperatures.¹⁷ The faster α_2 -process is assigned to the dynamics of the low- T_g additive. This process shows an anti-plasticizer effect, i.e., a slowdown of the dynamics with decreasing additive concentration. Furthermore, one observes

strong broadening of the relaxation spectra, i.e., frequency-temperature superposition (FTS) does not apply. According to NMR investigations, the process reflects isotropic reorientation and exhibits strong dynamic heterogeneities; the corresponding correlation function shows quasi-logarithmic decays in the low concentration limit of the additive.^{7,16} Time constants attributed to the second, slower α_1 -process are equal to those of the polymer and the well-known plasticizer effect is observed. The corresponding dielectric spectra and equivalently the correlation functions only weakly broaden upon mixing, and FTS is fulfilled. These findings were interpreted in terms of two sub-ensembles of additive molecules, one associated with highly decoupled fast dynamics in the virtually rigid polymer matrix, the other attached to the slow dynamics of the polymer. Thus, while the dynamics of the polymer remains essentially unchanged in the mixed glass former, the spectral evolution of the additive is qualitatively different and exhibits pronounced dynamic heterogeneities. Two dimensional (2D) NMR techniques proved their transient nature with lifetimes on the order of τ_{α_2} . Analyzing the corresponding relaxation strengths it turned out that the fraction of the additive molecules involved in the glass process of the polymer continuously decreases upon increasing temperature until the process is only performed by the polymer above a certain temperature. In a similar study, this led to a possible interpretation in terms of a type-A glass transition predicted by mode coupling theory.⁹

^{a)} Author to whom correspondence should be addressed. Electronic mail: ernst.roessler@uni-bayreuth.de.

Covering the full additive concentration (c) range, two T_g were identified for all concentrations, $T_{g1}(c)$ (associated with α_1) and $T_{g2}(c)$ (associated with α_2) $< T_{g1}(c)$.^{10,16} While T_{g1} continuously decreases with increase of the low- T_g component, T_{g2} exhibits a maximum at an intermediate concentration, specifically, at low additive concentrations T_{g2} decreases again. Up to our knowledge, this finding was not reported before; most studies display two T_g values only for a limited concentration range. The maximum in T_{g2} results from the fact that the time constant $\tau_{\alpha_2}(T)$ changes from a non-Arrhenius behavior above to an Arrhenius law below T_{g1} (“fragile-to-strong” transition), i.e., at temperatures for which the high- T_g component is virtually immobile. From the dielectric spectra alone, the manifestation of the α_2 -process resembles a β -process. Actually, as said, many binary glasses exhibit in addition such a β -process.^{17–19}

This rather complex scenario of the dynamics in polymer-plasticizer systems raises the question, whether the observed effects are related to the fact that polymers are involved or whether the scenario generally holds for highly asymmetric binary glass formers. Therefore, in the present contribution, we extend our joint investigations by ^1H and ^{31}P NMR as well as by DS to a binary system consisting of two non-polymeric components, yet, with a high T_g contrast. The well-studied glass former *m*-tri-cresyl phosphate (*m*-TCP; $T_g = 206$ K)^{20–22} is mixed with the high- T_g component DH 379, a spirobichroman derivative (cf. Fig. 1; $T_g = 382$ K). Preliminary NMR studies of *m*-TCP mixed with the low- T_g glass former 2-methyltetrahydrofuran²³ and toluene in PCB (polychlorinated biphenyl) were recently published,²⁴ while several dielectric studies on such systems exist, yet covering only a limited range of concentration or temperature.^{25–28} As we will demonstrate, indeed similar dynamics are identified as in the case of polymer-additive systems. In particular, we find again a maximum in $T_{g2}(c)$, while $T_{g1}(c)$ continuously decreases with increasing *m*-TCP concentration.

II. EXPERIMENTAL SECTION

A. Systems

We investigated binary mixtures of the glass former *m*-TCP and an azobenzene-containing spirobichroman derivative, which will be called DH 379 (cf. Fig. 1). The low- T_g component *m*-TCP was received (97%) from Acros Organics, and the high- T_g DH 379 compound was synthesized at Macromolecular Chemistry I at the University of Bayreuth and belongs to the class of photochromic molecular glasses, which can be applied in holography.^{29–33} The synthesis and properties of DH 379 were described in Refs. 30 and 33. The glass tran-

sition temperature T_g of DH 379 is at 382 K (DSC: differential scanning calorimetry). With a T_g of 206 K for *m*-TCP a large T_g contrast of 176 K governs the dynamics. Mixtures with $c_{m\text{-TCP}} = 20\%$, 37%, 48%, 66%, 85%, and 100% mass concentration of *m*-TCP in DH 379 were investigated by different NMR techniques. Furthermore, DS measurements on neat DH 379, neat *m*-TCP, and mixtures with $c_{m\text{-TCP}} = 20\%$, 34%, 46%, 56%, 67%, 73%, and 80% were performed. The concentration error is $\pm 2\%$.

The binary system showed a tendency to demix; the DH 379 started to crystallize at temperatures above room temperature, depending on concentration and temperature within days to hours but was completely stable at lower temperatures.

To assure that the sample is in a single, stable macroscopic phase, all measurements were performed twice for both NMR and for dielectric spectroscopy. All results could be perfectly reproduced. If demixing occurred at higher temperatures, sudden changes in the NMR observables and the dielectric spectra were recognized. For example, any phase separation would lead to bi-exponential spin-lattice relaxations which are generally not observed. Furthermore, in the case of NMR measurements, the samples were visually inspected at higher temperatures between the measurements to assure that a single transparent phase was present.

B. NMR spectroscopy

The ^{31}P and ^1H experiments were performed on a Bruker Avance III spectrometer and a 400 MHz Spectrospin cryomagnet. The Larmor frequency of ^{31}P holds $\omega_L = 2\pi * 161.98$ MHz for a magnetic field of 9.4 T. The home-built (in cooperation with Bruker Biospin GmbH) double resonance probe was cooled by liquid nitrogen with an Oxford CF1200 cryostat and an Oxford ITC-503 temperature controller with a temperature accuracy better than ± 2 K and a temperature stability better than ± 0.2 K.

1. ^{31}P NMR spectra

The dominating interaction in the ^{31}P NMR spectrum of *m*-TCP is the chemical shift anisotropy (CSA). In the case of a symmetric CSA tensor $\eta = 0$, what is the case for *m*-TCP, the shift of the angular NMR frequency $\omega(\theta)$ with respect to the Larmor frequency ω_L depends solely on the angle θ between the direction of the magnetic field and the principal CSA tensor axis,³⁴

$$\omega(\theta) = \delta_{\text{CSA}}/2(3\cos^2\theta - 1). \quad (1)$$

The parameter δ_{CSA} specifies the anisotropy of the CSA tensor. It depends linearly on the strength of the magnetic field B_0 :

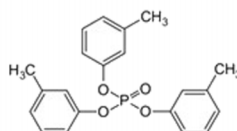
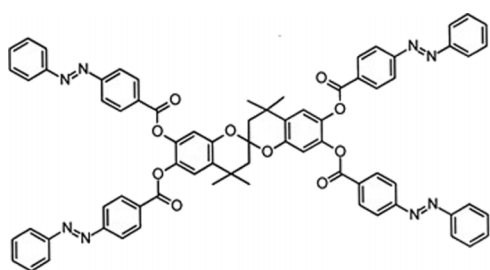


FIG. 1. High- T_g component DH 379 (left) ($T_g = 382$ K) with molar mass of $M_{\text{mol}} = 1205.3$ g/mol and low- T_g component *m*-TCP (right) ($T_g = 206$ K) with a molar mass of $M_{\text{mol}} = 368.4$ g/mol.

$\omega_L \Delta\sigma_{CSA} = \frac{3}{2} \delta_{CSA}$ with $\omega_L = \gamma B_0$ and the frequency independent chemical shielding anisotropy $\Delta\sigma_{CSA}$. The CSA leads to a characteristic asymmetric powder spectra if molecular reorientation is slower than the NMR time scale ($\tau_\alpha \gg \frac{1}{\delta_{CSA}}$) and if molecular orientation is isotropically distributed as it is the case in glasses. For high temperatures well above T_g fast isotropic reorientation characterized by the time constant τ_α leads to a collapse of the powder spectrum into a central Lorentzian line. In this limit ($\tau_\alpha \ll \frac{1}{\delta_{CSA}}$), the width of the Lorentzian line $\Delta\omega$ (in angular frequency) is related to the transversal relaxation time T_2 via $\Delta\omega = 2/T_2$. At even higher temperatures, the inhomogeneity of the magnetic field determines the line width.

Such solid-state spectra were recorded with a Hahn-echo pulse sequence (90° - t_p - 180°), with an inter-pulse delay of $t_p = 20 \mu\text{s}$. For all spectra ^1H - ^{31}P dipolar decoupling was applied during the acquisition of the FID (free induction decay) to eliminate the heteronuclear dipole-dipole interaction.

Upon heating from low temperatures, due to pronounced dynamical heterogeneities typical of binary systems and therefore a broad distribution of correlation times $G(\ln\tau_\alpha)$, one observes so-called two-phase spectra instead of a gradual collapse from the solid-state spectrum to the liquid line. Such two-phase spectra can be described by a superposition of a solid-state spectrum S_{powder} and a liquid line S_{Lorentz} ,^{7,15,16,35,36}

$$S(\omega; T) = W(T)S_{\text{Lorentz}}(\omega) + (1 - W(T))S_{\text{powder}}(\omega), \quad (2)$$

with a weighting factor $W = \int_0^{\tau_{\text{cut}}} G(\ln\tau_\alpha) d \ln\tau_\alpha$, while τ_{cut} is defined by the typical time scale of the experiment: $\tau_{\text{cut}} \approx 1/\delta_{CSA}$. Spectral parts from sub-ensembles with correlation times on the order of the NMR time scale ($\tau_\alpha \approx \frac{1}{\delta_{CSA}}$) can be neglected in good approximation due to the reduction of the intensity of the signal of these sub-ensembles in the Hahn-echo and the small fraction of $G(\ln\tau_\alpha)$ on the order of the NMR time scale.

In the case of ^1H NMR, the dominant interaction is the dipole-dipole interaction between the different protons. In a dense system, the interaction leads to a broad Gaussian-like spectrum. At high temperatures, similar to the CSA interaction, all the orientation dependent couplings get averaged out and only the isotropic chemical shift interaction is left over, which again leads to a narrow Lorentzian line. The dipole-dipole interaction is (partly) refocused by a solid-echo pulse sequence (90° - t_p - 90°) with a short inter-pulse delay t_p .³⁷

2. Relaxation times

The ^{31}P NMR relaxation is determined by the fluctuation of the CSA interaction.^{34,38,39} The contribution from heteronuclear dipolar coupling is weak at the applied high magnetic field and in the case of homonuclear coupling it is neglectable due to the large distance between the phosphorus nuclei in the different m-TCP molecules.²² The relaxation rates $1/T_{1,2}$ which are linked to the spectral density $J(\omega)$ at the Larmor frequency ω_L and $\omega = 0$ write

$$\frac{1}{T_1^{CSA}} = K^{CSA} J(\omega_L), \quad (3)$$

$$\frac{1}{T_2^{CSA}} = \frac{1}{6} K^{CSA} (3J(\omega_L) + 4J(0)), \quad (4)$$

with

$$K^{CSA} = \frac{2}{15} (\Delta\sigma_{CSA} \omega_L)^2. \quad (5)$$

One can easily gain time constants from the T_2 data in the slow motion limit ($\omega_L \tau_\alpha \gg 1$), where $J(\omega) \approx 0$ and $J(0) = \langle \tau \rangle = \tau_\alpha$; thus, one finds $\frac{1}{T_2^{CSA}} = \frac{2}{3} K^{CSA} \tau_\alpha$. Furthermore holds $\omega_\alpha \tau_\alpha \approx 1$ at the T_1 -minimum.

The spin-lattice relaxation measurements were performed with an inversion recovery pulse sequence at high temperature and with the saturation recovery pulse sequence at low temperature. The spin-spin relaxation time T_2 was obtained from the spectral width $\Delta\omega$ of the Lorentzian line in the liquid when inhomogeneous broadening can be neglected (cf. above).

3. Stimulated echo experiment

From the decay of the stimulated echo, the full correlation function of the second Legendre polynomial is directly accessible, i.e., the rank-two reorientational correlation function $C_2(t)$ is probed. A three-pulse echo sequence (90° - t_p - 90° - t_m - 90°) with appropriate pulse phases is applied and the echo amplitude is measured for different mixing times t_m , for a constant evolution time t_p . If the second pulse is shifted by 90° compared to the first pulse, then the sine-sine reorientational correlation function $F_{t_p}^{\text{sin}}(t_m)$ is probed,^{36,40,41}

$$\begin{aligned} I(t_m, t_p) &\propto \langle \sin(\omega(0)t_p) \sin(\omega(t_m)t_p) \rangle \exp(-t_m/T_1) \\ &= F_{t_p}^{\text{sin}}(t_m) \exp(-t_m/T_1), \end{aligned} \quad (6)$$

which is damped by spin-lattice relaxation and which represents an upper limit for the accessible time window in a stimulated echo experiment. For short evolution time t_p , the correlation function $F_{t_p}^{\text{sin}}(t_m)$ approximates $C_2(t)$,

$$\lim_{t_p \rightarrow 0} F_{t_p}^{\text{sin}}(t_m) \propto \langle \omega(0) \omega(t_m) \rangle \propto C_2(t_m) = C_2(t), \quad (7)$$

which is interpolated with a stretched exponential (Kohlrausch) function,^{20,36}

$$C_2(t) = \exp\left(-\left(\frac{t}{\tau_K}\right)^{\beta_K}\right) \quad (8)$$

in the neat and the binary system, except for very low concentrations, where $C_2(t)$ follows a quasi-logarithmic decay. The (mean) correlation time is given by $\tau_\alpha = \frac{\tau_K}{\beta_K} \Gamma(\frac{1}{\beta_K})$. An evolution time $t_p = 10 \mu\text{s}$ was applied, whereby the short-time limit is fulfilled (cf. Eq. (7)).

4. Two-dimensional ^{31}P NMR spectra

With the TPPI (time proportional phase incrementation) pulse sequence followed by two dimensional Fourier transform, one obtains 2D spectra.⁴¹ As the NMR frequency is linked to the orientation of a molecular axis (of a presumed rigid molecule) with respect to the external field one can directly visualize the evolution of the reorientational process. Similar

to the stimulated echo experiment a three-pulse sequence with a fixed mixing time t_m and evolution time t_p is applied. An additional Hahn-echo pulse is added after the third pulse in order to avoid dead time effects. While the evolution time gets linearly incremented beginning from $t_p = 0$ up to $t_p \approx T_2$ one measures alternately the sine ($90^\circ_x-t_p-90^\circ_y-t_m-90^\circ-t_p-180^\circ$) and cosine ($90^\circ_x-t_p-90^\circ_x-t_m-90^\circ-t_p-180^\circ$) part of the echo (TPPI).⁴¹

The 2D NMR spectrum, $S(\omega_1, \omega_2; t_m)$, measures the joint probability, $P(\omega_2, t_m | \omega_1, 0)$, to find molecules with a frequency ω_2 at the mixing time t_m and a frequency ω_1 at time $t = 0$. The probability $P(\omega_2, t_m | \omega_1, 0)$ can be expressed as a product of an *a priori* probability $P(\omega_1)$ that one molecule has the NMR frequency ω_1 (in the rotating frame) before the mixing time and the conditional probability $P(\omega_2, t_m; \omega_1, 0)$ that a molecule has the NMR frequency ω_2 after the mixing time if it had the NMR frequency ω_1 before; explicitly^{40,41}

$$S(\omega_1, \omega_2; t_m) = P(\omega_1)P(\omega_2, t_m; \omega_1, 0). \quad (9)$$

Considering isotropic reorientation and complete exchange ($t_m \gg \tau_\alpha \gg 1/\delta_{CSA}$), $P(\omega_2, t_m; \omega_1, 0)$ is completely independent of ω_1 and the spectrum, $S_{reo}(\omega_1, \omega_2)$, can be calculated from⁴²

$$S_{reo}(\omega_1, \omega_2) = P_{slow}(\omega_1) P_{slow}(\omega_2), \quad (10)$$

where $P(\omega) = P_{slow}(\omega)$ provides the *a priori* probability to find a NMR frequency ω and is given by the 1D CSA spectrum. For short mixing times when no exchange has taken place ($\tau_\alpha \gg t_m$) ω_1 equals ω_2 , and one obtains a diagonal spectrum⁴²

$$S_{dia}(\omega_1, \omega_2) = P_{slow}(\omega) \delta(\omega_1 - \omega_2). \quad (11)$$

For fast molecules $\tau_\alpha \ll \delta_{CSA}$ all frequencies get averaged and one obtains a liquid line S_{liq} in the center of the spectra whereby $P_{fast}(\omega)$ is given by a 1D Lorentzian line,

$$S_{liq}(\omega_1, \omega_2) = P_{fast}(\omega_1) P_{fast}(\omega_2). \quad (12)$$

If molecules perform a slow reorientation before the mixing time and a fast reorientation after the mixing time and vice versa, one measures exchange spectra⁴²

$$S_{ex}(\omega_1, \omega_2) = P_{fast}(\omega_1) P_{slow}(\omega_2) + P_{slow}(\omega_1) P_{fast}(\omega_2). \quad (13)$$

At temperatures where 1D two-phase spectra are obtained, things get more complicated. Then the 2D spectra have to be written as a superposition of all four sub-spectra (Eqs. (10)–(13)),^{7,42}

$$S(\omega_1, \omega_2) = P_{dia}(t_m)S_{dia}(\omega_1, \omega_2) + P_{reo}(t_m)S_{reo}(\omega_1, \omega_2) + P_{liq}(t_m)S_{liq}(\omega_1, \omega_2) + P_{ex}(t_m)S_{ex}(\omega_1, \omega_2), \quad (14)$$

whereby $P_{dia}(t_m) + P_{reo}(t_m) + P_{liq}(t_m) + P_{ex}(t_m) = 1$ holds. Due to a broad distribution $G(\ln \tau_\alpha)$, one measures only a superposition of these well-defined limiting case spectra in Eqs. (10)–(13).

C. Dielectric spectroscopy

The dielectric measurements were carried out with an Alpha-A Analyzer from Novocontrol in the frequency range $\nu = 10^{-2}$ – 10^6 Hz. Temperature was kept constant within ± 0.2 K by using a Quatro-H temperature controller from

Novocontrol yielding an absolute accuracy better than ± 0.2 K. The sample cell was constructed by a design of Wagner and Richert and assures a constant sample volume.⁴³

Generally, the dielectric permittivity is defined by the equation⁴⁴

$$\varepsilon^*(\omega) = \varepsilon'(\omega) - i\varepsilon''(\omega) = \varepsilon_\infty + \Delta\varepsilon \int_0^\infty -\frac{d\phi(t)}{dt} e^{-i\omega t} dt, \quad (15)$$

where $\varepsilon^*(\omega)$ is the complex dielectric constant, ω is the angular frequency, ε_∞ is the high frequency permittivity, and $\phi(t)$ is the step-response function. Regarding the main relaxation peak of the neat components and the α_1 -relaxation peaks in the mixture (reflecting DH 379 dynamics), a Kohlrausch stretched exponential function (cf. Eq. (8)) was used for $\phi(t)$ to fit the data. Regarding the α_2 -peak (reflecting m-TCP dynamics) in the mixture, a Havriliak-Negami (HN)⁴⁴ function had to be used with a low-frequency exponent a significantly less than unity, explicitly

$$\varepsilon^* - \varepsilon_\infty = \Delta\varepsilon/[1 + i(\omega\tau_0)^a]^b. \quad (16)$$

The time constants are extracted by “peak picking,” i.e., $\tau_{\alpha 2} = 1/(2\pi\nu_{max})$. In some cases, both α_1 - and α_2 -peaks are observed simultaneously in the frequency window; the data are then interpolated with a weighted sum of Eqs. (8)/(15) and (16), respectively. At low frequencies, a pronounced dc conductivity is observed, which is subtracted from the dielectric loss by using the expression

$$\varepsilon''_{dc}(\omega) = \frac{\sigma_{dc}}{\varepsilon_0\omega}. \quad (17)$$

III. RESULTS

A. Dielectric spectra

1. Neat components

The dielectric spectra of the neat components DH 379 and m-TCP are shown for temperatures close to and above T_g (382 K and 206 K, respectively) in Figs. 2(a) and 2(b), respectively. A pronounced (main) α -relaxation is observable in both cases and can be interpolated by a Kohlrausch function (Eq. (8)/(15)). Upon heating, this process shifts to higher frequencies. Yet, in the case of DH 379 at $T > 400$ K the liquid starts to crystallize leading to a decrease of the signal. At highest frequencies a secondary relaxation (β -process) is well recognizable in Fig. 2(a), so the DH 379 is a type-B glass former with a well separated β -process.^{45,46} The low amplitude of the dielectric signal of DH 379 reflects its low molecular dipole moment. In the case of m-TCP (Fig. 2(b)), the spectra are reproduced from Ref. 21. Here, the high-frequency flank of the α -process crosses over from one power-law to another, the latter is known as “excess wing,”⁴⁷ and a power-law $\nu^{-\gamma}$ is added to Eq. (8)/(15) to interpolate the DS spectra (cf. Fig. 2(b)) with $\gamma < \beta_K$. At temperatures below T_g , the α -relaxation leaves the frequency window while the excess wing persists. No β -process is identified in m-TCP in the investigated temperature range. The amplitude of the α -relaxation peak of m-TCP is about ten times larger than that of DH 379. Thus, we expect that in the mixtures the dielectric response will be

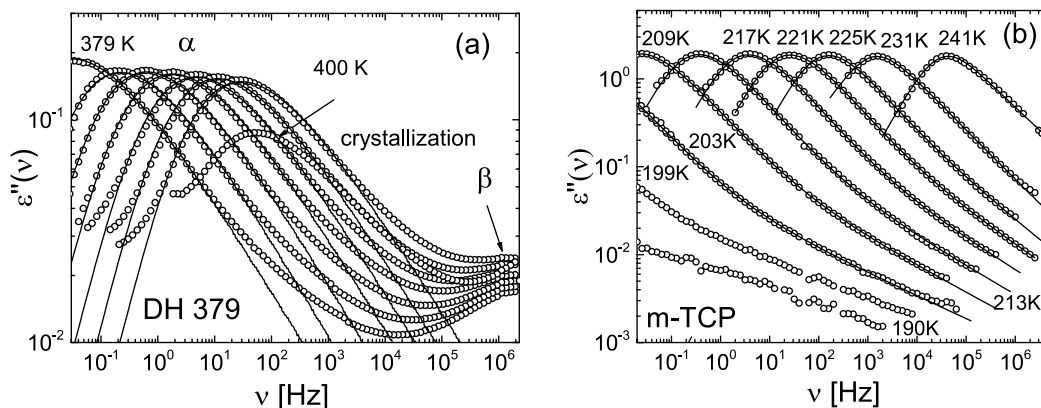


FIG. 2. (a) Dielectric spectra of DH 379 (cf. Fig. 1) in a temperature range of $T = 379$ K to 400 K, where the primary (α -) process is observable. (b) Dielectric spectra of m-tri-cresyl phosphate (m-TCP) in a temperature range of $T = 190$ K to 241 K; data taken from Ref. 21. Solid lines: fits by Eq. (8)/(15); for m-TCP in addition a power-law contribution for the excess wing is included.

predominated by that of m-TCP. The time constants of neat DH 379 and m-TCP are extracted by fitting a Kohlrausch function to the spectra (solid lines), and they are displayed in Fig. 14(a) for later discussion. We note that the stretching parameter ($\beta_K = 0.42$ for DH 379 and $\beta_K = 0.77$ for m-TCP) does not change with temperature, thus FTS applies.

2. Mixtures

Figure 3(a) displays the dielectric spectra of the $c_{m-TCP} = 80\%$ sample; for comparison one spectrum of neat m-TCP is included. While the original data display a single relaxation peak, after subtraction of the contribution of the dc conductivity (open symbols) a weak shoulder is recognized on the low-frequency flank of the main relaxation. The latter is assigned to the dynamics of the high- T_g component DH 379 which we call α_1 -process and the former to the m-TCP dynamics called α_2 -process. This assignment will be further substantiated in due course. Clearly, with respect to neat m-TCP the α_2 -spectra are broader in particular on the low-frequency flank ($\omega\tau_{max} \ll 1$), in addition they become wider with decreasing temperature, i.e., FTS does not apply. As

expected, the signal strength of the α_2 -process is somewhat lower than that of neat m-TCP and the peak is shifted to lower frequencies as a consequence of the anti-plasticizer effect due to the presence of the high- T_g component DH 379. The time constants of the α_2 -relaxation extracted via the condition $\tau_{\alpha_2} = 1/(2\pi\nu_{max})$ are included in Fig. 14(a) and will be discussed below (Sec. IV). In the case of the α_1 -relaxation, due to its small intensity we refrain from extracting time constants. For the other samples with $c_{m-TCP} = 73\%$ (see the Appendix, Fig. 16), $c_{m-TCP} = 56\%$, $c_{m-TCP} = 46\%$ (spectra not shown), $c_{m-TCP} = 34\%$ (see Fig. 3(b)), and $c_{m-TCP} = 20\%$ (see Fig. 4), the situation is somewhat more favorable and one can apply a fit with a weighted sum of a Kohlrausch (α_1 -process) and HN spectrum (α_2 -process) along Eqs. (8)/(15) and (16), respectively, and extract $\tau_{\alpha_i}(T)$ from the Kohlrausch function; as said, $\tau_{\alpha_2}(T)$ was extracted by “peak picking.”

Fig. 3(b) shows the dielectric spectra of the low-concentration mixture with $c_{m-TCP} = 34\%$. At high temperatures, already the original data display two relaxation processes, yet the dc conductivity contribution partly covers the slower one. Subtracting the conductivity contribution results in two well resolved relaxations with similar amplitudes (open symbols).

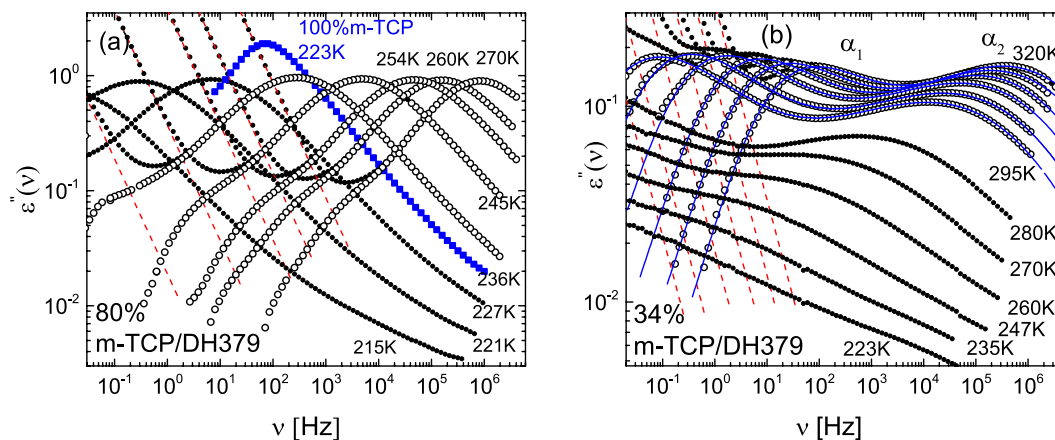


FIG. 3. (a) Original dielectric spectra of the mixture $c_{m-TCP} = 80\%$ (filled black circles; temperatures indicated) and after subtraction of the dc conductivity contribution (open black circles). Data of neat m-TCP at $T = 221$ K for comparison (filled blue squares). (b) Original spectra for the $c_{m-TCP} = 34\%$ sample (filled circles). For high temperatures (295 K–320 K) the conductivity contribution was subtracted (open circles). Dashed lines: conductivity contribution; solid lines: fit applying Kohlrausch and HN susceptibility (cf. Eqs. (8)/(15) and (16), respectively).

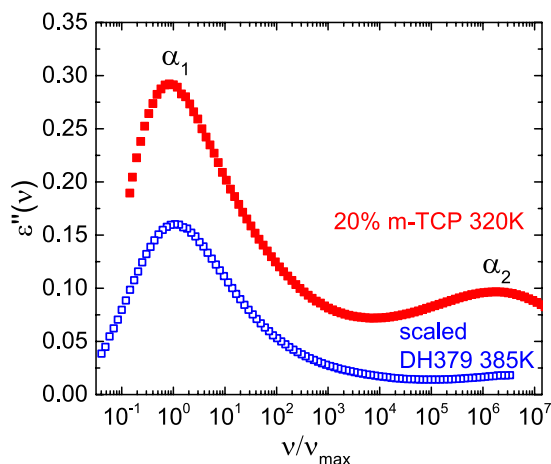


FIG. 4. Dielectric susceptibility at 320 K for the $c_{m-TCP}=20\%$ sample at $\nu_{max} \approx 1$ Hz (red squares, frequency axis scaled to the peak frequency). For comparison, the spectrum of neat DH 379 at 385 K multiplied by 0.8 and 385 K/320 K (Curie correction) (open blue squares).

The relaxation at higher frequencies is again attributed to the α_2 -process of m-TCP while the slower one is assigned to the dynamics of the high- T_g component DH 379 (α_1 -process). Yet, the amplitude of the latter signal is somewhat larger than that of the neat DH 379 although the sample contains only 66% DH 379. An even larger signal enhancement is documented in Fig. 4 for the $c_{m-TCP} = 20\%$ sample, where the α_1 -relaxation of the mixture is compared to the spectrum of neat DH 379 multiplied in amplitude by a factor $0.8 \cdot 385 \text{ K}/320 \text{ K}$ assuming a linear concentration dependence and validity of the Curie law for the relaxation strength. Here, an enhancement by a factor of 1.8 is found, while the widths of the spectra are similar. We think an enhancement factor of almost two for the relaxation of DH 379 at low m-TCP concentration is difficult to explain by a possible non-linear concentration dependence of the relaxation strength. Thus, as in our previous investigation,¹⁰ as well as in Refs. 8 and 9, our results suggest that the α_1 -relaxation contains a contribution from the low- T_g component m-TCP, i.e., a fraction of m-TCP molecules participates in the α_1 -process of DH 379. Of course, a final conclusion needed the determination of the total relaxation strength $\Delta\epsilon(c_{m-TCP})$, which, actually, is not easily done in the present case of the highly viscous mixtures as the filling factor in the capacity cannot be controlled accurately enough. Moreover, a contribution by the β -process would be necessary to be accounted for. Thus, in the present case, the conclusion that a small fraction of m-TCP molecules follow the α_1 -process remains preliminary.

Inspecting Fig. 3(b) one recognizes a trend that the α_1 -relaxation decreases with increasing temperature while the α_2 -relaxation grows. Again, this was observed before,^{8,10} possibly indicating that the contribution of m-TCP to the α_1 -relaxation disappears above some high temperature.

In Fig. 5 we present the dielectric spectra of the α_2 -process (reflecting m-TCP dynamics) at constant temperature $T = 247$ K for different concentrations. The low-frequency flank changes from a Debye dependence of $\epsilon''(\nu)\alpha\nu^1$ typical of neat glass formers to a behavior with a strongly broadened low-frequency flank with decreasing m-TCP concentration.

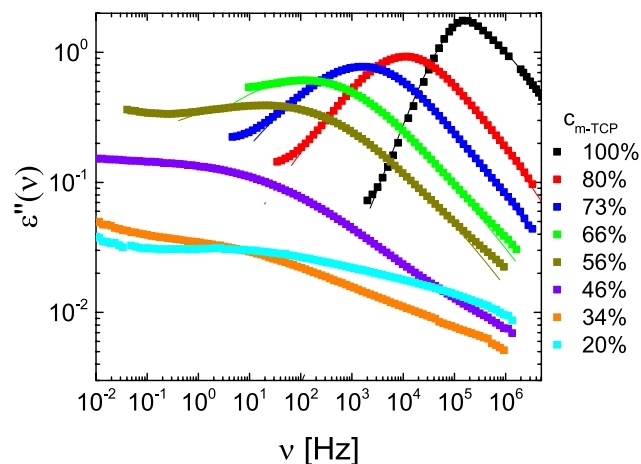


FIG. 5. Dielectric susceptibility for different concentrations of m-TCP/DH 379 mixtures at the temperature $T = 247$ K. Solid lines: fits by Eq. (16) (HN function) for $c_{m-TCP} < 100\%$, for $c_{m-TCP} = 100\%$ a Kohlrausch function (Eq. (8)/(15)) was used.

Also a broadening at the high-frequency flank, yet weaker is observed. The systematic broadening is a clear indication of increasing dynamic heterogeneity upon decreasing m-TCP concentration. In addition, the process slows down and its amplitude decreases as expected due to the dilution of m-TCP and the spectral broadening.

B. NMR measurements

1. ^{31}P NMR spectra

In Fig. 6 the ^{31}P NMR spectra probing the dynamics of the low- T_g component m-TCP are depicted for the entire concentration range. At low temperatures, typical asymmetric powder spectra determined by the CSA interaction (cf. Sec. II) are found, which means all m-TCP molecules are immobile on the NMR time scale ($1/\delta_{CSA}$). At highest temperatures a Lorentzian liquid line is observed, which indicates that all molecules perform isotropic reorientation faster than the NMR time scale. This behavior is found for all concentrations of the mixture. In between these low- and high-temperature limiting spectra a concentration dependent crossover from solid-state spectrum to a liquid line is observable. While for neat m-TCP a gradual collapse from a powder spectrum to a Lorentzian line is discernible, one finds “two-phase spectra” in the entire concentration range of the mixture, i.e., spectra which are described by a superposition of a central Lorentzian line and a solid-state powder spectra (cf. Sec. II). Such two-phase spectra are a clear indication of a broad distribution of correlation times $G(\ln\tau_{\alpha_2})$ of an isotropic reorientation, i.e., a signature of pronounced dynamic heterogeneities.^{7,35,36} The temperature range in which they are observed becomes broader with lower c_{m-TCP} (cf. black dashed lines in Fig. 6). Interestingly, two-phase spectra are also observed below T_{g1} (cf. below) clearly indicating the presence of isotropic m-TCP reorientation in a matrix of virtually immobilized DH 379 molecules.

Thus, as it will become further clear below, ^{31}P NMR essentially probes the α_2 -process. The identification of the

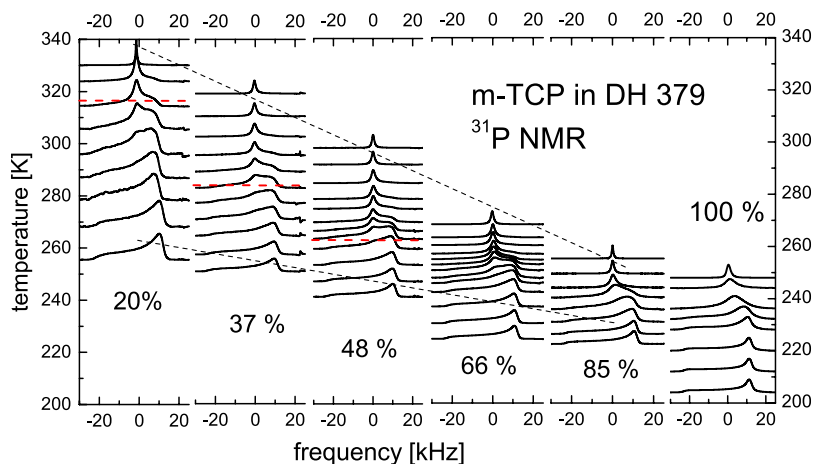


FIG. 6. ^{31}P NMR spectra of m-TCP for the mass concentrations $c_{m\text{-TCP}} = 20\%$, 37% , 48% , 66% , 85% , and 100% . The baseline of the spectra corresponds to the temperature at which they were measured. The dashed lines mark the region in which two-phase spectra are observable. The red dashed lines mark T_g values (associated with DH 379 dynamics) from dielectric spectroscopy for $c_{m\text{-TCP}} = 20\%$, 34% , and 46% for comparison.

small fraction m-TCP molecules involved in the α_1 -process of the DH 379 is difficult to achieve.

As discussed in Sec. II, one can fit these spectra by a superposition of a liquid (Lorentzian) line and a solid-state spectrum (Eq. (2)). The corresponding weighting factor $W(T)$ specifies the fraction of molecules which perform a fast liquid-like reorientation on the NMR time scale. An example of such a “two-phase fit” for a spectrum at 314.4 K of the 20% mixture is shown in Fig. 7(a). As one can see, the two-phase model works well due to a broad distribution $G(\ln\tau_{\alpha 2})$ of reorientational correlation times. The spectral contribution from molecules with time constants in the intermediate exchange regime ($\tau_{\alpha 2} \approx 1/\delta_{\text{CSA}}$) is negligible.

Fits with the two-phase model are applied to all spectra of all mixtures and the thus obtained weighting factor $W(T)$ is shown in Fig. 7(b). As already mentioned, with decreasing m-TCP concentration the temperature range which shows two-phase spectra shifts to higher temperatures and gets significantly broader. The shift to higher temperatures corresponds to the anti-plasticizer effect while the broadening of the two-phase region is a clear sign of increasing dynamical heterogeneities with decreasing additive concentration as it will be further proved below with stimulated echo measurements.

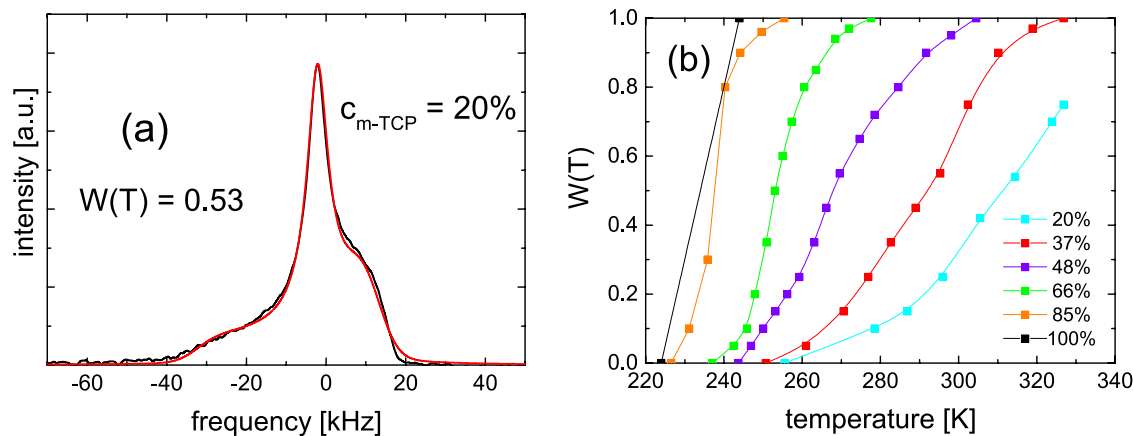


FIG. 7. (a) ^{31}P NMR spectrum of the $c_{m\text{-TCP}} = 20\%$ mixture at 314.4 K (black line) and a two-phase fit (red line) with a weighting factor $W(T)$ indicated. (b) Weighting factor $W(T)$ denoting the fraction of fast (liquid-like) reorienting m-TCP molecules obtained from the analysis of the two-phase spectra for samples with $c_{m\text{-TCP}} = 20\%$, 37% , 48% , 66% , 85% , and 100% . In the case of neat m-TCP, the two (black) points correspond to the beginning and the end of the line collapse in Fig. 6.

2. ^{31}P NMR spin-lattice relaxation

An analogue behavior can be seen in the ^{31}P NMR spin-lattice relaxation time T_1 displayed in Fig. 8 where T_1 of all mixtures is plotted as a function of temperature. In neat m-TCP a minimum is observed and attributed to the main (α -) relaxation. In the mixtures, the T_1 minimum shifts to higher temperatures and the value of T_1 at the minimum increases with decreasing concentration. For low m-TCP concentrations (48% and below), the minimum could not be reached due to crystallization of the high- T_g component at higher temperatures. The increasing T_1 minimum value reflects the increasing width of the distribution $G(\ln\tau_{\alpha 2})$. We observe a non-exponential T_1 relaxation in ^{31}P NMR for the lowest m-TCP concentrations of 37% and 20% at temperatures lower than 270 K, while for all other temperatures and concentrations the T_1 decay is straight exponential. A non-exponential magnetization recovery can occur if all T_1 averaging processes like spin diffusion or molecular exchange are slower than the magnetization recovery.

Given that the relaxation is measured only for a single NMR frequency, a quantitative interpolation of $T_1(T)$ is not an easy task. Thus, we refrain from attempting it here (cf. however Ref. 23). In the case of the relaxation controlling α_2 -process FTS does not hold, consequently the width parameter

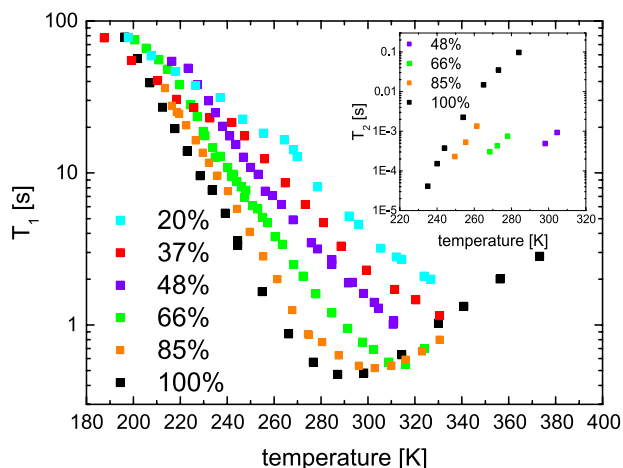


FIG. 8. Spin-lattice relaxation time $T_1(T)$ for mixtures of m-TCP/DH397 with $c_{m-TCP} = 20\%$, 37% , 48% , 66% , 85% and neat m-TCP in a temperature regime from 180 K to 360 K. Inset: spin-spin relaxation time $T_2(T)$ obtained from the width of the Lorentzian line (cf. Fig. 6).

of $G(\ln\tau_{\alpha 2})$ is a function of temperature in addition to the time constants. Moreover, assuming that dielectric spectroscopy and NMR essentially probe the same dynamics, one has to extrapolate the dielectric spectral density to the (higher) Larmor frequency. Thus, a simple analysis of the spin-lattice relaxation as in the case of neat glass-formers, for which a Cole-Davidson susceptibility with temperature-independent stretching parameter suffices to describe the temperature

dependence of the relaxation rate,^{20,48} is not possible in the case of mixed systems.

The inset of Fig. 8 shows the spin-spin relaxation time $T_2(T)$ obtained from the width of the Lorentzian line (cf. Sec. II) at temperatures above the two-phase region. From these T_2 values time constants are calculated and added to Fig. 14(a) (cf. Sec. II). As will be discussed below, the corresponding time constants fit well to the time constants from dielectric spectroscopy.

3. ^{31}P NMR stimulated echo decays

A most direct access to the rank-two reorientational correlation function $C_2(t)$ becomes possible when one studies the decay of the ^{31}P stimulated echo, in particular, for short evolution times t_P (cf. Sec. II). Stimulated echo decays were measured for all concentrations except for $c_{m-TCP} = 20\%$. After correction of the T_1 relaxation, selected normalized correlation functions are shown in Fig. 9 for $c_{m-TCP} = 48\%$, 66% , and 85% m-TCP in DH 379.

The stretching of the correlation function for neat m-TCP is $\beta_K = 0.62$,^{20,22} which is typical of neat glass formers.²¹ In the binary mixtures, with decreasing m-TCP concentration, the correlation functions become more and more stretched. The parameter β_K decreases from 0.62 in neat m-TCP to $\beta_K = 0.52 \pm 0.02$ in the 85% mixture, $\beta_K = 0.34 \pm 0.03$ in the 66% mixture and $\beta_K \approx 0.2$ in the 48% mixture. For the 37% mixture no appropriate Kohlrausch fit can be applied due to

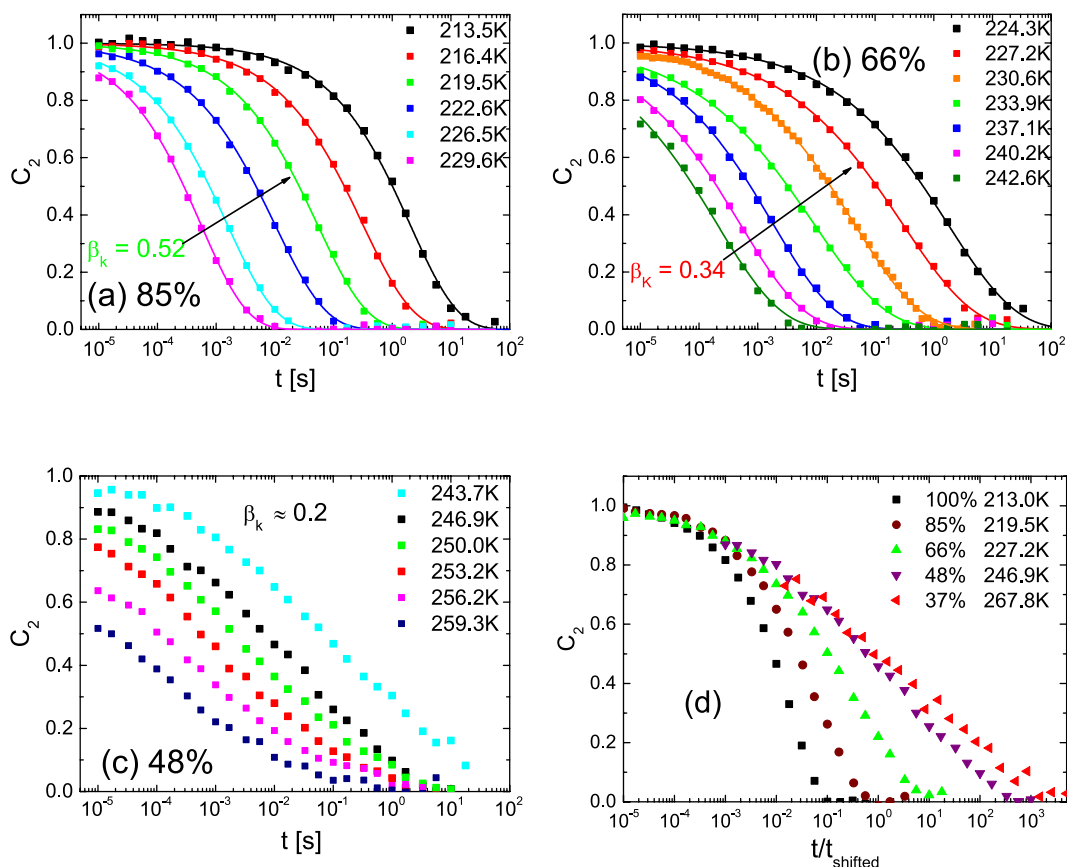


FIG. 9. Reorientational correlation function $C_2(t)$ for m-TCP in DH 379: (a) $c_{m-TCP} = 85\%$; (b) $c_{m-TCP} = 66\%$; and (c) $c_{m-TCP} = 48\%$. The solid lines are Kohlrausch fits to the correlation functions for $c_{m-TCP} \geq 66\%$. (d) Correlation functions for all concentrations (except for $c_{m-TCP} = 20\%$) as a function of scaled time.

the quasi-logarithmic decay of the correlation function. Time-temperature superposition appears to be valid in the small temperature range studied here as seen in the nearly temperature independent stretching parameters at each concentration. Yet, we emphasize that the DS spectra, covering a broader temperature range, clearly show that FTS fails in the mixtures for the α_2 -process (cf. Fig. 3).

So in accordance with the manifestation of the dielectric and NMR spectra (as well as of the NMR relaxation) an increasing extent of dynamic heterogeneities with decreasing concentration of the low- T_g component is rediscovered in the highly stretched reorientational correlation functions detected by the stimulated echo decay. The corresponding time constants are shown in Fig. 14(a) (open diamonds).

4. 2D ^{31}P spectra

Further insight into the nature of the dynamical heterogeneities can be gained by measuring 2D ^{31}P NMR spectra. Therefore 2D spectra with different mixing times were measured for all concentrations in the temperature region where 1D two-phase spectra were found (cf. Fig. 6). Results are shown in Fig. 10 for the $c_{m\text{-TCP}} = 48\%$ mixture and mixing times of $t_m = 50 \mu\text{s}$, 5 ms, and 100 ms, respectively. For the short mixing time (Fig. 10 left) the diagonal cut through the 2D spectra is equivalent to the 1D spectra at this temperature, i.e., no reorientation, except reorientation of the molecules in the fast motion limit ($\tau_\alpha \ll 1/\delta_{\text{CSA}}$) takes place during the mixing time. Slow molecules stay slow and are arrested on the experimental time scale, while fast molecules stay fast during the experiment. The situation changes with increasing mixing time. More and more intensity off the diagonal is observable. Especially at the longest mixing time (Fig. 10 right) it becomes clear that the spectrum has to be described by a superposition of the four sub-spectra introduced in Eq. (14) (cf. Sec. II). In other words, there are molecules which perform an isotropic liquid-like motion before and after the mixing time (Lorentzian line at the center of the spectrum $\omega_1(0) = \omega_2(t_m) = 0$), there are molecules which are arrested before the mixing time and after the mixing time (intensity on the diagonal at $\omega_1(0) = \omega_2(t_m)$),

there are molecules which perform a reorientation on the time scale of the mixing time (S_{reo} in Eq. (10), the intensity is spread over the whole (ω_1, ω_2) -plane), and most interestingly, that there are molecules which perform a liquid-like reorientation before the mixing time and are arrested on the NMR time scale after the mixing time and vice versa (exchange spectra with a cross like pattern at $(\omega_1(0) = 0, \omega_2(t_m))$ and $(\omega_1(0), \omega_2(t_m) = 0)$).

This clearly demonstrates that the dynamical heterogeneities are of transient nature, i.e., there is an exchange of molecules in the fast motion limit with molecules in the slow motion limit. Furthermore, the 2D spectra are measured around T_{g1} , i.e., the α_1 -process (related to the high T_g component) is slow compared to the mixing time. This leads to the assumption that the dynamical exchange only occurs between molecules which perform the faster α_2 -process. The same exchange patterns are found in the whole concentration range (cf. Fig. 11) and have also been observed in polymer additive systems, where again the additive components show pronounced dynamic heterogeneities.^{7,16,42}

5. ^1H NMR measurements

To gain information on the dynamics of the high- T_g component, ^1H NMR spectra were measured with a solid-echo pulse sequence for the $c_{m\text{-TCP}} = 66\%$ mixture. In this case, the spectra reflect the dynamics of both DH 379 and m-TCP. The spectra are shown in Fig. 12(a). At low temperatures, a broad Gaussian line is observable typical of a solid-state ^1H NMR spectrum. With increasing temperature and thus increasing speed of the molecular reorientation, the dipole-dipole interaction gets averaged out and the spectrum collapses to two narrow Lorentzian lines. The two lines are the result of the different isotropic chemical shifts of the protons in the molecules (cf. Fig. 1). Methyl and methylene group protons have a chemical shift of about 1.5 ppm, benzene rings about 7 ppm. For a proton frequency of 400 MHz the line separation is expected to be 2200 Hz, which is in accordance with the measured spectra; also the intensity scales with the number of protons in the respective sub-ensemble (40:16 protons, ca. 2:1 intensity ratio

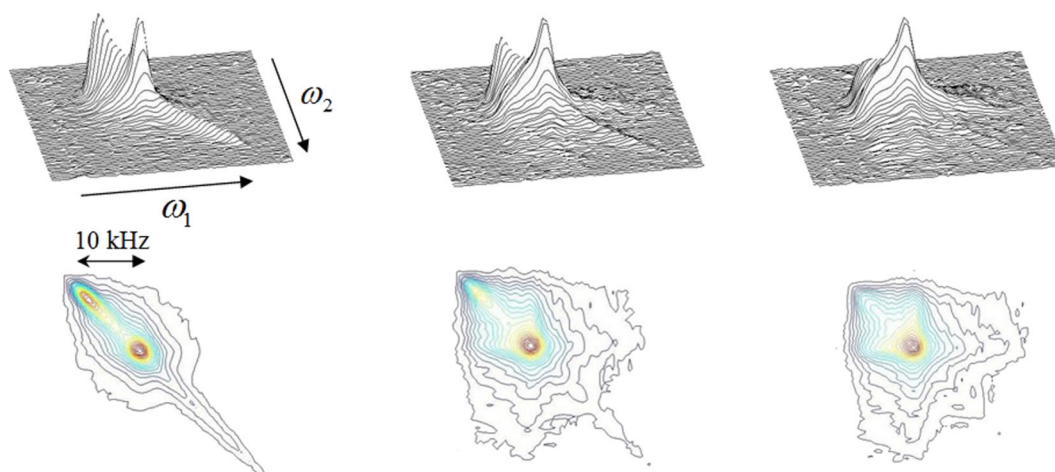


FIG. 10. 2D NMR spectra for the $c_{m\text{-TCP}} = 48\%$ mixture of m-TCP/DH 379 measured for mixing times of $t_m = 50 \mu\text{s}$ (left), $t_m = 5 \text{ms}$ (middle), and $t_m = 100 \text{ms}$ (right) in a stack plot (top) and in contour plot (bottom) representation at $T = 267.7 \text{K}$.

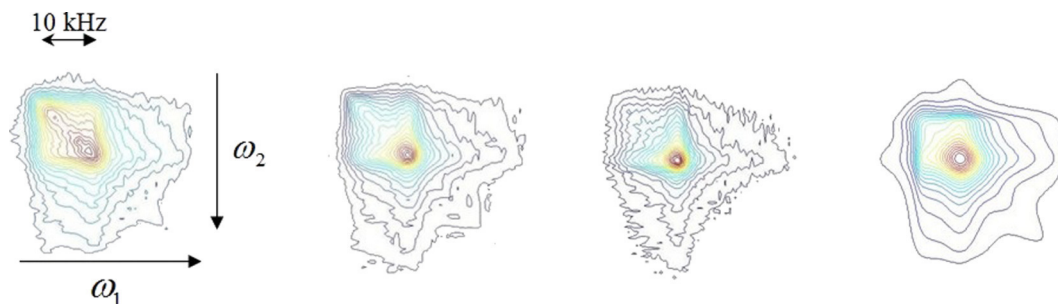


FIG. 11. 2D NMR spectra for $c_{m-TCP} = 37\%$, 48% , and 66% (from left to right) in a contour plot representation for long mixing times. Exchange pattern characteristics of transient dynamic heterogeneities are observable for all concentrations. For comparison a simulated exchange spectra (see Eq. (14)) are added (right side).

of the two lines, cf. molecular structure in Fig. 1). In between these motional limits one observes, similar to the ^{31}P spectra, two-phase spectra, i.e., a superposition of the Gaussian and the two Lorentzian lines.

In analogy to the analysis of the ^{31}P NMR spectra, all the ^1H NMR spectra are fitted with a superposition of a broad Gaussian (cf. Fig. 12(a)) and two Lorentzian lines, and the spectral weight of the two Lorentzian lines gives the fraction of protons attached on fast (liquid-like) moving molecules of both DH 379 and m-TCP. At $T = 269.4$ K and $T = 259.6$ K, in the two-phase region, fits are shown in Figs. 12(b) and 12(c). The fits work well and one gets a weighting factor of $W = 0.70$

and $W = 0.52$, respectively. All weighting factors $W(T)$ are shown in Fig. 13. For comparison, the ^{31}P NMR weighting factors for the $c_{m-TCP} = 66\%$ sample are added. Similar results are revealed. Yet, when one compares the weighting factors in detail, it is obvious that the two-phase region for the proton NMR is significantly broader than in the case of ^{31}P NMR, especially at high temperatures, where still two-phase spectra are observable, while in the ^{31}P NMR spectra only a liquid line is present (270 K–290 K). Thus, the protons yielding at such high temperatures a solid-state spectrum belong to DH 379 molecules which are still arrested on the NMR time scale. Furthermore, the total percentage of protons attached to the

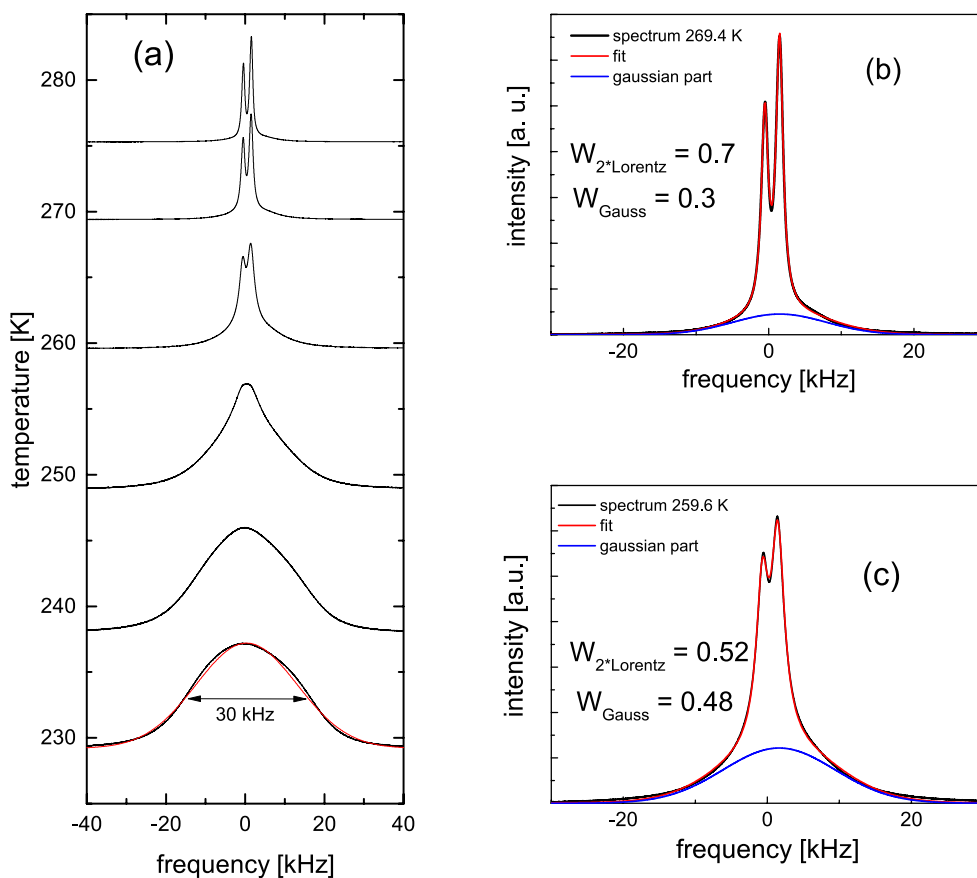


FIG. 12. (a) ^1H NMR spectra for $c_{m-TCP} = 66\%$. The baseline of the spectra corresponds to the temperature at which they were measured. A Gaussian fit to the spectra at lowest temperature is shown (red). (b) ^1H spectrum at $T = 269.4$ K (black) and fit with a superposition of two Lorentzian and one Gaussian line (red). The Gaussian part of the spectrum is shown as a blue line. (c) ^1H spectrum at $T = 259.6$ K (black) and fit with the superposition of two Lorentzian and one Gaussian line (red). The Gaussian part of the spectrum is also shown (blue).

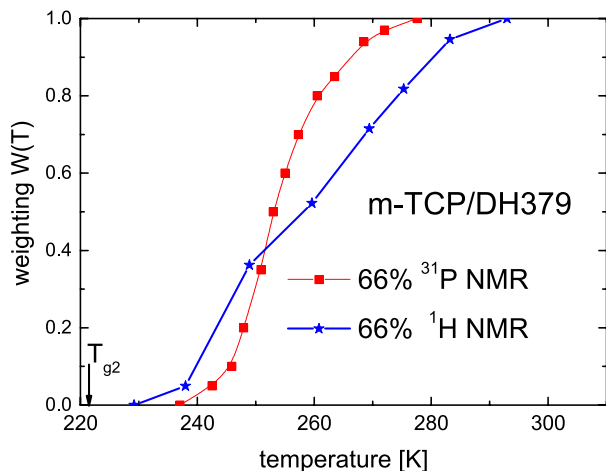


FIG. 13. Weighting factor $W(T)$ obtained from the spectral analysis of m-TCP for the $c_{m-TCP} = 66\%$ sample from ^1H NMR (blue stars) and from ^{31}P NMR (red squares).

DH 379 molecules in the 66% sample is 31% of the total protons. At $T = 269.8$ K 30% ($W = 0.70$) of the molecules are immobilized that means that all or almost all DH 379 molecules are arrested, while almost all m-TCP molecules perform a liquid-like motion within the matrix of the high- T_g component. At even higher temperatures above 290 K, also all the matrix molecules move isotropically and the mixture forms a binary liquid. At lowest temperatures, $W(T)$ by ^1H NMR increases almost parallel with that of ^{31}P NMR. Here, the first m-TCP molecules become mobile enough to contribute to both weighting factors. The somewhat bimodal character of $W(T)$ from ^1H NMR is indicative of the decoupling of the dynamics of m-TCP and DH 379.

IV. DISCUSSION

Figure 14(a) shows the relaxation times for both α_1 - and α_2 -processes as obtained by NMR and DS in the whole concentration range. The time constants of the slow α_1 -process reflecting DH 379 dynamics and obtained from the DS spectra shift to lower temperatures when adding more and more of the low- T_g component m-TCP (filled circles). This corresponds to

the well documented plasticizer effect. Analyzing the dielectric relaxation strengths by assuming a linear concentration dependence of the total relaxation strength, there are indications that a (small) fraction of m-TCP molecules also takes part in the α_1 -process which confirms previous results for other asymmetric binary systems.^{8,9,16} We note that we were not able so far to directly identify this slower m-TCP sub-ensemble by ^{31}P NMR, for example, in the stimulated echo decay. This may be explained by its low magnitude and a very long correlation time with the corresponding correlation loss interfering with a rather fast spin-lattice relaxation fixing the long-time limit of the stimulated echo experiment. The α_1 -process weakly broadens with increasing m-TCP concentration, but the broadening is essentially temperature independent, i.e., FTS holds.

The time constant of the α_2 -process (open symbols) shifts to higher temperatures with decreasing m-TCP concentration which reflects the anti-plasticizer effect. Here, the ^{31}P NMR time constants from T_1 and T_2 data (open triangles) as well as from stimulated echo experiments (open diamonds) fit perfectly to the results gained by DS (open squares). Due to the fact that ^{31}P NMR only probes the m-TCP dynamics it is clear that the α_2 -process (as probed by DS) corresponds to the dynamics of the m-TCP molecules. While at high m-TCP concentrations the corresponding time constant $\tau_{\alpha_2}(T)$ shows a non-Arrhenius temperature dependence resembling that of neat m-TCP yet shifted on the temperature scale, for low concentration the temperature dependence becomes very weak and a qualitative change with temperature is recognized. This is exemplified in Fig. 15(a), where the time constants for the $c_{m-TCP} = 20\%$ and the $c_{m-TCP} = 34\%$ mixture are once again shown. Especially for the $c_{m-TCP} = 34\%$ mixture there is an apparent change from a non-Arrhenius high-temperature behavior to an Arrhenius dependence of the time constant at low temperatures, while for the $c_{m-TCP} = 20\%$ mixture the α_2 -process shows an apparent Arrhenius behavior at all temperatures. Interestingly, the crossover to Arrhenius behavior (or “fragile-to-strong” transition) occurs close to T_{g1} (cf. Fig. 14(b)), i.e., when the dynamics of the high- T_g component gets arrested. A similar change in the temperature dependence of the time constants was recently observed in a polymer-plasticizer system¹⁶ which is reproduced in Fig. 15(b) for comparison. Again, T_{g1} is

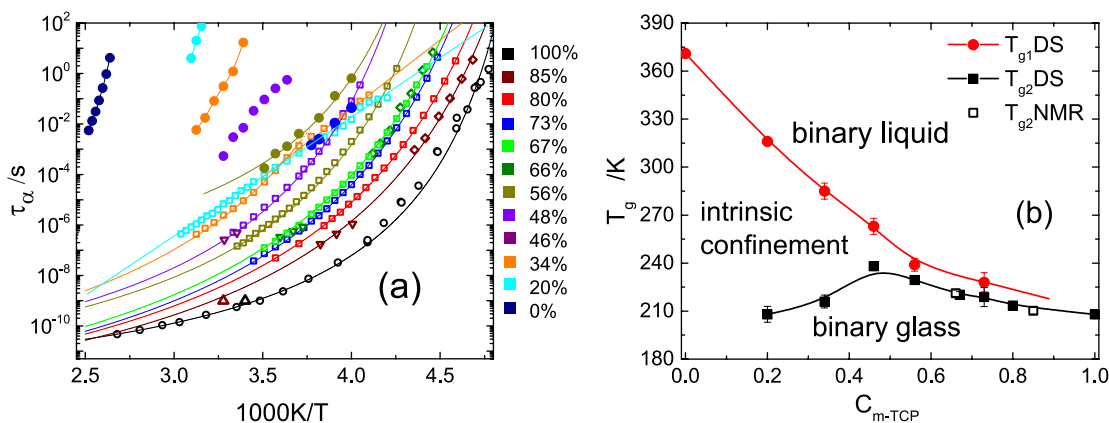


FIG. 14. (a) Time constants for the mixture DH 379/m-TCP in the whole concentration range (color code defines concentration); α_2 -process as obtained from dielectric spectroscopy (open squares), NMR stimulated echo (open diamonds), T_1 minimum (open up triangle), T_2 data (open down triangle), and neat TCP from Ref. 21 (open black circles); α_1 -process from dielectric spectroscopy (filled circles). (b) Glass transition temperatures for both processes α_1 (red circles) and α_2 (black squares) with guide for the eyes (solid lines).

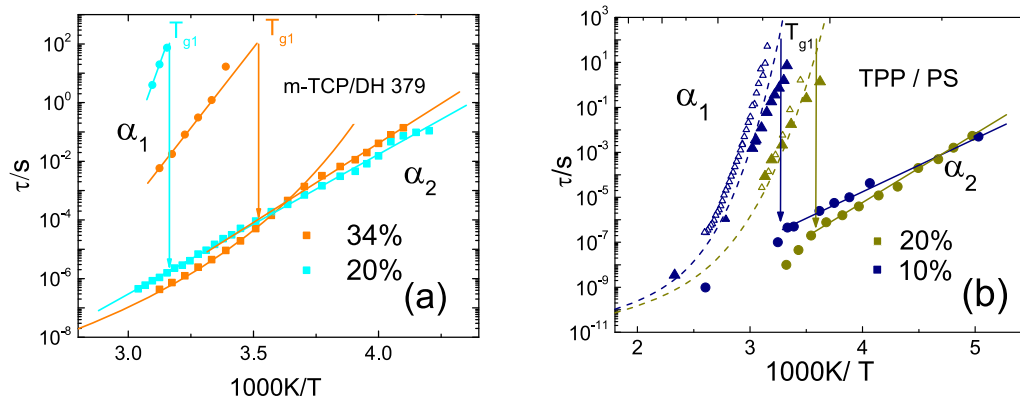


FIG. 15. (a) Time constants for the mixture m-TCP/DH 379 for $c_{m-TCP}=20\%$ and for $c_{m-TCP}=34\%$. The arrows indicate the estimated T_{g1} . A crossover from non-Arrhenius to Arrhenius behavior is observed for $c_{m-TCP}=34\%$ and indicated by the solid lines. (b) The same behavior is found in the polymer additive system TPP/PS (tripropyl phosphate/polystyrene).¹⁶

marked by arrows. We also note that analogous results were reported for another series of mixtures.⁹

Figure 14(b) shows the two $T_g(c_{m-TCP})$ values obtained by extrapolating the time constants of the α_1 -process and the α_2 -process (cf. Fig. 14(a)), respectively, to $\tau_\alpha(T_g) = 100$ s. $T_{g1}(c_{m-TCP})$ reflects the plasticizer effect, the glass point continuously decreases upon adding m-TCP. In contrast, $T_{g2}(c)$ displays a maximum around $c_{m-TCP} = 50\%$. This is explained by the just discussed transition to a weak Arrhenius temperature dependence of the time constants below T_{g1} which leads to a re-decrease of $T_{g2}(c)$ at lowest m-TCP concentrations. Most reports on binary glass formers cover only a restricted concentration range. The present results verify our previous reports showing also a T_{g2} maximum in a polymer-plasticizer system.^{10,16} Three dynamics regimes can be distinguished in Fig. 14(b): At high temperatures ($T > T_{g1}$) the dynamics correspond to that of a binary liquid. For temperatures below T_{g1} and a low m-TCP concentration, the low- T_g molecules move liquid-like in a more or less arrested matrix of DH 379. At lowest temperatures a dynamically arrested binary glass is present.

We note that although no time constants $\tau_{\alpha_1}(T)$ could be extracted for the $c_{m-TCP} = 80\%$ sample, the spectra (cf. Fig. 3(a)) clearly demonstrate that even at highest concentrations two relaxation processes can be distinguished. Actually, this is the first time that both processes are identified in the entire concentration range investigated. This is in contrast to previous reports⁹ where in the case of polystyrene/methyltetrahydrofuran mixtures a merging of both processes is suggested at high additive concentrations, i.e., only a single T_g is measured above a certain additive concentration.

Asymmetric binary glass formers show pronounced dynamic heterogeneities first of all due to the decoupling of the component dynamics. Yet, while the α_1 -relaxation (high- T_g component) remains essentially narrow and similar to that of neat glass formers, the DS spectra as well as the NMR observables measured for the α_2 -process (low- T_g component) clearly indicate a strong broadening of the corresponding distribution $G_{\alpha_2}(\ln\tau_{\alpha_2})$ with decreasing concentration of the low- T_g component. Furthermore, the 2D ³¹P NMR exchange spectra demonstrate exchange within $G_{\alpha_2}(\ln\tau_{\alpha_2})$ even below

T_{g1} . Thus, especially at low concentration and below T_{g1} , the dynamics of the low- T_g component is qualitatively different from that of the high- T_g component. We note that an Arrhenius temperature dependence, as found for the α_2 -process at $T < T_{g1}$, is also characteristic of secondary (β -) relaxations at temperatures below T_g . Thus, from DS spectra alone it is difficult to distinguish an α_2 -process from a β -process. Here, NMR proofs that the α_2 -process reflects isotropic reorientation while the β -process is associated with spatially highly restricted motion.^{49,50}

All the described features were recently also reported for polymer-plasticizer systems which by their very nature display a large T_g contrast of the components.^{7-10,16} It appears that introducing a high T_g contrast also in non-polymeric mixtures leads to very similar effects in the dynamics. In the literature, the dynamic heterogeneities in binary glass formers were usually explained in terms of local concentration variations, which lead to a local distribution of glass transition temperatures in the mixture, and which are either attributed to thermally driven concentration fluctuations⁵¹⁻⁵³ or so-called self-concentration effects, i.e., the variation of the local concentration around one polymer segment due to chain connectivity^{54,55} or a combination of both mechanisms.^{56,57} However, in dynamically very asymmetric mixtures additional effects appear to emerge. Specifically, the low- T_g component may experience intrinsic confinement effects due to the presence of a rigid matrix, much akin to super-cooled liquids inside nanometer size pores.^{58,59} Indeed, the NMR findings in the latter case reflecting as well pronounced dynamic heterogeneities are very similar to those reported here for asymmetric mixtures.²³ Interestingly, such a behavior is predicted in the framework of MCT⁶⁰ as well as documented by MD simulations,⁶¹ where a dynamic decoupling of large and small particles is found for components of sufficiently large size disparity. In that case, the smaller particles retain mobility below the glass point of the larger ones until they undergo a localization transition in the confinement of a frozen matrix. In particular, MCT work on fluids confined in disordered rigid matrices⁶² predicts higher order singularities in the vicinity of which the correlation functions of the smaller molecules become particularly broad, e.g., quasi-logarithmic, consistent with our observations as well as MD simulations.⁶³

V. CONCLUSIONS

The aim of the paper was to study the dynamics of a dynamically asymmetric non-polymeric binary glass former, namely, m-TCP ($T_g = 206$ K) and an azobenzene-containing spirochroman derivative (DH 379 $T_g = 382$ K), by means of dielectric spectroscopy as well as ^1H NMR and ^{31}P NMR and to compare the behavior of this mixed glass former to that of the widely investigated polymer plasticizer systems. As in the latter case, the T_g contrast is rather large. Dielectric spectroscopy identifies two relaxation processes: one associated with the high- T_g component (α_1 -process) and another related to the low- T_g species (α_2 -process). The α_1 -process shows only weak broadening in its spectral shape with increasing m-TCP concentration, while with decreasing m-TCP concentration the α_2 -process displays increasing dynamic heterogeneities, which manifest themselves by highly stretched reorientational correlation functions probed by NMR becoming quasi-logarithmic at lowest concentrations. Furthermore, FTS does not hold in contrast to neat systems. Comparing the relaxation strengths for the α_1 -process in neat DH 379 and in the mixtures it is suggested that a small fraction of m-TCP molecules takes part in the α_1 -process in accordance with other recent reports. ^1H and ^{31}P NMR reveal that the α_2 -process still involves a liquid-like motion below T_{g1} , i.e., within the matrix of the arrested high- T_g component. 2D ^{31}P NMR exchange spectroscopy proves that the dynamical heterogeneities of the α_2 -process are of transient nature, i.e., exchange occurs within the distribution $G(\ln\tau_{\alpha_2})$ below T_{g1} . The time constants compiled from all the methods fit perfectly together and display the evolution of the dynamics of the two relaxations in the full concentration range. The plasticizer effect for the slow α_1 -relaxation and the anti-plasticizer effect for the fast m-TCP relaxation are documented. At the glass transition temperature T_{g1} of the large component a dynamical crossover is found for $\tau_{\alpha_2}(T)$, from a non-Arrhenius behavior above to an Arrhenius behavior below T_{g1} and attributed to intrinsic confinement dynamics. This “fragile-to-strong” transition also leads again to a decrease of the $T_{g2}(c)$ at low m-TCP concentration, thus a maximum in the $T_{g2}(c)$ value is found at concentrations around 50%. So all features known from polymer additive systems are also found in this non-polymeric system, and it appears that essentially the T_g contrast of the components determines the dynamics in binary glass formers.

ACKNOWLEDGMENTS

Dr. Klaus Kreger, Doris Hanft, and Professor Hans-Werner Schmidt (Macromolecular Chemistry I, University of Bayreuth) are gratefully acknowledged for providing the photochromic molecular glass and for fruitful discussions. Furthermore, Björn Pötzschnner appreciates financial support of the Elitenetzwerk Bayern.

APPENDIX: ADDITIONAL DIELECTRIC SPECTRA

Fig. 16 shows the dielectric spectra for the $c_{m\text{-TCP}} = 73\%$ sample with pronounced α_2 -process. After subtraction of the

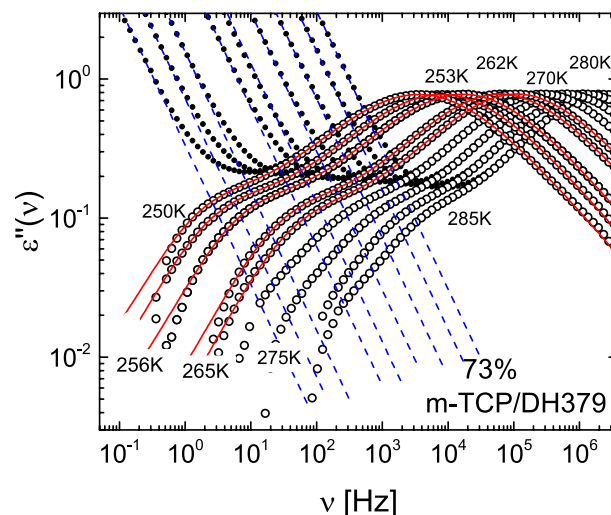


FIG. 16. Dielectric spectra of the sample $c_{m\text{-TCP}} = 73\%$ (filled circles). Open circles: spectra after subtracting the contribution of the dc conductivity. Dashed lines: conductivity contribution. Solid lines: fit by a weighted superposition along of Eqs. (8)/(15) and (16), respectively.

conductivity contribution a shoulder at low frequencies is observed and attributed to the α_1 -process.

- ¹P. J. Hains and G. Williams, *Polymer* **16**, 725 (1975).
- ²M. A. Desando, S. Walker, and W. H. Baarschers, *J. Chem. Phys.* **73**, 3460 (1980).
- ³M. Scandola, G. Ceccorulli, and M. Pizzoli, *Polymer* **28**, 2081 (1987).
- ⁴M. Nakazawa, O. Urakawa, and K. Adachi, *Macromolecules* **33**, 7898 (2000).
- ⁵J. Colmenero and A. Arbe, *Soft Matter* **3**, 1474 (2007).
- ⁶K. L. Ngai, *Relaxation and Diffusion in Complex Systems* (Springer-Verlag, Berlin, Heidelberg, 2011).
- ⁷D. Bingemann, N. Wirth, J. Gmeiner, and E. A. Rössler, *Macromolecules* **40**, 5379 (2007).
- ⁸T. Blochowicz, S. Lusceac, P. Gutfreund, S. Schramm, and B. Stühn, *J. Phys. Chem. B* **115**, 1623 (2011).
- ⁹T. Blochowicz, S. Schramm, S. Lusceac, M. Vogel, B. Stühn, P. Gutfreund, and B. Frick, *Phys. Rev. Lett.* **109**, 035702 (2012).
- ¹⁰R. Kahlau, D. Bock, B. Schmidtke, and E. A. Rössler, *J. Chem. Phys.* **140**, 044509 (2014).
- ¹¹R. P. Kambour, J. M. Kelly, B. J. McKinley, B. J. Cauley, P. T. Inglefield, and A. A. Jones, *Macromolecules* **21**, 2937 (1988).
- ¹²Y. Liu, A. K. Roy, A. A. Jones, P. T. Inglefield, and P. Ogden, *Macromolecules* **23**, 968 (1990).
- ¹³C. Zhang, P. Wang, A. A. Jones, P. T. Inglefield, and R. P. Kambour, *Macromolecules* **24**, 338 (1991).
- ¹⁴Y. Liu, M. M. Turnbull, A. A. Jones, P. T. Inglefield, and R. P. Kambour, *Solid State Nucl. Magn. Reson.* **2**, 289 (1993).
- ¹⁵T. Blochowicz, C. Karle, A. Kudlik, P. Medick, I. Roggatz, M. Vogel, Ch. Tschirwitz, J. Wolber, J. Senker, and E. A. Rössler, *J. Phys. Chem. B* **199**, 4032 (1999).
- ¹⁶D. Bock, R. Kahlau, B. Pötzschnner, T. Körber, E. Wagner, and E. A. Rössler, *J. Chem. Phys.* **140**, 094505 (2014).
- ¹⁷D. Bock, R. Kahlau, B. Micko, B. Pötzschnner, G. J. Schneider, and E. A. Rössler, *J. Chem. Phys.* **139**, 064508 (2013).
- ¹⁸G. Floudas, M. Paluch, A. Grzybowski, and K. L. Ngai, *Molecular Dynamics of Glass-Forming Systems* (Springer, Berlin, 2011).
- ¹⁹T. Blochowicz and E. A. Rössler, *Phys. Rev. Lett.* **92**, 225701 (2004).
- ²⁰E. A. Rössler and P. Eiermann, *J. Chem. Phys.* **100**, 5237 (1994).
- ²¹T. Blochowicz, C. Gainaru, P. Medick, C. Tschirwitz, and E. A. Rössler, *J. Chem. Phys.* **124**, 134503 (2006).
- ²²S. Adichtchev, D. Bock, C. Gainaru, R. Kahlau, B. Micko, N. Petzold, B. Pötzschnner, and E. A. Rössler, *Z. Phys. Chem.* **226**, 1149 (2012).
- ²³D. Bock, N. Petzold, R. Kahlau, S. Gradmann, B. Schmidtke, N. Benoit, and E. A. Rössler, *J. Non-Cryst. Solids* **407**, 88 (2015).
- ²⁴B. Micko, C. Tschirwitz, and E. A. Rössler, *J. Chem. Phys.* **138**, 154501 (2012).

- ²⁵D. Cangialosi, A. Alegría, and J. Colmenero, *J. Chem. Phys.* **126**, 204904 (2007).
- ²⁶K. Kessairi, S. Capaccioli, D. Prevosto, M. Lucchesi, and P. Rolla, *J. Chem. Phys.* **127**, 174502 (2007).
- ²⁷M. D. Ediger, T. R. Lutz, and Y. He, *J. Non-Cryst. Solids* **352**, 4718 (2006).
- ²⁸S. Capaccioli, K. Kessairi, M. Shahin, D. Prevosto, and M. Lucchesi, *J. Non-Cryst. Solids* **357**, 251 (2011).
- ²⁹H. Audorff, K. Kreger, R. Walker, D. Haarer, L. Kador, and H.-W. Schmidt, *Adv. Polym. Sci.* **228**, 59 (2010).
- ³⁰K. Kreger, P. Wolfer, H. Audorff, L. Kador, N. Stingelin-Stutzmann, P. Smith, and H.-W. Schmidt, *J. Am. Chem. Soc.* **132**, 509 (2010).
- ³¹P. Wolfer, H. Audorff, K. Kreger, L. Kador, H.-W. Schmidt, N. Stingelin, and P. Smith, *J. Mater. Chem.* **21**, 4339 (2011).
- ³²H. Audorff, R. Walker, L. Kador, and H.-W. Schmidt, *Chem.–Eur. J.* **17**, 12722 (2011).
- ³³R. Walker, H. Audorff, L. Kador, and H.-W. Schmidt, *Adv. Funct. Mater.* **19**, 2630 (2009).
- ³⁴A. Abragam, *The Principles of Nuclear Magnetism* (Clarendon Press, Oxford, 1961).
- ³⁵E. A. Rössler, M. Taupitz, K. Börner, M. Schulz, and H.-M. Vieth, *J. Chem. Phys.* **92**, 5847 (1990).
- ³⁶R. Böhmer, G. Diezemann, G. Hinze, and E. A. Rössler, *Prog. Nucl. Magn. Reson. Spectrosc.* **39**, 191 (2001).
- ³⁷C. P. Slichter, *Principles of Magnetic Resonance* (Springer-Verlag, Berlin, Heidelberg, 1990).
- ³⁸H. W. Spiess, *Dynamic NMR Spectroscopy, NMR Basic Principles and Progress Vol. 15* (Springer Verlag, Berlin, 1978).
- ³⁹J. Kowalewski and L. Maler, *Nuclear Spin Relaxation in Liquids: Theory, Experiments and Applications* (Taylor and Francis, International, 2006).
- ⁴⁰F. Fujara, S. Wefing, and H. W. Spiess, *J. Chem. Phys.* **84**, 4579 (1986).
- ⁴¹K. Schmidt-Rohr and H. W. Spiess, *Multidimensional Solid-State NMR and Polymers* (Academic Press, New York, 1994).
- ⁴²M. Vogel and E. A. Rössler, *J. Phys. Chem. A* **102**, 2102 (1998).
- ⁴³H. Wagner and R. Richert, *J. Phys. Chem. B* **103**, 4071 (1999).
- ⁴⁴C. J. F. Böttcher and P. Bordewijk, *Theory of Electric Polarization* (Elsevier, Amsterdam, 1978).
- ⁴⁵A. Kudlik, S. Benkhof, T. Blochowicz, C. Tschirwitz, and E. A. Rössler, *J. Mol. Struct.* **479**, 201 (1999).
- ⁴⁶C. Gainaru, R. Kahlau, E. A. Rössler, and R. Böhmer, *J. Chem. Phys.* **131**, 184510 (2009).
- ⁴⁷P. Lunkenheimer, U. Schneider, R. Brand, and A. Loidl, *Contemp. Phys.* **41**, 15 (2000).
- ⁴⁸T. Dries, F. Fujara, M. Kiebel, E. A. Rössler, and H. Sillescu, *J. Chem. Phys.* **88**, 2139 (1988).
- ⁴⁹M. Vogel and E. A. Rössler, *J. Chem. Phys.* **114**, 5802 (2001).
- ⁵⁰M. Vogel and E. A. Rössler, *J. Chem. Phys.* **115**, 10883 (2001).
- ⁵¹A. Zetsche and E. W. Fischer, *Acta Polym.* **45**, 168 (1994).
- ⁵²S. K. Kumar, R. H. Colby, S. H. Anastasiadis, and G. Fytas, *J. Chem. Phys.* **105**, 3777 (1996).
- ⁵³R. Kant, S. K. Kumar, and R. H. Colby, *Macromolecules* **36**, 10087 (2003).
- ⁵⁴G. C. Chung, J. A. Kornfield, and S. D. Smith, *Macromolecules* **27**, 964 (1994).
- ⁵⁵T. P. Lodge and T. C. B. McLeish, *Macromolecules* **33**, 5278 (2000).
- ⁵⁶E. Leroy, A. Alegria, and J. Colmenero, *Macromolecules* **36**, 7280 (2003).
- ⁵⁷S. Shenogin, R. Kant, R. H. Colby, and S. K. Kumar, *Macromolecules* **40**, 5767 (2007).
- ⁵⁸A. Schönhals, H. Goering, C. Schick, B. Frick, M. Mayorova, and R. Zorn, *Eur. Phys. J.: Spec. Top.* **141**, 255 (2007).
- ⁵⁹F. Kremer, A. Huwe, M. Arndt, P. Behrens, and W. Schwieger, *J. Phys.: Condens. Matter* **11**, A175 (1999).
- ⁶⁰J. Bosse and Y. Kaneko, *Phys. Rev. Lett.* **74**, 4023 (1995).
- ⁶¹T. Voigtmann and J. Horbach, *Phys. Rev. Lett.* **103**, 205901 (2009).
- ⁶²V. Krakoviack, *Phys. Rev. Lett.* **94**, 065703 (2005).
- ⁶³A. J. Moreno and J. Colmenero, *Phys. Rev. E* **74**, 021409 (2006).

6. Publication III

Publication III

Non-polymeric asymmetric binary glass-formers. I. Main relaxations studied by dielectric, ^2H NMR, and ^{31}P NMR spectroscopy

B. Pötzschner, F. Mohamed, C. Bächer, E. Wagner, A. Lichtinger,
R. Minikejew, K. Kreger, H.-W. Schmidt, and E. A. Rössler

J. Chem. Phys. 146, 164503 (2017)

Doi: 10.1063/1.4980084

© 2017 AIP Publishing LLC

Non-polymeric asymmetric binary glass-formers. I. Main relaxations studied by dielectric, ^2H NMR, and ^{31}P NMR spectroscopy

B. Pötzschner, F. Mohamed, C. Bächer, E. Wagner, A. Lichtinger, R. Minikejew, K. Kreger, H.-W. Schmidt, and E. A. Rössler^{a)}

Experimentalphysik II, University of Bayreuth, 95447 Bayreuth, Germany and Macromolecular Chemistry I, University of Bayreuth, 95447 Bayreuth, Germany

(Received 4 February 2017; accepted 31 March 2017; published online 27 April 2017)

In Paper I of this series of two papers we study the main relaxations of a binary glass former made of the low- T_g component tripropyl phosphate (TPP, $T_g = 134$ K) and of a specially synthesized (deuterated) spirobichroman derivative (SBC, $T_g = 356$ K) as the non-polymeric high- T_g component for the full concentration range. A large T_g contrast of the neat components is put into effect. Dielectric spectroscopy and different techniques of ^2H nuclear magnetic resonance (NMR) as well as of ^{31}P NMR spectroscopy allow to selectively probe the dynamics of the components. For all concentrations, two well separated liquid-like processes are identified. The faster α_2 -process associated with the low- T_g component TPP shows pronounced dynamic heterogeneities reflected by quasi-logarithmic correlation functions at low TPP concentrations. The slower α_1 -process involves the reorientation of the high- T_g component SBC. Its correlation function is Kohlrausch-like as in neat glass formers. The corresponding time constants and consequently their glass transition temperatures T_{g1} and T_{g2} differ more the lower the TPP concentration is. Plasticizer and anti-plasticizer effect, respectively, is observed. At low temperatures a situation arises that the TPP molecules isotropically reorient in an arrested SBC matrix ($T_{g2} < T < T_{g1}$). At $T < T_{g2}$ the liquid-like reorientation of TPP gets arrested too. We find indications that a fraction of the TPP molecule takes part in the slower α_1 -process of the high- T_g component. All the features known from polymer-plasticizer systems are rediscovered in this non-polymeric highly asymmetric binary mixture. In Paper II [B. Pötzschner *et al.*, *J. Chem. Phys.* **146**, 164504 (2017)] we study the secondary (β -) relaxations of the mixtures. *Published by AIP Publishing.* [<http://dx.doi.org/10.1063/1.4980084>]

I. INTRODUCTION

In recent years, pure glass formers were extensively investigated in terms of the evolution of their dynamic susceptibility covering many decades in frequency or time.^{1–7} The next challenge is to characterize and understand the dynamics in binary glass forming systems. While technologically relevant polymer-additive systems were the subject of intensive research,^{8–15} less is known about non-polymeric mixed systems, in particular, about such systems with a high- T_g contrast of their components as it is the case in the usual polymer-plasticizer systems. Extending our previous activities on polymer-plasticizer systems, we recently started a project synthesizing non-polymeric high- T_g glass formers which are mixed with a low- T_g component.^{13,16,17} We note that such systems may also be of technological relevance.¹⁸ Our first experiments with a spirobichroman derivative as the high- T_g component demonstrated so far that, as in the case of polymer-plasticizer systems, the T_g contrast determines the dynamics of the mixture.¹⁹ Given a large enough T_g contrast strong dynamical heterogeneities appear and two glass transition temperatures can be identified as in the case of polymer-plasticizer systems.^{20–22}

In detail the following picture emerged which applies to both polymer and non-polymer binary glass formers.^{13,16,17,23} With the aid of dielectric spectroscopy (DS) and component selective nuclear magnetic resonance (NMR) spectroscopy two main relaxation processes, α_1 and α_2 , were identified. The faster (α_2 -)process is assigned to the dynamics of the (low- T_g) additive molecule, showing the anti-plasticizer effect and strong dynamic heterogeneities, i.e., a very broad distribution of correlation times $G(\ln \tau_{\alpha_2})$ is found which leads to quasi-logarithmic correlation functions observed by NMR techniques. Both effects become more pronounced with decreasing additive concentration. The slower (α_1 -)process is attributed to the dynamics of the high- T_g component showing the well documented plasticizer effect with increasing additive concentration. Its correlation function essentially remains similar to that of the pure high- T_g component following frequency-temperature superposition (FTS). In the case of the mixture tripropyl phosphate (TPP)/polystyrene (PS), dielectric spectroscopy, predominantly probing the low- T_g component TPP, actually identified two relaxation processes (in addition to a secondary process²⁴). In agreement with other reports,^{20,21} this was interpreted in terms of two sub-ensembles of additive molecules, one participating in the slow dynamics of the high- T_g components and the other displaying the highly decoupled (α_2 -)dynamics in the slowly moving matrix consisting essentially of the high- T_g component. Furthermore,

^{a)} Author to whom correspondence should be addressed. Electronic mail: ernst.roessler@uni-bayreuth.de.

a change in the temperature dependence of the α_2 -process is observed when surpassing T_{g1} associated with the glassy arrest of the high- T_g component (α_1 -process). While above T_{g1} , $\tau_{\alpha_2}(T)$ shows a non-Arrhenius behavior, an Arrhenius law is observed below T_{g1} . This “fragile-to-strong” transition was observed in the polymer blend PS/PVME.²⁵ Later it was also found in both polymer-additive and non-polymeric binary systems.^{16,19,21} As the α_2 -process displays an Arrhenius temperature dependence it could be confused with a secondary (β -) process. However, our 2D NMR experiments clearly demonstrated that a broad distribution of isotropic reorientations is involved, i.e., below T_{g1} a liquid-like motion occurs in the rigid matrix of the high- T_g component. The fragile-to-strong transition in $\tau_{\alpha_2}(T)$ is also responsible that the (mass) concentration dependence of $T_{g2}(c)$ exhibits a maximum around $c = 50\%$ while $T_{g1}(c)$ shows the well-known monotonic plasticizer effect.

The present investigation continues our studies on non-polymeric binary systems. In our previous works, a non-deuterated high- T_g spirobichroman derivative ($T_g = 382$ K) together with *m*-tricresyl phosphate ($T_g = 206$ K) as an additive was employed with a T_g contrast of $\Delta T_g = 176$ K. This time we synthesized and deuterated a new non-polymeric high- T_g component (again a spirobichroman derivative called SBC, cf. Fig. 1). As the low- T_g component we chose TPP (like in our PS study¹⁷) which leads to a larger T_g contrast of $\Delta T_g = 222$ K. By means of ^{31}P NMR and ^2H NMR as well as by DS, the component-specific dynamics of TPP and SBC were probed. The study is decomposed into two parts. Paper I focuses on the synthesis of (deuterated) SBC and on the main relaxation processes (α_1 and α_2) of the components and of the mixtures. Also the methodological part of DS and NMR is included. In Paper II⁵⁵ we investigate the β -process which is observable below T_{g2} . Our previous TPP/PS study²⁴ on the β -process demonstrated that, while pure PS does not show a β -process, in the mixture the activation energy of $\tau_\beta(T)$ essentially does not change in the entire concentration regime being virtually the same as that in neat TPP. Characterized by NMR spectroscopy as a spatially highly hindered reorientation as found in neat glasses,^{24,26–28} the β -process in the mixed glasses was actually identified for both components, TPP as well as PS. Thus, it appears that TPP “enslaves” the PS segments to participate in the β -process introduced by TPP. This we took as an indication that the β -process is of cooperative nature. Consequently, we address in Paper II⁵⁵ the question whether in the present mixtures the molecularly “large” component SBC is enslaved by the “small” component TPP.

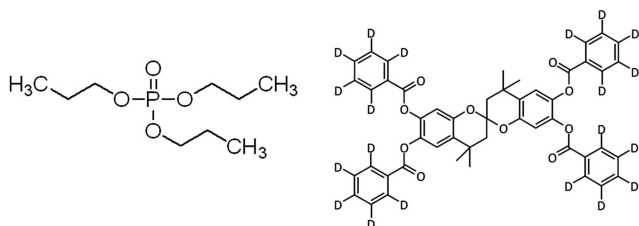


FIG. 1. Low- T_g component tripropyl phosphate (TPP) (left) ($M_{mol} = 224.23$ g/mol, $T_g = 134$ K) and high- T_g spirobichroman component SBC (right) ($M_{mol} = 809.0$ g/mol, $T_g = 356$ K).

II. EXPERIMENTAL AND METHODOLOGICAL SECTION

A. Systems

The binary mixtures of the (low- T_g) glass former tripropyl phosphate (TPP) and a (high- T_g) spirobichroman derivative functionalized with four deuterated benzoic acids, which will be subsequently called SBC, were investigated (cf. Fig. 1). The TPP (99%) was received from Sigma-Aldrich and the SBC compound was specifically synthesized for this study (see below). With a T_g of 134 K for TPP²⁹ and a T_g of 356 K for SBC, a T_g contrast of $\Delta T_g = 222$ K is reached. The SBC was employed in a non-deuterated form for ^{31}P NMR and dielectric measurements and deuterated at the phenyl rings (cf. Fig. 1) for the ^2H NMR experiments. Mixtures with mass concentration $c_{TPP} = 10\%$ (only β -process), 21%, 34%, 47%, 61%, 76%, 89%, and 100% of TPP in SBC were investigated by ^{31}P NMR spectroscopy and mixtures with $c_{TPP} = 0\%$, 10%, 22%, 39%, 59%, and 80% by ^2H NMR spectroscopy. Additionally, we performed DS measurements on neat SBC, neat TPP, and mixtures with $c_{TPP} = 61\%$, 70%, and 85%. The concentration error is $\pm 2\%$. They confirmed that both, the non-deuterated and the deuterated SBC components, show the same dielectric loss for the main and secondary relaxations and thus are dynamically identical.

The mixture showed a tendency to de-mix at temperatures around room temperature or slightly above. Hence, no NMR measurements above room temperature were possible. To assure a stable glass phase at temperatures below, all samples were measured twice and regularly inspected for transparent appearance. Regarding the DS measurements, the tendency to de-mix limited measurements to $c_{TPP} \geq 61\%$. Possibly the mixture shows a lower critical solution temperature. In the case of the NMR experiments, measurements down to lowest concentrations were possible.

The deuterated spirobichroman derivative (SBC) 4,4,4',4'-tetramethyl-2,2'-spirobichroman-6,6',7,7'-tetrol-tetrabenzoate- d_5 was synthesized by an esterification of benzoyl- d_5 chloride (Aldrich) and 6,6',7,7'-tetrahydroxy-4,4,4',4'-tetramethyl-2,2'-spirobichroman (ABCR). The amount of 0.56 g (1.5 mmol) of the 2,2'-spirobichroman-6,6',7,7'-tetrol was dissolved in 30 ml of anhydrous tetrahydrofuran (THF) and 0.9 ml (6.5 mmol) of triethylamine under inert atmosphere. The mixture was cooled to 0°C and 0.75 ml (6.5 mmol) of benzoic- d_5 -acid chloride was added dropwise. The mixture was allowed to warm to room temperature and was refluxed for 12 h. After cooling the solution to room temperature, approximately 50 ml of ethyl acetate was added. The organic mixture was washed three times with water and brine. Subsequently, the solvents were removed under reduced pressure and the crude product was re-crystallized from ethanol and acetone, respectively. An amount of 0.56 mg (47%) of SBC was obtained as white solid.

Molecular characterization: ^1H NMR spectra in solution were recorded on a Bruker Avance 300 spectrometer at 300.1 MHz at room temperature. Mass spectrometry (MS) was conducted on a Finnigan MAT 8500 GC/MS. Thermogravimetric analysis was performed with a Mettler Toledo

SDTA 851 at a heating rate of 10 K min⁻¹ under nitrogen. The following results were obtained.

¹H NMR (CDCl₃): *d* = 1.42 (s, 6H), 1.65 (s, 6H), 2.07 (d, 2H), 2.17 (d, 2H), 6.82 (s, 2H), and 7.33 (s, 2H) ppm.

Mass spectroscopy (MS): 809 (M⁺ 7); 794 (32); 621 (15); 410 (55); 167 (14); 110 (30); 82 (21) m/z (%).

Thermogravimetric analysis: *T*_{dec}: 658 K (385 °C) (decomposition temperature, *T*_{dec}, refers to a weight loss of 5 wt. %).

B. Nuclear magnetic resonance (NMR) spectroscopy

The ³¹P NMR experiments were performed on a Bruker Avance III spectrometer with a 400 MHz (9.4 T) Spectrospin cryomagnet corresponding to a ³¹P nuclear frequency of $\omega_L/2\pi = 161.98$ MHz. A home-built (in cooperation with Bruker Biospin GmbH) double resonance probe was employed and cooled with liquid nitrogen applying an Oxford CF1200 cryostat and an Oxford ITC-503 temperature controller. Temperature accuracy was better than ± 2 K and stability was better than ± 0.2 K. The ²H NMR experiments were carried out on an upgraded Bruker Avance DSX spectrometer and an Oxford 300 MHz cryomagnet resulting in an NMR frequency of $\omega_L/2\pi = 46.067$ MHz. A CryoVac Konti cryostat together with an Oxford ITC-503 temperature controller cooled the home-built probe with liquid nitrogen. The temperature accuracy was better than ± 1 K and stability was better than ± 0.2 K.

1. NMR spectra

The interaction of the nuclear quadrupolar moment (Q) with the electric field gradient (EFG) determines the ²H NMR spectra. The shift of the NMR frequency $\omega(\theta, \varphi)$ with respect to the Larmor frequency is given by

$$\omega(\theta, \varphi) = \pm \delta_Q/2(3 \cos^2 \theta - 1 - \eta \sin^2(\theta) \cos(2\varphi)) \quad (1)$$

and depends on the spherical angles (θ, φ) between the direction of the magnetic field and the principal EFG tensor axis.³⁰ The anisotropy of the quadrupolar tensor is specified by the parameter δ_Q , and the asymmetry by the parameter η . For SBC at low temperatures a symmetric EFG tensor is found ($\eta = 0$), i.e., the shift of the angular NMR frequency $\omega(\theta)$ depends only on the angle θ . For an anisotropic fast motion, for example, the phenyl ring jump of SBC, δ_Q and η have to be replaced by their motional averaged values $\overline{\delta_Q}$ and $\overline{\eta}$.

In the case of ³¹P NMR, the dominant interaction is the chemical shift anisotropy (CSA). The dependence of the NMR frequency on the reorientation is similar to that of ²H NMR (cf. Eq. (1)); δ_Q has to be replaced by the CSA anisotropy δ_{CSA} and only the positive sign is valid. Also for TPP a symmetric CSA tensor $\eta = 0$ is found. The parameter δ_{CSA} depends linearly on the magnetic field B_0 : $\omega_L \Delta\sigma_{CSA} = \frac{3}{2} \delta_{CSA}$ with $\omega_L = \gamma B_0$ and the frequency independent shielding parameter $\Delta\sigma_{CSA} = \sigma_{\parallel} - \sigma_{\perp}$ (for $\eta = 0$), while σ_{\parallel} and σ_{\perp} are the CSA tensor components parallel to the symmetry axis of the molecule and to a perpendicular axis.

The CSA interaction leads to a characteristic asymmetric powder spectrum, the quadrupolar interaction to a Pake spectrum, provided that the molecular reorientation is slower than the NMR time scale ($\tau_\alpha \gg \frac{1}{\delta}$) and that the molecular orientation is isotropically distributed as it is the case in glasses.

For high temperatures well above T_g , fast isotropic reorientation characterized by the time constant τ_α leads to a collapse of the solid-state spectrum to a central Lorentzian line. In this limit ($\tau_\alpha \ll \frac{1}{\delta}$) the full width of the Lorentzian line $\Delta\omega$ (in angular frequency) is related to the transversal relaxation time T_2 via $\Delta\omega = 2/T_2$.^{30,31} At even higher temperatures the inhomogeneity of the magnetic field determines the line width.

Static density fluctuations in the case of the phenyl jumps observed in SBC ($T < T_g$), as well as the dynamic heterogeneity of the α_2 -process, lead to a broad distribution of correlation times $G(\ln \tau)$ which yields the so-called “two-phase spectra.” They can be described by a superposition of a fast exchange S_{fast} and a slow exchange S_{slow} spectra,^{32,33}

$$S(\omega; T) = W(T)S_{fast}(\omega) + (1 - W(T))S_{slow}(\omega) \quad (2)$$

with a weighting factor $W = \int_{-\infty}^{\ln \tau_{cut}} G(\ln \tau) d \ln \tau$, where τ_{cut} is defined by the typical time scale of the experiment: $\tau_{cut} \approx 1/\delta$. In the case of a broad distribution $G(\ln \tau)$, spectral contributions from subensembles with correlation times on the order of the NMR time scale ($\tau_\alpha \approx \frac{1}{\delta}$) can be neglected due to the small fraction of molecules in the intermediate exchange limit and due to the reduction of their signal intensity in the NMR echo (applied for monitoring the spectra, see below). In the case of the isotropic, α_2 -relaxation of TPP S_{fast} corresponds to a Lorentzian line and S_{slow} to the CSA solid-state spectrum. In the case of the phenyl ring jumps observed in SBC, S_{fast} corresponds to a motional averaged spectrum with $\overline{\delta_Q}$ and $\overline{\eta} \neq 0$, while S_{slow} again is the solid-state spectrum. Here, assuming a distribution of activation energies $g(E)$ as the cause for $G(\ln \tau_{ph})$ ($T < T_g$), one is able to estimate $g(E)$ from the weighting factor $W(T) = W_{ph}(T)$ via

$$g(E) = (R \ln \left(\frac{\tau_{cut}}{\tau_0} \right))^{-1} * \frac{dW_{ph}(T)}{dT} \quad (3)$$

with $\tau_{cut} \approx 10^{-5}$ s and taking $1/\tau_0 \approx 10^{12}$ s⁻¹ being the attempt frequency.³²

Solid-state spectra were recorded with a Hahn echo pulse sequence (³¹P: 90°-*t*_p-180°) or a solid echo pulse sequence (²H: 90°-*t*_p-90°) with an inter-pulse delay of *t*_p = 20 μs and 25 μs, respectively. For investigating the β-process, *t*_p was systematically varied (cf. Paper II⁵⁵). ¹H-³¹P dipolar decoupling was applied for all ³¹P NMR spectra during the acquisition of the FID to eliminate the heteronuclear dipole-dipole interaction.

2. Relaxation times

The ³¹P NMR relaxation is determined by the fluctuation of the CSA interaction.^{30,31,34} The relative contribution from heteronuclear dipolar coupling is weak at the applied high magnetic field and in the case of homonuclear coupling it is neglectable due to the large distance between the phosphorus nuclei in the different TPP molecules.²⁹ The ²H relaxation is caused by the fluctuation of the quadrupolar interaction.^{30,31,34} The relaxation rates $1/T_1$ and $1/T_2$ are linked to the spectral density $J(\omega)$ at multiples of the Larmor frequency ω_L .³⁰ In the case of the CSA interaction one gets

$$\frac{1}{T_1} = K^{CSA} J(\omega_L), \quad (4)$$

$$\frac{1}{T_2} = \frac{1}{6} K^{CSA} (4J(0) + 3J(\omega_L)), \quad (5)$$

with

$$K^{CSA} = \frac{2}{15} (\Delta\sigma_{CSA}\omega_L)^2. \quad (6)$$

In the case of the quadrupolar interaction it holds

$$\frac{1}{T_1} = \frac{2}{15} \delta_Q^2 [J(\omega_L) + 4J(2\omega_L)], \quad (7)$$

$$\frac{1}{T_2} = \frac{1}{15} \delta_Q^2 [3J(0) + 5J(\omega_L) + 2J(2\omega_L)]. \quad (8)$$

For an estimate of the time constants, we took the condition $\omega_L\tau_{\alpha 2} \approx 1$ at the T_1 -minimum for ^{31}P NMR and $\omega_L\tau_{\alpha 1} \approx 0.616$ for ^2H NMR.³⁰ In the slow motion limit ($\omega_L\tau_{\alpha} \gg 1$) $1/T_2$ is directly linked to the time constant τ_{α} and independent of a specific model for $J(\omega)$:³⁰ $\frac{1}{T_2} = \frac{2}{3} K^{CSA} \tau_{\alpha 2}$ for ^{31}P NMR and $\frac{1}{T_2} = \frac{1}{5} \delta_Q^2 \tau_{\alpha 1}$ for ^2H NMR.

The spin-lattice relaxation measurements were performed with a saturation recovery pulse sequence at low and with an inversion recovery pulse sequence at high temperatures. The spin-spin relaxation time T_2 was obtained with the Carr-Purcell-Meiboom-Gill (CPMG) pulse sequence³⁰ and from the spectral width $\Delta\omega$ of the Lorentzian line in the liquid when inhomogeneous broadening can be neglected.

3. Stimulated echo experiment

From the decay of the stimulated echo the correlation function of the second Legendre polynomial $P_2(\theta)$ is accessible, i.e., the rank-two reorientational correlation function $C_2(t)$ is probed. In the case of ^{31}P NMR, a three-pulse echo sequence (90° - t_{ev} - 90° - t_m - 90°) with appropriate pulse phases is applied and the echo amplitude is measured for different mixing times t_m at constant evolution time t_{ev} . Regarding ^2H NMR a four-pulse sequence (90° - t_{ev} - 45° - t_m - 45° - t_p - 90°) is employed.³⁵ Here an additional solid-echo pulse sequence is added after the third pulse. The decay in the sine-sine experiment is described by³⁵

$$\begin{aligned} I(t_m, t_{ev}) &\propto \langle \sin(\omega(0)t_{ev}) \sin(\omega(t_m)t_{ev}) \rangle \exp\left(-\left(t_m/T_{1Q}\right)\right) \\ &= F_{t_{ev}}^{\sin}(t_m) \exp\left(-\left(t_m/T_{1Q}\right)\right). \end{aligned} \quad (9)$$

In the case of ^2H NMR, the correlation function $F_{t_{ev}}^{\sin}(t_m)$ is damped by the quadrupolar relaxation (T_{1Q}) while for ^{31}P NMR by the spin-lattice relaxation (T_1). $F_{t_{ev}}^{\sin}(t_m)$ can be written as³⁶

$$F_{t_{ev}}^{\sin} = (1 - F_{\infty}) F(t_m, t_{ev}) + F_{\infty}. \quad (10)$$

For a short evolution time t_{ev} and isotropic reorientation, the function $F_{t_{ev}}^{\sin}(t_m)$ approximates the reorientational correlation function $C_2(t)$,

$$\lim_{t_{ev} \rightarrow 0} F_{t_{ev}}^{\sin}(t_m) \propto \langle \omega(0)\omega(t_m) \rangle \propto C_2(t_m) = C_2(t). \quad (11)$$

$C_2(t)$ is interpolated by a stretched exponential (Kohlrausch) function, so the normalized data is fitted with

$$C_2(t) = \exp\left(-\left(\frac{t}{\tau_K}\right)^{\beta_K}\right) \quad (12)$$

except at very low additive concentrations, where $C_2(t)$ follows a quasi-logarithmic decay. The (mean) correlation time is given by $\tau_{\alpha} = \frac{\tau_K}{\beta_K} \Gamma\left(\frac{1}{\beta_K}\right)$. An evolution time $t_{ev} = 10 \mu\text{s}$ was applied for both ^{31}P and ^2H NMRs, whereby the short-time limit is fulfilled (cf. Eq. (11)).

C. Dielectric spectroscopy

The dielectric measurements were achieved by applying an Alpha-A analyzer from Novocontrol in the frequency range $\nu = 10^{-2} \text{ Hz} - 10^6 \text{ Hz}$. Temperature was regulated within $\pm 0.1 \text{ K}$ by using a Quatro-H temperature controller from Novocontrol with an absolute accuracy better than $\pm 0.2 \text{ K}$. The sample cell was constructed by a design of Wagner and Richert and assures a constant sample volume.³⁷

The (complex) dielectric constant $\varepsilon^*(\omega)$ is defined by³⁸

$$\varepsilon^*(\omega) = \varepsilon'(\omega) - i\varepsilon''(\omega) = \varepsilon_{\infty} + \Delta\varepsilon \int_0^{\infty} -\frac{d\phi(t)}{dt} e^{-i\omega t} dt, \quad (13)$$

where ε_{∞} denotes its high-frequency limit and $\phi(t)$ the step-response function. For the α_1 -relaxation peak (reflecting essentially SBC dynamics), a Kohlrausch stretched exponential function (cf. Eq. (12)) was used for $\phi(t)$ to fit the data. For the α_2 -peak (reflecting TPP dynamics), a Havriliak-Negami (HN) function was taken explicitly,³⁸

$$\varepsilon^* - \varepsilon_{\infty} = \Delta\varepsilon / [1 + i(\omega\tau_0)^a]^b. \quad (14)$$

In the case that both α_1 - and α_2 -peak are observed simultaneously in the frequency window, the spectra are interpolated by a weighted sum of Eqs. (12)/(13) and (14). Anyway, the time constant $\tau_{\alpha 2}$ is always extracted by ‘‘peak picking’’, i.e., $\tau_{\alpha 2} = 1/(2\pi\nu_{max})$, while $\tau_{\alpha 1}$ is given by the mean correlation time of the Kohlrausch function (cf. above). At low frequencies, a dc conductivity is observed, which is subtracted from $\varepsilon''(\omega)$ along $\varepsilon''_{dc}(\omega) = \frac{\sigma_{dc}}{\varepsilon_0\omega}$.

III. RESULTS

A. Dielectric spectra of the neat components

The dielectric spectra of neat SBC ($T_g = 356 \text{ K}$) and of neat TPP ($T_g = 134 \text{ K}$)²⁹ are shown in Fig. 2. Above T_g , the main (α -)relaxation process is observed which shifts to higher frequencies upon heating in both components. At frequencies higher than that of the α -relaxation, a secondary relaxation (β -process) is well recognized in both components which persists for temperatures below T_g . The signal amplitude of SBC is about a factor of 50 smaller than that of TPP. In terms of the relaxation strength $\Delta\varepsilon$ (given by the integral over $\varepsilon''(\omega)$) corrected for the Curie law, we find that $\Delta\varepsilon_{TPP}/\Delta\varepsilon_{SBC} \cong 11$. At $T \geq 388 \text{ K}$ the signal of SBC decreased due to crystallization. The time constants τ_{α} are extracted via $\tau_i = 1/2\pi\nu_{imax}$ and included in Fig. 11. They will be discussed below; those of the β -process are presented in Paper II.⁵⁵ We emphasize that both non- and deuterated SBC show the same time constants for α - and β -process (see Fig. 11).

B. Dielectric spectra of the mixtures

The spectra of the $c_{TPP} = 85\%$ sample are displayed in Fig. 3(a). The original data (open circles) show the main

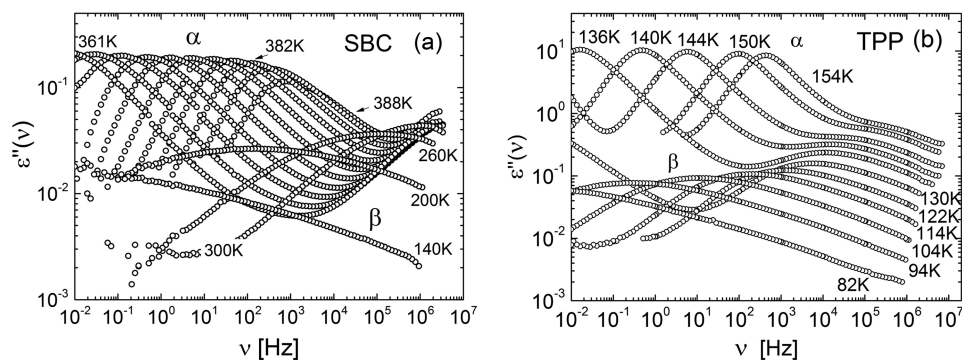


FIG. 2. (a) Dielectric spectra of neat SBC ($T_g = 356$ K) in the temperature range of $T = 361$ K to 391 K in 3 K steps and at distinct lower temperatures down to 140 K. (b) Corresponding spectra of neat TPP ($T_g = 134$ K) in the temperature range of $T = 82$ K to 154 K. (Adapted with permission from J. Chem. Phys. **139**, 064508 (2013). Copyright 2013 AIP Publishing LLC.)

relaxation together with dc conductivity. For comparison a spectrum of neat TPP is included (filled squares). Due to the low dipole moment and the low concentration of SBC, the TPP relaxation is monitored predominantly. As expected, the signal is lower than that of 100% TPP and shifted to lower frequencies as a consequence of the anti-plasticizer effect. Moreover, the relaxation peak is significantly broader, in particular on the low-frequency side. Specifically $\chi''(\omega) \propto \omega^a$ with $a < 1$ is found at $\omega\tau_\alpha \ll 1$ in contrast to neat glass formers, for which $\chi''(\omega) \propto \omega^1$ holds. The relaxation peak also becomes broader upon cooling, i.e., frequency-temperature superposition (FTS) does not apply. On the high-frequency side of the main relaxation, a β -relaxation is observed. After subtracting the dc conductivity contribution (dashed lines), a shoulder is recognized on the low-frequency side of the main relaxation (filled circles). The latter is assigned to the main relaxation of the high- T_g component SBC subsequently called α_1 -process, whereas the main peak reflects the dynamics of the low- T_g component TPP hereafter called α_2 -process. Above $T = 194$ K measurements were not possible due to phase separation and crystallization.

Figure 3(b) shows the dielectric spectra of the mixture with $c_{TPP} = 70\%$. The α_2 -process is even broader than that for $c_{TPP} = 85\%$, especially at the low-frequency flank. Again, subtracting the conductivity contribution yields a well-defined shoulder, reflecting the α_1 -relaxation. The two relaxations are more separated than in the case of the 85% mixture and the α_1 -relaxation is relatively stronger, as expected. Again, FTS does not apply. For $c_{TPP} \leq 61\%$ (cf. Fig. 12 of the Appendix), the sample in the (metallic) dielectric cell always crystallizes above 200 K. Therefore the α_1 -process could not be detected;

only the α_2 -process and the secondary relaxation were observable. Yet, crystallization did not occur in the NMR glass ampules, thus NMR measurements were still possible. The time constants of the (strong) α_2 -relaxation are extracted again by “peak picking,” while those of the (weak) α_1 -process are taken from an interpolation of the full spectra with a superposition of HN (α_2 -process) and Kohlrausch function (α_1 -process) along Eqs. (12)/(13) and (14) (red lines). All time constants are included in Fig. 11 for later discussion.

In our previous study of the TPP/PS mixtures,¹⁶ we reported indications that the relaxation strength of the α_1 -relaxation (PS) in the mixture was larger than expected given the small relaxation strength $\Delta\epsilon_1$ of neat PS. In agreement with a study on PS mixed with methyltetrahydrofuran,^{20,21} we concluded that a fraction of the TPP molecules takes part in the α_1 -process. In order to further test this hypothesis in the present case, we determined the experimental ratio of the strength of the two relaxations, α_1 and α_2 . We found that $\Delta\epsilon_1/\Delta\epsilon_2 \approx 0.12$ for the $c_{TPP} = 70\%$ mixture and $\Delta\epsilon_1/\Delta\epsilon_2 \approx 0.035$ for the 85% mixture. This value can be compared to the expected ratio $(\Delta\epsilon_1/\Delta\epsilon_2)_{calc} = \frac{(1-c_{TPP})\Delta\epsilon_{1n}T_1}{c_{TPP}\Delta\epsilon_{2n}T_2}$ which is calculated assuming a Curie law and ideal mixing. Here, $\Delta\epsilon_{in}$ is the relaxation strength of the neat system and T_i the temperature at which it is measured. We can use the weight concentration c_{TPP} instead of the molar concentration because both components have comparable densities. We obtain $(\Delta\epsilon_1/\Delta\epsilon_2)_{calc} \approx 0.04$ for the $c_{TPP} = 70\%$ mixture and $(\Delta\epsilon_1/\Delta\epsilon_2)_{calc} \approx 0.016$ for the $c_{TPP} = 85\%$ mixture. The measured ratios, $\Delta\epsilon_1/\Delta\epsilon_2 \approx 0.12$ and $\Delta\epsilon_1/\Delta\epsilon_2 \approx 0.035$, respectively, are significantly larger than the ratios calculated. This may be taken again as an indication that some TPP molecules participate in main relaxation of SBC

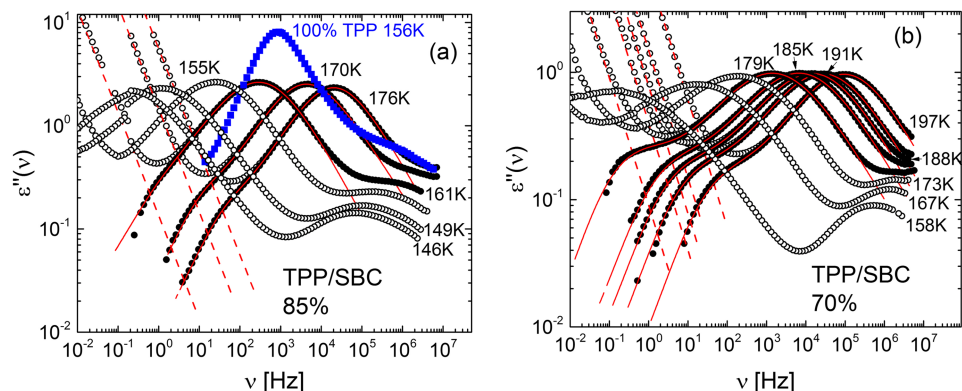


FIG. 3. (a) Selected dielectric spectra of the $c_{TPP} = 85\%$ mixture TPP/SBC (temperatures indicated); open circles: data as measured; filled circles: data after subtracting the conductivity contribution; dashed (red) lines: conductivity contribution; solid (red) lines: interpolations by a superposition of a Kohlrausch and a HN susceptibility; for comparison a spectrum of neat TPP (blue squares) is shown; (b) DS spectra of the $c_{TPP} = 70\%$ mixture TPP/SBC; symbols and interpolation as in (a).

in the mixture. Of course, ideal mixing may not apply; yet, the differences of the experimental and calculated ratios are rather large.

C. NMR experiments

1. NMR spectra

In Fig. 4 the ^2H NMR spectra of neat (phenyl group deuterated) SBC ($c_{\text{TPP}} = 0\%$) and of the mixtures with TPP down to $c_{\text{TPP}} = 10\%$ are shown. Only the dynamics of SBC is probed, and temperatures up to 400 K were accessible for neat SBC, while in the mixtures phase separation limits the experiments to $T < 300$ K. In the neat system one finds at low temperatures the typical Pake spectrum with an anisotropy parameter $\delta_Q/2\pi \approx 135 \pm 2$ kHz, indicating that all molecules are slow on the NMR time scale ($1/\delta_Q$). At temperatures above 220 K, two additional peaks appear in the middle of the broad spectra indicative of fast 180° flips of a fraction of the phenyl rings. At highest temperatures, all phenyl groups reorient fast yielding a motional averaged spectrum with $\bar{\delta}_Q/2\pi \approx 120$ kHz and $\bar{\eta} \approx 0.64$. For a well-defined 180° flip, an $\bar{\eta}$ of 0.6 is calculated. The fit (red lines) does not perfectly match the measured phenyl jump spectra. Probably additional small-angle fluctuations of the phenylene groups about the flip axis contribute to the observed line shape as found in similar cases.³⁹ At intermediate temperatures, the spectra are described by a kind of “two-phase” spectrum with a weighted superposition of a broad Pake and a phenyl flip spectrum; no intermediate exchange spectra are recognized. The weighting factor $W_{\text{ph}}(T)$ is shown in Fig. 5 (black squares). As discussed in the experimental part, such two-phase spectra reflect a broad distribution of jump times $G(\ln \tau_{\text{ph}})$. Assuming a thermally activated process, one directly gets an estimate of the distribution of activation energies $g(E)$ (dashed lines) from the temperature derivative of $W_{\text{ph}}(T)$ via Eq. (3) (red and blue dashed lines in Fig. 5).³² The distribution $g(E)$ is rather broad. This is typical of amorphous systems with their pronounced static density fluctuations.

In the mixtures for $c_{\text{TPP}} = 10\%$ and 22% , one finds quite similar two-phase spectra; however, the full temperature range

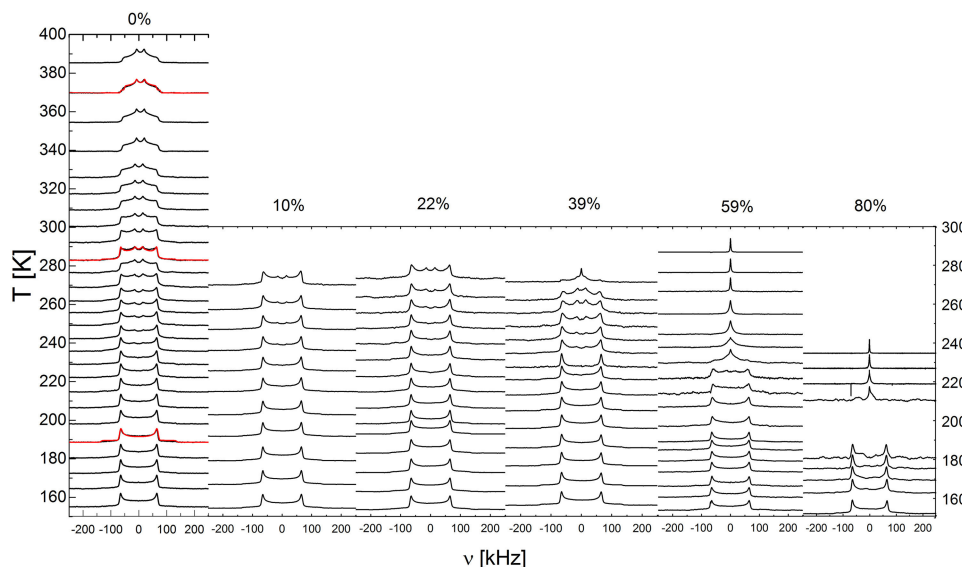


FIG. 4. ^2H NMR spectra of neat SBC ($c_{\text{TPP}} = 0\%$) and in the mixture TPP/SBC for concentrations as indicated. The baseline of the spectra corresponds to the temperature for which the spectra were measured. The red lines for $c_{\text{TPP}} = 0\%$ are fits with a weighted superposition of the Pake and the phenyl flip spectrum; the corresponding weighting factors are given in Figure 5.

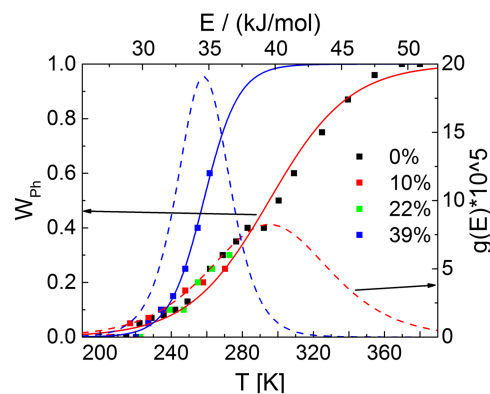


FIG. 5. Temperature dependent weighting factor $W_{\text{ph}}(T)$ of the phenyl group jump for the mixtures with $c_{\text{TPP}} = 0\%$, 10% , 22% , and 39% with interpolations by a logistic function (solid lines). The corresponding activation energy distributions $g(E)$ are shown as dashed lines.

cannot be covered due to crystallization. The corresponding weighting factors $W_{\text{ph}}(T)$ are very similar to those for neat SBC, indicating that the local density distribution virtually does not change (cf. Fig. 5). Yet, in the case of the $c_{\text{TPP}} = 39\%$ sample, the motional averaged spectra appear at somewhat lower temperatures, consequently $W_{\text{ph}}(T)$ sets in at lower temperature and grows faster with temperature, indicating now a change of $g(E)$. The corresponding distribution of activation energies $g(E)$ is narrower and shifts to lower energies. For $c_{\text{TPP}} = 59\%$ the plasticizer effect is strong and the crossover to the central line of the (fast) isotropic reorientation associated with the α_1 -process is well documented at $T > 240$ K. Still some traces of the phenyl flip spectrum are recognized. The spectrum around 230 K is described by a superposition of a liquid line and a solid-state spectrum. Thus, in the case of the α_1 -process a somewhat broadened distribution $G(\ln \tau_{\alpha_1})$ is observed which also leads to “two-phase” spectra. Yet, the temperature range for which such spectra are observed is rather narrow, in contrast to spectra observed for the low- T_g component (see below). In the case of the $c_{\text{TPP}} = 80\%$, the low-temperature Pake spectrum directly collapses to yield a liquid line around 210 K.

In Fig. 6 we display the ^{31}P NMR spectra for the additive TPP; concentrations $c_{\text{TPP}} = 21\%$, 34% , 47% , 61% , 76% ,

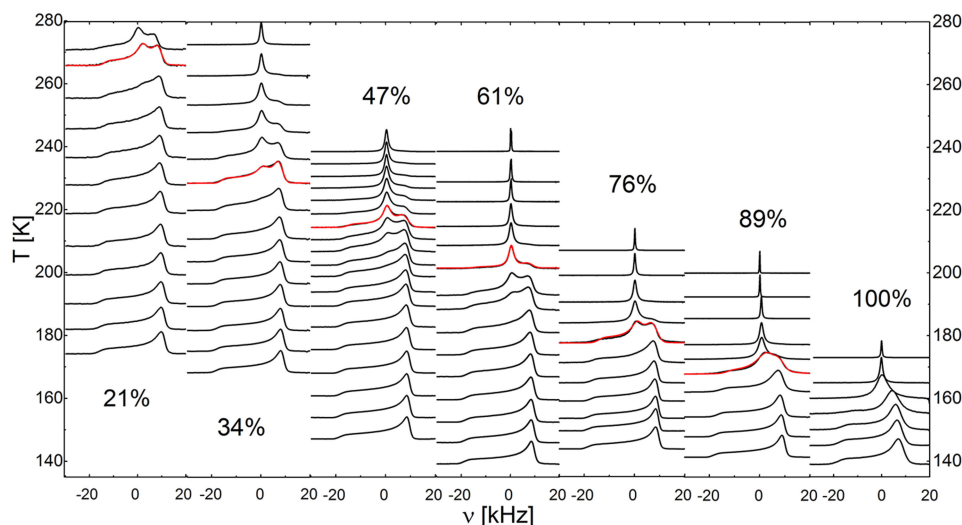


FIG. 6. ^{31}P NMR spectra of TPP in the mixture TPP/SBC for the concentrations as indicated. The baseline of the spectra corresponds to the temperature at which they were measured. The red lines are fits along the two-phase model (cf. Eq. (2)).

and 89% and neat TPP are covered. At low temperatures powder spectra now dominated by the CSA interaction are found with an anisotropy parameter $\delta_{\text{CSA}}/2\pi \approx 20 \pm 0.5$ kHz, reflecting the TPP molecules reorienting slowly on the NMR time scale. At highest temperatures a Lorentzian line is observed, i.e., all molecules perform a fast liquid-like (isotropic) reorientation. This is found for all concentrations, except for $c_{\text{TPP}} = 21\%$, where the measured temperatures are not high enough to reveal the full liquid line. At intermediate temperatures, two-phase spectra are observed over a wide temperature range; they comprise a superposition of a solid-state spectrum and a central Lorentzian line. As explained, such spectra are indicative of a broad distribution of correlation times $G(\ln \tau_{\alpha_2})$. In contrast, in the case of neat TPP a continuous collapse from powder spectra to a Lorentzian line is observed upon heating which reflects a rather narrow distribution $G(\ln \tau_{\alpha_2})$ as found in most neat glass formers.³³ In other words, in the mixture the low- T_g component TPP displays pronounced dynamic heterogeneities not found in neat glass formers, which qualitatively change the NMR spectra. The red lines in Fig. 6 are fits consisting of a superposition of both, a CSA powder spectrum and a Lorentzian line. The fits yield the corresponding

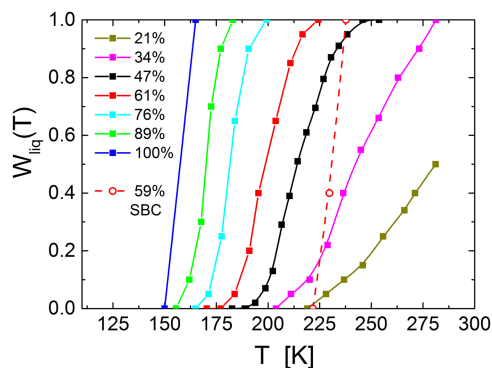


FIG. 7. Weighting factor $W_{\text{liq}}(T)$ of TPP (full symbols) in the mixtures TPP/SBC as a function of temperature. For neat TPP the two points at $W_{\text{liq}} = 0$ and $W_{\text{liq}} = 1$ indicate the temperature at which the beginning and the end of the spectral collapse occurs. For comparison $W_{\text{liq}}(T)$ as obtained for $c_{\text{TPP}} = 59\%$ by ^2H NMR is shown (open symbols), indicating significant decoupling of the α_1 - and α_2 -process. Lines are guides for the eye.

weighting factors $W_{\text{liq}}(T)$ reflecting the fraction of liquid-like moving molecules (cf. Fig. 7). With decreasing TPP concentration, the temperature range in which two-phase spectra are observed becomes broader, shifts to higher temperatures, and reflects the “anti-plasticizer” effect.

Inspecting Figs. 4 and 6, it is obvious that the liquid-like dynamics of the low- and high- T_g components are well decoupled. This is directly demonstrated in Fig. 8 for the $c_{\text{TPP}} \approx 60\%$ mixture. There are temperatures for which almost all TPP molecules perform a liquid-like motion (ca. 220 K), while the SBC molecules are still arrested displaying a powder spectrum. Finally, at lower temperatures also the low- T_g component gets arrested confined in a rigid matrix of the high- T_g component. This decoupling is also evidenced in Fig. 7 when the weighting factor $W_{\text{liq}}(T)$ of SBC ($c_{\text{TPP}} = 59\%$; from Fig. 4), obtained by ^2H NMR and of TPP ($c_{\text{TPP}} = 61\%$) are compared to each other. The weighting factor of TPP reaches almost one at around 215 K, while that of SBC is still zero at 220 K and then grows fast with increasing temperature until a liquid-like spectrum is

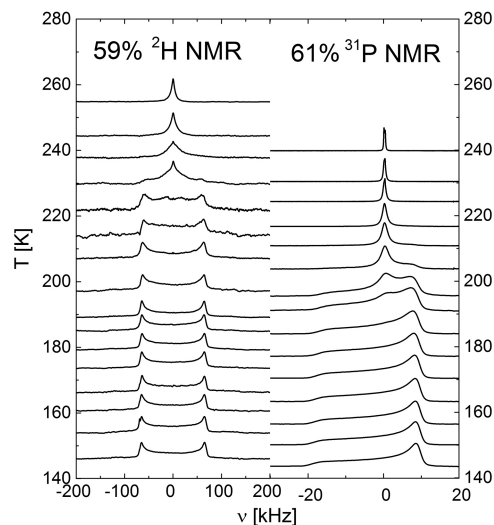


FIG. 8. ^2H NMR spectra of SBC and ^{31}P NMR spectra of TPP, respectively, in the mixture TPP/SBC for the concentrations $c_{\text{TPP}} = 59\%$ and $c_{\text{TPP}} = 61\%$. The baseline of the spectra corresponds to the temperature at which they were measured.

observed at 238 K. In between, a narrow “two-phase” region is observed for the SBC component, as discussed. Clearly, two isotropic processes associated with two glass transitions are involved and the difference of the corresponding T_{g1} and T_{g2} (see below) increases with decreasing c_{TPP} . Yet, while the distribution $G(\ln \tau_{\alpha 1})$ is rather narrow and still similar to that in neat glass formers,⁷ the distribution $G(\ln \tau_{\alpha 2})$ is broad becoming extremely wide at low TPP concentration. This becomes further evident when the reorientational correlation functions are directly probed by the stimulated echo technique (see below).

2. Reorientational correlation functions

³¹P stimulated echo decays of TPP were measured for all concentrations. After corrections of the T_1 decay and the residual correlation F_∞ (cf. Sec. II), one obtains the reorientational correlation function $C_2(t)$. In addition to a damping due to the spin-lattice relaxation, we had to take into account the effect of spin-diffusion which leads to a temperature independent decay at lowest temperatures. The correlation functions are shown in Fig. 9 for $c_{TPP} = 21\%$, 47%, 61%, 76%, and 89% with the corresponding Kohlrausch fits. Starting with $\beta_K = 0.66$ for neat TPP (not shown),²⁹ with decreasing additive concentration the correlation functions get increasingly stretched and reach a stretching parameter of $\beta_K = 0.18$ for

$c_{TPP} = 47\%$. For $c_{TPP} = 21\%$ and 37%, no Kohlrausch fit is possible any longer; the decays become quasi-logarithmic, i.e., an extremely broad distribution $G(\ln \tau_{\alpha 2})$ is revealed. The decays occur at higher temperatures, the lower the TPP concentration is, again reflecting the anti-plasticizer effect. Time temperature superposition (TTS) seems to be valid in the narrow temperature range measured. Yet, as discussed above, covering a much broader temperature range the dielectric spectra clearly show the violation of FTS/TTS (cf. Fig. 3). The conclusion which can be drawn from the stimulated echo decays agrees with that of the observation of two-phase ³¹P NMR spectra: the lower the c_{TPP} the broader is the two-phase region and the more stretched is the correlation function. This is explicitly shown in Fig. 9, right bottom. Here, a single correlation decay for each concentration is shown on a reduced time scale so that the correlation functions are comparable. The crossover from a Kohlrausch to a quasi-logarithmic decay is clearly visible. The time constants obtained from these fits are shown in Fig. 11; they coincide with those collected by analyzing the dielectric spectra fairly well.

In the case of ²H NMR on the SBC component stimulated echo decays for $c_{TPP} = 22\%$ and 80% are shown in Fig. 10. For $c_{TPP} = 22\%$ the T_{1Q} decays could be accounted for since the low temperature limit, where the stimulated echo solely decays along T_{1Q} , was reached. Here T_{1Q} is

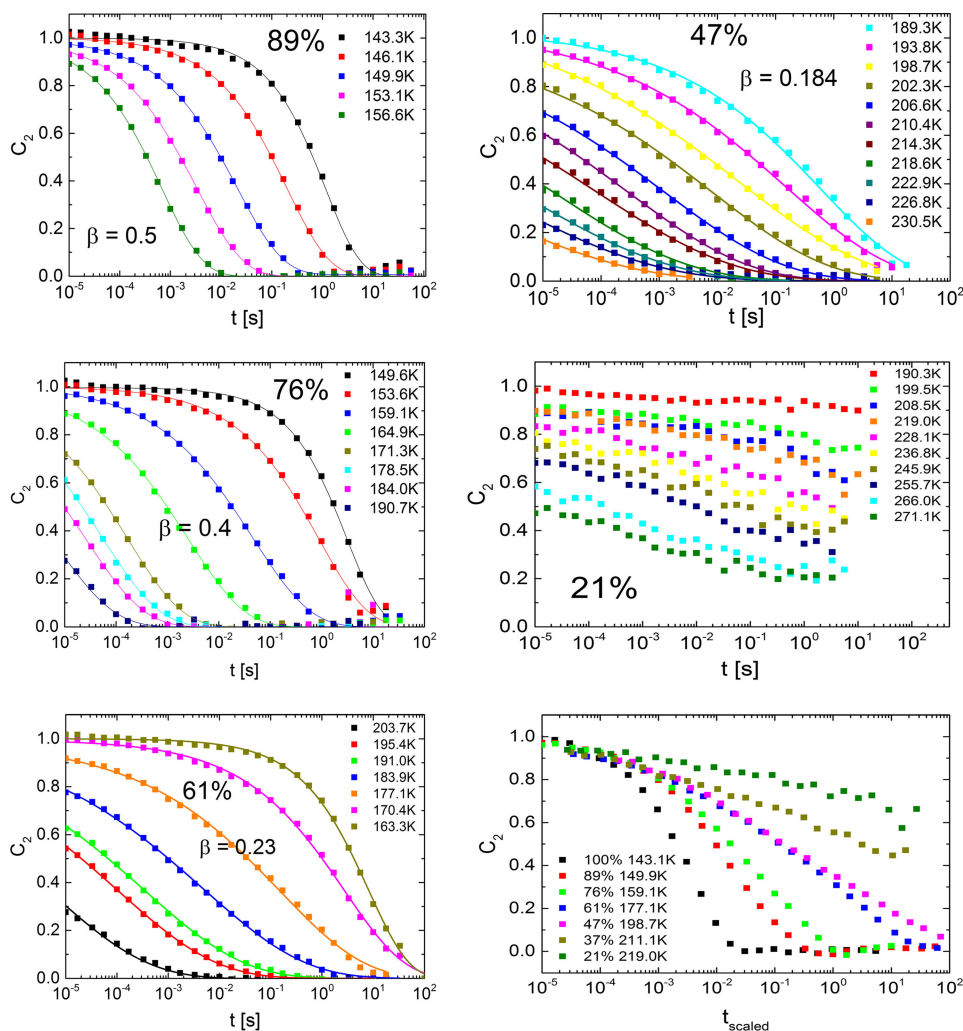


FIG. 9. Reorientational correlation function $C_2(t)$ of the TPP component in the mixture TPP/SBC for different concentrations as indicated, corrected for the T_1 decay and effects of spin diffusion. Solid lines for $c_{TPP} = 47\%$, 61%, 76%, and 89% represent Kohlrausch fits. For $c_{TPP} = 21\%$ no Kohlrausch fits are possible. The figure at the right bottom shows a comparison of the correlation functions on a reduced time scale for the different concentrations.

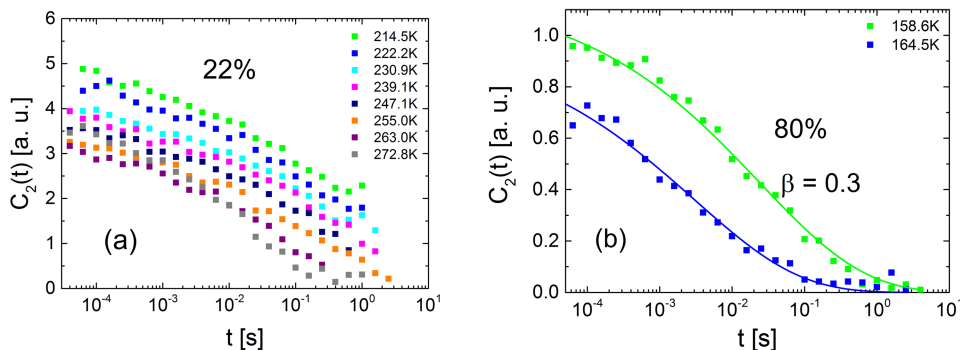


FIG. 10. (a) ^2H NMR stimulated echo decays of the SBC component in the mixture TPP/SBC for $c_{\text{TPP}} = 22\%$ corrected for the T_{1Q} decay. (b) ^2H NMR stimulated echo decays for $c_{\text{TPP}} = 80\%$; T_{1Q} decay can be ignored; Kohlrausch fits are applied to the correlation functions (solid lines).

proportional to T_1 and the latter is almost temperature independent in the relevant temperature interval. Also SBC (α_1 -process) shows strongly stretched decays (cf. Fig. 10(a)). In the first place, this is unusual, as for the high- T_g component according to the ^2H NMR spectra (cf. Fig. 4) the stretching should be moderate and similar to that of neat SBC. Inspecting the ^2H NMR spectra, the observation finds its explanation in the interference of the phenyl jump and α_1 -relaxation. In the case of $c_{\text{TPP}} = 59\%$ (not shown), the stimulated echo decay is less stretched and at $c_{\text{TPP}} = 80\%$ a Kohlrausch function with $\beta_K = 0.3$ fits the data well (see Fig. 10(b)). At such high TPP concentrations, T_{g1} has decreased strongly and the α_1 -process is observable at low temperatures before the phenyl jumps are activated (cf. again Fig. 4). Time constants gained from the Kohlrausch fit to the $c_{\text{TPP}} = 80\%$ data are shown in Fig. 11.

3. Time constants

Figure 11 shows the time constants $\tau_{\alpha_1}(T)$ (open symbols and dashed lines) and $\tau_{\alpha_2}(T)$ (filled symbols and lines) as obtained from dielectric spectroscopy (squares) and from the different NMR methods, namely, stimulated echo (up triangle), T_2 relaxation (down triangle), T_1 minimum (diamond). The $T_1(T)$ data of both ^2H and ^{31}P NMR are shown in Paper II.⁵⁵ The different concentrations are coded by different colors; similar concentrations are coded by the same color (e.g., $c_{\text{TPP}} = 85\%$ DS and $c_{\text{TPP}} = 89\%$ NMR). The NMR and dielectric time constants fit well together in the whole concentrations' range. With decreasing additive concentration the α_2 -process shifts to higher

temperatures representing the anti-plasticizer effect. For concentrations lower than $c_{\text{TPP}} = 34\%$, no time constants could be obtained as the α_2 -process was too slow to be accessed in the measurable temperature window. The same problem occurs for NMR measurements of the α_1 -process at low concentrations. Dielectric measurements could only be performed at high concentrations ($c_{\text{TPP}} \geq 60\%$). Both for $c_{\text{TPP}} = 70\%$ and 85% time constants from the DS spectra, for $c_{\text{TPP}} = 80\%$ from stimulated echo measurements and also for $c_{\text{TPP}} = 59\%$ from relaxation measurements, could be obtained. The dynamics are much faster than in the neat SBC due to the plasticizer effect. Both processes α_1 and α_2 are only slightly separated at high concentrations. The inset in Fig. 11 shows the T_{g1} and T_{g2} values, with T_g defined by $\tau_a = 1$ s. A maximum in $T_{g2}(c)$ was observed in Ref. 16 at concentrations around $c_{\text{additive}} = 0.5$, caused by a crossover in the behavior of the time constants of the α_2 process from Arrhenius at low TPP concentration to non-Arrhenius at high concentrations. This could not be seen here due to the inaccessibility of time constants for lower concentrations.

IV. DISCUSSION

The present paper (Paper I) focuses on the main relaxations in a dynamically asymmetric non-polymeric binary mixture, while the second paper (Paper II⁵⁵) reports on its secondary (β -)relaxations. A large T_g contrast of $\Delta T_g = 222$ K is reached as it is usually the case in polymer-plasticizer-systems. In addition to the low- T_g component TPP, due to deuteration

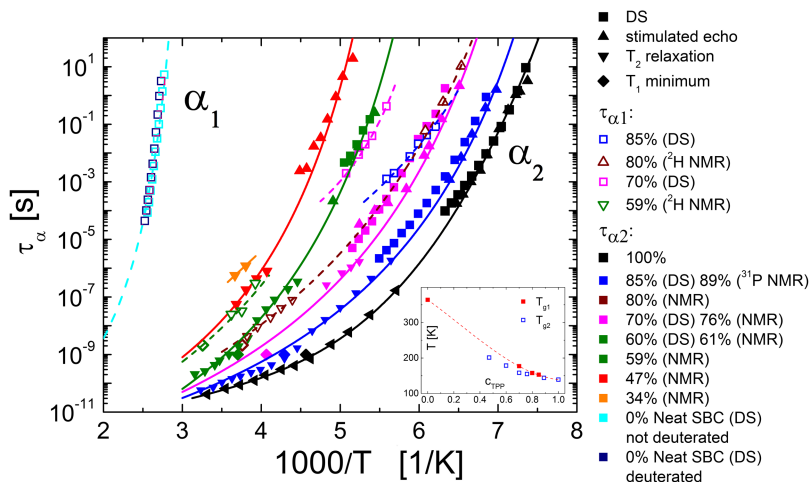


FIG. 11. Mean relaxation times of α_1 - and α_2 -process in the mixture TPP/SBC for the concentrations as indicated. Symbols are coded by process, method, and concentration: α_1 -process: open symbols; α_2 -process: filled symbols; dielectric spectroscopy: squares; stimulated echo: up triangles; T_2 relaxation: down triangles; T_1 minimum: diamonds; concentration are indicated by color code, similar concentrations (e.g., 60% and 61%) are shown in the same color. The solid and dashed lines are guide for the eyes. Inset: $T_{g1/2}$ ($\tau = 1$ s) data for both processes. The dashed line is a guide for the eye.

of the high- T_g component SBC, the dynamics of each component is accessible by NMR separately. For all concentrations investigated, SBC and TPP perform distinct isotropic, liquid-like reorientations. The corresponding time constants $\tau_{\alpha_1}(T)$ and $\tau_{\alpha_2}(T)$ differ more the lower the c_{TPP} is. We emphasize that even at very low SBC concentrations two separate processes, yet with rather close time constants, can be identified by DS (cf. Fig. 3), a result also found in our previous studies.¹⁹ Thus, merging of the two α -processes at high c_{TPP} as suggested in Refs. 20 and 21 is not confirmed. At a higher SBC content a situation results, where the low- T_g component TPP performs isotropic reorientations in a matrix of essentially rigid SBC molecules. At lower temperatures the TPP molecules get arrested too. In this sense one can speak of a glass transition of small molecules in a random matrix of large molecules, and two glass temperatures T_{g1} and T_{g2} may be defined by choosing an appropriate iso-dynamical temperature, i.e., $\tau_{\alpha}(T_g) = \text{const.}$ (compare Fig. 11). An identification of the second T_{g2} by DSC is often not possible due to the extremely broad distribution of relaxation times associated with the α_2 -process.

There is a fundamental difference between the α_1 - and α_2 -process: While the α_1 -process resembles the α -process in neat glass formers with an only weakly broadened relaxation spectrum, the α_2 -process shows an extremely broad distribution $G(\ln \tau_{\alpha_2})$, at low TPP concentration reflected by quasi-logarithmic correlation functions. The NMR as well as the DS observables display features, which are also reported for glass formers embedded in nano-confinement,^{40–44} i.e., pronounced dynamic heterogeneities are revealed which are not found in neat systems. We conclude that the high- T_g component in the asymmetric mixtures provides an intrinsic confinement for the low- T_g component. The features known from polymer-additive systems are rediscovered in the non-polymeric system.¹⁶ It appears that the T_g contrast of the components determines the dynamics of the main relaxations in binary glass formers. We note that previously, the dynamic heterogeneities typical of binary glass formers were explained in terms of thermally driven concentration fluctuations^{45–47} or the so-called self-concentration effects.^{48,49} In the present case of dynamically very asymmetric mixtures, however, additionally confinement effects appear to come into play.

The behavior of binary mixtures consisting of two particles with different sizes was also investigated by molecular dynamics (MD) simulations.⁵⁰ Also here a dynamical decoupling of both particle species was reported. The large particles exhibit a standard glass transition controlled by the cage effect, while the small particle still remain mobile within the arrested matrix of the large particles. The small component first shows a sub-diffusive behavior at low particle density until they perform a localization transition at high density. As in our experiments, the dynamics of the small particles is qualitatively different compared to the large particle. The phenomenon was also investigated by the mode coupling theory (MCT) where a dynamic decoupling of large and small particles is anticipated, if the components differ sufficiently in size.⁵¹ In that case the smaller particles retain mobility below T_g of the larger ones and undergo a localization transition in the confinement of a frozen matrix. In this respect, work

on MCT in the so-called quenched-annealed systems⁵² and simulations for a Lorentz-gas model⁵³ may be relevant. In such systems MCT predicts higher order singularities⁵² in the vicinity of which the correlation functions of the smaller molecules become extremely broad and quasi-logarithmic decay curves are expected as observed in simulations⁵⁴ and in our experiments.

In contrast to many polymer-plasticizer systems, which allow investigating the full concentration range, in the case of the non-polymeric asymmetric mixtures we face the problem of de-mixing. In the present case, this hampered the study of α_1 - and α_2 -relaxation at $c_{TPP} < 60\%$, while in our previous study¹⁶ we were able to measure almost the whole concentration range. Yet, in the present case one is able to investigate the secondary (β -) relaxation below T_{g2} for all concentrations, as will be demonstrated in Paper II.⁵⁵ We were not able to monitor the dynamics of the high- T_g component in Ref. 16 as it was not labelled. In the present study the high- T_g component was deuterated at the phenyl ring sites, which, however, leads to a situation that at high TPP concentrations the isotropic α_1 -process and the phenyl ring jumps showed up in the ²H NMR spectra at similar temperatures. This again hampered a clear cut analysis of the α_1 -process.

The preparation of mixtures with a high SBC concentration led to highly viscous liquids when filling the dielectric capacitor and controlling the filling factor was not possible. Hence a quantitative analysis of the strength of the different relaxation and their change with temperature is not feasible. Yet, from determining the relative contribution of the relaxation strengths $\Delta\epsilon_1/\Delta\epsilon_2$ and assuming ideal mixing we concluded in accordance with previous studies^{16,21} that a fraction of TPP molecules also participates in the α_1 -process. Still, this fraction of TPP molecules is difficult to identify in the NMR experiments due to the extreme dynamical heterogeneities revealed for the TPP molecules. In our study on the mixture TPP/PS^{16,17} as well as in Ref. 21, the fraction of the low- T_g molecules involved in the α_1 -process appears to decrease with temperature. This implies that above some temperature no more low- T_g molecules participate in the α_1 -relaxation. Finally, let us speculate what happens at $c_{TPP} \rightarrow 0$, i.e., at very low concentrations of the low- T_g component. It is well established that for this situation the additive may serve as a probe for the dynamics of a matrix; similar time constants as those of the α_1 -process are expected. Thus, one expects that the α_2 -process disappears and only the fraction of the TPP molecules attached to the high- T_g component survives. Further experiments are needed to test this crossover.

V. CONCLUSION

We study the dynamics of the main relaxations in a binary glass former consisting of tripropyl phosphate (TPP, $T_g = 134$ K) and a spirobichroman derivative (SBC, $T_g = 356$ K). This especially synthesized non-polymeric high- T_g glass former was functionalized with four deuterated phenyl rings to allow monitoring its dynamics by ²H NMR. The dynamics of TPP was probed by dielectric and ³¹P NMR spectroscopy. A high T_g contrast of $\Delta T_g = 222$ K was put in effect to reach a comparable dynamic asymmetry as in

the case of typical polymer-plasticizer systems. At all concentrations, two separated main relaxation processes (in addition to a β -process) were identified by dielectric spectroscopy. The faster α_2 -process is associated with the low- T_g TPP component, while the slower α_1 -process is related to the reorientation of the high- T_g component SBC. The α_1 -relaxation shows the well documented plasticizer effect, while the anti-plasticizer effect is observed for the faster α_2 -relaxation. The corresponding time constants $\tau_{\alpha_1}(T)$ and $\tau_{\alpha_2}(T)$ and consequently their glass transition temperatures T_{g1} and T_{g2} differ more the lower the TPP concentration is. An estimate of the dielectric relaxation strength of the α_1 -process in the mixtures indicates that some fraction of the TPP molecules is also involved in the α_1 -process in agreement with previous reports.

Dielectric spectroscopy and ^2H and ^{31}P NMR spectra as well as stimulated echo decays demonstrate that the dynamics of the low- T_g component TPP molecules is governed by a broad distribution $G(\ln \tau_a)$ becoming extremely wide resulting in quasi-logarithmic correlation functions at low TPP concentrations. In contrast, the correlation function of the α_1 -process is Kohlrausch-like as in neat glass formers, yet, somewhat more stretched. As quite similar relaxation features are observed for glass formers in nano-confinement, we conclude that the high- T_g component in the asymmetric mixtures provides an intrinsic confinement for the low- T_g component. All in all, the main features known from polymer-plasticizer systems are rediscovered in this non-polymeric binary mixture. In Paper II⁵⁵ of this series we study the secondary (β -) relaxations of the system.

ACKNOWLEDGMENTS

The authors appreciate financial support by Deutsche Forschungsgemeinschaft (DFG) through Project No. RO 907/19.

APPENDIX: DIELECTRIC SPECTRA OF THE $c_{\text{TPP}} = 61\%$ TPP/SBC MIXTURE

Figure 12 shows the dielectric spectra of the mixture $c_{\text{TPP}} = 61\%$. Only the α_2 -process and the secondary relaxation are observable due to crystallization at $T = 200$ K before the α_1 -process shifts into the frequency window.

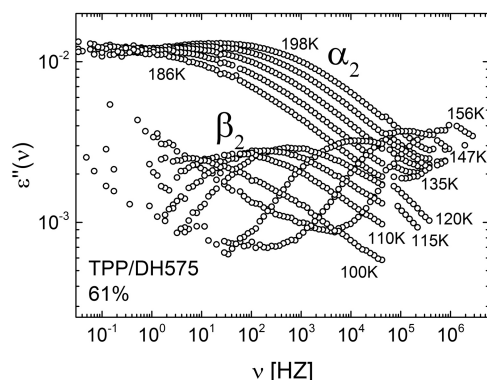


FIG. 12. Dielectric spectra of 61% TPP/SBC; temperatures are indicated.

- ¹A. Cavagna, *Phys. Rep.* **476**, 51 (2009).
- ²L. Berthier and G. Biroli, *Rev. Mod. Phys.* **83**, 587 (2011).
- ³R. Richert, *Annu. Rev. Phys. Chem.* **62**, 65 (2011).
- ⁴G. Floudas, M. Paluch, A. Grzybowski, and K. L. Ngai, *Molecular Dynamics of Glass-Forming Systems* (Springer, Berlin, 2011).
- ⁵P. G. Wolyne and V. Lubchenko, *Structural Glasses and Supercooled Liquids* (Wiley, Hoboken, 2012).
- ⁶M. D. Ediger and P. Harrowell, *J. Chem. Phys.* **137**, 080901 (2012).
- ⁷N. Petzold, B. Schmidtke, R. Kahlau, D. Bock, R. Meier, B. Micko, D. Krug, and E. A. Rössler, *J. Chem. Phys.* **138**, 12A510 (2013).
- ⁸P. J. Hains and G. Williams, *Polymer* **16**, 725 (1975).
- ⁹M. A. Desando, S. Walker, and W. H. Baarschers, *J. Chem. Phys.* **73**, 3460 (1980).
- ¹⁰M. Scandola, G. Ceccorulli, and M. Pizzoli, *Polymer* **28**, 2081 (1987).
- ¹¹M. Nakazawa, O. Urakawa, and K. Adachi, *Macromolecules* **33**, 7898 (2000).
- ¹²J. Colmenero and A. Arbe, *Soft Matter* **3**, 1474 (2007).
- ¹³D. Bingemann, N. Wirth, J. Gmeiner, and E. A. Rössler, *Macromolecules* **40**, 5379 (2007).
- ¹⁴S. Schramm, T. Blochowicz, E. Gouirand, R. Wipf, B. Stühn, and Y. Chuchkin, *J. Chem. Phys.* **132**, 224505 (2010).
- ¹⁵K. L. Ngai, *Relaxation and Diffusion in Complex Systems* (Springer-Verlag, Berlin, Heidelberg, 2011).
- ¹⁶R. Kahlau, D. Bock, B. Schmidtke, and E. A. Rössler, *J. Chem. Phys.* **140**, 044509 (2014).
- ¹⁷D. Bock, R. Kahlau, B. Pötzschnner, T. Körber, E. Wagner, and E. A. Rössler, *J. Chem. Phys.* **140**, 094505 (2014).
- ¹⁸Y. Shirota, *J. Mater. Chem.* **10**, 1–25 (2000).
- ¹⁹B. Pötzschnner, F. Mohamed, A. Lichtinger, D. Bock, and E. A. Rössler, *J. Chem. Phys.* **143**, 154506 (2015).
- ²⁰T. Blochowicz, S. Lusceac, P. Gutfreund, S. Schramm, and B. Stühn, *J. Phys. Chem. B* **115**, 1623 (2011).
- ²¹T. Blochowicz, S. Schramm, S. Lusceac, M. Vogel, B. Stühn, P. Gutfreund, and B. Frick, *Phys. Rev. Lett.* **109**, 035702 (2012).
- ²²D. Cangialosi, A. Alegría, and J. Colmenero, *Phys. Rev. E* **80**, 041505 (2009).
- ²³T. Blochowicz, C. Karle, A. Kudlik, P. Medick, I. Roggatz, M. Vogel, C. Tschirwitz, J. Wolber, J. Senker, and E. A. Rössler, *J. Phys. Chem. B* **103**, 4032 (1999).
- ²⁴D. Bock, R. Kahlau, B. Micko, B. Pötzschnner, G. J. Schneider, and E. A. Rössler, *J. Chem. Phys.* **139**, 064508 (2013).
- ²⁵C. Lorthioir, A. Alegria, and J. Colmenero, *Phys. Rev. E* **68**, 031805 (2003).
- ²⁶M. Vogel and E. A. Rössler, *J. Chem. Phys.* **114**, 5802 (2001).
- ²⁷M. Vogel and E. A. Rössler, *J. Chem. Phys.* **115**, 10883 (2001).
- ²⁸M. Vogel, C. Tschirwitz, G. Schneider, C. Koplin, P. Medick, and E. Rössler, *J. Non-Cryst. Solids* **307**, 326 (2002).
- ²⁹S. Adichtchev, D. Bock, C. Gainaru, R. Kahlau, B. Micko, N. Petzold, B. Pötzschnner, and E. A. Rössler, *Z. Phys. Chem.* **226**, 1149 (2012).
- ³⁰A. Abragam, *The Principles of Nuclear Magnetism* (Clarendon Press, Oxford, 1961).
- ³¹J. Kowalewski and L. Maler, *Nuclear Spin Relaxation in Liquids: Theory, Experiments and Applications* (Taylor and Francis, International, 2006).
- ³²E. A. Rössler, M. Taupitz, K. Börner, M. Schulz, and H.-M. Vieth, *J. Chem. Phys.* **92**, 5847 (1990).
- ³³R. Böhmer, G. Diezemann, G. Hinze, and E. A. Rössler, *Prog. Nucl. Magn. Reson. Spectrosc.* **39**, 191 (2001).
- ³⁴H. W. Spiess, *NMR Basic Principles and Progress*, Dynamic NMR Spectroscopy Vol. 15 (Springer Verlag, Berlin, 1978).
- ³⁵K. Schmidt-Rohr and H. W. Spiess, *Multidimensional Solid-State NMR and Polymers* (Academic Press, New York, 1994).
- ³⁶F. Fujara, S. Wefing, and H. W. Spiess, *J. Chem. Phys.* **84**, 4579 (1986).
- ³⁷H. Wagner and R. Richert, *J. Phys. Chem. B* **103**, 4071 (1999).
- ³⁸C. J. F. Böttcher and P. Bordewijk, *Theory of Electric Polarization* (Elsevier, Amsterdam, 1978).
- ³⁹H. W. Spiess, *Colloid Polym. Sci.* **261**, 193 (1983).
- ⁴⁰A. Schönhals, H. Goering, C. Schick, B. Frick, M. Mayorova, and R. Zorn, *Eur. Phys. J.: Spec. Top.* **141**, 255 (2007).
- ⁴¹S. Gradmann, P. Medick, and E. A. Rössler, *J. Phys. Chem. B* **113**, 8443 (2009).
- ⁴²D. Bock, N. Petzold, R. Kahlau, S. Gradmann, B. Schmidtke, N. Benoit, and E. A. Rössler, *J. Non-Cryst. Solids* **407**, 88 (2015).
- ⁴³S. A. Lusceac, C. Koplin, P. Medick, M. Vogel, C. LeQuelllec, N. Brodie-Linder, C. Alba-Simionesco, and E. A. Rössler, *J. Phys. Chem.* **108**, 16601 (2004).

- ⁴⁴F. Kremer, A. Huwe, M. Arndt, P. Behrens, and W. Schwieger, *J. Phys.: Condens. Matter* **11**, A175 (1999).
- ⁴⁵A. Zetsche and E. W. Fischer, *Acta Polym.* **45**, 168 (1994).
- ⁴⁶S. K. Kumar, R. H. Colby, S. H. Anastasiadis, and G. Fytas, *J. Chem. Phys.* **105**, 3777 (1996).
- ⁴⁷R. Kant and S. K. Kumar, *Macromolecules* **36**, 10087 (2003).
- ⁴⁸G. C. Chung, J. A. Kornfield, and S. D. Smith, *Macromolecules* **27**, 964 (1994).
- ⁴⁹T. P. Lodge and T. C. B. McLeish, *Macromolecules* **33**, 5278 (2000).
- ⁵⁰T. Voigtmann and J. Horbach, *Phys. Rev. Lett.* **103**, 205901 (2009).
- ⁵¹J. Bosse and Y. Kaneko, *Phys. Rev. Lett.* **74**, 4023 (1995).
- ⁵²V. Krakoviack, *Phys. Rev. Lett.* **94**, 065703 (2005).
- ⁵³F. Höfling, T. Franosch, and E. Frey, *Phys. Rev. Lett.* **96**, 165901 (2006).
- ⁵⁴A. J. Moreno and J. Colmenero, *J. Chem. Phys.* **125**, 164507 (2006).
- ⁵⁵B. Pötzschner, F. Mohamed, C. Bächer, E. Wagner, A. Lichtinger, D. Bock, K. Kreger, H.-W. Schmidt, and E. A. Rössler, *J. Chem. Phys.* **146**, 164504 (2017).

7. Publication IV

Publication IV

Non-polymeric asymmetric binary glass-formers. II. Secondary relaxation studied by dielectric, ^2H NMR, and ^{31}P NMR spectroscopy

B. Pötzschner, F. Mohamed, C. Bächer, E. Wagner, A. Lichtinger,

K. Kreger, H.-W. Schmidt, and E. A. Rössler

J. Chem. Phys. 146, 164504 (2017)

Doi: 10.1063/1.4980085

© 2017 AIP Publishing LLC

Non-polymeric asymmetric binary glass-formers. II. Secondary relaxation studied by dielectric, ^2H NMR, and ^{31}P NMR spectroscopy

B. Pötzschner, F. Mohamed, C. Bächer, E. Wagner, A. Lichtinger, D. Bock, K. Kreger, H.-W. Schmidt, and E. A. Rössler^{a)}

Experimentalphysik II, University of Bayreuth, 95447 Bayreuth, Germany and Macromolecular Chemistry I, University of Bayreuth, 95447 Bayreuth, Germany

(Received 4 February 2017; accepted 31 March 2017; published online 27 April 2017)

We investigate the secondary (β -) relaxations of an asymmetric binary glass former consisting of a spirobichroman derivative (SBC; $T_g = 356$ K) as the high- T_g component and the low- T_g component tripropyl phosphate (TPP; $T_g = 134$ K). The main relaxations are studied in Paper I [B. Pötzschner *et al.*, *J. Chem. Phys.* **146**, 164503 (2017)]. A high T_g contrast of $\Delta T_g = 222$ K is put into effect in a non-polymeric system. Component-selective studies are carried out by combining results from dielectric spectroscopy (DS) for mass concentrations $c_{\text{TPP}} \geq 60\%$ and those from different methods of ^2H and ^{31}P NMR spectroscopy. In the case of NMR, the full concentration range ($10\% \leq c_{\text{TPP}} \leq 100\%$) is covered. The neat components exhibit a β -relaxation (β_1 (SBC) and β_2 (TPP)). The latter is rediscovered by DS in the mixtures for all concentrations with unchanged time constants. NMR spectroscopy identifies the β -relaxations as being alike to those in neat glasses. A spatially highly restricted motion with angular displacement below $\pm 10^\circ$ encompassing all molecules is involved. In the low temperature range, where TPP shows the typical ^{31}P NMR echo spectra of the β_2 -process, very similar spectral features are observed for the (deuterated) SBC component by ^2H NMR, in addition to its “own” β_1 -process observed at high temperatures. Apparently, the small TPP molecules enslave the large SBC molecules to perform a common hindered reorientation. The temperature dependence of the spin-lattice relaxation time of both components is the same and reveals an angular displacement of the SBC molecules somewhat smaller than that of TPP, though the time constants τ_{β_2} are the same. Furthermore, $T_1(T)$ of TPP in the temperature region of the β_2 -process is absolutely the same as in the mixture TPP/polystyrene investigated previously. It appears that the manifestations of the β -process introduced by one component are essentially independent of the second component. Finally, at $c_{\text{TPP}} \leq 20\%$ one finds indications that the β_2 -process starts to disintegrate. More and more TPP molecules get immobilized upon decreasing c_{TPP} . We conclude that the β -process is a cooperative process. *Published by AIP Publishing.* [<http://dx.doi.org/10.1063/1.4980085>]

I. INTRODUCTION

In the first part of this study (Paper I),¹ we investigated the main, liquid-like relaxations in an asymmetric binary glass former, consisting of a (deuterated) spirobichroman derivative (SBC, molar mass $M = 809.0$ g/mol), especially synthesized to achieve a high $T_g = 356$ K, and tripropyl phosphate (TPP, $T_g = 134$ K). A high T_g contrast of $\Delta T_g = 222$ K was put in effect to reach a comparable dynamic asymmetry as in the case of typical polymer-plasticizer systems. Strong differences of the dynamics among the components were found by dielectric spectroscopy (DS) and by ^2H and ^{31}P NMR. For all concentrations, an α_1 -process associated with the high- T_g component SBC and a faster α_2 -relaxation reflecting the dynamics of the TPP molecules were identified. The α_1 -relaxation shows the well-documented plasticizer effect, while the anti-plasticizer effect is observed for the faster α_2 -relaxation. Correspondingly, two glass transition temperatures T_{g1} and T_{g2} can be defined. The dynamics of the low- T_g component

is governed by a broad distribution of correlation times resulting in quasi-logarithmic correlation functions for low TPP concentrations. In contrast, the correlation function of the α_1 -process is Kohlrausch-like as in neat glass formers, yet, somewhat more stretched. As quite similar relaxation features as for glass formers in nano-confinement are observed, we concluded that the high- T_g component in the asymmetric mixtures provides an intrinsic confinement for the low- T_g component. In this disordered matrix, the low- T_g component becomes immobilized itself at $T < T_{g2}$. In agreement with previous reports, we found indications that some fraction of the TPP molecules is also involved in the α_1 -process. All in all, the scenario of the dynamics appears to be very similar to that of polymer-plasticizer systems.^{2–10}

In addition to the main (α -) relaxations, secondary (β -) relaxations are often observed in glass forming systems at higher frequencies than those of the α -relaxation and they persist at $T < T_g$. In most cases, DS is applied as a probe,^{10–15} in a few cases also mechanical relaxation^{16,17} or neutron scattering.^{18,19} It was shown that a secondary relaxation may also appear for rigid molecules and must therefore be of intermolecular nature. This was first stressed by Johari and

^{a)} Author to whom correspondence should be addressed. Electronic mail: ernst.roessler@uni-bayreuth.de.

Goldstein.¹¹ Below T_g , the relaxation time of the β -process follows an Arrhenius law with an activation energy in the range $E/R = 11\text{--}26 T_g$,²⁰ while above T_g merging of α - and β -relaxations is often but not always observed. Relying mainly on DS studies, much effort was undertaken to achieve an experimental classification scheme distinguishing generic and non-generic β -relaxations, i.e., such secondary processes which are intrinsic to the glass state or other processes reflecting structural particularities of the glass forming molecule.^{10,21,22} In particular, the pressure dependence of the β -process may be an important classification criterion.^{15,23–25} We mention that further relaxations occur at cryogenic temperatures,^{26,27} which are usually connected to the low-temperature anomalies of glasses.²⁸ We also note that a well resolved β -process is not always found. Instead an “excess wing” on the high-frequency side of the α -peak is observed, which may also be regarded as a special secondary relaxation or an intrinsic spectral feature of the α -process.^{10,15,29,30} In some cases, even both, an excess wing and a β -process, are observed.^{10,14,15} Still, unraveling the involved molecular mechanism is difficult to answer when restricting to dielectric studies alone. Here, solid-state NMR spectroscopy and neutron scattering,^{18,19} the latter, however, being usually limited to temperatures above T_g , provided deeper insight. Also simulations of Lennard-Jones binary mixtures of asymmetric, dumbbell-shaped molecules were carried out attempting to access the nature of the β -process.^{31,32}

Applying solid-state ^2H NMR measurements on glass formers like toluene^{33–36} and glassy crystals like ethanol³⁶ and cyano cyclohexane,^{37,38} the nature of the β -process was thoroughly investigated. Due to the high sensitivity of the NMR echo technique regarding small-angular motion it was shown that essentially all molecules take part in spatially highly restricted reorientations. A wobbling-on-a-cone or within-a-cone model^{39–41} with opening angles smaller than $\pm 10^\circ$ was proposed to reproduce the salient features of the NMR spectra due to the β -process ($T < T_g$).^{35,38,42} This model is close to the ideas forwarded by Williams and co-workers,⁴³ who proposed a partial fast decay (β -process) of the reorientational correlation which relaxes on long times due to the α -process. Implicitly, it was assumed by the interpretation of the NMR experiments that an isotropic, small-angle process not much depending on the particular structure of the glass-forming molecule is involved. Very recently, however, we found indications that the β -process may exhibit some extent of anisotropy reflecting the molecular structure of the glass former.⁴⁴ For example, in the case of studying the ^2H NMR echo spectra of toluene- d_3 , it essentially involves only fluctuations around the pseudo C_2 -axis, a finding actually suggested by measurements of the ^2H spin-lattice relaxation quite a while ago.⁴⁵ In contrast, measurements on toluene- d_5 suggested that all deuterons of toluene take part in the secondary relaxation thus indicating reorientation of the C_2 -axis as well.³⁵ Yet, assuming only fluctuations around the C_2 -axis, one is left with a situation which does not easily explain the dielectric activity of the β -process in the case of toluene, since such a kind of motion does not change the dipole moment. These experimental discrepancies still have to be settled.

In the case of a polymer, namely, poly(ethylene-propylene) (PEP) we found⁴⁴ that the β -process is not only

anisotropic but may also be dynamically inhomogeneous, i.e., not all polymer segments participate below T_g , a finding also reported for other polymers.^{46,47} It appears that the concept of “islands of mobility” or “islands of rigidity”^{48,49} first discussed by Johari and Goldstein^{11,21} may reappear, at least in the case of polymers or in some mixtures.

Secondary processes in binary glass formers and their phenomenology may turn out to be even more puzzling.^{9,10,15,49–52} In the case of the mixed glass TPP/polystyrene (PS), we investigated the component dynamics by DS and ^{31}P as well as ^2H solid-state NMR.⁴⁹ While neat PS does not show indications of a β -process, TPP displays one. In the mixture down to $c_{\text{TPP}} = 10\%$, yet both PS and TPP participate in a secondary process with an activation energy which does not change with c_{TPP} , i.e., it is essentially the same as in neat TPP. It appears that the small molecules “enslave” the polymer segments. Similar results were reported for the mixture chlorobenzene/decalin, both components showed very similar ^2H NMR echo spectra.^{36,42}

In the present case of the dynamically asymmetric non-polymeric mixture TPP/SBC, both neat components exhibit a β -process, and it is the goal of this paper to unravel the changes of the β -processes due to mixing. Again, combining DS, ^{31}P and ^2H solid-state NMR techniques we were able to selectively probe the dynamics of each component. We will demonstrate that, as in the case of the mixture TPP/PS, a common β -process appears; TPP and SBC both participate in a β -process originating from the TPP component. The “small” TPP molecules enslave the “large” SBC molecules.

Paper II is organized as follows. First, we characterize the mixed systems by dielectric spectroscopy and display time constants for both secondary processes. Then, we analyze the ^{31}P and ^2H NMR echo spectra in the mixtures probing both components selectively. Experimental details and description of the methods are mainly found in Paper I.¹

II. EXPERIMENTAL AND METHODOLOGICAL PART

We investigated binary mixtures of the (low- T_g) glass former tripropyl phosphate (TPP) and a (high- T_g) spirobichroman derivative which will be called SBC (see Fig. 1). TPP (99%) was received from Sigma Aldrich. The SBC compound was especially synthesized (see Paper I). A T_g contrast of $\Delta T_g = 222$ K is reached with a T_g of 134 K for TPP and T_g of 356 K for SBC. The SBC was employed in a non-deuterated form for the ^{31}P NMR and dielectric measurements and deuterated at the phenyl rings for ^2H NMR experiments (compare

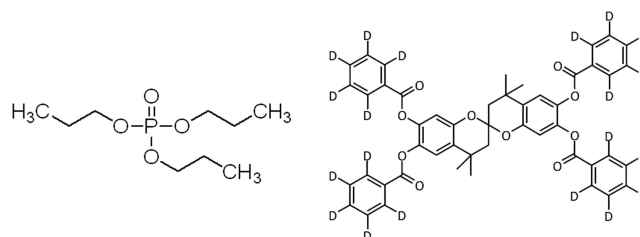


FIG. 1. Low- T_g component tripropyl phosphate (TPP) (left) ($M_{\text{mol}} = 224.23$ g/mol, $T_g = 134$ K) and the high- T_g spirobichroman component SBC (right) ($M_{\text{mol}} = 809.0$ g/mol, $T_g = 356$ K).

Fig. 1). Dielectric measurements confirmed that both, the non-deuterated and the deuterated SBC components, are dynamically identical. Mixtures with mass concentration $c_{TPP} = 10\%$ (only β -process), 21%, 34%, 47%, 61%, 76%, 89%, and 100% of TPP in SBC were investigated by ^{31}P NMR spectroscopy and mixtures with $c_{TPP} = 0\%$, 10%, 22%, 39%, 59%, and 80% by ^2H NMR spectroscopy. Additionally, we performed DS measurements on neat SBC, neat TPP, and mixtures with $c_{TPP} = 61\%$, 70%, and 85%. The concentration error is $\pm 2\%$. For experimental details regarding the DS experiments and the corresponding T_g values of the mixtures, see Paper I.¹

The dependence of the solid-state ^2H and ^{31}P NMR frequency on the angle ϑ between the molecular axis and the external magnetic field follows the second Legendre polynomial for systems with a symmetric interaction tensor as it is the case for deuterated SBC and TPP, respectively. The second Legendre polynomial has the highest pitch at $\vartheta = 45^\circ$ which corresponds to frequencies $\omega = 1/4 \cdot \delta$. Due to the symmetry of the ^2H Pake spectrum (involving two NMR transitions), the sensitivity with respect to changes of the NMR frequency due to some small-angle displacements of the C– ^2H -bonds is largest in the center and smallest at the singularities at $\pm\delta/2$, (cf. Paper I¹). It can be increased by enlarging the inter-pulse delay t_p of the applied solid-echo sequence leading to a relative decrease of the center of the powder spectrum.^{33,42,53} Indeed, a stronger relaxation of the center of the spectrum upon extending t_p is observed as the NMR fingerprint of the β -process in glasses or polymers.^{33–36,44,49} In order to quantify these subtle spectral changes, we introduced the spectral shape ratio $R(t_p)$ which defines the intensity $S(\omega; t_p)$ of the echo spectrum at $\omega = 0$ normalized to its intensity at the singularities explicitly^{48,49,54}

$$R(t_p) = \frac{S(\omega = 0; t_p)}{S(\omega = \delta/2; t_p)}. \quad (1)$$

In the case of the ^{31}P NMR echo spectra determined by the chemical shift anisotropy (CSA) interaction the maximum decay is at $\omega = 1/4 \cdot \delta$; experimentally the $R(t_p)$ value is obtained at $\omega = 0$, nevertheless. The value $R(t_p)$ for sufficiently large t_p exhibits a minimum as a function of temperature when the time scale of the secondary process fulfills the condition $\tau_\beta \cong 2\pi/\delta$.^{49,54} Therefore, an estimate of the time constant τ_β can be obtained. In some cases, the ^2H NMR spectra were symmetrized to improve the signal to noise ratio to allow an unambiguous determination of $R(t_p)$.

In the case of ^{31}P NMR, the relaxation rate $1/T_1$ is linked to the spectral density $J(\omega)$ at the Larmor frequency ω_L ,⁵⁵

$$\frac{1}{T_1} = K_{CSA} J(\omega_L) \quad \text{with} \quad K_{CSA} = \frac{3}{10} \delta_{CSA}^2. \quad (2)$$

In the case of the ^2H relaxation one finds the following:

$$\frac{1}{T_1} = K_Q [J(\omega_L) + 4J(2\omega_L)] \quad \text{with} \quad K_Q = \frac{2}{15} \delta_Q^2. \quad (3)$$

If one assumes $J(\omega_L) \approx J(2\omega_L)$ and uses the coupling constants gained from the solid-state NMR spectra ($\delta_Q/2\pi \approx 135$ kHz, $\delta_{CSA}/2\pi \approx 20$ kHz) (see Paper I¹) one can directly calculate the spectral density from these equations. The normalized susceptibility $\chi''(T) = \omega \cdot J(\omega = \omega_L, T)$ can be split into two

fractions, one describing the relaxation of the α -process (f) and one describing the spatial restricted reorientation of the secondary relaxation $(1-f)$:⁵⁶ $\chi''(T) = f\chi''_\alpha(T) + (1-f)\chi''_\beta(T)$. The quantity of $(1-f)$ reflects the relaxation strength and depends on the geometry of the secondary relaxation, i.e., the extents of angular displacement involved. This will be applied to compare the relaxation strength of the β -process shared by TPP and SBC.

III. RESULTS

A. Dielectric spectra

As demonstrated in Paper I,¹ both (neat) components SBC and TPP are type B glass formers,¹⁴ i.e., they show a secondary process (β_1 and β_2 , respectively) which is well recognized in the glass ($T < T_g$). The corresponding time constants $\tau_{\beta_1}(T)$ and $\tau_{\beta_2}(T)$ are shown in Fig. 2 as given via “peak picking” (i.e., $\tau_\beta = 1/(2\pi\nu_{\max})$ with ν_{\max} being the frequency at the maximum of the dielectric spectrum). An Arrhenius temperature dependence with activation energies $E_{\beta_1} = 15.6 RT_g$ and $E_{\beta_2} = 23.5 RT_g$, respectively, is observed. Compared to the α -process, the β_1 -process (SBC) is much faster than the β_2 -process. Dielectric spectra regarding the β -process were also measured in the mixture TPP/SBC for the concentrations $c_{TPP} = 60\%$, 70%, and 85% (mass percentage). In Fig. 3, they are compared to those of neat TPP. The spectra at the same temperatures $T = 105$ K, $T = 115$ K, and $T = 125$ K are plotted. Clearly, regarding the β_2 -process introduced by TPP, time scale as well as spectral shape do not change, they agree with those for neat TPP; except the magnitude of the spectra decreases due to the dilution of the TPP dipoles. The time constants in the mixtures are also included in Fig. 2. In all cases, they follow the same Arrhenius law as those of neat TPP. Below $c_{TPP} < 60\%$, we were unable to measure the dielectric spectra as the mixture shows phase separation. By contrast, in the case of NMR, the glass ampoules could be quenched fast enough in order to get true mixtures with $c_{TPP} < 60\%$ (see below). Anticipating the NMR results (stars in Fig. 2) we can state that even at $c_{TPP} = 21\%$ a β_2 -process is identified by ^{31}P NMR with a

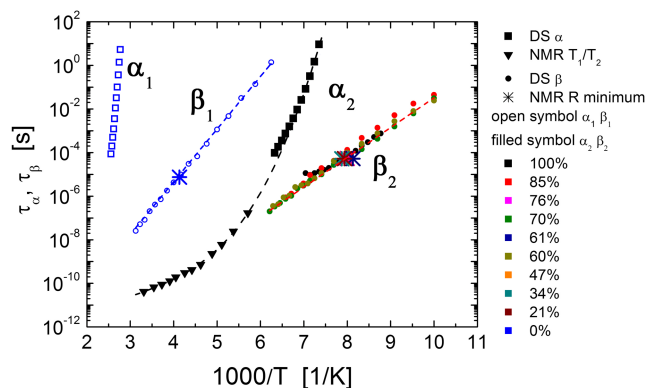


FIG. 2. Time constants of the main relaxations α_1 and α_2 of the neat systems and of the secondary relaxations β_1 and β_2 in the mixture TPP/SBC for $c_{TPP} = 21\%$, 34%, 47%, 60%, 61%, 70%, 76%, 85%, 100%, and neat SBC ($c_{TPP} = 0\%$). Every symbol is coded by the relaxation process, measurement method, and concentration. α_1 -process (open squares); α_2 -process (filled squares from DS and down triangles from NMR T_1/T_2 measurements⁵⁷); dielectric spectroscopy β -process (open circles β_1 , filled circles β_2); time constants from minimum of the NMR echo spectra (crosses).

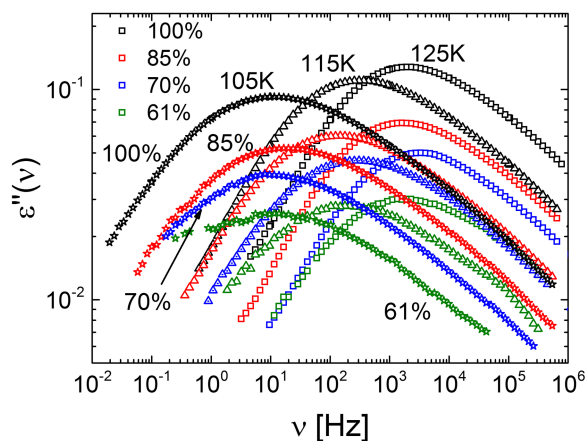


FIG. 3. Dielectric spectra of the mixture TPP/SBC showing the β -process at $T = 105$ K, 115 K, and 125 K for the concentrations indicated. The amplitudes of the spectra are adapted for better comparison.

time constant which essentially is that of neat TPP. Regarding the β_1 -process, introduced by SBC, we were unable to observe it in the mixtures by DS. As its time scale lies between those of the main relaxations of TPP and SBC, it is covered by the α_1 - and the broad α_2 -relaxation (if one assumes that $\tau_{\beta_1}(T)$ also does not change significantly with concentration as it is implied by the NMR measurements—see below).

B. NMR measurements

For the further investigation of the β -relaxation, we measured ^{31}P Hahn echo (TPP) and ^2H solid echo spectra (SBC) (compare Experimental in Paper I¹). In particular, the inter-pulse delay t_p of the echo pulse sequence was systematically enlarged. Thereby, the sensitivity on the spatially highly restricted angular displacement is enhanced as demonstrated in previous works.^{36,42} In Fig. 4(a) such ^{31}P echo spectra are shown for neat TPP at 123 K, and in Fig. 4(b) ^2H echo spectra for neat SBC at 122.4 K are shown. In the case of TPP, the

effect of the β -process is well recognized: By increasing the inter-pulse delay t_p , the spectral intensity decreases mainly in the center of the spectra, while the singularities, i.e., the intensity at the edges of the spectrum, are essentially unaffected. In the case of SBC, its β -process is much too slow at this temperature (cf. Fig. 2) and no changes of the ^2H spectra with t_p are expected—as observed (Fig. 4(b)). For all t_p values, the same spectral shape (Pake) is found.⁴²

In the mixtures, the β_2 -process (introduced by TPP) is identified by the Hahn echo spectra for all concentrations down to $c_{\text{TPP}} = 10\%$ (see below). In Fig. 4(c), the ^{31}P NMR spectra at $T = 124.2$ K for $c_{\text{TPP}} = 61\%$ are shown. Clearly, the same features as in the neat TPP are reproduced. Figure 4(d) shows the ^2H spectra of SBC in the mixture at a very similar temperature. Now spectral changes typical of a spatially highly restricted motion are observed in contrast to neat SBC (Fig. 4(b)). Thus, while in neat SBC no spectral changes are observed at temperatures around 125 K, they are well seen in the mixtures. It appears that the β_2 -process involves also the SBC molecules.

We measured the NMR echo spectra of TPP and SBC over a large temperature range ($T < T_{g1}$). The results are displayed in Fig. 5 for the neat systems TPP (left side) and SBC (right side) and two TPP/SBC mixtures with comparable concentrations, $c_{\text{TPP}} = 34\%$ (middle left) monitored by ^{31}P NMR and $c_{\text{TPP}} = 39\%$ (middle right) monitored by ^2H NMR. At each temperature, the inter-pulse delay is varied. On the left side (neat TPP), the characteristic line-shape effects of the β -process are recognized. As the β -process becomes slow at low temperatures, the spectral change at large t_p disappears finally, indicating that the slow motion limit is reached. The fast motion limit expected at high temperatures is not observable because of the collapse of the solid-state spectrum due to the α -relaxation. In the case of the ^{31}P spectra in the mixture (middle left of Fig. 5), the line-shape effects due to the β_2 -process are even better recognized. Because of the anti-plasticizer

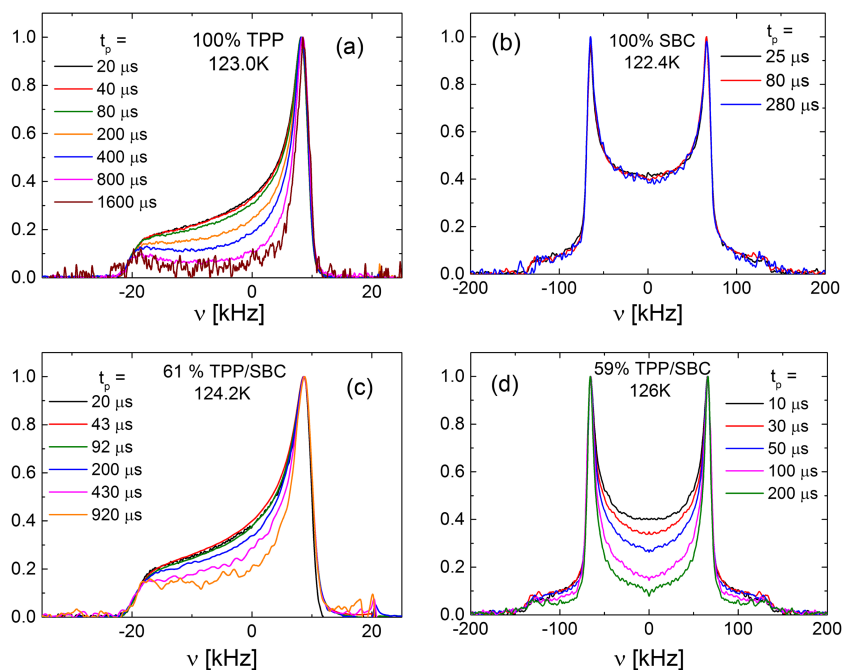


FIG. 4. NMR echo spectra at different inter-pulse delays t_p : (a) neat TPP: ^{31}P NMR spectra at $T = 123.0$ K; (b) neat SBC: ^2H NMR spectra at $T = 122.4$ K; (c) mixture TPP/SBC with $c_{\text{TPP}} = 61\%$: ^{31}P NMR spectra at $T = 124.2$ K; (d) mixture TPP/SBC with $c_{\text{TPP}} = 59\%$: ^2H NMR spectra (symmetrized) at $T = 126.0$ K.

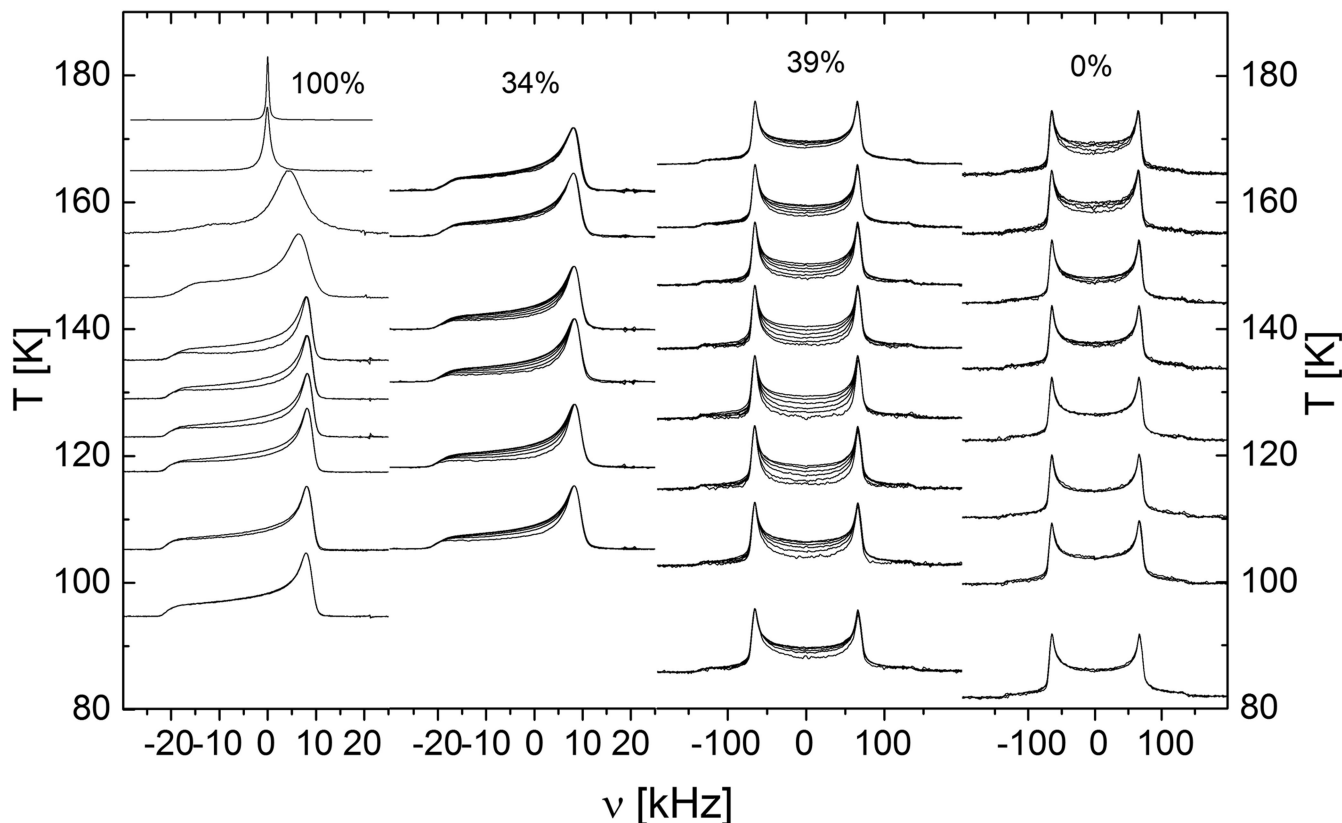


FIG. 5. Temperature and inter-pulse dependent ^{31}P and ^2H NMR echo spectra of the neat systems TPP (100%) (left, some data taken from Ref. 57) and SBC (0%) (right), and of the mixtures with $c_{\text{TPP}} = 34\%$ (probed via ^{31}P NMR, middle left) and with $c_{\text{TPP}} = 39\%$ (probed via ^2H NMR, middle right). The baseline of the spectra corresponds to the temperature at which they were measured. At each temperature, spectra with different inter-pulse delays are shown as follows: $25\ \mu\text{s}$ – $280\ \mu\text{s}$ for ^2H NMR, $20\ \mu\text{s}$ – $920\ \mu\text{s}$ for $c_{\text{TPP}} = 34\%$ and $20\ \mu\text{s}$, and $200\ \mu\text{s}$ for neat TPP; at high temperatures for neat TPP only spectra with $t_p = 20\ \mu\text{s}$ are shown.

effect T_{g2} increases in the mixtures, while the β_2 -process does not change as already found by DS, i.e., α_2 - and β_2 -process are well separated. While at high temperature essentially no spectral changes occur with varying t_p , they appear at intermediate temperatures, and at lowest temperatures they start to disappear again. This is the typical spectral behavior for a motional process passing through the NMR time window: At high temperature the process is in the fast motion (exchange) limit, whereas at low temperatures it is in the slow motion (exchange) limit. Importantly, the spectral widths in the fast and slow exchange limit, respectively, are essentially the same. Thus, the angular displacements associated with the β_2 -process are very small – say, below $\pm 10^\circ$. It is the great advantage of the NMR echo method to enhance the sensitivity on such small angular displacements via increasing the inter-pulse distance t_p .^{33,53}

Concerning neat SBC (Fig. 5, right side) essentially no spectral changes are observed at temperatures for which spectral changes are observed for TPP. Only at high temperatures (150 K and higher), changes due to the fast β -process of SBC (β_1) are recognized which will be further discussed below. In contrast, clear line-shape changes are observed for SBC at $c_{\text{TPP}} = 39\%$. Again they are small at high temperatures, large at intermediate temperatures, and small again at low temperatures. The spectral effects occur at similar temperatures as those for TPP in the $c_{\text{TPP}} = 34\%$ mixture (middle left). The fast and slow exchange ^2H NMR spectra alters its width only

by less than 1% ($(\delta_Q/2\pi) = 131.6\ \text{kHz}$ at low temperatures and $(\delta_Q/2\pi) = 130.6\ \text{kHz}$ at high temperatures). Thus, again angular displacements smaller than $\pm 10^\circ$ are also characteristic of the large SBC molecules. Clearly, in the mixtures, the β_2 -process introduced by the TPP molecules induces a similar small-angle motion for the SBC molecules.

While no secondary process is observable at low temperatures for neat SBC, an onset of spectral changes is found at high temperatures, as mentioned (cf. Fig. 5, right column). As revealed by DS (see Fig. 2), the β -process of SBC is expected to show up in the NMR spectra only at high temperatures. This is demonstrated in Fig. 6. At the low temperature, no spectral change is observable; the β -process is too slow to be seen in the NMR spectra. By increasing the temperature, the spectral shape starts to change for long t_p values with the intensity decreasing in the center of the spectra. Additionally, for temperatures higher than 230 K, two additional peaks in the middle of the spectra appear, typical of fast phenyl jumps—as discussed in Paper I.¹

For the characterization of the subtle spectral changes caused by the β -process, we previously introduced the ratio $R(T, t_p)$ of the spectral intensity in the center with respect to that of the singularities (see Section II).^{48,49} In Fig. 7(a), $R(T, t_p)$ normalized by $R(t_p = 15\ \mu\text{s})$ is shown for all t_p values measured for neat SBC. This normalization is necessary because, due to the influence of the phenyl jump, the spectral intensity increases in the middle of the spectra for higher

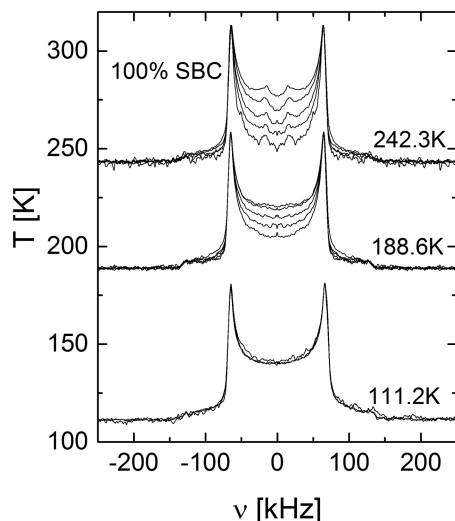


FIG. 6. Inter-pulse dependent echo spectra (symmetrized) ($t_p = 25 \mu\text{s}$, $50 \mu\text{s}$, $80 \mu\text{s}$, $120 \mu\text{s}$, and $180 \mu\text{s}$) of neat SBC revealing spectral effects due to the β_1 -process. The baseline of the spectra corresponds to the temperature at which they were measured.

temperatures and distorts the behavior of $R(T, t_p)$ (compare Fig. 6). A minimum in $R(T, t_p)$ is seen for all t_p delays at a temperature around 250 K again reflecting the situation that the β_1 -relaxation passes through the NMR time window. The larger t_p is, the lower the minimum is; in particular, for $t_p = 180 \mu\text{s}$, $R(T, t_p)$ reaches almost zero. This indicates that essentially all SBC molecules participate.^{33,34,42} At the minimum, the condition $\tau_\beta \cong 2\pi/\delta\omega$ holds^{49,54} and the corresponding decay time is added in Fig. 2 (crosses). It well agrees with the data collected by DS for SBC, although a small dependence of the time constant on t_p is expected, but irrelevant on logarithmic scales.

A similar behavior is shown in Fig. 7(b), where $R(T, t_p)$ for the ^{31}P echo spectra of TPP in the mixture with $c_{\text{TPP}} = 34\%$ is presented. In this case, the $R(T, t_p)$ minimum due to the β_2 -process introduced by TPP is monitored at low temperatures around $T = 125 \text{ K}$. At $T \cong 170 \text{ K}$ the influence of the β_2 -relaxation has almost vanished, while at even higher temperatures the α_2 -process leads to a full line collapse, which is also reflected in $R(T, t_p)$. Again, an estimate of the time constant τ_{β_2} can be made. It is shown in Fig. 2 together with τ_{β_2} of all other concentrations extracted by the echo method. Good accordance with the dielectric data is found. Even for mixtures with concentrations lower than

those investigated by DS $\tau_{\beta_2}(T)$ remains the same down to $c_{\text{TPP}} = 21\%$.

In order to compare the spectral changes induced by the β -process in the different mixtures, we discuss the temperature dependence of $R_{ip}(T)$ at a fixed, yet, large t_p value. For such a t_p value, the effect of β -process in the spectra is largest. Figure 8(a) displays $R_{ip}(T)$ for the TPP component. Two observations can be made: First, within the error margin, the minimum in $R_{ip}(T)$ occurs at the same temperature, and second, the depth of the minimum is essentially the same, both indicating that the involved dynamics of the TPP component do not significantly change in the mixtures, except for the $c_{\text{TPP}} = 10\%$ mixture, where $R_{ip}(T)$ is much higher. We take this as an indication that the β_2 -process starts to disintegrate as expected for $c_{\text{TPP}} \rightarrow 0\%$. At high TPP concentrations, the α -process interferes. This is not any longer the case at lower concentrations due to the anti-plasticizer effect, which shifts the α -relaxation to higher temperatures, while $\tau_\beta(T)$ remains independent of the concentration.

Regarding the SBC component, the corresponding $R_{ip}(T)$ data sets are displayed in Fig. 8(b). As already shown in Fig. 7(a), for neat SBC the minimum corresponding to the β_1 -process is observed at high temperatures (ca. $T = 250 \text{ K}$). For the mixture, another secondary relaxation is observed at much lower temperatures between 100 K and 170 K. It appears at the same temperatures as the β_2 -relaxation of the TPP component (see Fig. 8(a)). As already concluded above, the TPP component induces a secondary process in SBC. Again, the depth of the minima is rather similar except for the $c_{\text{TPP}} = 10\%$ mixture. Here, the $R_{ip}(T)$ is much higher, yet the position of the minimum essentially remains the same. As for TPP, we take this as an indication that for $c_{\text{TPP}} \rightarrow 0\%$ the β_2 -process vanishes. Whether the amplitude of the angular displacements involved in the β_2 -process decreases or whether the fraction of the SBC molecules participating diminishes cannot be decided so far (see below). For $c_{\text{TPP}} = 10\%$, the α_1 -process is slow enough that traces of another secondary relaxation, the β_1 -process (the original SBC secondary process), are observable, too. A low plateau value $R_{ip=180\mu\text{s}}(T) \cong 0.12$ is recognized for temperatures between 210 K and 260 K which follows that of neat SBC. At higher temperatures, the main relaxation interferes and $R_{ip}(T)$ decays even further. So at least for $c_{\text{TPP}} = 10\%$ both secondary relaxations are observable by NMR with time constants being essentially the same as in the neat systems SBC and TPP, respectively. The observation of two restricted

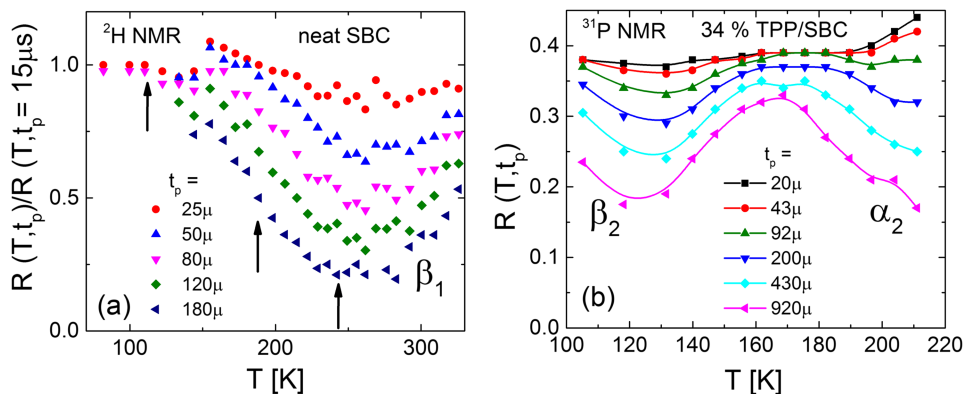


FIG. 7. (a) Normalized spectral shape ratio $R(T, t_p)$ characterizing the changes of the echo spectra for different inter-pulse delays t_p for neat SBC measured by ^2H NMR. The arrows indicate the temperatures for which spectra are shown in Fig. 6. (b) $R(T, t_p)$ of TPP for the $c_{\text{TPP}} = 34\%$ mixture measured by ^{31}P NMR. The interpolations are guides for the eye.

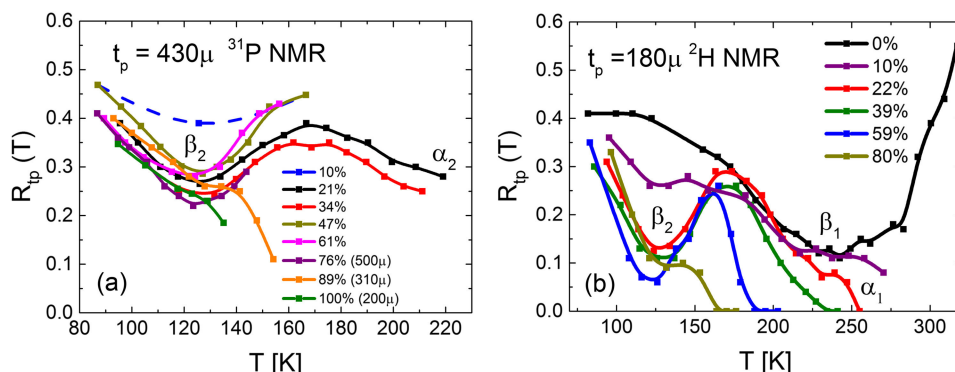


FIG. 8. (a) Spectral shape ratio $R_{tp}(T)$ characterizing the changes of the ^{31}P Hahn echo spectra of the TPP component as a function of temperature for the concentrations indicated at a large inter-pulse delay of $t_p = 430 \mu\text{s}$ ($500 \mu\text{s}$ for $c_{TPP} = 76\%$, $310 \mu\text{s}$ for $c_{TPP} = 89\%$, and $200 \mu\text{s}$ for $c_{TPP} = 100\%$). (b) $R_{tp}(T)$ as measured by the solid echo ^2H spectra of the SBC component for the concentrations and inter-pulse delay indicated. Lines are guides for the eyes.

small angle movements is at first glance contra-intuitive. As discussed below, $R_{tp}(T)$ of the β_2 -process for SBC in the $c_{TPP} = 10\%$ mixture is higher compared to $R_{tp}(T)$ at higher concentrations; thus the β_2 relaxation starts to disintegrate. However, the extent of molecular motion is further enhanced by its own β_1 -process at high temperatures.

Figure 9 shows $R(t_p)$ at temperatures for which $R_{tp}(T)$ is minimal for both, ^{31}P NMR (a) and ^2H NMR (b). Regarding TPP, for concentrations $c_{TPP} \geq 34\%$, the ratio $R(t_p)$ decays to zero on a similar time scale. An exponential function can be fit to the decays. For $c_{TPP} = 10\%$ and 21% , the R value does not decay to zero any longer; finite long-time values $R_\infty \approx 0.5$ for $c_{TPP} = 21\%$ and $R_\infty \approx 0.8$ for $c_{TPP} = 10\%$ are found. A finite R_∞ value signals that only a fraction of TPP molecules takes part in the secondary relaxation. For $c_{TPP} \rightarrow 0\%$, the β_2 -process, of course, has to disappear. Apparently, its disintegration sets in at $c_{TPP} < 25\%$: The lower c_{TPP} , the lower is the fraction of TPP molecules participating.

In the case of ^2H NMR of SBC, the $R(t_p)$ decay (Fig. 9(b)) is about a factor of 6 faster than it is in the case for ^{31}P NMR as expected for the larger coupling constant ($\delta_Q \approx 6 \delta_{CSA}$). For the SBC component, the decay for all concentrations is the same, except for $c_{TPP} = 10\%$. The ratio $R(t_p)$ at $c_{TPP} > 10\%$ decays exponentially to zero; all SBC molecules participate in the induced β -relaxation. For the $c_{TPP} = 10\%$ mixture, the decay takes place on a longer time scale, which is also the reason for the high $R_{tp}(T)$ value in Fig. 8(b). However, it is not clear whether the decay of $R(t_p)$ reaches zero or a finite value R_∞ is approached for long inter-pulse delays as it is the case for TPP at low concentrations. Due to the too fast T_2 decay, longer t_p values cannot be explored in the case of ^2H NMR. In any case, as for TPP, the disintegration

of the β_2 -process in terms of changes in amplitude and/or of fewer molecules participating is also recognized in the SBC signal.

C. Relaxation data

The mixtures were also characterized by measuring the spin-lattice relaxation over a large temperature range. The magnetization recovery was found to be exponential for the TPP component (^{31}P) and mostly non-exponential for the SBC component (^2H) in particular at low temperatures. In the latter case, fits by a Kohlrausch function yield the mean relaxation time $\langle T_1 \rangle(T)$. In Fig. 10(a), the T_1 data of the TPP component is shown. At high temperature, a T_1 minimum which is attributed to the main relaxation of TPP (α_2 -process). It shifts to higher temperatures with decreasing TPP concentration reflecting the anti-plasticizer effect. The minimum value increases with decreasing c_{TPP} , which signals that the distribution $G(\ln\tau_{\alpha_2})$ becomes broader as discussed in Paper I.¹ At low temperatures, however, within the error margin, $T_1(T)$ becomes the same for all mixtures. Actually, given the results from the spectral analysis (see above), this is expected: Time scale and relaxation strength of the β_2 -process are virtually not changing in the mixtures, except at lowest concentrations. However, the T_1 relaxation times for $c_{TPP} = 10\%$ and $c_{TPP} = 21\%$ coincide with the T_1 data at higher concentrations which probably is caused by spin diffusion. Although not all molecules are involved in the β -relaxation any longer, the mobile fraction controls the spin-lattice relaxation. For $c_{TPP} \leq 47\%$, one observes a shoulder in the T_1 data at higher temperatures, indicating the relaxation rate maximum due to the β_2 -process at $T > T_{g_2}$ as observed in Ref. 58.

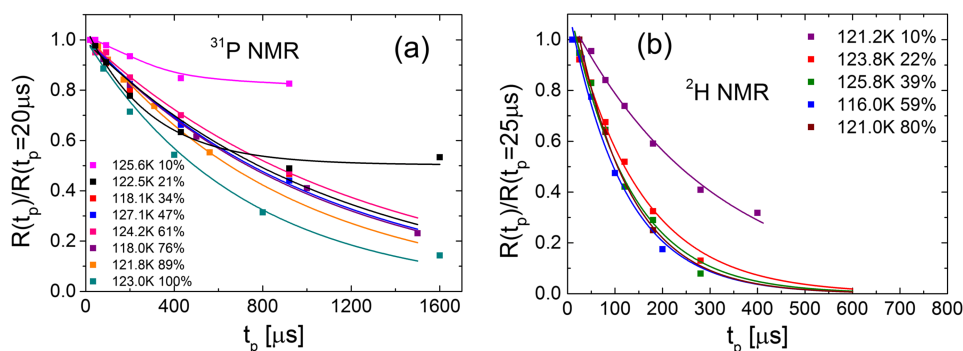


FIG. 9. (a) Normalized spectral shape parameter $R(t_p)$ at the $R_{tp}(T)$ minimum for all concentrations measured by ^{31}P NMR on the TPP component. (b) Normalized $R(t_p)$ for all concentrations measured by ^2H NMR on the SBC component. Solid lines are fits by an exponential function, except for $c_{TPP} = 10\%$ and 21% in (a); here only guides for the eyes are shown.

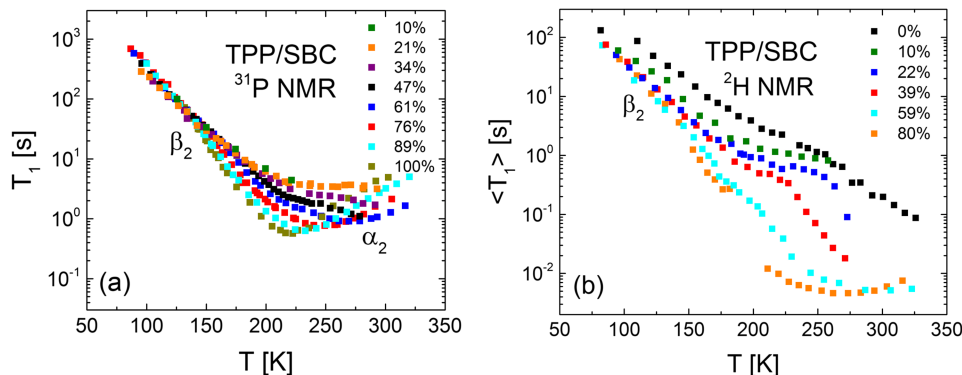


FIG. 10. (a) Spin-lattice relaxation time of TPP in the neat system and in the mixtures TPP/SBC for concentrations indicated. (b) Relaxation data of SBC in the neat system and in the mixtures for concentrations indicated. Between 180 K and 210 K in the 80% mixture no T_1 data could be measured because of the low signal intensity.

The ^2H NMR relaxation data $\langle T_1 \rangle(T)$ for the SBC component are shown in Fig. 10(b). The stretching parameter β_K as given by a Kohlrausch fit is found in the Appendix (Fig. 12) and shows a temperature dependent behavior as expected.⁵⁹ The data $\langle T_1 \rangle(T)$ exhibits a rather complex behavior at high temperatures due to the presence of two motional processes, namely, the α_1 -process and the phenyl group jumps identified in the ^2H spectra (cf. Paper I¹ and Fig. 6 above). At low temperatures and for $c_{\text{TPP}} \geq 22\%$, the relaxation times become essentially the same. Only for $c_{\text{TPP}} = 10\%$ and neat SBC they are longer. As will be demonstrated below (see Fig. 11), the temperature dependence of the spin-lattice relaxation of SBC ($c_{\text{TPP}} > 10\%$) at low temperatures is the same like that of TPP and thus reflects the β_2 -process, too. As in the case of ^2H relaxation, spin-diffusion is less efficient; thus the different behavior of the mixture with $c_{\text{TPP}} = 10\%$ reflects the disintegration of the β -process. The case $c_{\text{TPP}} = 0\%$ with its even longer relaxation time is obvious as no β_2 -process is present.

For both components, an estimate of the time constants is obtained from the T_1 minimum via $\omega_\alpha \tau_\alpha \approx 0.616$ for ^2H NMR and $\omega_L \tau_\alpha \approx 1$ for ^{31}P NMR and discussed in Paper I.¹ In the case of TPP, the α_2 -process and in the case of SBC the α_1 -process are probed.

As the relaxation rate $1/T_1$ is linked to a spectral density and a coupling constant K_i , the latter known from the

solid-state spectrum (cf. Section II), we can attempt to quantitatively compare the susceptibility characterizing the β_2 -process as probed by TPP (via ^{31}P NMR) and SBC (via ^2H NMR). Since both rates show the same temperature dependence at low temperatures, any difference among the susceptibility can be mapped to a different extent of angular displacement of the molecules TPP and SBC. Figure 11 shows the normalized susceptibility $\chi'' = \omega_L J(\omega_L) = \chi''(T)$ of TPP and SBC in the mixture calculated from the T_1 data and assuming $J(\omega_L) \approx J(2\omega_L)$ in the case of ^2H relaxation (cf. Section II, Eqs. (2) and (3); $J(\omega_L) = 1/(K_i * T_1)$). As anticipated, the slope of the susceptibility $\chi''(T)$ for both, TPP and SBC, is the same for $c_{\text{TPP}} \geq 20\%$, yet the absolute values are different for TPP and SBC but the same for each component in the mixture. In the case of SBC, $\chi''(T)$ is by about a factor of seven lower than that of TPP. The difference between the susceptibility of both components is larger than it can be caused by the different Larmor frequencies. As introduced in Section II, the normalized susceptibility $\chi''(T)$ can be split into two fractions,⁵⁶ one describing the relaxation of the α -process (f) and one describing the spatial restricted β -process ($1-f$).⁵⁶ In the glass ($T < T_{g2}$), the contribution of the α -process can be ignored and one gets $\chi''(T) = (1-f)\chi''_\beta(T)$. The quantity $(1-f)$ reflects the relaxation strength of the β -process and is linked to the extent of angular displacement of the molecules. The lower susceptibility in the case of SBC indicates a lower extent of angular displacement of the SBC molecules compared to that of TPP, which might be caused by the larger size of SBC molecules. We note that the different amplitudes of the β -process for TPP and SBC, respectively, should also be seen in the behavior of the line shape parameter $R(t_p)$ (see Fig. 9), yet it is difficult to estimate quantitatively the extent of its influence on the decay of $R(t_p)$. We previously investigated the β -relaxation in the mixture TPP/PS.⁴⁹ As in the present case, TPP enslaves PS to participate in the β_2 -process. For comparison, data of the TPP relaxation in the system TPP/PS⁴⁹ are added. Remarkably, $\chi''(T)$ is the same as in the TPP/SBC mixture. It appears that the manifestations of the β -process introduced by TPP are essentially independent of the second component.

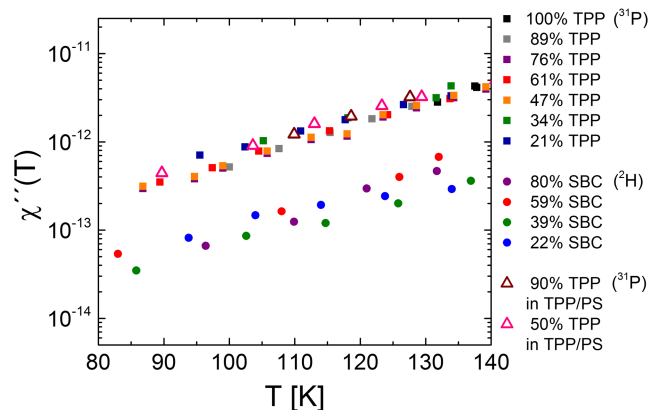


FIG. 11. Temperature dependence of the normalized susceptibility $\chi''(T) = \omega_L J(\omega_L)$ of neat TPP and TPP in the mixture at low temperatures where the β -relaxation determines the spin-lattice relaxation for concentrations as indicated and of the SBC component in the mixture (c_{TPP} as indicated). For comparison, $\chi''(T)$ data from the system TPP/PS⁴⁹ is added showing the same behavior as the TPP/SBC mixture.

IV. DISCUSSION

In Paper I¹ of this series of two papers, we focused on the main relaxations (α_1 and α_2) of the dynamically asymmetric binary glass former consisting of the low- T_g component TPP ($T_g = 134$ K) and the non-polymeric high- T_g component

SBC ($T_g = 356$ K), a spirobichroman derivative. Component-specific dynamics were revealed by applying dielectric spectroscopy as well as ^2H and ^{31}P NMR spectroscopy. Both components exhibit a secondary (β -) relaxation which is dealt with in the present contribution (Paper II). While the β -process of SBC is present at temperatures where it interferes with the α_2 -process of TPP, that of TPP is well observable by DS and NMR at low temperatures. In the mixture, remarkably, the time constants as well as the relaxation strength of the β -process introduced by TPP (β_2 -process) do not change with concentration. Similar results were reported in the system TPP/PS⁴⁹ for which τ_β slightly changes with concentration. Also for the mixtures toluene/PCB54,⁵² m-toluidine/aniline,⁶⁰ methyl tetrahydrofuran/PS,⁹ and toluene/picoline,⁴⁸ no change in time constants and the distribution $G(\ln(\tau_\beta))$ are found. However, in mixtures of water and propylene glycol, the time scale of the β -process decreases with decreasing propylene glycol concentration.⁵⁰

NMR echo experiments with their high resolution of small-angle processes demonstrate that the β -process in the mixture displays the same characteristics as in neat glasses. A spatially highly hindered motion is revealed, which is in contrast to MD simulations where rather large reorientation angles were found.³¹ As the NMR spectral widths essentially agree in the slow and fast exchange limit, the involved angular displacements can be estimated to be below $\pm 10^\circ$. We are not aware of any other technique, which allows to probe such small angular amplitudes. Interestingly, while the relative dielectric relaxation strength of the β -process varies significantly,²⁰ the NMR manifestation of the β -process appears to be very similar.

In the mixtures for all concentrations, solid-state NMR identifies a secondary process also for the SBC component in the same temperature interval as that of the β_2 -process of TPP. The spectral manifestation as well as its temperature dependence are essentially the same. As in our previous study,⁴⁹ we conclude that the β -process introduced by TPP enslaves the large SBC molecules to perform a similar motion. We emphasize that the line shape changes due to the β -process are very similar to those observed in neat systems,^{35,36} and no concentration dependence of the effect is observed, except for very low c_{TPP} for which the β -process starts to disintegrate. Moreover, a significant shortening of the ^2H T_1 values at low temperatures (together with the same temperature dependence of the ^{31}P T_1 data) is seen in the mixtures (compare Fig. 10(b)). Similar relaxation effects were reported for TPP/PS.⁴⁹ We therefore rule out that the intermolecular dipole-dipole interaction between the deuterons of SBC and the protons of TPP can be the cause of the ^2H NMR findings. In particular, given the ratio of the relaxation rates of the dipolar over the quadrupolar interaction $R_{\text{DD}}/R_{\text{Q}} = (\delta_{\text{DD}}/\delta_{\text{Q}})^2 \approx (5/100)^2$,⁶¹ the influence due to the dipole-dipole coupling can be neglected.

The extent of angular displacement of SBC is smaller than that of the TPP molecules as is suggested by a quantitative comparison of the ^2H and ^{31}P spin-lattice relaxation times, a result which may be rationalized by the larger size of the SBC molecule. All molecules TPP and SBC participate. This only changes at low concentrations, say, $c_{\text{TPP}} \leq 20\%$, for which less and less molecules take part in the β_2 -process. In other words, the β -process, involving both TPP and SBC molecules,

starts to disintegrate at low concentrations forming “islands of rigidity”^{48,49} or “islands of mobility.”¹¹ Finally, for $c_{\text{TPP}} \rightarrow 0\%$, the β_2 -process has to disappear. Similar observations were made for TPP/PS,⁴⁹ toluene/PCB,^{52,54} and toluene/picoline⁴⁸ where again “islands of rigidity” were found, however, they appear already at a higher additive concentration.

Summarizing, one could say that the remarkable fact that the time constant $\tau_{\beta_2}(T)$ does not change with concentration might indicate a “local” process controlled by some structural particularity of the TPP molecule. Yet, two observations strongly point to another interpretation. (i) The enslavement of the high- T_g component SBC. (ii) The disintegration of the process at low TPP concentration. We take these facts as a strong indication that the β -process is a cooperative process which involves all molecules of the mixture at least above some concentration limit above which cooperativity can be established. Furthermore, a high activation energy ($E_{\beta_2} = 23.5 RT_g$) was quoted as a hint for a cooperative process.^{14,62,63}

V. CONCLUSION

The paper investigates the secondary (β -) relaxations of the asymmetric binary mixture TPP/SBC over a broad temperature and concentration range. The components exhibit a very large T_g contrast ($\Delta T_g = 222$ K) to mimic a situation as in a typical polymer-plasticizer system. Employing dielectric and ^2H as well as ^{31}P NMR spectroscopy the component-selective dynamics are probed. The β -relaxation observed in neat TPP is also seen in the mixtures with time constants not changing down to $c_{\text{TPP}} \approx 10\%$. NMR echo experiments with their high sensitivity to small-angle processes identify the β -relaxations as a spatially highly restricted process of all molecules with angular amplitudes below, say, $\pm 10^\circ$, as it is also reported for neat glass formers like toluene.

At low temperatures, for which TPP shows the ^{31}P NMR spectra typical of a β -process in the mixture, very similar spectral features are revealed for the (deuterated) SBC component by ^2H NMR, in addition to its “own” β -process observed at high temperatures. Apparently, the small TPP molecules enslave the large SBC molecules to perform a similar hindered reorientation. This confirms the previous results for the mixture TPP/PS where TPP enslaves the PS segments to participate in the β -process introduced again by TPP. By investigating the spin-lattice relaxation time $T_1(T)$ of both components, it is shown that the angular displacement of SBC is somewhat smaller than that of TPP though the time constant is the same like that of TPP. Furthermore, $T_1(T)$ of TPP in the temperature region of the β_2 -process is absolutely the same as in the mixture TPP/polystyrene investigated previously. Thus, it appears that the manifestations of the β -process introduced by one component are not only independent of concentration but also independent of the second component. Below $c_{\text{TPP}} \leq 20\%$, the NMR experiments indicate that the β_2 -process starts to disintegrate—as expected for $c_{\text{TPP}} \rightarrow 0$. While at higher concentrations all molecules, TPP as well SBC, participate, more and more TPP molecules get immobilized upon decreasing concentration, i.e., “islands of rigidity” appear. All in all, we take these results as a strong indication that the β -process in glasses is a cooperative phenomenon.

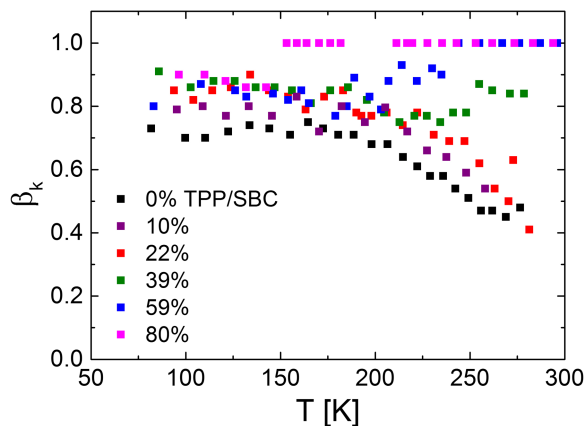


FIG. 12. Stretching parameters β_K of the Kohlrausch fits of the spin-lattice relaxation of SBC at different concentrations.

ACKNOWLEDGMENTS

The authors appreciate financial support by Deutsche Forschungsgemeinschaft (DFG) through Project No. RO 907/19.

APPENDIX: TEMPERATURE DEPENDENCE OF THE KOHLRAUSCH STRETCHING PARAMETER OF SBC

Figure 12 displays the temperature dependence of the stretching parameter β_K of the Kohlrausch fits to the ^2H NMR spin-lattice relaxation data (compare Fig. 10). With decreasing additive concentration β_K decreases at high temperatures, while it is almost concentration independent at low temperatures. At low temperatures with its long relaxation times, spin-diffusion becomes more efficient and leads to higher β_K values compared to those at high temperatures.

- ¹B. Pötzschnner, F. Mohamed, C. Bächer, E. Wagner, A. Lichtinger, R. Minikejew, K. Kreger, H.-W. Schmidt, and E. A. Rössler, *J. Chem. Phys.* **146**, 164503 (2017).
- ²P. J. Hains and G. Williams, *Polymer* **16**, 725 (1975).
- ³M. A. Desando, S. Walker, and W. H. Baarschers, *J. Chem. Phys.* **73**, 3460 (1980).
- ⁴M. Scandola, G. Ceccorulli, and M. Pizzoli, *Polymer* **28**, 2081 (1987).
- ⁵M. Nakazawa, O. Urakawa, and K. Adachi, *Macromolecules* **33**, 7898 (2000).
- ⁶J. Colmenero and A. Arbe, *Soft Matter* **3**, 1474 (2007).
- ⁷D. Bingemann, N. Wirth, J. Gmeiner, and E. A. Rössler, *Macromolecules* **40**, 5379 (2007).
- ⁸S. Schramm, T. Blochowicz, E. Gouirand, R. Wipf, B. Stühn, and Y. Chuchkin, *J. Chem. Phys.* **132**, 224505 (2010).
- ⁹T. Blochowicz, S. A. Lusceac, P. Gutfreund, S. Schramm, and B. Stuh, *J. Phys. Chem. B* **115**, 1623 (2011).
- ¹⁰K. L. Ngai, *Relaxation and Diffusion in Complex Systems* (Springer, New York, 2011).
- ¹¹G. Johari and M. Goldstein, *J. Chem. Phys.* **53**, 2372 (1970).
- ¹²L. Wu, *Phys. Rev. B* **43**, 9906 (1991).
- ¹³F. Garwe, A. Schönhals, H. Lockwenz, M. Beiner, K. Schröter, and E. Donth, *Macromolecules* **29**, 247 (1996).
- ¹⁴A. Kudlik, S. Benkhof, T. Blochowicz, C. Tschirwitz, and E. A. Rössler, *J. Mol. Struct.* **479**, 201 (1999).
- ¹⁵G. Floudas, M. Paluch, A. Grzybowski, and K. L. Ngai, *Molecular Dynamics of Glass-Forming Systems* (Springer, Berlin, 2011).
- ¹⁶N. G. McCrum, B. E. Read, and G. Williams, *Anelastic and Dielectric Effects in Polymer Solids* (Wiley, New York, 1967).
- ¹⁷B. Jakobsen, K. Niss, C. Maggi, N. B. Olsen, T. Christensen, and J. C. Dyre, *J. Non-Cryst. Solids* **357**, 267 (2011).

- ¹⁸A. Arbe, D. Richter, J. Colmenero, and B. Farago, *Phys. Rev. E* **54**, 3853 (1996).
- ¹⁹A. Arbe, J. Colmenero, B. Frick, M. Monkenbusch, and D. Richter, *Macromolecules* **31**, 4926 (1998).
- ²⁰C. Gainaru, R. Kahlau, E. A. Rössler, and R. Böhmer, *J. Chem. Phys.* **131**, 184510 (2009).
- ²¹G. P. Johari, *J. Non-Cryst. Solids* **307**, 317 (2002).
- ²²K. L. Ngai and M. Paluch, *J. Chem. Phys.* **120**, 857 (2004).
- ²³K. Kessairi, S. Capaccioli, D. Prevosto, S. Sharifi, and P. Rolla, *J. Non-Cryst. Solids* **353**, 4273 (2007).
- ²⁴M. Mierzwa, S. Pawlus, M. Paluch, E. Kaminska, and K. L. Ngai, *J. Chem. Phys.* **128**, 044512 (2008).
- ²⁵S. Capaccioli, M. Paluch, D. Prevosto, W. Li-Min, and K. L. Ngai, *J. Phys. Chem. Lett.* **3**, 735–743 (2012).
- ²⁶C. Gainaru, A. Rivera, S. Putselyk, G. Eska, and E. A. Rössler, *Phys. Rev. B* **72**, 174203 (2005).
- ²⁷C. Gainaru, R. Böhmer, R. Kahlau, and E. A. Rössler, *Phys. Rev. B* **82**, 104205 (2010).
- ²⁸R. O. Pohl, X. Liu, and E. Thompson, *Rev. Mod. Phys.* **74**, 991 (2002).
- ²⁹P. Lunkenheimer, U. Schneider, R. Brand, and A. Loidl, *Contemp. Phys.* **41**, 15 (2000).
- ³⁰N. Petzold, B. Schmidtke, R. Kahlau, D. Bock, R. Meier, B. Micko, D. Krug, and E. A. Rössler, *J. Chem. Phys.* **138**, 12A510 (2013).
- ³¹D. Fragiadakis and C. M. Roland, *Phys. Rev. E* **86**, 020501 (2012).
- ³²D. Fragiadakis and C. M. Roland, *Phys. Rev. E* **89**, 052304 (2014).
- ³³M. Vogel and E. A. Rössler, *J. Phys. Chem. B* **104**, 4285 (2000).
- ³⁴M. Vogel and E. A. Rössler, *J. Chem. Phys.* **114**, 5802 (2001).
- ³⁵M. Vogel and E. A. Rössler, *J. Chem. Phys.* **115**, 10883 (2001).
- ³⁶M. Vogel, C. Tschirwitz, G. Schneider, C. Koplin, P. Medick, and E. A. Rössler, *J. Non-Cryst. Solids* **307**, 326 (2002).
- ³⁷B. Micko, S. A. Lusceac, H. Zimmermann, and E. A. Rössler, *J. Chem. Phys.* **138**, 074503 (2013).
- ³⁸B. Micko, D. Kruk, and E. A. Rössler, *J. Chem. Phys.* **138**, 074504 (2013).
- ³⁹K. J. Kinoshita, S. Kawato, and A. Ikegami, *Biophys. J.* **20**, 289 (1977).
- ⁴⁰C. C. Wang and R. Pecora, *J. Chem. Phys.* **72**, 5333 (1980).
- ⁴¹A. E. Sitnitsky, *J. Magn. Reson.* **213**, 58 (2011).
- ⁴²M. Vogel, P. Medick, and E. A. Rössler, *Annu. Rep. NMR Spectrosc.* **56**, 231 (2005).
- ⁴³G. Williams and D. C. Watts, *NMR Basic Principles and Progress*, edited by P. Diehl, E. Flick, and E. Kosfeld (Springer, Berlin, 1971), Vol. 4, p. 271.
- ⁴⁴T. Körber, F. Mohamed, M. Hofmann, A. Lichtinger, L. Willner, and E. A. Rössler, *Macromolecules* **50**, 1554 (2017).
- ⁴⁵G. Hinze, F. Fajara, and H. Sillescu, *Chem. Phys. Lett.* **232**, 154 (1995).
- ⁴⁶K. Schmidt-Rohr, A. S. Kulik, H. W. Beckham, A. Ohlemacher, U. Pawelzik, C. Boeffel, and H. W. Spiess, *Macromolecules* **27**, 4733 (1994).
- ⁴⁷A. S. Kulik, H. W. Beckham, K. Schmidt-Rohr, D. Radloff, U. Pawelzik, C. Boeffel, and H. W. Spiess, *Macromolecules* **27**, 4746 (1994).
- ⁴⁸B. Micko, C. Tschirwitz, and E. A. Rössler, *J. Chem. Phys.* **138**, 154501 (2013).
- ⁴⁹D. Bock, R. Kahlau, B. Micko, B. Pötzschnner, G. J. Schneider, and E. A. Rössler, *J. Chem. Phys.* **139**, 064508 (2013).
- ⁵⁰J. Sjöström, J. Mattsson, R. Bergman, E. Johanson, K. Josefsson, D. Svanteson, and J. Swenson, *Phys. Chem. Chem. Phys.* **12**, 10452 (2010).
- ⁵¹T. Blochowicz and E. A. Rössler, *Phys. Rev. Lett.* **92**, 225701 (2004).
- ⁵²D. Cangialosi, A. Alegria, and J. Colmenero, *J. Chem. Phys.* **128**, 224508 (2008).
- ⁵³M. Vogel and E. A. Rössler, *J. Magn. Reson.* **147**, 43 (2000).
- ⁵⁴S. A. Lusceac, “Study of relaxation processes in simple glass formers by means of ^2H NMR spectroscopy,” Ph.D. dissertation (University of Bayreuth, 2005).
- ⁵⁵A. Abragam, *The Principles of Nuclear Magnetism* (Clarendon Press, Oxford, 1961).
- ⁵⁶T. Blochowicz, A. Kudlick, S. Benkhof, J. Senker, G. Hinze, and E. A. Rössler, *J. Chem. Phys.* **110**, 12011 (1999).
- ⁵⁷S. Adichtchev, D. Bock, C. Gainaru, R. Kahlau, B. Micko, N. Petzold, B. Pötzschnner, and E. A. Rössler, *Z. Phys. Chem.* **226**, 1149 (2012).
- ⁵⁸D. Bock, N. Petzold, R. Kahlau, S. Gradmann, B. Schmidtke, N. Benoit, and E. A. Rössler, *J. Non-Cryst. Solids* **407**, 88 (2015).
- ⁵⁹W. Schnauss, F. Fajara, and H. Sillescu, *J. Chem. Phys.* **97**, 1378 (1992).
- ⁶⁰G. Kasper and A. Reiser, *J. Chem. Phys.* **120**, 10339 (2004).
- ⁶¹R. Richert and A. Blumen, *Disorder Effects on Relaxational Processes, Glasses, Polymers, Proteins* (Springer-Verlag, Berlin, 1994).
- ⁶²H. W. Starkweather, *Macromolecules* **21**, 1798 (1988).
- ⁶³J. F. Mano and S. Lanceros-Méndez, *J. Appl. Phys.* **89**, 1844 (2001).

References

1. A. Kudlik: *Dielektrische Spectroskopie an organischen Glasbildnern*, PhD thesis, University of Bayreuth (1997).
2. M. Cukierman, J. W. Lane, and D. R. Uhlmann: *High temperature flow behavior of glass forming liquids: A free-volume interpretation*, J. Chem. Phys. 59, 3639 (1973). <http://dx.doi.org/10.1063/1.1680531>
3. H. Vogel: *Das Temperaturabhängigkeitsgesetz der Viskosität von Flüssigkeiten*, Phys. Z. 22, 645 (1921).
4. G. Tarjus, S. A. Kivelson, Z. Nussinov, and P. Viot: *The frustration-based approach of supercooled liquids and the glass transition: a review and critical assessment*, J. Phys. Condens. Matter 17, R1143 (2005). <http://dx.doi.org/0.1088/0953-8984/17/50/R01>
5. B. Schmidtke, N. Petzold, R. Kahlau, and E. A. Rössler: *Reorientational dynamics in molecular liquids as revealed by dynamic light scattering: From boiling point to glass transition temperature*, J. Chem. Phys. 139, 084504 (2013). <http://dx.doi.org/10.1063/1.4817406>
6. S. Mirigian and K. S. Schweizer: *Unified Theory of Activated Relaxation in Liquids over 14 Decades in Time*, J. Phys. Chem. Lett. 4, 3648 (2013). <http://dx.doi.org/10.1021/jz4018943>
7. S. Adishchev, D. Bock, C. Gainaru, R. Kahlau, B. Micko, N. Petzold, B. Pötzschner, and E. A. Rössler: *Reorientational Dynamics of Organophosphate Glass Formers - a Joint Study by ³¹P NMR, Dielectric Spectroscopy and Light Scattering*, Z. Phys. Chem. 226, 1149 (2012). <http://dx.doi.org/10.1524/zpch.2012.0281>
8. R. Kohlrausch: *Theorie des elektrischen Rückstandes in der Leidener Flasche*, Annalen der Physik 91, 1854 (1854).
9. G. Williams and D. C. Watts: *Non-symmetrical dielectric relaxation behaviour arising from a simple empirical decay function*, Trans. Faraday Soc. 66, 80 (1970). <http://dx.doi.org/10.1039/tf9706600080>

10. B. Schmidtke, N. Petzold, B. Pötzschner, H. Weingärtner, and E. A. Rössler: *Relaxation Stretching, Fast Dynamics, and Activation Energy: A Comparison of Molecular and Ionic Liquids as Revealed by Depolarized Light Scattering*, J. Phys. Chem. B 118, 7108 (2014). <http://dx.doi.org/10.1021/jp412297u>
11. W. Götze and L. Sjögren: *Relaxation Processes in Supercooled Liquids*, Rep. Prog. Phys. 55, 241 (1992). <http://dx.doi.org/10.1088/0034-4885/55/3/001>
12. H. Sillescu: *Heterogeneity at the glass transition: a review*, J. Non-Cryst. Solids 243, 81 (1999). [http://dx.doi.org/10.1016/S0022-3093\(98\)00831-X](http://dx.doi.org/10.1016/S0022-3093(98)00831-X)
13. K. Schmidt-Rohr and H. W. Spiess: *Nature of nonexponential loss of correlation above the glass-transition investigated by multidimensional NMR*, Phys. Rev. Lett. 66, 3020 (1991). <http://dx.doi.org/10.1103/PhysRevLett.66.3020>
14. U. Tracht, M. Wilhelm, A. Heuer, H. Feng, K. Schmidt-Rohr, and H. W. Spiess: *Length scale of dynamic heterogeneities at the glass transition determined by multidimensional nuclear magnetic resonance*, Phys. Rev. Lett. 81, 2727 (1998). <http://dx.doi.org/10.1103/PhysRevLett.81.2727>
15. B. Schiener, R. Böhmer, A. Loidl, and R. V. Chamberlin: *Nonresonant spectral hole burning in the slow dielectric response of supercooled liquids*, Science 274, 752 (1996). <http://dx.doi.org/10.1126/science.274.5288.752>
16. B. Schiener, R. V. Chamberlin, G. Diezemann, and R. Böhmer: *Nonresonant dielectric hole burning spectroscopy of supercooled liquids*, J. Chem Phys. 107, 7746 (1997). <http://dx.doi.org/10.1063/1.475089>
17. M. T. Cicerone and M. D. Ediger: *Relaxation of spatially heterogeneous dynamic domains in supercooled orthoterphenyl*, J. Chem. Phys. 103, 5684 (1995). <http://dx.doi.org/10.1063/1.470551>
18. M. M. Hurley and P. Harrowell: *Kinetic structure of a 2-dimensional liquid*, Phys. Rev. E 52, 1694 (1995). <http://dx.doi.org/10.1103/PhysRevE.52.1694>
19. W. Kob, C. Donati, S. J. Plimpton, P. H. Poole, and S. C. Glotzer: *Dynamical heterogeneities in a supercooled Lennard-Jones liquid*, Phys. Rev. Lett. 79, 2827 (1997). <http://dx.doi.org/10.1103/PhysRevLett.79.2827>

20. L. Berthier and G. Biroli: *Theoretical perspective on the glass transition and amorphous materials*, Rev. Mod. Phys. 83, 587 (2011). <http://dx.doi.org/10.1103/RevModPhys.83.587>
21. E. Flenner and G. Szamel: *Lifetime of dynamic heterogeneities in a binary Lennard-Jones mixture*, Phys. Rev. E 70, 052501 (2004). <http://dx.doi.org/10.1103/PhysRevE.70.052501>
22. R. Böhmer, G. Hinze, G. Diezemann, B. Geil and H. Sillescu: *Dynamic heterogeneity in supercooled ortho-terphenyl studied by multidimensional deutron NMR*, Europhys. Lett 36, 55 (1996). <http://dx.doi.org/10.1209/epl/i1996-00186-5>
23. L. Berthier, G. Biroli, J. P. Bouchaud, L. Cipelletti, D. El Masri, D. L'Hôte, F. Ladieu, and M. Pierno: *Direct experimental evidence of a growing length scale accompanying the glass transition*, Science 310, 1797 (2005). <http://dx.doi.org/10.1126/science.1120714>
24. C. Dalle-Ferrier, C. Thibierge, C. Alba-Simionesco, L. Berthier, G. Biroli, J.-P. Bouchaud, F. Ladieu, D. L'Hôte, and G. Tarjus: *Spatial correlations in the dynamics of glassforming liquids: Experimental determination of their temperature dependence*, Phys. Rev. E 76, 041510 (2007). <http://dx.doi.org/10.1103/PhysRevE.76.041510>
25. W. M. Du, G. Li, H. Z. Cummins, M. Fuchs, J. Toulouse, and L. A. Knauss: *Light-scattering study of the liquid-glass transition in propylene carbonate*, Phys. Rev. E 49, 2192 (1994). <http://dx.doi.org/10.1103/PhysRevE.49.2192>
26. W. Götze and T. Voigtmann: *Universal and nonuniversal features of glassy relaxation in propylene carbonate*, Phys. Rev. E 61, 4133 (2000). <http://dx.doi.org/10.1103/PhysRevE.61.4133>
27. E. Leutheusser: *Dynamical model of the liquid-glass transition*, Phys. Rev. A 29, 2765 (1984). <http://dx.doi.org/10.1103/PhysRevA.29.2765>
28. W. Götze: *Recent tests of the mode-coupling theory for glassy dynamics*, J. Phys. Condens. Matter 11, A1 (1999). <http://dx.doi.org/10.1088/0953-8984/11/10A/002>
29. W. Götze and T. Voigtmann: *Ideale Glasübergänge*, Phys. Bl. 57 Nr. 4, 41 (2001). <http://dx.doi.org/0031-9279/01/0404-41>
30. W. Götze: *Complex dynamics of glass-Forming Liquids – A Mode coupling Theory*, New York, Oxford University Press (2009).

31. L. M. C. Janssen, P. Mayer, and D. R. Reichman: *Relaxation patterns in supercooled liquids from generalized mode-coupling theory*, Phys. Rev. E 90, 052306 (2014). <https://doi.org/10.1103/PhysRevE.90.052306>
32. W. Götze and L. Sjögren: The glass-transition singularity, Z. Phys. B. Con. Mat. 65, 415 (1987). <https://doi.org/10.1007/BF01303763>
33. S. Kämmerer, W. Kob, and R. Schilling: *Test of mode coupling theory for a supercooled liquid of diatomic molecules. I. Translational degrees of freedom*, Phys Rev. E 58, 2131 (1998). <http://dx.doi.org/10.1103/PhysRevE.58.2131>
34. S. Kämmerer, W. Kob, and R. Schilling: *Test of mode coupling theory for a supercooled liquid of diatomic molecules. II. q-dependent orientational correlators*, Phys Rev. E 58, 2141 (1998). <http://dx.doi.org/10.1103/PhysRevE.58.2141>
35. K. Binder and W. Kob: *Glassy materials and Disordered Solids*, World Scientific, New Jersey (2005).
36. T. R. Kirkpatrick, D. Thirumalai, and P. G. Wolynes: *Scaling concepts for the dynamics of viscous-liquids near an ideal glassy state*, Phys. Rev. A 40, 1045 (1989). <http://dx.doi.org/10.1103/PhysRevA.40.1045>
37. J. P. Bouchaud and G. Biroli: *On the Adam-Gibbs-Kirkpatrick-Thirumalai-Wolynes scenario for the viscosity increase in glasses*, J. Chem. Phys. 121, 7347 (2004). <http://dx.doi.org/10.1063/1.1796231>
38. V. Lubchenko and P. G. Wolynes: *Theory of structural glasses and supercooled liquids*, Annu. Rev. Phys. Chem. 58, 235 (2007). <http://dx.doi.org/10.1146/annurev.physchem.58.032806.104653>
39. J. C. Dyre, T. Christensen, and N. B. Olsen: *Elastic models for the non-Arrhenius viscosity of glass-forming liquids*, J. Non.-Cryst. Solids 352, 4635 (2006). <http://dx.doi.org/10.1016/j.jnoncrysol.2006.02.173>
40. G. Hinze: *Geometry and time scale of the rotational dynamics in supercooled toluene*, Phys. Rev. E 57, 2010 (1998). <http://dx.doi.org/10.1103/PhysRevE.57.2010>
41. R. Böhmer, G. Diezemann, G. Hinze, and E. A. Rössler: *Dynamics of supercooled liquids and glassy solids*, Prog. Nucl. Magn. Reson. Spectrosc. 39, 191 (2001). [http://dx.doi.org/10.1016/S0079-6565\(01\)00036-X](http://dx.doi.org/10.1016/S0079-6565(01)00036-X)

42. D. Krug, A. Herrmann, and E. A. Rössler: *Field-cycling NMR relaxometry of viscous liquids and polymers*, Prog. Nucl. Magn. Reson. Spectrosc. 63, 33 (2012). <http://dx.doi.org/10.1103/PhysRevE.57.2010>
43. T. Blochowicz: *Broadband Dielectric Spectroscopy in Neat and Binary Molecular Glass Formers*, PhD thesis, University of Bayreuth (2003).
44. R. Casalini and C. M. Roland: *Excess wing in the dielectric loss spectra of propylene glycol oligomers at elevated pressure*, Phys. Rev. B 69, 094202 (2004). <http://dx.doi.org/10.1103/PhysRevB.69.094202>
45. U. Schneider, R. Brand, P. Lunkenheimer, and A. Loidl: *Excess wing in the dielectric loss of glass formers: A Johari-Goldstein beta relaxation?*, Phys. Rev. Lett. 84, 5560 (2000). <http://dx.doi.org/10.1103/PhysRevLett.84.5560>
46. N. Petzold, B. Schmidtke, R. Kahlau, D. Bock, R. Meier, B. Micko, D. Krug, and E. A. Rössler: *Evolution of the dynamic susceptibility in molecular glass formers: Results from light scattering, dielectric spectroscopy, and NMR*, J. Chem. Phys. 138, 12A510 (2013). <http://dx.doi.org/10.1063/1.4770055>
47. K. L. Ngai: *Relaxation and Diffusion in Complex Systems*, Springer, New York (2011).
48. N. G. McCrum, B. E. Read, and G. Williams: *Anelastic and dielectric effects in polymeric solids*, John Wiley & Sons, London (1967).
49. G. P. Johari and M. Goldstein: *Viscous liquids and glass transition. II. secondary relaxations in glasses of rigid molecules*, J. Chem. Phys. 53, 2372 (1970). <http://dx.doi.org/10.1063/1.1674335>
50. G. P. Johari: *Intrinsic mobility of molecular glasses*, J. Chem. Phys. 58, 1766 (1973). <http://dx.doi.org/10.1063/1.1679421>
51. G. P. Johari: *Glass-transition and secondary relaxations in molecular liquids and crystals*, Ann. N. Y. Acad. Sci. 279, 117 (1976). <http://dx.doi.org/10.1111/j.1749-6632.1976.tb39701.x>
52. A. Rivera and E. A. Rössler: *Evidence of secondary relaxations in the dielectric spectra of ionic liquids*, Phys. Rev. B 73, 212201 (2006). <http://dx.doi.org/10.1103/PhysRevB.73.212201>

53. P. Rösner, K. Samwer, and P. Lunkenheimer: *Indications for an "excess wing" in metallic glasses from the mechanical loss modulus in Zr₆₅Al_{7.5}Cu_{27.5}*, Europhys. Lett. 68, 226 (2004). <http://dx.doi.org/10.1209/epl/i2004-10193-6>
54. A. Arbe, D. Richter, J. Colmenero, and B. Farago: *Merging of the alpha and beta relaxations in polybutadiene: A neutron spin echo and dielectric study*, Phys. Rev. E 54, 3853 (1996). <http://dx.doi.org/10.1103/PhysRevE.54.3853>
55. A. Arbe, J. Colmenero, B. Frick, M. Monkenbusch, and D. Richter: *Investigation of the dielectric beta-process in polyisobutylene by incoherent quasielastic neutron scattering*, Macromolecules 31, 4926 (1998). <http://dx.doi.org/10.1021/ma9717810>
56. B. Jakobsen, K. Niss, C. Maggi, N. B. Olsen, T. Christensen, and J. C. Dyre: *Beta relaxation in the shear mechanics of viscous liquids: Phenomenology and network modeling of the alpha-beta merging region*, J. Non-Cryst. Solids 357, 267 (2011). <http://dx.doi.org/10.1016/j.jnoncrysol.2010.08.010>
57. A. Kudlik, S. Benkhof, T. Blochowicz, C. Tschirwitz, and E. A. Rössler: *The dielectric response of simple organic glass formers*, J. Mol. Struct. 479, 201 (1999). [http://dx.doi.org/10.1016/S0022-2860\(98\)00871-0](http://dx.doi.org/10.1016/S0022-2860(98)00871-0)
58. K. L. Ngai and M. Paluch: *Classification of secondary relaxation in glass-formers based on dynamic properties*, J. Chem. Phys. 120, 857 (2004). <http://dx.doi.org/10.1063/1.1630295>
59. M. Mierzwa, S. Pawlus, M. Paluch, E. Kaminska, and K. L. Ngai: *Correlation between primary and secondary Johari-Goldstein relaxations in supercooled liquids: Invariance to changes in thermodynamic conditions*, J. Chem. Phys. 128, 044512 (2008). <http://dx.doi.org/10.1063/1.2828496>
60. S. Capaccioli, M. Paluch, D. Prevosto, L. M. Wang, and K. L. Ngai: *Many-Body Nature of Relaxation Processes in Glass-Forming Systems*, J. Phys. Chem. Let. 3, 735 (2012). <http://dx.doi.org/10.1021/jz201634p>
61. A. Kudlik, C. Tschirwitz, T. Blochowicz, S. Benkhof, and E. A. Rössler: *Slow secondary relaxation in simple glass formers*, J. Non-Cryst. Solids 235, 406 (1998). [http://dx.doi.org/10.1016/S0022-3093\(98\)00510-9](http://dx.doi.org/10.1016/S0022-3093(98)00510-9)
62. L. Wu: *Relaxation mechanisms in a benzyl-chloride toluene glass*, Phys. Rev. B 43, 9906 (1991). <http://dx.doi.org/10.1103/PhysRevB.43.9906>

63. R. Kahlau, T. Dörfler, and E. A. Rössler: *Secondary relaxations in a series of organic phosphate glasses revealed by dielectric spectroscopy*, J. Chem. Phys. 139, 134504 (2013). <http://dx.doi.org/10.1063/1.4822002>
64. A. Kudlik, C. Tschirwitz, S. Benkhof, T. Blochowicz and E. A. Rössler: *Slow secondary relaxation process in supercooled liquids*, Europhys. Lett. 40, 649 (1997). <http://dx.doi.org/10.1209/epl/i1997-00518-y>
65. C. Gainaru, R. Kahlau, E. A. Rössler, and R. Böhmer: *Evolution of excess wing and β -process in simple glass formers*, J. Chem. Phys. 131, 184510 (2009). <http://dx.doi.org/10.1063/1.3258430>
66. S. Benkhof: *Dielektrische Relaxation zur Untersuchung der molekularen Dynamik in unterkühlten Flüssigkeiten und plastischen Kristallen*, PhD thesis, University of Bayreuth (2000).
67. C. Tschirwitz, S. Benkhof, T. Blochowicz, and E. A. Rössler: *Dielectric spectroscopy on the plastically crystalline phase of cyanocyclohexane*, J. Chem. Phys. 117, 6281 (2002). <http://dx.doi.org/10.1063/1.1501582>
68. M. Vogel, C. Tschirwitz, G. Schneider, C. Koplin, P. Medick, and E. A. Rössler: *A ^2H NMR and dielectric spectroscopy study of the slow beta-process in organic glass formers*, J. Non-Cryst. Solids 307, 326 (2002). [http://dx.doi.org/10.1016/S0022-3093\(02\)01492-8](http://dx.doi.org/10.1016/S0022-3093(02)01492-8)
69. C. Hansen, F. Stickel, T. Berger, R. Richert, and E. W. Fischer: *Dynamics of glass-forming liquids. III. Comparing the dielectric alpha- and beta-relaxation of 1-propanol and o-terphenyl*, J. Chem. Phys. 107, 1086 (1997). <http://dx.doi.org/10.1063/1.474456>
70. M. Goldstein: *Viscous liquids and glass transition - a potential energy barrier picture*, J. Chem. Phys. 51, 3728 (1969). <http://dx.doi.org/10.1063/1.1672587>
71. M. Vogel and E. A. Rössler: *Slow beta process in simple organic glass formers studied by one- and two-dimensional ^2H nuclear magnetic resonance. I*, J. Chem. Phys. 114, 5802 (2001). <http://dx.doi.org/10.1063/1.1351159>
72. M. Vogel and E. A. Rössler: *Slow beta process in simple organic glass formers studied by one- and two-dimensional ^2H nuclear magnetic resonance. II. Discussion of motional models*, J. Chem. Phys. 115, 10883 (2001). <http://dx.doi.org/10.1063/1.1415495>
73. H. Wagner and R. Richert: *Spatial uniformity of the beta-relaxation in D-sorbitol*, J. Non-Cryst. Solids 242, 19 (1998). [http://dx.doi.org/10.1016/S0022-3093\(98\)00777-7](http://dx.doi.org/10.1016/S0022-3093(98)00777-7)

74. M. Vogel and E. A. Rössler: *On the nature of slow beta-process in simple glass formers: A ^2H NMR study*, J. Phys. Chem. B 104, 4285 (2000). <http://dx.doi.org/10.1021/jp9942466>
75. M. Vogel and E. A. Rössler: *Effects of various types of molecular dynamics on 1D and 2D ^2H NMR studied by random walk simulations*, J. Magn. Reson. 147, 43 (2000). <http://dx.doi.org/10.1006/jmre.2000.2160>
76. B. Micko, S. A. Lusceac, H. Zimmermann, and E. A. Rössler: *Primary and secondary relaxation process in plastically crystalline cyanocyclohexane studied by ^2H nuclear magnetic resonance. I*, J. Chem. Phys. 138, 074503 (2013). <http://dx.doi.org/10.1063/1.4790397>
77. B. Micko, D. Krug, and E. A. Rössler: *Primary and secondary relaxation process in plastically crystalline cyanocyclohexane studied by ^2H nuclear magnetic resonance. II. Quantitative analysis*, J. Chem. Phys. 138, 074504 (2013). <http://dx.doi.org/10.1063/1.4790398>
78. G. Williams and D. C. Watts: *Molecular motion in the glassy state. The effect of temperature and pressure on the dielectric β relaxation of polyvinyl chloride*, Trans. Faraday Soc. 67, 1971 (1971). <http://dx.doi.org/10.1039/TF9716701971>
79. M. Vogel, P. Medick, and E. A. Rössler: *Secondary Relaxation Processes in Molecular Glasses Studied by Nuclear Magnetic Resonance Spectroscopy*, Annu. Rep. NMR Spectro. 56, 231 (2005). [http://dx.doi.org/10.1016/S0066-4103\(05\)56005-8](http://dx.doi.org/10.1016/S0066-4103(05)56005-8)
80. C. C. Wang and R. Pecora: *Time-correlation functions for restricted rotational diffusion*, J. Chem. Phys. 72, 5333 (1980). <http://dx.doi.org/10.1063/1.439024>
81. A. E. Sitnitsky: *Analytic treatment of nuclear spin–lattice relaxation for diffusion in a cone model*, J. Magn. Res. 213, 58 (2011). <http://dx.doi.org/10.1016/j.jmr.2011.08.041>
82. B. Micko, C. Tschirwitz, and E. A. Rössler: *Secondary relaxation processes in binary glass formers: Emergence of "islands of rigidity"*, J. Chem. Phys. 138, 154501 (2013). <http://dx.doi.org/10.1063/1.4798655>
83. T. Körber, F. Mohamed, M. Hofmann A. Lichtinger, L. Willner, and E. A. Rössler: *The Nature of Secondary Relaxations: The Case of Poly(ethylene-alt-propylene) Studied by Dielectric and Deuteron NMR Spectroscopy*, Macromolecules 50, 1554 (2017). <http://dx.doi.org/10.1021/acs.macromol.6b02536>

84. G. Hinze, H. Sillescu, and F. Fujara: *Anisotropic motion of toluene above and below the glass-transition studied by ^2H NMR*, Chem. Phys. Lett. 232, 154 (1995).
[http://dx.doi.org/10.1016/0009-2614\(94\)01322-M](http://dx.doi.org/10.1016/0009-2614(94)01322-M)
85. D. Fragiadakis and C. M. Roland: *Molecular dynamics simulation of the Johari-Goldstein relaxation in a molecular liquid*, Phys. Rev. E 86, 020501 (2012).
<http://dx.doi.org/10.1103/PhysRevE.86.020501>
86. D. Fragiadakis and C. M. Roland: *Dynamic correlations and heterogeneity in the primary and secondary relaxations of a model molecular liquid*, Phys. Rev. E 89, 052304 (2014).
<http://dx.doi.org/10.1103/PhysRevE.89.052304>
87. G. Braun and A. J. Kovacs: *Variations de la temperature de transition vitreuse du polystyrolene en fonction de la concentration en plastifiant*, C. R. Hebd. Seances Acad. Sci. 260, 2217 (1965).
88. L. A. Utracki: *Polymer alloys and blends: Thermodynamics and rheology*, Carl Hauser Verlag, Munich (1990).
89. T. Sakaguchi, N. Taniguchi, O. Urakawa, and K. Adachi: *Calorimetric study of dynamical heterogeneity in blends of polyisoprene and poly(vinylethylene)*, Macromolecules 38, 422 (2005). <http://dx.doi.org/10.1021/ma048280g>
90. Y. Miwa, K. Usami, K. Yamamoto, M. Sakaguchi, M. Sakai, and S. Shimada: *Direct detection of effective glass transitions in miscible polymer blends by temperature-modulated differential scanning calorimetry*, Macromolecules 38, 2355 (2005).
<http://dx.doi.org/10.1021/ma0480401>
91. T. P. Lodge, E. R. Wood, and J. C. Haley: *Two calorimetric glass transitions do not necessarily indicate immiscibility: The case of PEO/PMMA*, J. Polym. Sci. Pol. Phys 44, 756 (2006). <http://dx.doi.org/10.1002/polb.20735>
92. A. N. Gaikwad, E. R. Wood, T. Ngai, and T. P. Lodge: *Two calorimetric glass transitions in miscible blends containing poly(ethylene oxide)*, Macromolecules 41, 2502 (2008).
<http://dx.doi.org/10.1021/ma702429r>
93. K. Adachi and Y. Ishida: *Effect of diluent on molecular-motion and glass-transition in polymers. IV. The system poly(methyl acrylate) - toluene*, Polymer J. 11, 233 (1979).
<http://dx.doi.org/10.1295/polymj.11.233>

94. M. Pizzoli, M. Scandola, and G. Ceccorulli: *Molecular motion in polymer-diluent systems: polystyrene-tritolylphosphate*, Eur. Polym. J. 23, 843 (1987). [http://dx.doi.org/10.1016/0014-3057\(87\)90055-3](http://dx.doi.org/10.1016/0014-3057(87)90055-3)
95. G. Ceccorulli, M. Pizzoli, and M. Scandola: *Composition dependence of the glass-transition temperature of polymer diluent systems. 1. experimental-evidence of a dual behavior in plasticized pvc*, Polymer 28, 2077 (1987). [http://dx.doi.org/10.1016/0032-3861\(87\)90044-9](http://dx.doi.org/10.1016/0032-3861(87)90044-9)
96. M. Scandola, G. Ceccorulli, and M. Pizzoli: *Composition dependence of the glass-transition of polymer diluent mixtures. 2. 2 concomitant glass-transition processes as a general feature of plasticized polymers*, Polymer 28, 2081 (1987). [http://dx.doi.org/10.1016/0032-3861\(87\)90045-0](http://dx.doi.org/10.1016/0032-3861(87)90045-0)
97. D. A. Savin, A. M. Larson, and T. P. Lodge: *Effect of composition on the width of the calorimetric glass transition in polymer-solvent and solvent-solvent mixtures*, J. Polym. Sci. Pol. Phys 42, 1155 (2004). <http://dx.doi.org/10.1002/polb.10776>
98. J. E. G. Lipson and S. T. Milner: *Multiple glass transitions and local composition effects on polymer solvent mixtures*, J. Polym. Sci. Pol. Phys 44, 3528 (2006). <http://dx.doi.org/10.1002/polb.21023>
99. S. Schramm, T. Blochowicz, E. Gouirand, R. Wipf, B. Stühn, and Y. Chushkin: *Concentration fluctuations in a binary glass former investigated by x-ray photon correlation spectroscopy*, J. Chem. Phys. 132, 224505 (2010). <http://dx.doi.org/10.1063/1.3431537>
100. J. Colmenero and A. Arbe: *Segmental dynamics in miscible polymer blends: recent results and open questions*, Soft Matter 3, 1474 (2007). <http://dx.doi.org/10.1039/b710141d>
101. P. J. Hains and G. Williams: *Molecular-motion in polystyrene - plasticizer systems as studied by dielectric-relaxation*, Polymer 16, 725 (1975). [http://dx.doi.org/10.1016/0032-3861\(75\)90188-3](http://dx.doi.org/10.1016/0032-3861(75)90188-3)
102. M. A. Desando, S. Walker, and W. H. Baarschers: *Relaxation processes of some aromatic sulfides, sulfoxides, anekessarid sulfones in a polystyrene matrix*, J. Chem. Phys. 73, 3460 (1980). <http://dx.doi.org/10.1063/1.440497>

103. M. Nakazawa, O. Urakawa, and K. Adachi: *Effect of local heterogeneity on dielectric relaxation spectra in concentrated solutions of poly(vinyl acetate) and poly(vinyl octanoate)*, *Macromolecules* 33, 7898 (2000). <http://dx.doi.org/10.1021/ma000102+>
104. D. Bingemann, N. Wirth, J. Gmeiner, and E. A. Rössler: *Decoupled dynamics and quasi-logarithmic relaxation in the polymer-plasticizer system poly(methyl methacrylate)/tri-m-cresyl phosphate studied with 2D NMR*, *Macromolecules* 40, 5379 (2007). <http://dx.doi.org/10.1021/ma070519g>
105. R. Kahlau, D. Bock, B. Schmidtke, and E. A. Rössler: *Dynamics of asymmetric binary glass formers. I. A dielectric and nuclear magnetic resonance spectroscopy study*, *J. Chem. Phys.* 140, 044509 (2014). <http://dx.doi.org/10.1063/1.4861428>
106. D. Bock, R. Kahlau, B. Pötzschner, T. Körber, E. Wagner, and E. A. Rössler: *Dynamics of asymmetric binary glass formers. II. Results from nuclear magnetic resonance spectroscopy*, *J. Chem. Phys.* 140, 094505 (2014). <http://dx.doi.org/10.1063/1.4865945>
107. T. Blochowicz, S. Schramm, S. Lusceac, M. Vogel, B. Stühn, P. Gutfreund, and B. Frick: *Signature of a Type-A Glass Transition and Intrinsic Confinement Effects in a Binary Glass-Forming System*, *Phys. Rev. Lett.* 109, 035702 (2012). <http://dx.doi.org/10.1103/PhysRevLett.109.035702>
108. T. Blochowicz and E. A. Rössler: *Beta relaxation versus high frequency wing in the dielectric spectra of a binary molecular glass former*, *Phys. Rev. Lett.* 92, 225701 (2004). <http://dx.doi.org/10.1103/PhysRevLett.92.225701>
109. K. Kessairi, S. Capaccioli, D. Prevosto, M. Lucchesi, and P. Rolla: *Relaxation dynamics in tert-butylpyridine/tristyrene mixture investigated by broadband dielectric spectroscopy*, *J. Chem. Phys.* 127, 174502 (2007). <http://dx.doi.org/10.1063/1.2784190>
110. D. Cangialosi, A. Alegria, and J. Colmenero: *Dielectric relaxation of polychlorinated biphenyl/toluene mixtures: Component dynamics*, *J. Chem. Phys.* 128, 224508 (2008). <http://dx.doi.org/10.1063/1.2937alegria449>
111. S. Capaccioli, K. Kessairi, M. S. Thayyil, D. Prevosto, and M. Lucchesi: *The Johari-Goldstein beta-relaxation of glass-forming binary mixtures*, *J. Non-Cryst. Solids* 357, 251 (2011). <http://dx.doi.org/10.1016/j.jnoncrysol.2010.08.007>

112. T. Blochowicz, S. A. Lusceac, P. Gutfreund, S. Schramm, and B. Stühn: *Two Glass Transitions and Secondary Relaxations of Methyltetrahydrofuran in a Binary Mixture*, J. Phys. Chem. B 115, 1623 (2011). <http://dx.doi.org/10.1021/jp110506z>
113. A. Alegria, J. Colmenero, K. L. Ngai, and C. M. Roland: *Observation of the component dynamics in a miscible polymer blend by dielectric and mechanical spectroscopies*, Macromolecules 27, 4486 (1994). <http://dx.doi.org/10.1021/ma00094a009>
114. T. Blochowicz, C. Karle, A. Kudlik, P. Medick, I. Roggatz, M. Vogel, C. Tschirwitz, J. Wolber, J. Senker, and E. A. Rössler: *Molecular dynamics in binary organic glass formers*, J. Phys. Chem. B 103, 4032 (1999). <http://dx.doi.org/10.1021/jp983754x>
115. D. Bock, N. Petzold, R. Kahlau, S. Gradmann, B. Schmidtke, N. Benoit, and E. A. Rössler: *Dynamic heterogeneities in glass-forming systems*, J. Non-Cryst. Solids 407, 88 (2015). <http://dx.doi.org/10.1016/j.jnoncrysol.2014.09.029>
116. A. Zetsche and E. W. Fischer: *Dielectric studies of the alpha-relaxation in miscible polymer blends and its relation to concentration fluctuations*, Acta Polym. 45, 168 (1994). <http://dx.doi.org/10.1002/actp.1994.010450306>
117. S. K. Kumar, R. H. Colby, S. H. Anastasiadis, and G. Fytas: *Concentration fluctuation induced dynamic heterogeneities in polymer blends*, J. Chem. Phys. 105, 3777 (1996). <http://dx.doi.org/10.1063/1.472198>
118. R. Kant, S. K. Kumar, and R. H. Colby: *What length scales control the dynamics of miscible polymer blends?*, Macromolecules 36, 10087 (2003). <http://dx.doi.org/10.1021/ma0347215>
119. G. C. Chung, J. A. Kornfield, and S. D. Smith: *Compositional dependence of segmental dynamics in a miscible polymer blend*, Macromolecules 27, 5729 (1994). <http://dx.doi.org/10.1021/ma00098a030>
120. T. P. Lodge and T. C. B. McLeish: *Self-concentrations and effective glass transition temperatures in polymer blends*, Macromolecules 33, 5278 (2000). <http://dx.doi.org/10.1021/ma9921706>
121. E. Leroy, A. Alegria, and J. Colmenero: *Segmental dynamics in miscible polymer blends: Modeling the combined effects of chain connectivity and concentration fluctuations*, Macromolecules 36, 7280 (2003). <http://dx.doi.org/10.1021/ma034144k>

122. S. Shenogin, R. Kant, R. H. Colby, and S. K. Kumar: *Dynamics of miscible polymer blends: Predicting the dielectric response*, *Macromolecules* 40, 5767 (2007). <http://dx.doi.org/10.1021/ma070503q>
123. K. Schmidt-Rohr and H. W. Spiess: *Multidimensional Solid State NMR and Polymers*, Acad. Press, New York (1994).
124. M. Vogel and E. A. Rössler: *Exchange processes in disordered systems studied by solid-state 2D NMR*, *J. Phys. Chem. A* 102, 2102 (1998). <http://dx.doi.org/10.1021/jp973461o>
125. A. J. Moreno and J. Colmenero: *Relaxation scenarios in a mixture of large and small spheres: Dependence on the size disparity*, *J. Chem. Phys.* 125, 164507 (2006). <http://dx.doi.org/10.1063/1.2361286>
126. A. J. Moreno and J. Colmenero: *Anomalous dynamic arrest in a mixture of large and small particles*, *Phys. Rev. E* 74, 021409 (2006). <http://dx.doi.org/10.1103/PhysRevE.74.021409>
127. T. Voigtmann and J. Horbach: *Double Transition Scenario for Anomalous Diffusion in Glass-Forming Mixtures*, *Phys. Rev. Lett.* 103, 205901 (2009). <http://dx.doi.org/10.1103/PhysRevLett.103.205901>
128. F. Höfling, T. Franosch, and E. Frey: *Localization transition of the three-dimensional Lorentz model and continuum percolation*, *Phys. Rev. Lett.* 96, 165901 (2006). <http://dx.doi.org/10.1103/PhysRevLett.96.165901>
129. J. Bosse and Y. Kaneko: *Self-diffusion in supercooled binary liquids*, *Phys. Rev. Lett.* 74, 4023 (1995). <http://dx.doi.org/10.1103/PhysRevLett.74.4023>
130. V. Krakoviack: *Liquid-glass transition of a fluid confined in a disordered porous matrix: A mode-coupling theory*, *Phys. Rev. Lett.* 94, 065703 (2005). <http://dx.doi.org/10.1103/PhysRevLett.94.065703>
131. Y. Kaneko and J. Bosse: *Dynamics of binary liquids near the glass transition: A mode-coupling theory*, *J. Non-Cryst-Solids* 207, 472 (1996). [http://dx.doi.org/10.1016/S0022-3093\(96\)00262-1](http://dx.doi.org/10.1016/S0022-3093(96)00262-1)
132. S. H. Chong, W. Götze, and A. P. Singh: *Mode-coupling theory for the glassy dynamics of a diatomic probe molecule immersed in a simple liquid*, *Phys. Rev. E* 63, 011206 (2001). <https://doi.org/10.1103/PhysRevE.63.011206>

133. K. Kim, K. Miyazaki, and S. Saito: *Molecular dynamics studies of slow dynamics in random media: Type A-B and reentrant transitions*, Eur. Phys. J. Special Topics 189, 135 (2010). <http://dx.doi.org/10.1140/epjst/e2010-01315-y>
134. A. Huwe, F. Kremer, P. Behrens, and W. Schwieger: *Molecular dynamics in confining space: From the single molecule to the liquid state*, Phys. Rev. Lett. 82, 2338 (1999). <http://dx.doi.org/10.1103/PhysRevLett.82.2338>
135. F. Kremer, A. Huwe, M. Arndt, P. Behrens, and W. Schwieger: *How many molecules form a liquid?*, J. Phys. Condens. Matter 11, A175 (1999). <http://dx.doi.org/10.1088/0953-8984/11/10A/013>
136. S. A. Lusceac, C. Koplin, P. Medick, M. Vogel, N. Brodie-Linder, C. LeQuellec, C. Alba-Simionesco, and E. A. Rössler: *Type A versus type B glass formers: NMR relaxation in bulk and confining geometry*, J. Phys. Chem. B 108, 16601 (2004). <http://dx.doi.org/10.1021/jp040376p>
137. G. B. McKenna: *Confit III. Summary and perspectives on dynamics in confinement*, Eur. Phys. J. Special Topics 141, 291 (2007). <http://dx.doi.org/10.1140/epjst/e2007-00056-4>
138. A. Schönhals, H. Goering, C. Schick, B. Frick, M. Mayorova, and R. Zorn: *Segmental dynamics of poly(methyl phenyl siloxane) confined to nanoporous glasses*, Eur. Phys. J. Special Topics 141, 255 (2007). <http://dx.doi.org/10.1140/epjst/e2007-00049-3>
139. S. Gradmann, P. Medick, and E. A. Rössler: *Glassy Dynamics in Nanoconfinement as Revealed by ^{31}P NMR*, J. Phys. Chem. B 113, 8443 (2009). <http://dx.doi.org/10.1021/jp9027518>
140. C. Lorthioir, A. Alegria, and J. Colmenero: *Out of equilibrium dynamics of poly(vinyl methyl ether) segments in miscible poly(styrene)-poly(vinyl methyl ether) blends*, Phys. Rev. E 68, 031805 (2003). <http://dx.doi.org/10.1103/PhysRevE.68.031805>
141. T. Blochowicz, C. Gainaru, P. Medick, C. Tschirwitz, and E. A. Rössler: *The dynamic susceptibility in glass forming molecular liquids: The search for universal relaxation patterns II*, J. Chem. Phys. 124, 134503 (2006). <http://dx.doi.org/10.1063/1.2178316>
142. D. Bock, R. Kahlau, B. Micko, B. Pötzschner, G. J. Schneider, and E. A. Rössler: *On the cooperative nature of the beta-process in neat and binary glasses: A dielectric and nuclear magnetic resonance spectroscopy study*, J. Chem. Phys. 139, 064508 (2013). <http://dx.doi.org/10.1063/1.4816374>

143. A. Reiser, G. Kaspar, and S. Hunklinger: *Effect of pressure on the secondary relaxation in a simple glass former*, Phys. Rev. Lett. 92, 125701 (2004). <http://dx.doi.org/10.1103/PhysRevLett.92.125701>
144. G. Kaspar and A. Reiser: *Variation of the secondary relaxation strength in a binary glass former*, J. Chem. Phys. 120, 10339 (2004). <http://dx.doi.org/10.1063/1.1735581>
145. C. Capaccioli, K. Kessairi, D. Prevosto, M. Lucchesi, and K. L. Ngai: *Genuine Johari–Goldstein β -relaxations in glass-forming binary mixtures*, J. Non-Cryst. Solids 42, 4643 (2006). <http://dx.doi.org/10.1016/j.jnoncrysol.2006.01.145>
146. K. Kessairi, S. Capaccioli, D. Prevosto, M. Lucchesi, S. Sharifi, and P. A. Rolla: *Interdependence of primary and Johari–Goldstein secondary relaxations in glass-forming systems*, J. Phys. Chem. B 112, 4470 (2008). <http://dx.doi.org/10.1021/jp800764w>
147. J. Sjöström, J. Mattsson, R. Bergman, E. Johansson, K. Josefsson, D. Svantesson, and J. Swenson: *Dielectric secondary relaxation of water in aqueous binary glass-formers*, Phys. Chem. Chem. Phys. 12, 10452 (2010). <http://dx.doi.org/10.1039/c001275k>
148. M. S. Thayyil, K. L. Ngai, D. Prevosto, and S. Capaccioli: *Revealing the rich dynamics of glass-forming systems by modification of composition and change of thermodynamic conditions*, J. Non-Cryst. Solids 407, 98 (2015). <http://dx.doi.org/10.1016/j.jnoncrysol.2014.10.025>
149. D. Bock: Personal correspondence.
150. T. Blochowicz, A. Kudlik, S. Benkhof, J. Senker, G. Hinze, and E. A. Rössler: *The spectral density in simple organic glass formers: Comparison of dielectric and spin-lattice relaxation*, J. Chem. Phys. 110, 12011 (1999). <http://dx.doi.org/10.1063/1.479178>
151. R. Richert and A. Blumen: *Disorder Effects on Relaxational Processes, Glasses, Polymers, Proteins*, Springer-Verlag, Berlin (1994).
152. H. W. Starkweather: *Noncooperative relaxations*, Macromolecules 21, 1798 (1988). <http://dx.doi.org/10.1021/ma00184a043>
153. J. F. Mano and S. Lanceros-Mendez: *Simple versus cooperative relaxations in complex correlated systems*, J. Appl. Phys. 89, 1844 (2001). <http://dx.doi.org/10.1063/1.1334937>

154. E. Buhleier, W. Wehner, and F. Vögtle: "Cascade"- and "Nonskid-Chain-like" Syntheses of Molecular Cavity Topologies, *Synthesis* 155 (1978). <http://dx.doi.org/10.1055/s-1978-24702>
155. M. Fischer and F. Vögtle: *Dendrimers: From design to application - A progress report*, *Angew. Chem. Int. Ed.* 38, 884 (1999). [http://dx.doi.org/10.1002/\(SICI\)1521-3773\(19990401\)38:7<884::AID-ANIE884>3.0.CO;2-K](http://dx.doi.org/10.1002/(SICI)1521-3773(19990401)38:7<884::AID-ANIE884>3.0.CO;2-K)
156. A. J. Khopade, F. Caruso, P. Tripathi, S. Nagaich, and N. K. Jain: *Effect of dendrimer on entrapment and release of bioactive from liposomes*, *Int. J. Pharm.* 232, 157 (2002). [http://doi.org/10.1016/S0378-5173\(01\)00901-2](http://doi.org/10.1016/S0378-5173(01)00901-2)
157. U. Boas and P. M. H. Heegaard: *Dendrimers in drug research*, *Chem. Soc. Rev.* 33, 43 (2004). <http://dx.doi.org/10.1039/b309043b>
158. R. N. Prajapati, R. K. Tekade, U. Gupta, V. Gajbhiye, and N. K. Jain: *Dendrimer-Mediated Solubilization, Formulation Development and in Vitro–in Vivo Assessment of Piroxicam*, *Mol. Pharm.* 6, 940 (2009). <http://dx.doi.org/10.1021/mp8002489>
159. A. W. Bosman, H. M. Janssen, and E. W. Maijer: *About dendrimers: Structure, physical properties, and applications*, *Chem. Rev.* 99, 1665, (1999). <http://dx.doi.org/10.1021/cr970069y>
160. A. D. Meltzer, D. A. Tirrell, A. A. Jones, P. T. Inglefield, D. M. Hedstrand, and D. A. Tomalia: *Chain dynamics in poly(amido amine) dendrimers - a study of ¹³C NMR relaxation parameters*, *Macromolecules* 25, 4541 (1992). <http://dx.doi.org/10.1021/ma00044a013>
161. A. D. Meltzer, D. A. Tirrell, A. A. Jones, and P. T. Inglefield: *Chain dynamics in poly(amido amine) dendrimers - a study of ²H NMR relaxation parameters*, *Macromolecules* 25, 4549 (1992). <http://dx.doi.org/10.1021/ma00044a014>
162. C. Malveau, W. E. Baille, X. X. Zhu, and W. T. Ford: *Molecular dynamics of hydrophilic poly(propylene imine) dendrimers in aqueous solutions by ¹H NMR relaxation*, *J. Polym. Sci.: Part B: Polym. Phys.* 41, 2969 (2003). <http://dx.doi.org/10.1002/polb.10584>
163. L. F. Pinto, J. Correa, M. Martin-Pastor, R. Riguera, and E. Fernandez-Megia: *The Dynamics of Dendrimers by NMR Relaxation: Interpretation Pitfalls*, *J. Am. Chem. Soc.* 135, 1972 (2013). <http://dx.doi.org/10.1021/ja311908n>

164. M. J. Jean and D. A. T. Frechet: *Dendrimers and other dendritic polymers*, John Wiley & Sons Ltd., New York (2002).
165. M. Ballauff and C. N. Likos: *Dendrimers in solution: Insight from theory and simulation*, *Angew. Chem. Int. Ed.* 43, 2998 (2004). <http://dx.doi.org/10.1002/anie.200300602>
166. K. Karatasos: *Glass transition in dendrimers*, *Macromolecules* 39, 4619 (2006). <http://dx.doi.org/10.1021/ma060545z>
167. Y. Y. Gotlib and D. A. Markelov: *Theory of orientational relaxation of individual specified units in a dendrimer*, *Polym. Sci. Ser. A* 49, 1137 (2007). <http://dx.doi.org/10.1134/S0965545X07100112>
168. D. A. Markelov, S. V. Lyulin, Y. Y. Gotlib, A. V. Lyulin, V. V. Matveev, E. Lähderanta, and A. A. Darinskii: *Orientational mobility and relaxation spectra of dendrimers: Theory and computer simulation*, *J. Chem. Phys.* 130, 044907 (2009). <http://dx.doi.org/10.1063/1.3063116>
169. D. A. Markelov, E. Lähderanta, and Y. Y. Gotlib: *Influence of Modified Terminal Segments on Dynamic Modulus and Viscosity of Dendrimer*, *Macromol. theory simul.* 19, 158 (2010). <http://dx.doi.org/10.1002/mats.200900062>
170. M. Dolgushev, G. Berezovska, and A. Blumen: *Branched Semiflexible Polymers: Theoretical and Simulation Aspects*, *Macromol. theory simul.* 20, 621 (2011). <http://dx.doi.org/10.1002/mats.201100049>
171. A. Kumar and P. Biswas: *Orientational relaxation in semiflexible dendrimers*, *Phys. Chem. Chem. Phys.* 15, 20294 (2013). <http://dx.doi.org/10.1039/c3cp53864h>
172. D. A. Markelov, M. Dolgushev, Y. Y. Gotlib, and A. Blumen: *NMR relaxation of the orientation of single segments in semiflexible dendrimers*, *J. Chem. Phys.* 140, 244904 (2014). <http://dx.doi.org/10.1063/1.4884024>
173. S. Uppuluri, F. A. Morrison, and P. R. Dvornic: *Rheology of dendrimers. 2. Bulk polyamidoamine dendrimers under steady shear, creep, and dynamic oscillatory shear*, *Macromolecules* 33, 2551 (2000). <http://dx.doi.org/10.1021/ma990634u>
174. B. M. Tande, N. J. Wagner, and Y. H. Kim: *Influence of end groups on dendrimer rheology and conformation*, *Macromolecules* 36, 4619 (2003). <http://dx.doi.org/10.1021/ma020801h>

175. S. Uppuluri, S. E. Keinath, D. A. Tomalia, and P. R. Dvornic: *Rheology of dendrimers. I. Newtonian flow behavior of medium and highly concentrated solutions of polyamidoamine (PAMAM) dendrimers in ethylenediamine (EDA) solvent*, *Macromolecules* 31, 4498 (1998). <http://dx.doi.org/10.1021/ma971199b>
176. J. Mijovic, S. Ristic, and J. Kenny: *Dynamics of six generations of PAMAM dendrimers as studied by dielectric relaxation spectroscopy*, *Macromolecules* 40, 5212 (2007). <http://dx.doi.org/10.1021/ma070624q>.
177. M. Doi and S. F. Edwards: *The Theory of Polymer Dynamics*, Oxford University Press, New York (1986).
178. N. Zacharopoulos and L. G. Economou: *Morphology and organization of poly(propylene imine) dendrimers in the melt from molecular dynamics simulation*, *Macromolecules* 35, 1814 (2002). <http://dx.doi.org/10.1021/ma010953x>
179. I. O. Götze and C. N. Likos: *Conformations of Flexible Dendrimers: A Simulation Study*, *Macromolecules* 36, 8189 (2003). <http://dx.doi.org/10.1021/ma030137k>
180. M. Murat and G. S. Grest: *Molecular Dynamics Study of Dendrimer Molecules in Solvents of Varying Quality*, *Macromolecules* 29, 1278 (1996). <http://dx.doi.org/10.1021/ma951219e>
181. B. Trahasch, B. Stühn, H. Frey, and K. Lorenz: *Dielectric relaxation in carbosilane dendrimers with perfluorinated end groups*, *Macromolecules* 32, 1962 (1999). <http://dx.doi.org/10.1021/ma981075e>
182. F. Noack: *NMR field-cycling spectroscopy - principles and applications*, *Prog. Nucl. Magn. Reson. Spectrosc.* 18, 171 (1986). [http://dx.doi.org/10.1016/0079-6565\(86\)80004-8](http://dx.doi.org/10.1016/0079-6565(86)80004-8)
183. R. Kimmich and E. Anzardo: *Field-cycling NMR relaxometry*, *Prog. Nucl. Magn. Reson. Spectrosc.* 44, 257 (2004). <http://dx.doi.org/10.1016/j.pnmrs.2004.03.002>
184. R. Kimmich: *Principles of Soft-Matter Dynamics: Basic Theories, Non-Invasive Methods, Mesoscopic Aspects*, Springer, Berlin (2012).
185. M. Hofmann: *Field-cycling NMR as a Tool of Molecular Rheology*, PhD thesis, University of Bayreuth (2016).

186. S. Kariyo, C. Gainaru, H. Schick, A. Brodin, V. N. Novikov, and E. A. Rössler: *From a simple liquid to a polymer melt: NMR relaxometry study of polybutadiene*, Phys. Rev. Lett. 97, 207803 (2006). <http://dx.doi.org/10.1103/PhysRevLett.97.207803>
187. M. Hofmann, A. Herrmann, A. Abou Elfadl, D. Krug, M. Wohlfahrt, and E. A. Rössler: *Glassy, Rouse, and Entanglement Dynamics As Revealed by Field Cycling ¹H NMR Relaxometry*, Macromolecules 45, 2390 (2012). <http://dx.doi.org/10.1021/ma202371p>
188. A. Garcia-Bernabe, R. Diaz-Calleja, and R. Haag: *Broadband dielectric spectroscopy studies of hyperbranched polyglycerols*, Macromol. Chem. Phys. 207, 970 (2006). <http://dx.doi.org/10.1002/macp.200600025>
189. J. R. Sangoro, G. Turkey, M. Abdel Rehim, C. Iacob, S. Naumov, A. Ghoneim, J. Kärger, and F. Kremer: *Charge Transport and Dipolar Relaxations in Hyperbranched Polyamide Amines*, Macromolecules 42, 1648 (2009). <http://dx.doi.org/10.1021/ma8024046>
190. G. Turkey, J. R. Sangoro, M. Abdel Rehim and F. Kremer: *Secondary Relaxations and Electrical Conductivity in Hyperbranched Polyester Amides*, J. Polym. Sci.: Part B: Polym. Phys. 48, 1651 (2010). <http://dx.doi.org/10.1002/polb.21966>
191. M. Hofmann, C. Gainaru, B. Catinkaya, R. Vaiullin, N. Fatkullin, and E. A. Rössler: *Field-Cycling Relaxometry as a Molecular Rheology Technique: Common Analysis of NMR, Shear Modulus and Dielectric Loss Data of Polymers vs Dendrimers*, Macromolecules 48, 7521 (2015). <http://dx.doi.org/10.1021/acs.macromol.5b01805>
192. D. W. Davidson and R. H. Cole: *Dielectric relaxation in glycerine*, J. Chem. Phys. 18, 1417 (1950). <http://dx.doi.org/10.1063/1.1747496>
193. D. W. Davidson and R. H. Cole: *Dielectric relaxation in glycerol, propylene glycol, and normal-propanol*, J. Chem. Phys. 19, 1484 (1951). <http://dx.doi.org/10.1063/1.1748105>
194. C. J. F. Böttcher and P. Bordewijk: *Theory of Electronic Polarization*, Elsevier Scientific Polarization, Amsterdam (1978).
195. A. Abou Elfadl, R. Kahlau, A. Herrmann, V. N. Novikov, and E. A. Rössler: *From Rouse to Fully Established Entanglement Dynamics: A Study of Polyisoprene by Dielectric Spectroscopy*, Macromolecules 43, 3340 (2010). <http://dx.doi.org/10.1021/ma902564b>
196. A. Abragam: *Principles of Nuclear Magnetism*, Oxford University Press, Oxford (1973).

197. S. A. Lusceac: *Study of relaxation processes in simple glass formers by means of ^2H NMR spectroscopy*, PhD thesis, University of Bayreuth (2005).
198. E. L. Hahn: *Spin echoes*, Phys. Rev. 80, 580 (1950).
<http://dx.doi.org/10.1103/PhysRev.80.580>
199. J. G. Powles and J. H. Strange: *Zero time resolution nuclear magnetic resonance transients in solids*, Proc. Phys. Soc. 82, 6 (1963). <http://dx.doi.org/10.1088/0370-1328/82/1/303>
200. E. A. Rössler, M. Taupitz, K. Börner, M. Schulz, and H.-M. Vieth: *A simple method analyzing ^2H nuclear-magnetic-resonance line-shapes to determine the activation-energy distribution of mobile guest molecules in disordered-systems*, J. Chem. Phys. 92, 5847 (1990). <http://dx.doi.org/10.1063/1.458354>
201. H. W. Spiess and H. Sillescu: *Solid echoes in the slow-motion region*, J. Magn. Res. 42, 381 (1981). [http://dx.doi.org/10.1016/0022-2364\(81\)90256-0](http://dx.doi.org/10.1016/0022-2364(81)90256-0)
202. N. Bloembergen, E. M. Purcell, and R.V. Pound: *Relaxation effects in nuclear magnetic resonance absorption*, Phys. Rev. 73, 679 (1948).
<http://dx.doi.org/10.1103/PhysRev.73.679>
203. H. Y. Carr and E. M. Purcell: *Effects of diffusion on free precession in nuclear magnetic resonance experiments*, Phys. Rev. 94, 630 (1954).
<http://dx.doi.org/10.1103/PhysRev.94.630>
204. S. Meiboom and D. Gill: *Modified spin-echo method for measuring nuclear relaxation times*, Rev. Sci. Instrum. 29, 688 (1958). <http://dx.doi.org/10.1063/1.1716296>
205. F. Fujara, S. Wefing, and H. W. Spiess: *Dynamics of molecular reorientations - analogies between quasi-elastic neutron-scattering and deuteron NMR spin alignment*, J. Chem. Phys. 84, 4579 (1986). <http://dx.doi.org/10.1063/1.450032>
206. M. Vogel: *^2H -NMR-Untersuchung der Sekundärrelaxation in organischen Glasbildnern*, PhD thesis, University of Bayreuth (2000).

List of figures and permissions for reuse

Figure: Description and copyright permission	Page Number
2.1 Reorientational correlation times and viscosity of salol.	13
2.2 Reorientational correlation function of TCP.	13
2.3 Single particle displacements of a Lennard-Jones mixture. Reprinted (figure 7) with permission from [L. Berthier and G. Biroli: Rev. Mod. Phys. 83, 587 (2011).] Copyright (2011) by the American Physical Society.	14
2.4 DLS spectra for propylene carbonate. Adapted (figure 1(a)) with permission from [W. Götze and T. Voigtmann:, Phys. Rev. E 61, 4133 (2000)]. Copyright (2000) by the American Physical Society.	15
2.5 Motional model for the α -process. Reproduced with permission from fig. 2 in Böhmer R., Diezemann G., Hinze G., and Rössler E. A. (2001): <i>Dynamics of Supercooled Liquids and Glassy Solids</i> . Amsterdam: Elsevier, Prog. Nucl. Magn. Reson. Spectrosc. .	16
2.6 Sketch of a DS spectra in a typical glass forming system.	17
2.7. (a) DS spectra of TCP. Reprinted with permission from J. Chem. Phys. 143, 154506 (2015), Copyright 2015 AIP Publishing.	18
2.7. (b) DS spectra of TPP. Adapted with permission from J. Chem. Phys. 1164503 (2017). Copyright 2017 AIP Publishing.	18
2.8 (a-c) Interpulse dependent ^2H NMR spectra of glycerol, of toluene and spectra obtained by simulations. Adapted with permission from (M. Vogel and E. A. Rössler: J. Phys. Chem. B 104, 4285, (2000)). Copyright (2000) American Chemical Society.	20
2.8 (d) Sketch of a “Motion-on-a-cone” model.	20
2.9 ^2H NMR spectra of cyano cyclohexane. Reprinted with permission from J. Chem. Phys. 138, 074503 (2013). Copyright 2013 AIP Publishing.	20
3.1 (a) DSC measurements of the mixture TTP/PS. Reprinted with permission from fig. 1 in Pizzoli M., Scandola M., and Ceccorulli G. (1987): <i>Molecular motions in polymer-diluent systems: Polystyrene-tritolylphosphate</i> . Amsterdam: Elsevier, Eur. Polym. J.	22

3.1 (b) Glass transition temperatures of the mixture TTP/PS. Reprinted with permission from fig. 2 in Pizzoli M., Scandola M., and Ceccorulli G. (1987): <i>Molecular motions in polymer-diluent systems: Polystyrene-tritolyolphosphate</i> . Amsterdam: Elsevier, Eur. Polym. J.	22
3.2 (a) Concentration dependent DS spectra of TPP in TPP/PS. Adapted with permission from J. Chem. Phys. 140, 094505 (2014). Copyright 2014 AIP Publishing.	23
3.2 (b) ^2H and ^{31}P NMR spectra of the system TCP/PMMA. Adapted with permission from (D. Bingemann, N. Wirth, J. Gmeiner, and E. A. Rössler: <i>Macromolecules</i> 40, 5379 (2007)). Copyright (2007) American Chemical Society.	23
3.3 Reorientational correlation function of the system TCP/PMMA. Reprinted with permission from fig. 9 (a) in Bock D., Petzold N., Kahlau R., Gradmann S., Schmidtke B., Benoit N., and Rössler E. A. (2015): <i>Dynamic Heterogeneities in Glass-Forming Systems</i> . Amsterdam: Elsevier, J. Non-Cryst. Solids.	24
3.4 DS spectra of the system MTHF in PS60k for $c_{\text{MTHF}} = 50\%$. Inset: Fraction of MTFH molecules participating in the α_1 -process. Adapted figure 2 (left) and figure 4 (inset) with permission from [T. Blochowicz, S. Schramm, S. Lusceac, M. Vogel, B. Stuhn, P. Gutfreund, and B. Frick: <i>Phys. Rev. Let.</i> 109, 035702 (2012)]. Copyright (2012) by the American Physical Society.	26
3.5 (a) Relaxation times in the system MTHF/PS60k. Adapted figure 3 with permission from [T. Blochowicz, S. Schramm, S. Lusceac, M. Vogel, B. Stuhn, P. Gutfreund, and B. Frick: <i>Phys. Rev. Let.</i> 109, 035702 (2012)]. Copyright (2012) by the American Physical Society.	27
3.5 (b) Glass transition temperatures in the system TPP/PS. Reprinted with permission from J. Chem. Phys. 140, 094505 (2014). Copyright 2014 AIP Publishing	27
3.6. Sketches of all low molecular systems used in this work.	29
3.7 (a) DS spectra of the system TCP/DH 379 for $c_{\text{TCP}} = 34\%$. Adapted with permission from J. Chem. Phys. 143, 154506 (2015). Copyright 2015 AIP Publishing.	30
3.7 (b) DS spectra of the system TPP/SBC for $c_{\text{TPP}} = 85\%$. Adapted with permission from J. Chem. Phys. 146, 1164503 (2017). Copyright 2017 AIP Publishing.	30
3.8 (a) Time constants for the system TCP/DH 379. Reprinted with permission from J. Chem. Phys. 143, 154506 (2015). Copyright 2015 AIP Publishing.	32

3.8 (b) Time constants for the system TCP/DH 379 for $c_{TCP} = 20\%$ and 34% . Reprinted with permission from J. Chem. Phys. 143, 154506 (2015). Copyright 2015 AIP Publishing.	32
3.9 Glass transition temperatures in the mixture TCP/DH 379. Adapted with permission from J. Chem. Phys. 143, 154506 (2015). Copyright 2015 AIP Publishing.	32
3.9 Inset: Glass transition temperatures of the system MTHF/tristyrene. Reprinted with permission from (T. Blochowicz, S. A. Luceac, P. Gutfreund, S. Schramm, and B. Stuhn., J. Phys. Chem. B 115, 1623 (2011)). Copyright (2011) American Chemical Society.	32
3.10 ^{31}P NMR spectra of TPP in the system TPP/SBC. Reprinted with permission from J. Chem. Phys. 146, 1164503 (2017). Copyright 2017 AIP Publishing.	34
3.10 Inset: Weighting factors in the system TPP/SBC. Reprinted with permission from J. Chem. Phys. 146, 1164503 (2017). Copyright 2017 AIP Publishing.	34
3.11 ^2H NMR spectra of SBC in the system TPP/SBC. Adapted with permission from J. Chem. Phys. 146, 1164503 (2017). Copyright 2017 AIP Publishing.	35
3.12 (a) Correlation functions of TPP in the system TPP/SBC. Reprinted with permission from J. Chem. Phys. 146, 1164503 (2017). Copyright 2017 AIP Publishing.	37
3.12 (b) Correlation functions of TCP in the system TCP/DH 379 for $c_{TCP} = 48\%$. Adapted with permission from J. Chem. Phys. 143, 154506 (2015). Copyright 2015 AIP Publishing.	37
3.13 2D NMR spectra in the system TCP/DH 379 for $c_{TCP} = 66\%$.	39
3.14 2D NMR spectra in the system TCP/DH 379 for $c_{TCP} = 48\%$.	40
3.15 Temperature dependence of T_g in the system TCP/DH 379. Reprinted with permission from J. Chem. Phys. 143, 154506 (2015). Copyright 2015 AIP Publishing.	41
3.16 Time constants of the main and secondary relaxation in the system toluene/PCB54. Adapted with permission from J. Chem. Phys. 128, 224508 (2008). Copyright 2008 AIP Publishing.	44
3.17 (a) Line shape parameter $R(t_p)$ in the system toluene/PCB54. Reprinted with permission from J. Chem. Phys. 138, 154501 (2013). Copyright 2013 AIP Publishing.	45

3.17 (b) Concentration dependent fraction of toluene molecules taking part in the secondary relaxation. Reprinted with permission from J. Chem. Phys. 138, 154501 (2013). Copyright 2013 AIP Publishing.	45
3.18 (a) Interpulse delay dependent ^2H NMR spectra of PS in the mixture TPP/PS. Reprinted with permission from J. Chem. Phys. 139, 064508 (2013). Copyright 2013 AIP Publishing.	46
3.18 (b) Interpulse delay dependent ^{31}P NMR spectra of TPP in the mixture TPP/PS. Reprinted with permission from J. Chem. Phys. 139, 064508 (2013). Copyright 2013 AIP Publishing.	46
3.19 Time constants of the main and secondary relaxation in the mixture TPP/SBC. Reprinted with permission from J. Chem. Phys. 146, 164504 (2017). Copyright 2017 AIP Publishing.	47
3.20 Interpulse delay dependent NMR spectra of the neat TPP and SBC and in a mixture of TPP/SBC. Reprinted with permission from J. Chem. Phys. 146, 164504 (2017). Copyright 2017 AIP Publishing.	48
3.21 (a,b) Line shape parameter $R(t_p)$ measured on the TPP (a) and the SBC component (b) in the TPP/SBC mixture. Reprinted with permission from J. Chem. Phys. 146, 164504 (2017). Copyright 2017 AIP Publishing.	49
3.22 (a,b) Spin-lattice relaxation times of TPP (a) and SBC (b) in the TPP/SBC mixture. Reprinted with permission from J. Chem. Phys. 146, 164504 (2017). Copyright 2017 AIP Publishing.	50
3.23 Susceptibility of TPP in the mixtures TPP/SBC and TPP/PS and of SBC in the mixture TPP/SBC. Reprinted with permission from J. Chem. Phys. 146, 164504 (2017). Copyright 2017 AIP Publishing.	52
4.1 Structure of the PPI dendrimer of generation 2.	55
4.2 (a) Dielectric spectra of generation 5 of the PPI dendrimer. Adapted with permission from (F. Mohamed, M. Hofmann, B. Pötzschner, N. Fatkullin, and E. A. Rössler: Macromolecules 48, 3294 (2015)). Copyright (2015) American Chemical Society.	56
4.2 (b) Time constants of generation 2-5 of the PPI dendrimer. Adapted with permission from (F. Mohamed, M. Hofmann, B. Pötzschner, N. Fatkullin, and E. A. Rössler: Macromolecules 48, 3294 (2015)). Copyright (2015) American Chemical Society.	56

4.3 Susceptibilities of generation 2-5 of the PPI dendrimer. Adapted with permission from (F. Mohamed, M. Hofmann, B. Pötzschner, N. Fatkullin, and E. A. Rössler: <i>Macromolecules</i> 48, 3294 (2015)). Copyright (2015) American Chemical Society.	57
4.4 ^2H NMR spectra of generation 2-5 of the PPI dendrimer. Adapted with permission from (F. Mohamed, M. Hofmann, B. Pötzschner, N. Fatkullin, and E. A. Rössler: <i>Macromolecules</i> 48, 3294 (2015)). Copyright (2015) American Chemical Society.	58
4.5 (a) Spectrum of the end group deuterated PPI dendrimer of generation 3. Reprinted with permission from (F. Mohamed, M. Hofmann, B. Pötzschner, N. Fatkullin, and E. A. Rössler: <i>Macromolecules</i> 48, 3294 (2015)). Copyright (2015) American Chemical Society.	59
4.5 (b) Relaxation times of generation 2-5 of the PPI dendrimer.	59
4.6 (a) Correlation function of the end branch deuterated $G = 3$ dendrimer.	60
4.6 (b) Line shape parameter $R(t_p)$ of the end branch deuterated $G = 3$ dendrimer.	60
5.1 GUI of the simulation program.	73
5.2 ^2H NMR solid echo spectra obtained by random walk simulations of a threefold methyl group jump.	74
5.3 Simulated residual correlation for a threefold methyl group jump.	74
5.4 Simulated 2D ^2H NMR spectrum for a threefold methyl group jump.	75
5.5 Solid-echo Pake spectra for a “motion-on-a-cone” model for different opening angles.	76
5.6 Solid-echo Pake spectra for a “motion-on-a-cone” model for an opening angle of $\chi = 5^\circ$ for different interpulse delays.	76

Acknowledgements

Hereby, I want to thank all people who supported me during my studies and my PhD thesis. First, I want to express my gratitude to Prof. Dr. Ernst Rössler, who always supported me during my time at his workgroup and provided perfect working conditions for my colleges and me.

Further, I want to thank all current and former members of our workgroup for the nice and kind working atmosphere and the help, which was provided at everyday scientific and non-scientific problems, especially I thank Dr. Björn Micko and Dr. Daniel Bock who introduced me to the experimental setup and always helped with technical problems. Further, I want to thank Fathia Mohamed, who greatly enhanced my work with her dielectric measurements. I want to thank the Elitenetzwerk Bayern who supported me financially with a 3-year long scholarship. Finally, I want to thank my family, in particular, my grandfather Manfred Gahn, who provided great support during all the years at the University.

Eidesstattliche Versicherung

Hiermit erkläre ich mich damit einverstanden, dass die elektronische Fassung meiner Dissertation unter Wahrung meiner Urheberrechte und des Datenschutzes einer gesonderten Überprüfung hinsichtlich der eigenständigen Anfertigung der Dissertation unterzogen werden kann.

Hiermit erkläre ich eidesstattlich, dass ich die Dissertation selbständig verfasst und keine anderen als die von mir angegebenen Quellen und Hilfsmittel benutzt habe.

Ich habe die Dissertation nicht bereits zur Erlangung eines akademischen Grades anderweitig eingereicht und habe auch nicht bereits diese oder eine gleichartige Doktorprüfung endgültig nicht bestanden.

Hiermit erkläre ich, dass ich keine Hilfe von gewerblichen Promotionsberatern bzw. –vermittlern in Anspruch genommen habe und auch künftig nicht nehmen werde.

.....

Ort, Datum, Unterschrift